The Dissertation Committee for Theresa Marie Diehl Certifies that this is the approved version of the following dissertation:

Gravity Analyses for the Crustal Structure and Subglacial Geology of West Antarctica, Particularly Beneath Thwaites Glacier

Committee:

Donald Blankenship, Supervisor

Vicki Childers

Ian Dalziel

Lawrence Lawver

Mrinal Sen

Clark Wilson

Gravity Analyses for the Crustal Structure and Subglacial Geology of West Antarctica, Particularly Beneath Thwaites Glacier

by

Theresa Marie Diehl, B.S.

Dissertation

Presented to the Faculty of the Graduate School of

The University of Texas at Austin

in Partial Fulfillment

of the Requirements

for the Degree of

Doctor of Philosophy

The University of Texas at Austin

August 2008

Dedication

To my family: parents Marilyn and Don; siblings Christina (and Stephen), Matthew (and Denise), Deborah, and Jessica (and Levi); and godparents Coletta and Art. You deserve more thanks than I could ever express for your tireless support, emotional and otherwise, during my time in Texas. You encouraged me when I decided to pursue my degree and your faith and encouragement has not wavered since. I could not have done this without knowing you were all behind me! Although it was tough with few visits home and spending many holidays apart, our frequent long phone calls and emails are evidence that we're never actually apart- even when we're living in different sections of the country.

I love you all so much!

Acknowledgements

To all:

Thank you to my supervisor, Don Blankenship, and all of my examining and dissertation committee members: Vicki Childers, Ian Dalziel, Steve Grand, Larry Lawver, Leon Long, Mrinal Sen, and Clark Wilson. I have learned more than I can say from your breadth and depth of experiences and am grateful for your support- especially of my desire to do field work and travel to conferences. Your thorough critiques of my work forced me to accept only my best work and I appreciate the time you invested in this dissertation. I am also very grateful to my colleagues, and friends, at the British Antarctic Survey (Tom Jordan and Fausto Ferraccioli) for patiently showing me the ropes of gravity analysis. Their willingness to share resources (especially by providing programs for analyses) and their welcoming attitudes came at a much-needed time during this degree. Thank you to all those who have served as collaborators and/or mentors (in research and otherwise), particularly: Duncan Young, Jack Holt, Ginny Catania, Philip Guerrero, Marcy Davis, and Vicki Childers. Our conversations helped my personal and professional development, as well as my research; I was glad for your ever-open doors and good advice. Special thanks to Scott Kempf for never tiring in teaching me to use our computer systems and codes; you taught me how to become self-sufficient.

Thanks to all the cryosphere graduate students for support, great conversations, and good times together: Sasha Carter, Irina Filina, Erick Leuro, Hunter Danque, and

Jamin Greenbaum. Thank you to Brad Wolaver for inviting me to do field work in Cuatro Cienegas, Mexico and for ever-enthusiastic collaboration on that gravity project. I'm looking forward to future projects together will all of you! I'd also like to thank all the good friends I've made while at UT for their encouragement and lots of good memories. There are too many of you to list, but I especially wanted to thank Danny Bailey, Shanna and Jack Bauer, Nedra and David Bonal, Nysha Chaderton, Kerin Claeson, and Lindsay Szramek.

Chapter 2:

I would like to thank the science crew and camp staff of the AGASEA and BBAS field parties, as well as Kenn Borek Air Ltd. for their hard work supporting this project. Special thanks to the geophysicists and engineers at Micro-G LaCoste for their willingness to train several of us on the operation of the Air/Sea II and many helpful conversations post-season. I would also like to thank Tom Richter and Scott Kempf for technical support and Vicki Childers for assistance with data processing and an insightful manuscript review. Thanks also to an anonymous reviewer for comments that improved the results and published manuscript. This project was funded by the National Science Foundation grant OPP-0230197, the Jackson School of Geosciences and the Geology Foundation at the University of Texas at Austin, the G. Unger Vetleson Foundation, the UK Natural Environment Research Council, and the LTMS-G Programme of the Geological Sciences Division at the British Antarctic Survey. This published manuscript version of this chapter was UTIG contribution no. 1940.

Chapters 3 and 5:

This work was supported by the National Science Foundation (grant OPP-0230197), the University of Texas Geology Foundation and Jackson School of Geosciences, the G. Unger Vetleson Foundation, the Institute for Geophysics Gale White Fellowship, and the British Antarctic Survey. I would like to thank Vicki Childers and Scott Kempf for their assistance with this work and Carol Finn for her suggestion of using GM-SYS for the forward modeling.

Chapter 4:

This work was supported by the University of Texas Geology Foundation and Jackson School of Geosciences and the G. Unger Vetleson Foundation. Thanks to Srinivas Bettadpur, Francis Condi, John Ries, and Byron Tapley at the University of Texas, Center for Space Research for their willingness to collaborate and provide GRACE satellite gravity data for this project. Thanks also to Larry Lawver for the idea to create an updated tectonic sketch map of West Antarctica and Dave McAdoo for providing the ERS-1 gravity anomalies. The inverse modeling work was aided by conversations with Irina Filina, Chaoshun Hu, Lopamundra Roy, and Mrinal Sen and additional assistance from Chaoshun Hu.

Gravity Analyses for the Crustal Structure and Subglacial Geology of West Antarctica, Particularly Beneath Thwaites Glacier

Publication No._____________

Theresa Marie Diehl, Ph.D.
The University of Texas at Austin, 2008

Supervisor: Donald D. Blankenship

The West Antarctic Ice Sheet (WAIS) is mostly grounded in broad, deep basins (down to 2.5 km below sea level) that are stretched between five crustal blocks. The geometry of the bedrock, being mostly below sea level, induces a fundamental instability in the WAIS through the possibility of runaway grounding line retreat. The crustal environment of the WAIS further influences the ice sheet's fast flow through conditions at the ice-bedrock boundary. This study focuses on understanding the WAIS by examining the subglacial geology (such as volcanoes and sedimentary basins) at the ice-bedrock boundary and the continent's deeper crustal structure- primarily using airborne gravity anomalies. The keystone of this study is a 2004-2005 aerogeophysical survey over one of the most negative mass balance glaciers on the continent: Thwaites Glacier (TG). The gravity anomalies derived from this dataset- as well as gravity-based modeling and spectral crustal boundary depth estimates- reveal a heterogeneous crustal environment beneath the glacier. The widespread Mesozoic rifting observed in the Ross

Sea Embayment (RSE) of West Antarctica extends beneath TG, where the crust is ~27 km thick and cool. Adjacent to TG, spectrally-derived shallow Moho depths for the Marie Byrd Land (MBL) crustal block can be explained by thermal support from warm mantle. I assemble here new compilations of free-air and Bouguer gravity anomalies across West Antarctica (from both airborne and satellite datasets) and re-interpret the extents of West Antarctic crustal block and their boundaries with the rift system. Airy isostatic gravity anomalies reveal that TG is relatively sediment starved, in contrast to the sediment-rich RSE. TG's fast flow velocities could be sustained in this sediment poor environment if higher heat flux in MBL was providing an ample source of subglacial melt water to the glacier. The isostatic anomalies also indicate that TG's outlet rests on a bedrock sill that will impede future grounding line retreat (up to ~100 km) and temporarily stabilize the glacier.

Table of Contents

List of Tables

List of Figures

Chapter 1: Introduction

1.1 Study Location

Antarctica is split into East and West, each named for the hemisphere in which it resides (Figure 1.1), but their true divisions are based on disparate tectonic histories, geology (Figure 1.2), and glaciology (Figure 1.3). The motivations for studying West Antarctica are inevitably rooted in understanding its unique marine ice sheet. The West Antarctic Ice Sheet holds the ice equivalent of approximately 5m of sea level rise [*Mercer*, 1978; *Oppenheimer*, 1998; *Alley and Bindschadler*, 2001] and is grounded mostly below sea level [*Bentley*, 1964; *Jankowski and Drewry*, 1981; *Drewry*, 1983; *Lythe, et al.*, 2001] (Figure 1.2). Recent observations show dynamic changes in ice flow on the order of decades or less, particularly in the Thwaites Glacier area of the Amundsen Sea Embayment [e.g. *Rignot, et al.*, 2004b] (Figure 1.3). Since recent work [*Holt et al.,* 2006a] has shown that bedrock topography drops to 2.5 km below sea level in the Byrd Subglacial Basin and Bentley Subglacial Trench (Figure 1.2), concerns first raised several decades ago about the instability of the ice sheet [*Hughes*, 1975; *Mercer*, 1978] are even more relevant today.

With the available data, increasingly complex models of ice flow [e.g. *Weertman*, 1974; *Schoof*, 2007] appear to have confirmed the instability of the ice sheet. However, basic boundary conditions needed for accurate ice flow models (from subglacial topography and lithological composition to crustal thickness) are lacking over vast areas of the ice sheet. To obtain these boundary conditions, we need to study the continent beneath the ice (Figure 1.4). The continent's tectonic history not only produced an environment hospitable to sustaining the West Antarctic Ice Sheet, but its resulting geologic features are believed to substantially impact the flow of the ice sheet (e.g.,

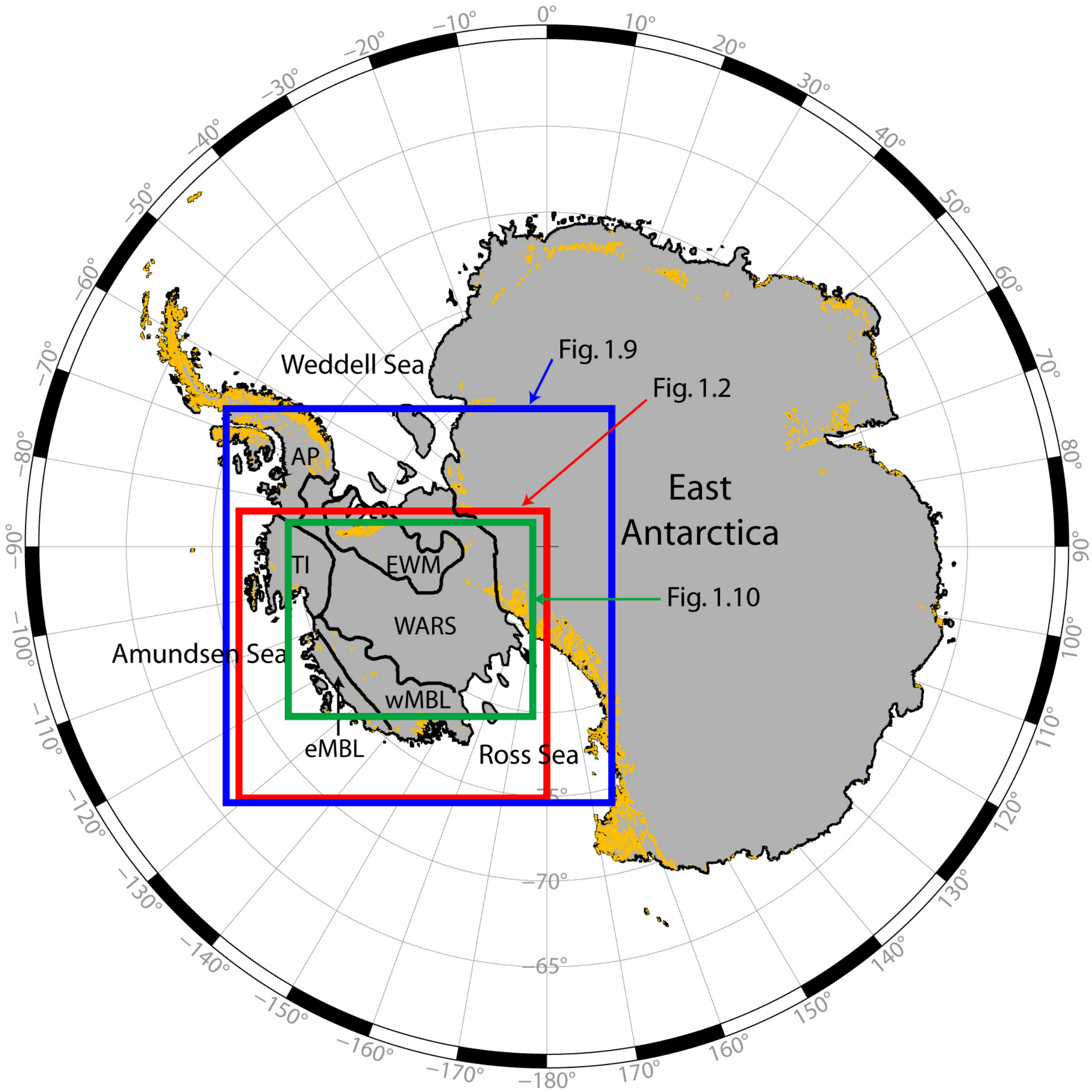

Figure 1.1: Antarctic index map showing the locations of Figure 1.3 (red box) and Figure 1.9 (blue box). Land is colored gray. Also shown: rock outcrop locations (gold lines) [*SCAR*, 2006] and West Antarctic crustal blocks (thick back lines) [*Dalziel and Elliot*, 1982; *Dalziel and Lawver*, 2001]. Crustal block names: AP= Antarctic Peninsula; TI= Thurston Island; EWM= Ellsworth-Whitmore Mountains; WARS= West Antarctic Rift System; eMBL and wMBL= eastern and western Marie Byrd Land.

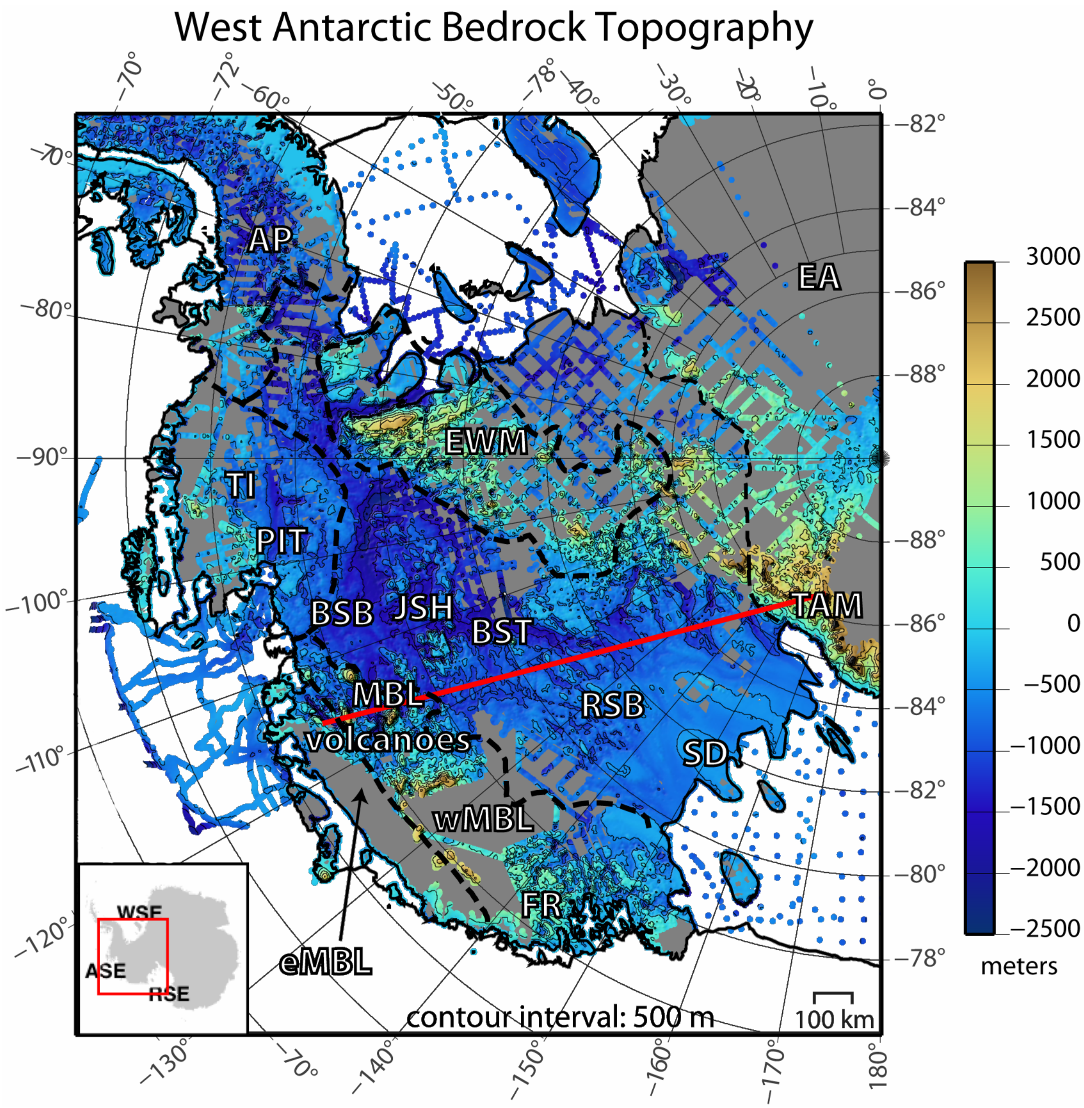

Figure 1.2: West Antarctic bedrock topography, primarily from airborne radar sounding [*Lythe, et al.*, 2001] (D. Young, unpub. data, 2008). Ice sheet-covered areas that lack data are gray. Solid black line=Antarctic coastline [*SCAR*, 2006], including ice shelves; dashed black lines=crustal blocks of West Antarctica [*Dalziel and Elliot*, 1982; *Dalziel and Lawver*, 2001]; red line=profile in Figure 1.4. Major bedrock features: PIT=Pine Island Trench [*Jordan, et al.*, submitted]; BSB=Byrd Subglacial Basin; JSH=Jankowski Subglacial Highlands (see section 1.4); BST=Bentley Subglacial Trench; TAM=Transantarctic Mountains; RSB=Rose Subglacial Basin (see section 1.4); SD=Siple Dome; FR=Ford Ranges; Crustal blocks: AP= Antarctic Peninsula, EWM=Ellsworth-Whitmore Mountains; EA=East Antarctica; TI=Thurston Island; MBL=Marie Byrd Land (east and west).

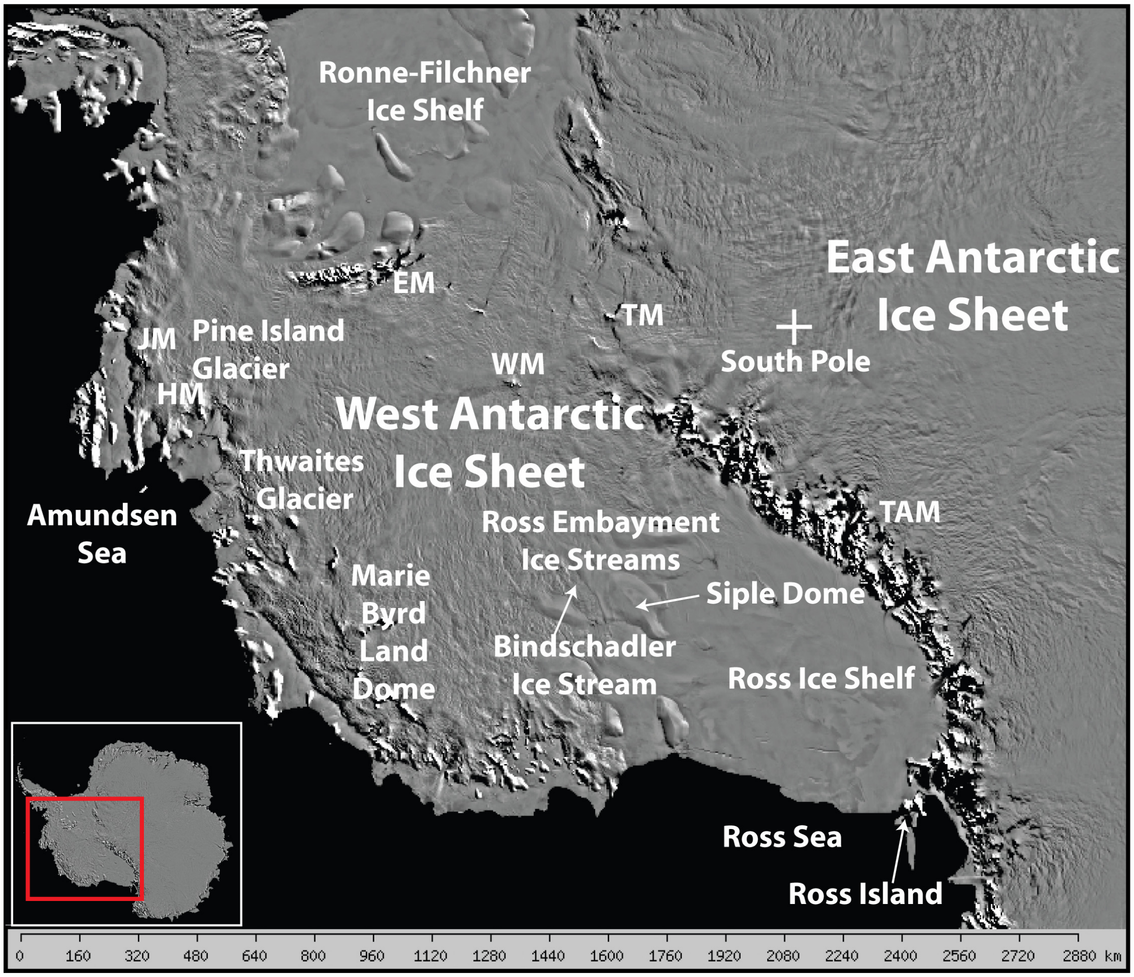

Figure 1.3: MODIS satellite visual image of West Antarctica [*Haran, et al.*, 2005] labeled with major glaciological and subaerial geological features mentioned in this study. EM=Ellsworth Mountains; WM=Whitmore Mountains; TM=Thiel Mountains; HM=Hudson Mountains; JM=Jones Mountains; TAM=Transantarctic Mountains. Inset: location of figure, also a MODIS image [*Haran, et al.*, 2005]

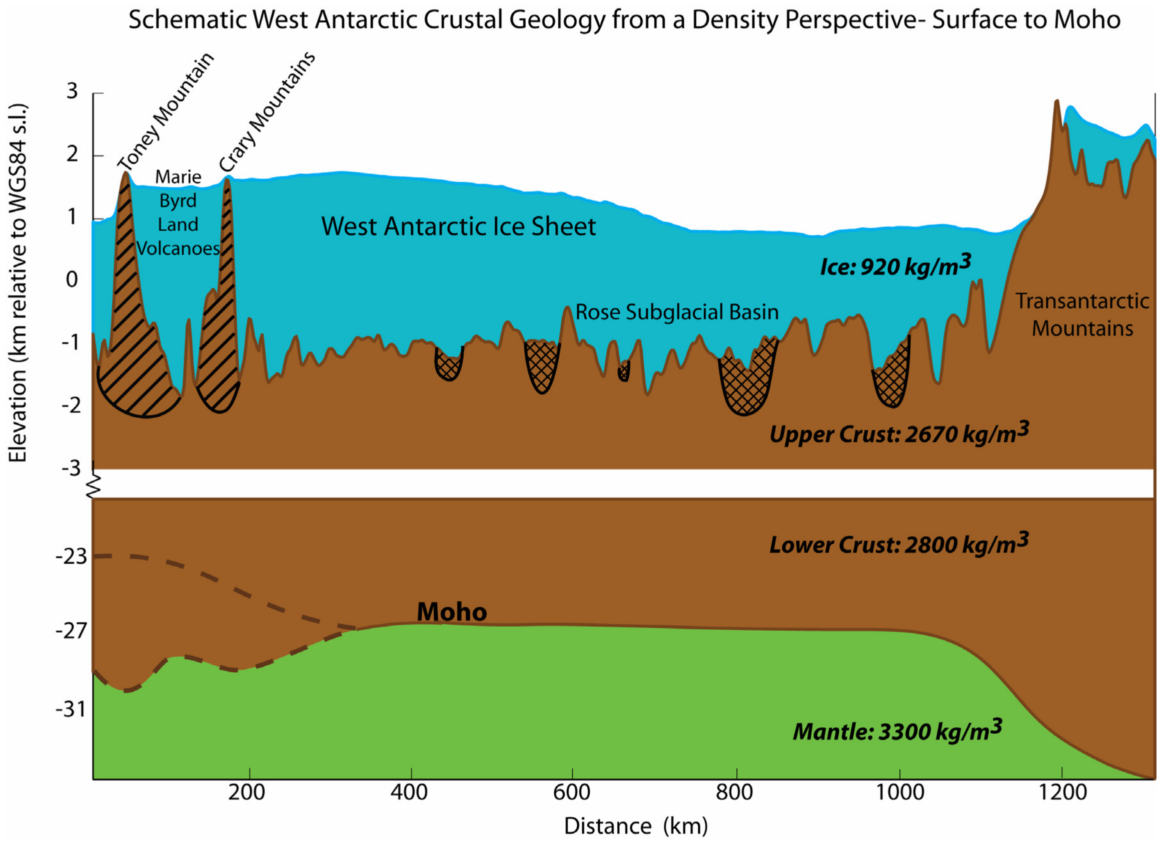

Figure 1.4: Schematic Cross Section of West Antarctica (located at red line on Figure 1.2), labeled with typical densities of major crustal bodies considered within this study. Schematic smaller density bodies include sedimentary basins (cross hatches, density 2100 kg/m^3) and volcanics (hatches, density 2800 kg/m^3). Ice sheet surface topography [*Bamber and Gomez-Dans*, 2005] and bedrock topography [*Lythe, et al.*, 2001] (D. Young, unpub. data, 2008) are an accurate cross section of the area. The Moho is a sketch based on published (see section 1.2.5) and possible (dashed, only in Marie Byrd Land) crustal thickness numbers.

sedimentary basins [*Blankenship, et al.*, 1986; *Anandakrishnan, et al.*, 1998; *Blankenship, et al.*, 2001; *Peters, et al.*, 2006] and enhanced geothermal flux [*Blankenship, et al.*, 1993]).

The goals of this study are focused on improving our understanding of West Antarctic crustal geology. The aim is to tie the crustal geology to both its tectonic history and its current influence on the overlying ice sheet. To do so, I undertook four research projects, primarily using airborne gravity but augmenting analyses with other datasets when available. Each of the four phases constitutes one of the four central chapters (Chapters 2-5). The first describes collecting and processing the largest airborne gravity dataset in West Antarctica, over 290,000 km^2 of the Thwaites Glacier catchment and surrounding area. The second establishes the crustal structure beneath Thwaites Glacier and links it to the tectonics and geology of the surrounding area. The third merges the Thwaites Glacier data with older datasets and updates crustal boundary interpretations over ~0.8 million km^2 of the West Antarctic ice sheet. The last examines geology near the base of the ice sheet and creates a template of potential sub-ice sedimentary basins, suitable for large-scale ice sheet modeling.

To accomplish these goals, geophysical interpretations were guided with a sound basis in West Antarctic geology and glaciology. To this end, a thorough review of the tectonic events leading to the formation of the crust in West Antarctica and a description of our understanding of West Antarctic Ice Sheet dynamics are necessary.

1.2 West Antarctic Tectonic History- Precambrian to Recent

1.2.1 Precambrian and Paleozoic: Assembling Gondwanaland

The tectonic history of West Antarctica is linked to that of East Antarctica and supercontinent creation in the early Phanerozoic. East Antarctica's current Pacific margin (now marked by the Cenozoic Transantarctic Mountains) obtained its present geometry during the breakup of Rodinia ~800 Ma. By latest Precambrian (550 Ma), East Antarctica became the "keystone" of the Gondwana supercontinent, at which time it was adjacent to South America, Africa, India, and Australia [*Dalziel and Lawver*, 2001]. Gondwana became the southern half of the supercontinent Pangea when Laurasia (made up of the current Northern Hemisphere continents) amalgamated at ~320 Ma [*Curtis*, 2001]. Gondwana remained in its 550 Ma configuration until it broke up at 200 Ma [*Dalziel, et al.*, 2000], by which time the crustal blocks of West Antarctica were in the proximity of the East Antarctic Gondwanan margin, although not in their current configuration [*Dalziel and Lawver*, 2001] (Figure 1.5) .

The pieces that make up West Antarctica are (Figure 1.2): five crustal blocks with Paleozoic (or earlier) basement and the West Antarctic Rift System. Development of the rift system started in the Cretaceous and will be discussed later. The crustal blocks are the Antarctic Peninsula, Ellsworth-Whitmore Mountains, Thurston Island, and East and West Marie Byrd Land. Geologic evidence has identified Paleozoic bedrock on all the crustal blocks (e.g. Antarctic Peninsula [*Dalziel and Elliot*, 1982], Ellsworth-Whitmore Mountains [*Curtis*, 2001], Thurston Island [*Pankhurst, et al.*, 1993], and Marie Byrd Land [*Luyendyk, et al.*, 2001]) and thus they must have existed before and/or been created during the time of the Gondwana supercontinent. In this study, I am particularly interested in the histories of the Ellsworth-Whitmore Mountains, Thurston Island, and both parts of Marie Byrd Land, and will refer to their tectonic histories (related below) extensively in Chapters 3 and 4.

In their Gondwanan configuration (Figure 1.5), the West Antarctic crustal blocks- plus the two that would eventually become New Zealand- can be grouped into two provinces with shared geochemical, paleomagnetic, and geologic signatures: the Amundsen (composed of the Antarctic Peninsula, Thurston Island, eastern Marie Byrd Land, and New Zealand's eastern province) and Ross (composed of East Antarctica's Victoria Land, western Marie Byrd Land, and New Zealand's western province) [*Divenere, et al.*, 1995; *Bradshaw, et al.*, 1997; *Pankhurst, et al.*, 1998]. Many lines of evidence link these provinces together; for example, Late Devonian to Carboniferous

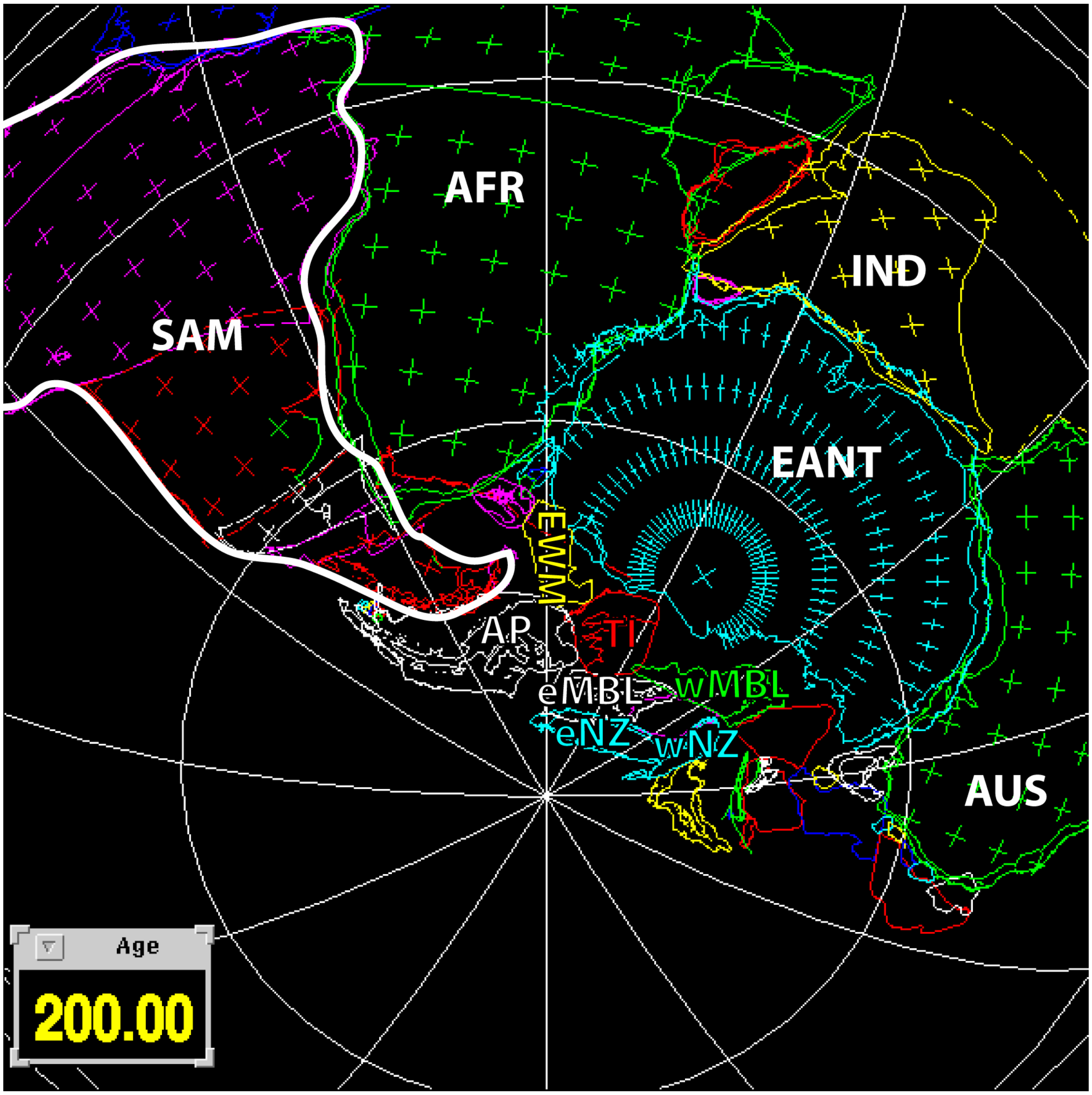

Figure 1.5: Tectonic reconstruction of the configuration of Gondwana at the start of breakup (200 Ma), including the West Antarctic and New Zealand crustal blocks. Major continents (clockwise): South America (SAM, all sections outlined by a thick white line); Africa (AFR, green); India (IND, yellow); East Antarctica (EANT, cyan); and Australia (AUS, green). Crustal blocks of interest: Ellsworth-Whitmore Mountains (EWM, yellow, boot-shaped); Antarctic Peninsula (AP, white); Thurston Island (TI, red); eastern Marie Byrd Land (eMBL, white); western Marie Byrd Land (wMBL, green); east and west New Zealand (eNZ and wNZ, cyan). White lines are latitude and longitude, converging at the South Pole. Modified with permission [*PLATES*, 1999].

Ford Granodiorite (from arc magmatism) on Edward VII Peninsula are similar to the Admirality Intrusives in the Transantarctic Mountains, placing western Marie Byrd Land and Victoria Land in close proximity during Gondwanan times [*Ferraccioli, et al.*, 2002]. Other such links, and in particular paleomagnetic poles [*Divenere, et al.*, 1995], suggest that the two Provinces were sub-parallel with the Amundsen Province close to the subduction zone, the Ross Province generally further inboard, and the Ellsworth-Whitmore Mountains block most distal to the subduction (Figure 1.5) [*Siddoway*, 2008].

Subduction along the East Antarctic crustal margin was extremely long-lived, starting in the late Neoproterozoic (ca. 1.7 Ga) and continuing into the late Cambrian (0.55 Ga)- resulting in a prolonged mountain-building event called the Ross Orogeny [*Curtis*, 2001]. The Ross Orogeny has corollaries on the other continents located along the subduction zone, suggesting an Andean-type margin [*Curtis*, 2001]. The oldest exposed rocks in the Ellsworth-Whitmore Mountains are early to mid- Cambrian, rift-related and subsequent passive margin deposits, suggesting that the block may have existed in a back-arc basin and that the Gondwana convergent margin was fairly complex along its length [*Curtis*, 2001; *Flowerdew, et al.*, 2007].

1.2.2 Late Triassic to Early Cretaceous: Gondwana Breakup, Opening of Weddell Sea, and Arc Magmatism

The start of Gondwana's breakup is generally placed at ~200 Ma and is thought to have been caused by the impingement of a plume beneath the crust in the area where Antarctica, South America, and Africa were adjacent to each other (Figure 1.5) [*Behrendt and Cooper*, 1991; *Dalziel and Lawver*, 2001]. One Antarctic-centered model of breakup [*Dalziel, et al.*, 2000] calls for several stages of development: 1. plume impingement on the underside of a subducting slab beneath the junction of Antarctica, South America, and Africa at ~260-230 Ma, 2. uplift of continental lithosphere above the plume head (including the Ellsworth-Whitmore Mountains [*Dalziel and Lawver*, 2001]) and heating that allowed ductile continental crustal rotation away from the plume area, from ~200-180 Ma, 3. break-through of the plume head and eruption of Karoo-Ferrar Large Igneous Province at 180 Ma, and 4. initiation of sea floor spreading between the continents.

This breakup scenario fits well with paleomagnetic evidence from the Ellsworth-Whitmore Mountains crustal block and the opening of the Weddell Sea. The Ellsworth-Whitmore Mountains block was translated to the northeast (toward the Antarctic Peninsula, Thurston Island, and eastern Marie Byrd Land) and rotated counterclockwise significantly by 175 Ma (Figure 1.6) [*Dalziel and Elliot*, 1982; *Grunow, et al.*, 1987; *Dalziel, et al.*, 2000]. The Weddell Sea Embayment formed during the Ellsworth-Whitmore Mountains block movement from the ductile extension of continental crust [*Dalziel and Lawver*, 2001] and the continental crust north of the current embayment thinned enough to start sea floor spreading by 165 Ma [*Grunow, et al.*, 1987]. The process of breaking the other four Gondwanan continents away from Antarctica continued through the Late Cretaceous (95 Ma) [*Dalziel and Lawver*, 2001].

Extensive studies in the western Marie Byrd Land Ford Ranges [*Siddoway*, 2008 and references therein] provide the best Antarctic record of activity along the Phoenix (proto-Pacific) subduction zone during Gondwana breakup. This subduction zone would have been just outboard of current-day West Antarctica and significant amounts of its resulting magmatism are exposed above the ice sheet today. Active subduction continued along the margin until ~100 Ma, producing widespread calc-alkaline magmatic arc rocks [*Pankhurst, et al.*, 1998; *Dalziel and Lawver*, 2001; *Siddoway*, 2008] and drawing the

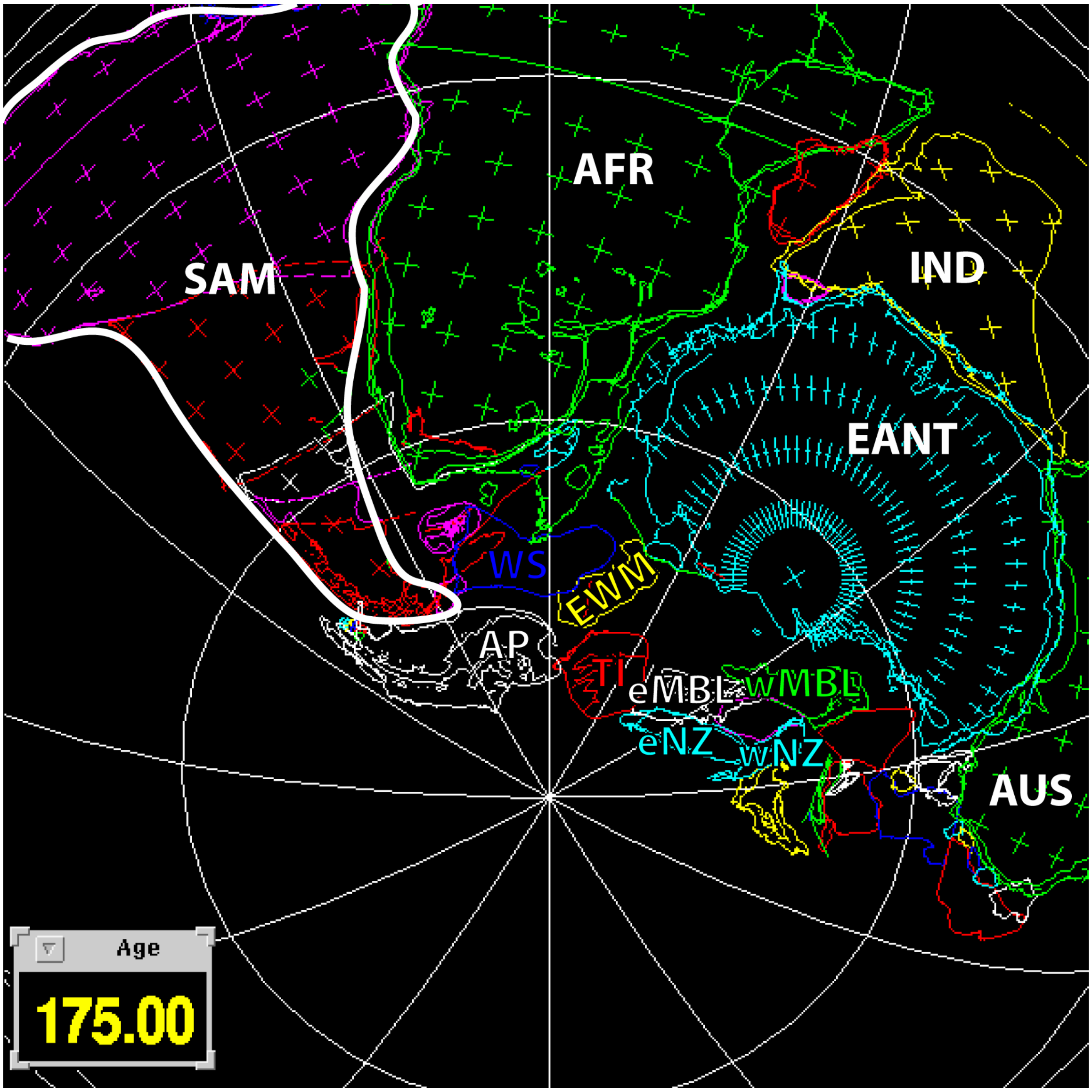

Figure 1.6: Tectonic reconstruction of the breakup of Gondwana at 175 Ma, showing significant rotation and/or translation of the Amundsen Province crustal blocks [*Divenere, et al.*, 1995; *Pankhurst, et al.*, 1998] (particularly the Ellsworth-Whitmore Mountains block, but also the Antarctic Peninsula, Thurston Island, and eastern Marie Byrd Land) by this time. Labeled as in Figure 1.5, plus the incipient Weddell Sea (WS, blue). Modified with permission [*PLATES*, 1999].

Phoenix-Pacific spreading ridge toward the subduction zone. An early Cretaceous strike-slip fault system may have existed across the Antarctic margin to accommodate oblique plate convergence [*Siddoway*, 2008]. Emplacement of Median Batholith in New Zealand occurred from ~145-120 Ma [*Bradshaw, et al.*, 1997; *Siddoway*, 2008] and similar plutonism has been suggested to continue throughout the Amundsen Province (eastern Marie Byrd Land, Thurston Island, and Antarctic Peninsula) from 124-96 Ma [*Bradshaw, et al.*, 1997; *Luyendyk, et al.*, 2001; *Siddoway*, 2008]. By 115 Ma, the young, hot, and buoyant crust of the Phoenix plate was being subducted beneath western Marie Byrd Land, raising the temperature and pressure of the lower crust to >800°C and ~7 kbar [*Siddoway*, 2008]. These conditions initiated wide-spread metamorphism and started ductile flow in the lower crust, creating the migmatized gneiss dome now exhumed in the Fosdick Mountains [*Siddoway*, 2008].

1.2.3 Mid-Late Cretaceous: Extensive Distributed Rifting, Opening of the Ross Sea, and Break Away of New Zealand

By this time (~100 Ma), Antarctica was in the last stages of breaking away from the remnants of Gondwana and had drifted into a stable polar position, where it has remained into the present [*van der Wateren and Cloetingh*, 1999; *Dalziel and Lawver*, 2001]. But stability in its location around the pole does not imply tectonic quiescence. Quite suddenly, from 105-92 Ma, there was a shift in the character of magmatism along the Ross Province from arc magmatism to bimodal, back-arc rifting [*Siddoway*, 2008]. Argon-argon dating and apatite fission track dating of the rocks along faults activated during this rifting indicate heating until 101 Ma and two subsequent cooling (exhumation?) episodes: 97-88 Ma and 80-70 Ma [*Siddoway*, 2008].

The first episode of cooling (i.e. exhumation of rocks along faults) was due to widespread rifting and opening of the Ross Sea (Figure 1.7) [*Luyendyk, et al.*, 2001;

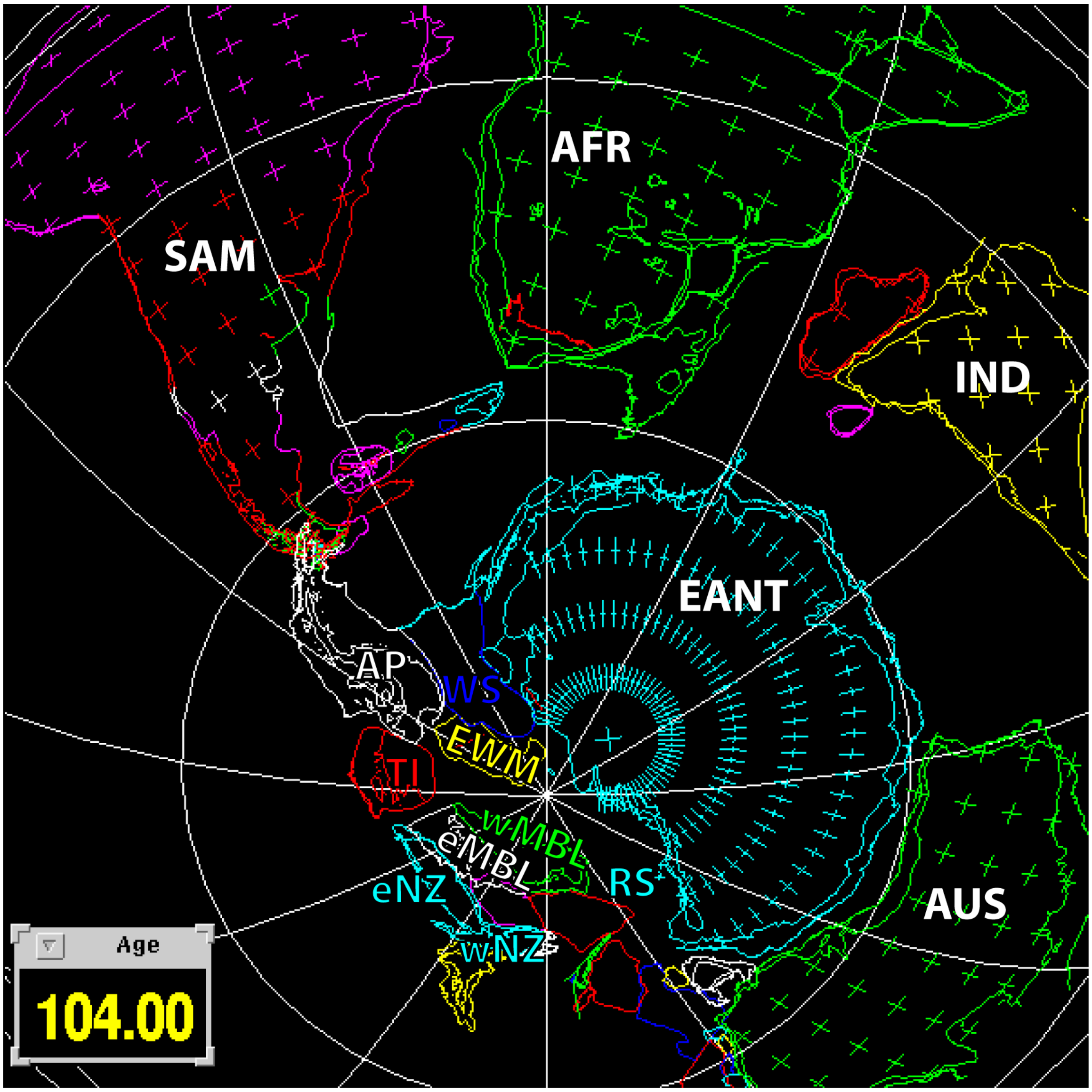

Figure 1.7: Tectonic reconstruction of West Antarctica in the process of opening of the Ross Sea and wide-scale, distributed rifting. Labeled as in Figure 1.6, plus the incipient Ross Sea (RS, cyan). Modified with permission [*PLATES*, 1999].

Siddoway, 2008]. The cause of the widespread Cretaceous rifting could be due to the start of continental rifting between Australia and East Antarctica just to the west of the now Ross Sea [*Siddoway*, 2008], impingement of a plume [*Behrendt and Cooper*, 1991; *Storey, et al.*, 1999; *Siddoway*, 2008], or slow-down of subduction due to buoyant Phoenix plate crust [*Luyendyk*, 1997]. The Ross Sea continental crust is thought to have been between 40 and 50 km thick prior to the onset of rifting (>105 Ma) and subsequently thinned by half, though it did not yet have its characteristic ridge-trough bathymetry [*Decesari, et al.*, 2007b]. Despite immature bathymetry, there is evidence for syn-rifting and post-rifting sediment deposition up to several kilometers thick, which was significantly eroded later [*Luyendyk, et al.*, 2001] (see section 1.2.4). Since extension in the Ross Sea was <50 km after the start of seafloor spreading between New Zealand and Marie Byrd Land [*Lawver and Gahagan*, 1994], several hundred kilometers of extension [*Divenere, et al.*, 1995] were accomplished during a period of time only 31-22 million years long [*Luyendyk, et al.*, 2001; *Eagles, et al.*, 2004]. This was a key episode of rifting because it accounts for up to 1.2×10^6 km^2 of extended continental crust across the continent (including the now ice-covered portions) and translated western Marie Byrd Land to its current location [*Siddoway*, 2008]. The NE limit of widespread rifting outside the Ross Sea is either in the Amundsen or Bellingshausen Seas [*LeMasurier and Landis*, 1997; *LeMasurier*, 2008].

A separate event at ~83-78 Ma commenced the separation of New Zealand from Marie Byrd Land and caused ocean floor spreading (Figure 1.8) [*Lawver and Gahagan*, 1994; *Luyendyk, et al.*, 2001; *Eagles, et al.*, 2004; *Siddoway*, 2008]. The presumed catalyst of this event, which cut through bedrock to rift away New Zealand, is the subduction of the Phoenix-Pacific spreading ridge [*Lawver, et al.*, 1991; *Luyendyk*, 1997; *Siddoway*, 2008]. This event changed the plate boundaries on both sides of the

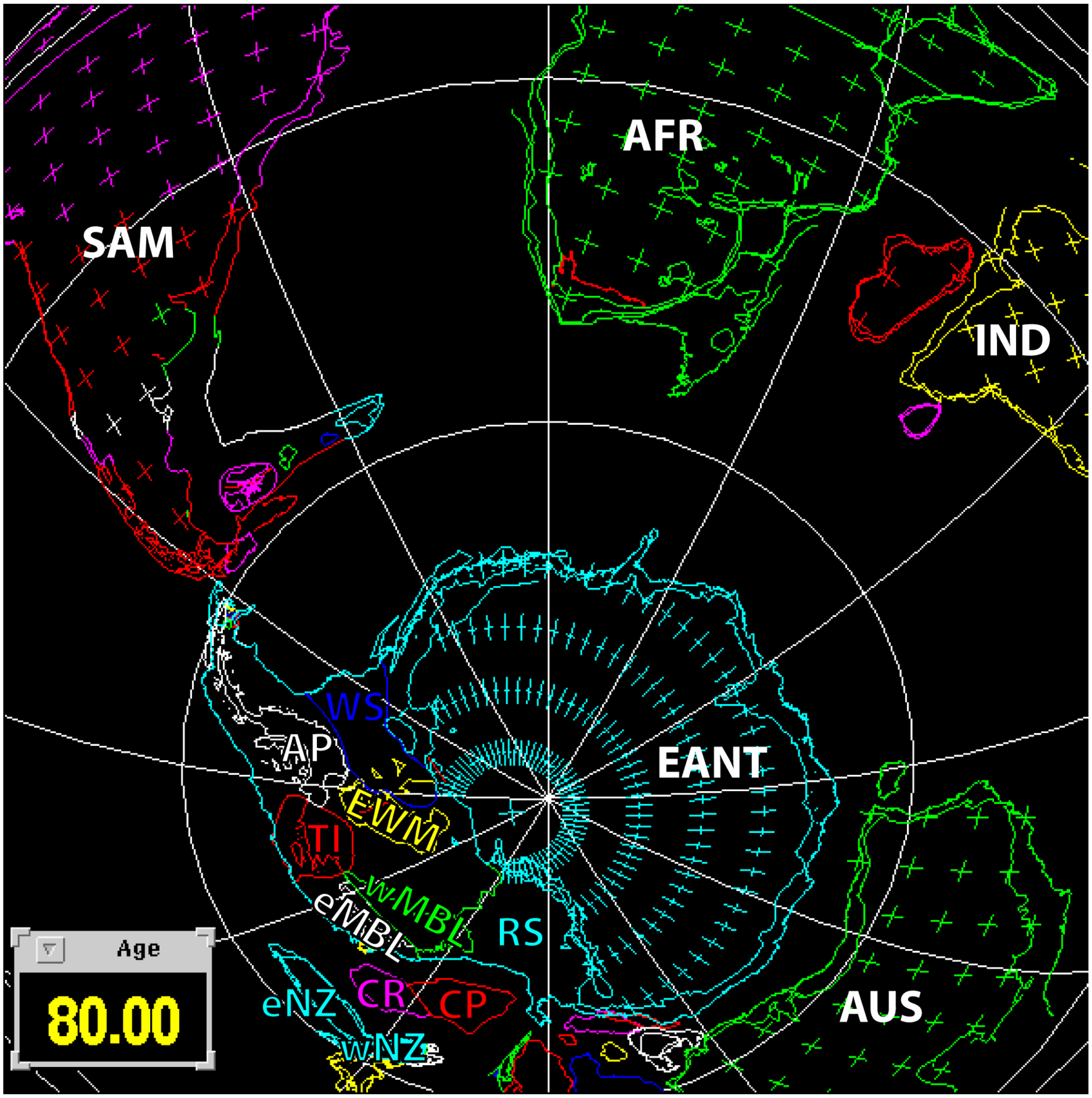

Figure 1.8: Tectonic reconstruction of 80 Ma, just after the initiation of sea floor spreading between West Antarctica and the Pacific plate, rifting New Zealand plus the Chatham Rise (CR, purple) and Campbell Plateau (CP, red) from Marie Byrd Land. Other labels as in Figure 1.7. Modified with permission [*PLATES*, 1999].

Antarctic-Pacific margin, causing seafloor spreading offshore of the eastern Ross Sea and Marie Byrd Land, as well as the creation of a Bellingshausen plate outboard of the current Amundsen Sea Embayment [*Eagles, et al.*, 2004]. The Bellingshausen plate rotated slightly over the course of 20 Ma while being consumed by a N-S subduction zone at the Antarctic Peninsula, but was captured by the Antarctic plate as part of a Pacific-wide plate reorganization at ~60 Ma [*Cunningham, et al.*, 2002] and was short-lived [*Eagles, et al*., 2004].

The importance of these Cretaceous events to the eventual creation of the West Antarctic Ice Sheet has been stated succinctly: "…the West Antarctic Ice Sheet is located on crust developed in association with microplate movement during the Mesozoic fragmentation of the Gondwanaland supercontinent" [*Dalziel and Lawver*, 2001].

1.2.4 Early Cenozoic: Transantarctic Mountains Uplift, Rift Subsidence

The Cenozoic marks the creation of the dramatic geographic divide between east and west Antarctica- the Transantarctic Mountain front. These mountains mark the boundary between the two physiographic halves of the continent and are usually considered to be the southern limit of rifting. The northern side of the mountains, particularly where it meets the Ross Sea, is a massive escarpment that may be evidence of large-scale brittle faulting [*Behrendt and Cooper*, 1991; *ten Brink, et al.*, 1993]. However, the uplift may also be due to isostatic rebound in response to glacial incision [*Stern, et al.*, 2005], thermal uplift due to nearby rifting [*ten Brink, et al.*, 1997], and/or flexural uplift between East and West Antarctica along a free boundary [*Stern and ten Brink*, 1989].

Though the average uplift (adjusting the total denudation for ~4 km of total downward erosion) from fission track dating is 100 m/my starting at 55 Ma [*Fitzgerald*, 1989], cosmogenic dating of erosional exposures shows that the denudation history varies across the Transantarctic Mountains [*van der Wateren, et al.*, 1999]. The mountains experienced periodic, differential uplift along apparent transverse faults of up to 1km/my since ~60Ma [*Behrendt and Cooper*, 1991]. Modeling of seismic and gravity data suggests that Transantarctic Mountains uplift happened mostly in the late Cretaceous (1.5-2 km across the range) and that additional Cenozoic uplift of 1.3 km was limited to Victoria Land [*Busetti, et al.*, 1999], though the timing of their initial uplifts are earlier than other estimates. It is likely that pre-rift rheological differences and/or preexisting faults along the mountain belt resulted in the differential uplift [*Behrendt and Cooper*, 1991; *Busetti, et al.*, 1999; *van der Wateren, et al.*, 1999].

A plate reorganization in the Southern Pacific also occurred around 60 Ma [*Cunningham, et al.*, 2002], terminating independent motion of the Bellingshausen Plate and creating a N-S spreading center that slowly subducted N-NE under the Antarctic Peninsula until ~3.3 Ma [*Cunningham, et al.*, 2002; *Eagles, et al.*, 2004]. Interestingly, the plate reorganization also slowed down the spreading rate along the Pacific-West Antarctic ridge near the Ross Sea, changed the ridge's orientation enough to cause its northward migration away from the Ross Sea, and increased the population of fracture zones at its southern end [*Eagles, et al.*, 2004].

1.2.5 Mid-Cenozoic to Holocene: Tectonics Coeval with Glaciations post-40 Ma

Most Cenozoic activity in the Ross Sea appears to have occurred slightly later than the Pacific plate reorganization- around 46-21 Ma when the Adare Trough was subject to sea floor spreading. The extension was roughly centered around the Oligocene [*Hamilton, et al.*, 2001], the time at which thermal subsidence of the Ross Sea crust allows it to reach elevations at and below sea level [*Decesari, et al.*, 2007a]. Any additional extension in the western and central Ross Sea would have further thinned the crust into horst and graben (or half-graben) bathymetry [*Decesari, et al.*, 2007b], though a second phase of rifting is not seen in the eastern Ross Sea [*Luyendyk, et al.*, 2001] and has been suggested (though is contentious) for the western and central Ross Sea [*Cande and Kent*, 1995]. The Adare Trough sea floor spreading and possible second episode of Ross Sea extension are closely timed with uplift and volcanism in Marie Byrd Land, though they are not necessarily tectonically related.

Late Cenozoic volcanism in Marie Byrd Land (and possibly in the interior rift and Transantarctic Mountains) may have exploited old lithospheric weaknesses [*LeMasurier and Thompson*, 1990; *Blankenship, et al.*, 1993; *Dalziel and Lawver*, 2001] and been generated by a plume [*Behrendt, et al.*, 1994; *van der Wateren and Cloetingh*, 1999], which is supported by geochemical analyses of Cenozoic volcanics [*Wörner*, 1999]. The Marie Byrd Land dome (Figure1.3), based on volcanic rocks overlying a regional erosional surface, began to rise at ~28-26 Ma at a rate of about 100 m/m.y. [*LeMasurier and Landis*, 1997]. Volcanism in Marie Byrd Land started around the time of domal uplift (28-30 Ma) but its main phases of activity based on the exposed rocks occurred from 8-12 Ma and 0-1 Ma, though older Cenozoic rocks are likely more abundant and simply obscured by the current ice sheet [*LeMasurier and Thompson*, 1990]. Subglacial volcanoes (both active and dormant/eroded) [*Blankenship, et al.*, 1993; *Behrendt, et al.*, 2004] and potentially extensive amounts of flood basalts exist in the rift area beneath the Ross Sea Embayment [*Behrendt, et al.*, 1994] and could be related to the hypothesized Marie Byrd Land plume but there are few to no age constraints on their creation, other than indications that they were erupted subaerially or subglacially [*Behrendt, et al.*, 1995].

Several lines of evidence support the hypothesis that continental extension is no longer active in the Recent (although volcanism certainly is). A drape of subglacial sediments across rift features in the Ross Sea Embayment indicates that they were not substantially reactivated in the Cenozoic [*Blankenship, et al.*, 2001; *Studinger, et al.*, 2001]. Magnetotelluric profiling and seismic results near the boundary between the rifted Ross Sea Embayment and the Ellsworth-Whitmore Mountains crustal block suggest cool mantle temperatures and thus no Cenozoic extension [*Wannamaker, et al.*, 1996; *Clarke, et al.*, 1997]. GPS-measured motion between East and West Antarctica do not exceed the measurements' noise level of 1-2 mm/yr, inferring that rifting in both the Ross Sea Embayment and the Ross Sea is very slow (or inactive) and that volcanism observed there is due to mantle upwelling, not rifting [*Donnellan and Luyendyk*, 2004].

The current continental crust of West Antarctica, after all the phases of magmatism and rifting, is topographically mostly below sea level and has significantly thinner than average crustal thicknesses (i.e. <35-40 km). The Ross Sea crust is thinnest at 15-24 km [*Behrendt and Cooper*, 1991; *Trey, et al.*, 1999; *Bannister, et al.*, 2003] but not dissimilar from the crustal thicknesses in the Amundsen Sea Embayment of 21-25 km [*Winberry and Anandakrishnan*, 2004; *Gohl, et al.*, 2007]. The crust in the Ross Sea Embayment rifted area is 27-28 km thick, intermediate for West Antarctica [*Winberry and Anandakrishnan*, 2004]. Transitional crust between the Ross Sea Embayment and the EW block is 28-30 km thick [*Clarke, et al.*, 1997]. The crust is thicker at the base of the Antarctic Peninsula, near Evans Ice Stream, where the Moho is ~32.5 km deep [*Jones, et al.*, 2002]. The thickest crust, under the high Transantarctic Mountains and not technically part of West Antarctica, is ~35-40 km thick [*ten Brink, et al.*, 1997; *Bannister, et al.*, 2003; *Studinger, et al.*, 2004]. Crustal thicknesses have been the focus of a number of studies and often reviewed [*Bentley*, 1983; *Kadmina, et al.*, 1983; *Bentley*, 1991; *Behrendt*, 1999; *Morelli and Danesi*, 2004]. However, there are still large areas of the ice sheet lacking crustal structure information and this study addresses that need in Chapters 3 and 4.

1.3 THE WEST ANTARCTIC ICE SHEET

The current West Antarctic Ice Sheet is waning as we enter an interglacial period. Classical understanding predicts that the ice sheet's current behavior is due to forcing that happened millennia ago- since that is the time period necessary for surface changes to propagate to the bed of the ice [*Alley and Bindschadler*, 2001]. This classical view of the ice sheet would consider the main driver of ice-bedrock conditions to be the relict surface temperature changes at the Last Glacial Maximum >11,000 yrs ago [*Alley and Bindschadler*, 2001]. These surface temperature changes are preserved in the ice and advected to the base of the ice over thousands of years. Over the last decade, satellites have taken repeat measurements of the speed and elevation of the ice sheet surface and seen changes on time scales much shorter than ever expected [*Rignot, et al.*, 2002; *Joughin, et al.*, 2003; *Shepherd, et al.*, 2004; *Thomas, et al.*, 2004; *Rignot*, 2006]. These changes in ice sheet flow happen over years to decades and must originate from conditions at the ocean-ice and bedrock-ice interfaces. In the Ross Sea Embayment, the glacier grounding lines are protected from changing ocean conditions by large ice shelves (Figure 1.3). Warm ocean temperatures are most threatening to outlet glaciers that are not buffered by larger ice shelves [*Alley*, 2002], such as the Thwaites and Pine Island Glaciers of the Amundsen Sea Embayment.

These two Amundsen Sea Embayment glaciers (Figure 1.9) drain smaller areas than the Ross Sea Embayment ice streams but have among the highest discharge velocities in West Antarctica [*Fahnestock and Bamber*, 2001]: ~250 km^3 of ice per year; 160% of the accumulation rate [*Thomas, et al.*, 2004]. These glaciers are threatened by the upwelling of the warm deep ocean waters onto the continental shelf by changes in

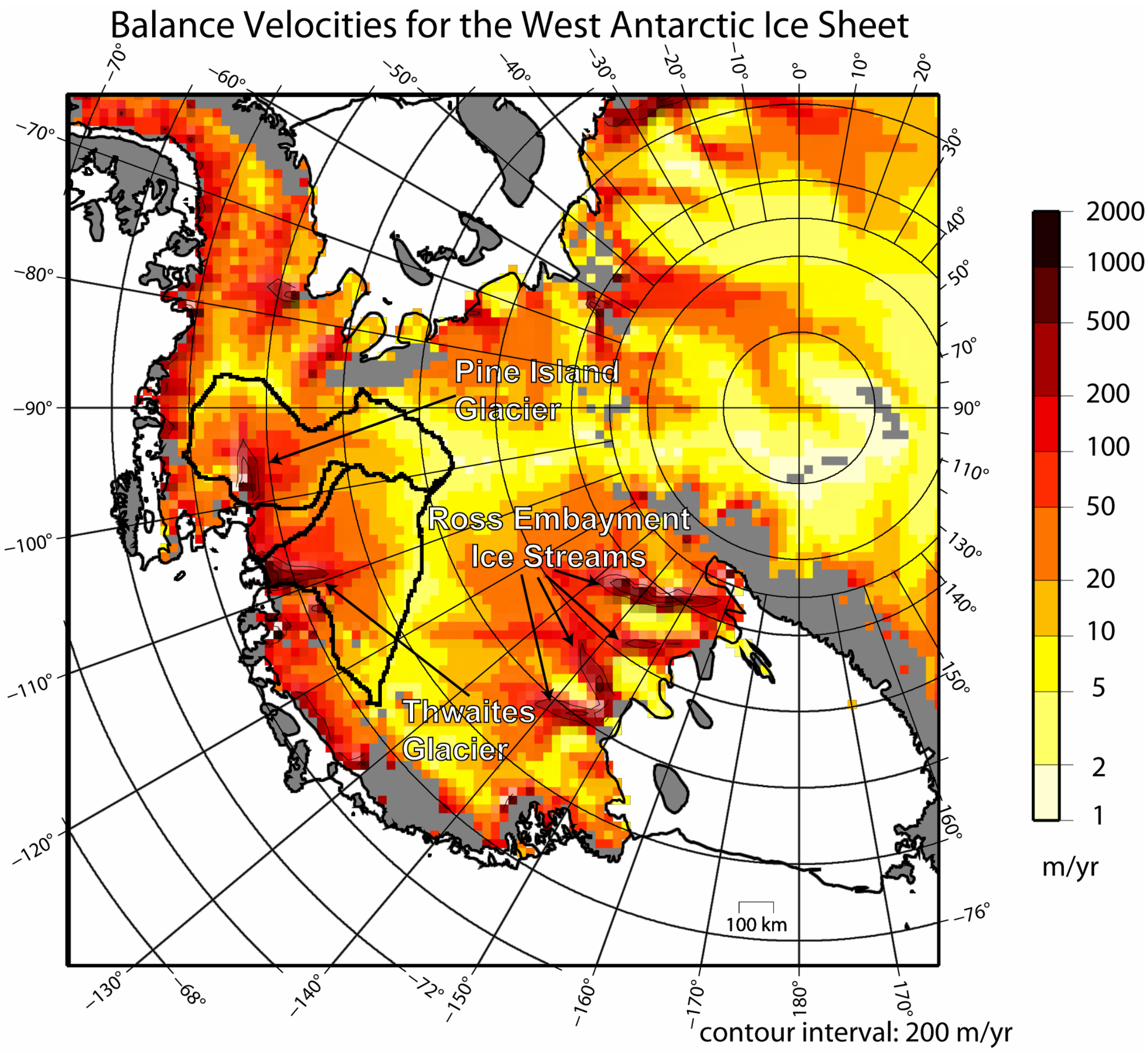

Figure 1.9: Balance velocities in West Antarctica (i.e. how fast the ice must flow to balance incoming and outgoing mass) [*LeBrocq, et al., 2006*] (D. Young, unpub. data, 2008). Thin black line = coastline [*SCAR*, 2006]; heavy black lines=glacier catchments [*Vaughan, et al.,* 1999]; TG=Thwaites Glacier; PIG=Pine Island Glacier.

wind patterns off the coast of the Amundsen Sea Embayment [*Vaughan, et al.*, 2007]. As a result, there is enhanced basal melting of the floating ice portions of glaciers around the Amundsen Sea [*Jacobs and Comiso*, 1997; *Shepherd, et al.*, 2004] and down-current freshening of the ocean that could affect the formation of cold ocean bottom water in the Ross Sea [*Jacobs, et al.*, 2002]. The effect of ice shelf degradation is not as pronounced as the massive speed up that the glacier undergoes when the shelf is finally lost, exemplified by the loss of the Antarctic Peninsula's Larson B ice shelf in 2002 [*Payne, et al.*, 2004; *Rignot, et al.*, 2004a; *Scambos, et al.*, 2004; *Shepherd, et al.*, 2004].

Of note is the unnamed inter-catchment sliver of ice between the Thwaites Glacier and Pine Island Glacier catchments, as defined by *Vaughan, et al.* [1999]. Since the definition of these catchment boundaries, InSAR ice velocity measurements have shown that Thwaites Glacier is widening [*Rignot, et al.*, 2002] beyond the eastern boundary defined in 1999 by *Vaughan, et al.* The newest InSAR velocities [*Rignot, et al.*, 2006] also show that this unnamed sliver of ice is flowing with velocities of 100-500 m/yr along its 1999 boundary with Thwaites Glacier. These high velocities extend across a continuous area ~75 km eastward and ~200 km upstream into the unnamed sliver. Along the unnamed sliver's *Vaughan, et al.,* [1999] boundary with Pine Island Glacier, InSAR velocities [*Rignot, et al.*, 2006] clearly show a confined tributary of Pine Island Glacier reaching ~60 km southwest into the unnamed sliver, flowing at velocities > 500 m/yr. This tributary intersects the fast flow that extends into the unnamed sliver from the Thwaites Glacier boundary. Clearly, the unnamed sliver of ice is not an area of slow-moving ice without outlets and there is a need for the glacier catchments in this area to be re-defined. Until new catchments have been rigorously interpreted for the area, the 5 km resolution glacier catchments defined by *Vaughan, et al.* [1999] are used.

With regards to the Ross Embayment ice streams (Figure 1.9), buffering by the largest ice shelf in the world (the Ross Ice Shelf) means that the ice-ocean interface plays less of a role in influencing fast flow of the ice streams. Instead, a major control on their velocities is the distribution of subglacial sediments [*Blankenship, et al.*, 2001; *Studinger,* *et al.*, 2001; *Anandakrishnan and Winberry*, 2004]. Several ice steams experience fast flow where these sediments become water saturated and the subglacial till dilates, allowing it to deform more easily and essentially lubricate the ice stream bed [*Alley, et al.*, 1986; *Blankenship, et al.*, 1986; *Anandakrishnan, et al.*, 1998; *Bell, et al.*, 1998]. The distribution of subglacial water is controlled by geothermal flux and is poorly constrained [*Blankenship, et al.*, 1993] but the locations of sedimentary basins are geologic in origin and slightly easier to identify. Studies have correlated the locations of deformable basal sediment to underlying long-lived sedimentary basins formed during Cretaceous, and possibly later, rifting [*Bell, et al.*, 1998; *Blankenship, et al.*, 2001; *Studinger, et al.*, 2001; *Peters, et al.*, 2006]. Though identification of basins with potential fields methods has proven problematic due to positive Bouguer gravity signals over basins [*Studinger, et al.*, 2001; *Karner, et al.*, 2005; *Bell, et al.*, 2006], seismic studies have been very successful at identifying basins [*Anandakrishnan, et al.*, 1998; *Anandakrishnan and Winberry*, 2004; *Peters, et al.*, 2006]. One of the challenges addressed in this study is using airborne gravity data (Chapter 1) to find potential sedimentary basins (Chapter 5) beneath the most dynamic portions of the West Antarctic Ice Sheet.

1.4 Renaming Prominent Subglacial Features Referred to in this Study

The newest subglacial topography from radar sounding (Figure 1.2) collected over the "Sinuous Ridge" beneath the ice flow divide in West Antarctica shows that the area was misinterpreted as a continuous ridge [*Holt, et al.*, 2006a]. Instead, the area is actually a series of subglacial highlands dissected by narrow, deep troughs. A temporary and informal name for this feature had become the "Former Sinuous Ridge" since 2006. However, I propose that this area should be permanently renamed and defined as the highlands (that rise above current sea level) between the Marie Byrd Land subaerial volcanoes and the Ellsworth-Whitmore Mountains (Figure 1.10). The name that I use in

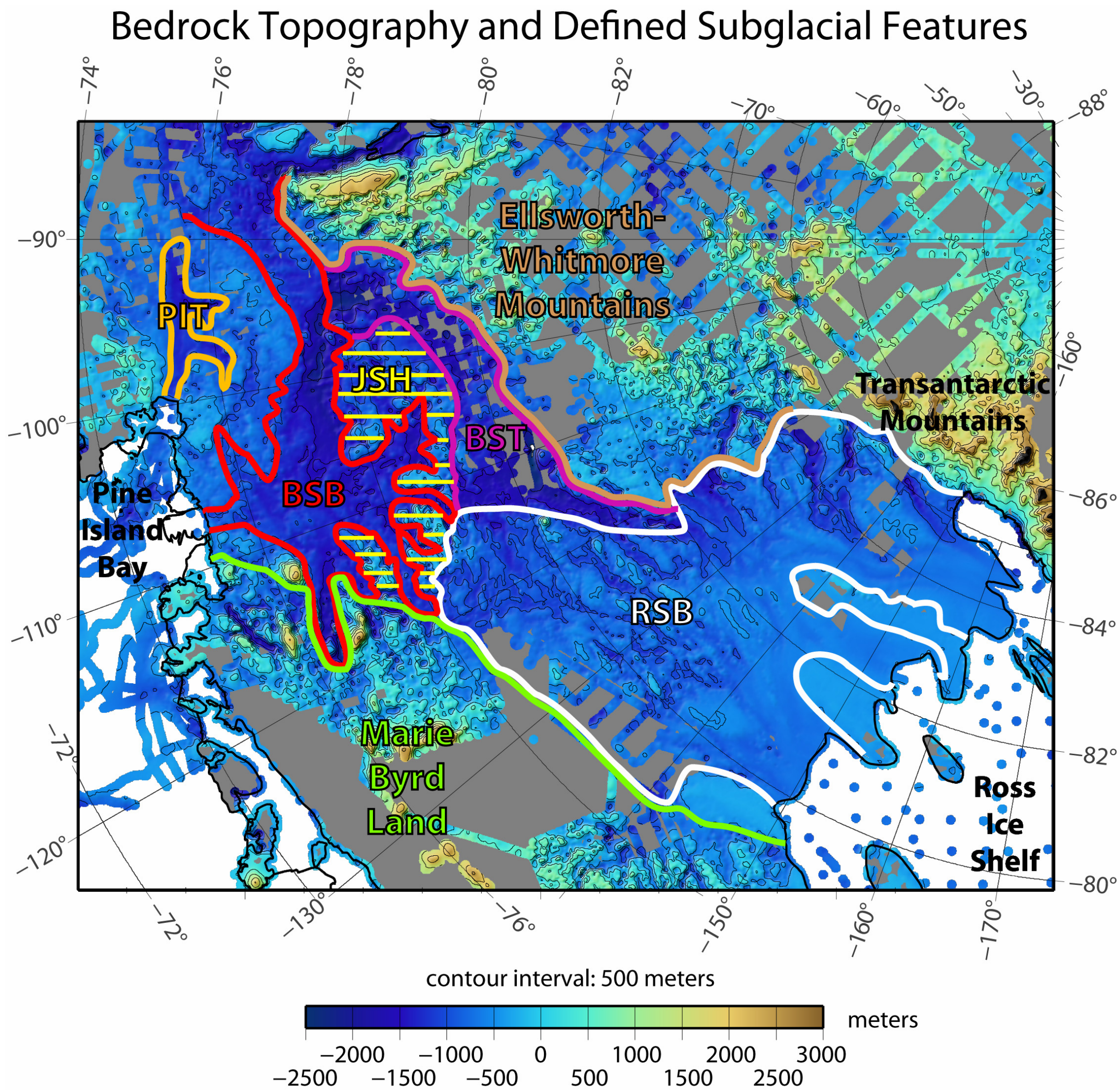

Figure 1.10: Bedrock topography, primarily from ice-penetrating radar [*Lythe, et al.,* 2001] (D. Young, unpub. data, 2008) overlain with sketch outlines of the newly redefined major subglacial features between the Ross Ice Shelf and Pine Island Bay. Features defined or refined in extent by the work presented in this study and *Holt, et al.* [2006]: RSB= Rose Subglacial Basin (outlined in white); BST= Bentley Subglacial Trench (outlined in fuchsia); JSH= Jankowski Subglacial Highlands (horizontally-hatched in yellow); BSB= Byrd Subglacial Basin (outlined in red). The PIT (Pine Island Trench, outlined in orange) was recently defined by *Jordan, et al.* [submitted]. Coastline, including ice shelves [*SCAR*, 2006]= light black line. Ice sheet-covered areas without data are grey.

this study is the “Jankowski Subglacial Highlands” (Figure 1.2), chosen to honor the scientist who discovered the feature (and coined the name “Sinuous Ridge”) [*Jankowski and Drewry*, 1981] and also to reflect our new knowledge of the area’s morphology.

Currently, the Byrd Subglacial Basin is defined by the US Board on Geographic Names as the broad basin extending from the Ross Sea Embayment into the Amundsen Sea Embayment, centered next to the Bentley Subglacial trench. The basin thus includes the now-renamed Jankowski Subglacial Highlands, which have been recognized since their discovery to appear to dissect the basin into two halves [*Jankowski and Drewry*, 1981]. The gravity results presented in this study (Chapters 3, 4, and 5) suggest that a division of the basin is appropriate- the character of the northeastern subglacial basin (bordered by Pine Island Bay) is very different from that of the southwestern subglacial basin (bordered by the Ross Ice Shelf). In fact, the term “Byrd Subglacial Basin” is commonly being used in current discussions to refer only to the basin bordering Pine Island Bay. To reflect this change in usage and to integrate the suggestions in this study that the two basins have differing crustal environments (and possibly rifting histories), I propose that the northeastern basin retain the name in common use (the Byrd Subglacial Basin) and that the southwestern basin be named the “Rose Subglacial Basin” (Figure 1.10) for the glaciologist who used the first large-scale airborne radar sounding campaign of the area to define major features both in the ice flow (i.e. the ice streams) and in the subglacial geology [*Rose*, 1978; *Rose*, 1979; *Rose*, 1982].

As a result of the proposed naming scheme, the area between Pine Island Bay and the Ross Ice Shelf (also bordered by Marie Byrd Land and the Ellsworth-Whitmore Mountains), is more specifically defined and divided (Figure 1.10). These names are only proposed at the moment and must be accepted by the US Board on Geographic Names before either being put into permanent use or being subject to further revision.

1.5 Datasets Available

1.5.1 Airborne Gravity Data

The earliest Antarctic airborne surveys were undertaken by the Naval Research Laboratory in the 1980s [*Brozena*, 1984; *Brozena and Peters*, 1988] and the first UTIG West Antarctic gravity data was collected in collaboration with Naval Research Laboratory in 1991 [*Brozena and Jarvis*, 1993; *Bell, et al.*, 1999]. A large portion of the airborne work on the West Antarctic Ice Sheet was carried out in the Ross Sea Embayment in the rest of the 1990s by the University of Texas at Austin and various collaborators (Figure 1.11) [*Blankenship, et al.*, 1993; *Behrendt, et al.*, 1994; *Bell, et al.*, 1999; *Blankenship, et al.*, 2001; *Luyendyk, et al.*, 2003]. The British Antarctic Survey has also performed aerogeophysical surveys in West Antarctica since the 1980s [recent e.g. *Jones, et al.*, 2002; *Ferraccioli, et al.*, 2006]. Most recently, University of Texas at Austin and the British Antarctic Survey successfully acquired the largest surveys yet attempted in West Antarctica- over the neighboring catchments of the Thwaites and Pine Island Glaciers in the Amundsen Sea Embayment [*Holt, et al.*, 2006a; *Vaughan, et al.*, 2006]. The coverage of the older datasets with the newest Amundsen Sea Embayment datasets expands the surveyed area of the West Antarctic Ice Sheet to ~800,000 km^2.

The six completed UTIG aerogeophysical surveys cover a significant portion of West Antarctica (Figure 1.11). IRE (1991-1993), BSB (1994-1996), and TKD (1996-1997) were part of the Corridor Aerogeophysics of the Southeastern Ross Transect Zone (CASERTZ) project (PI: D. Blankenship); while PPT and WMB (both 1998-1999) were completed as part of the Support Office for Aerogeophysical Research program, directed by D. Blankenship and coordinated by J. Holt. The AGASEA (2004-2005) campaign was accomplished by Blankenship and Holt as co-PIs and provides complete coverage of Amundsen Sea Embayment in combination with a neighboring survey (BBAS) completed by our British Antarctic Survey collaborators in 2004-2005.

Gravity (the focus of this study) is just one part of an aerogeophysical data suite that also includes ice-penetrating radar, magnetics, laser and pressure altimetry, and GPS for accurate timing and plane location. Each of the West Antarctic surveys has slightly different specifications for the primary instrumentation package due to availability of instrumentation each year and changes in technology over time (Tables 1.1-1.6). Each survey also carried a pressure altimeter as an additional navigation aid, though pressure altimetry drifts over the course of a flight and is not used in any final data analyses. The surveys' flight line spacings and gravity errors (based on differences in instrumentation, gravity ties, and processing) also vary (Table 1.7). Information is included here for the BBAS survey for radar, gravity, and resolution only (T. Jordan, pers. comm., 2008).

In relation to the hypothesized crustal and tectonic boundaries in West Antarctica, the CASERTZ dataset covers much of the Cretaceous rift basin in the Ross Sea Embayment and the northwestern edge of the Ellsworth-Whitmore block [*Blankenship, et al.*, 1993; *Brozena and Jarvis*, 1993; *Behrendt, et al.*, 1994; *Bell, et al.*, 1999; *Blankenship, et al.*, 2001; *Studinger, et al.*, 2001]. The WMB survey is located over the Ford Ranges, which represent the border between western Marie Byrd Land and the distributed Mesozoic extension and volcanism in the Ross Sea and Ross Sea Embayment [*Luyendyk, et al.*, 2003]. The BBAS survey area has been shown to contain the Hudson Mountains (possibly part of the Thurston Island block?), the rift system, and Ellsworth Subglacial Mountains [*Jordan, et al.*, submitted]; the AGASEA survey area is hypothesized to contain the intersection of the Marie Byrd Land and Thurston Island crustal blocks and the Cretaceous rift basin (Figure 1) [*Dalziel and Elliot*, 1982; *Dalziel and Lawver*, 2001].

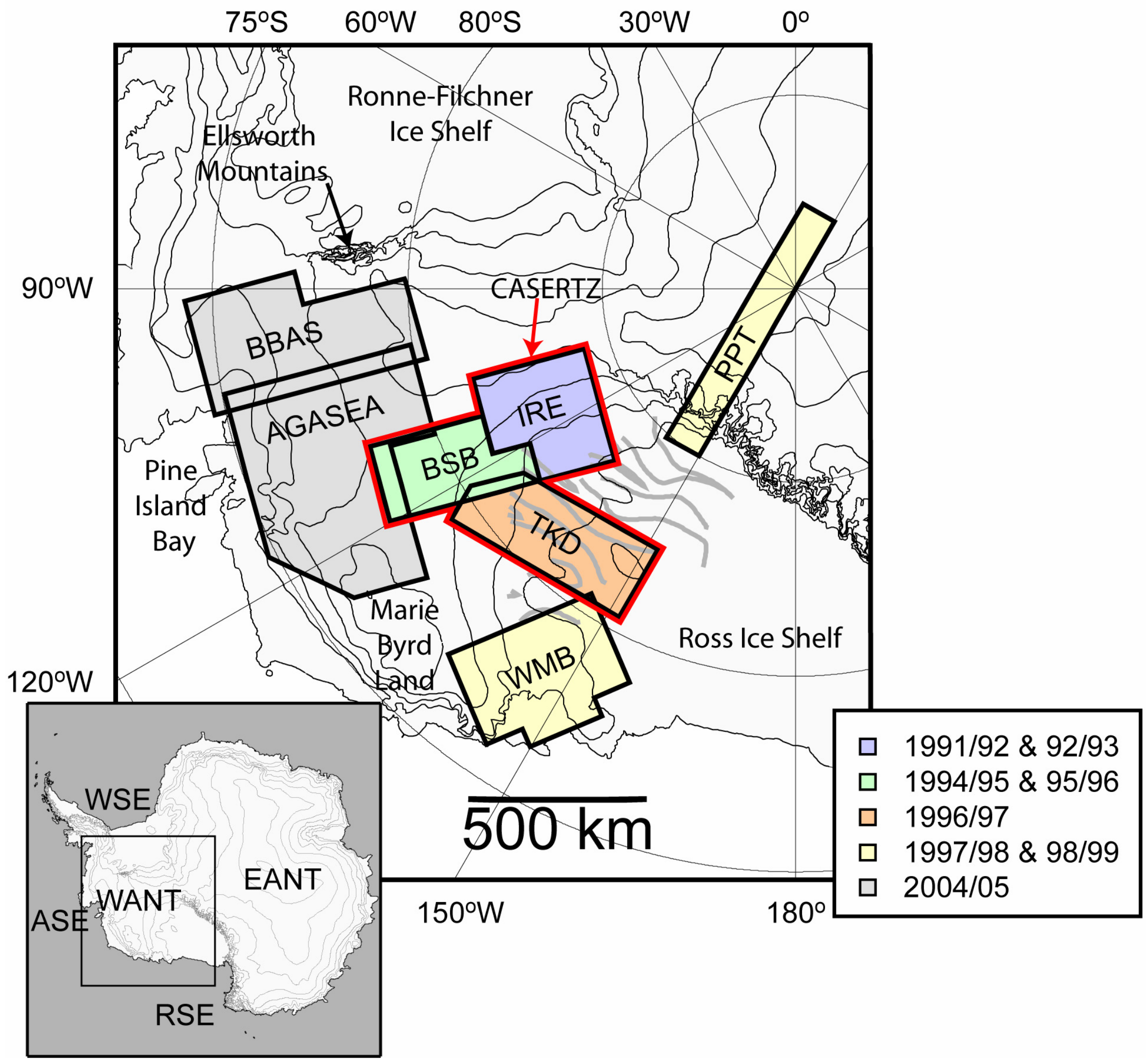

Figure 1.11: Location map of the West Antarctic airborne surveys available for this study. All were collected by the University of Texas at Austin except for BBAS (Basin Balance Analysis Survey), which was collected by the British Antarctic Survey. Displayed are the acronyms for each survey section. Together, IRE (Interior Ross Embayment), BSB (Byrd Subglacial Basin), and TKD (Trunk D) are called the CASERTZ project (outlined in red, Corridor Aerogeophysics of the Southeastern Ross Transect Zone). Since PPT (Pole-Pensacola Transect) did not overlap the other surveys, it is not included in analyses. Again, AGASEA (Airborne Geophysics of the Amundsen Sea Embayment, Antarctica) is the most recently collected University of Texas dataset. Inset: Ice surface topography, figure location indicated by black box, ASE=Amundsen Sea Embayment, RSE=Ross Sea Embayment, WSE=Weddell Sea Embayment, EANT=East Antarctica, and WANT=West Antarctica.

Table 1.1: Radar instrumentation for airborne surveys used in this study

Survey	System Name	Incoherent or Coherent	Frequency (MHz)	Bandwidth (MHz)	Recorded Along Track Sampling (Hz)
IRE, BSB (1994-5)	UT-TUD	Incoherent	Pulse 60	4	2.6
BSB (1995-6), TKD, WMB, AGASEA	UT-TUD	Incoherent	Pulse 60	4	4
AGASEA	HiCARS	Coherent	Center chirp 60	15	200
BBAS	PASIN	Coherent	Center chirp 150	10	312.5

Table 1.2: Laser altimeter instrumentation for airborne surveys used in this study

Survey	Make/Model	Track-line sampling distance (m)	Max Range (m)	Accuracy (cm)
IRE, BSB, TKD, WMB	Holometrix PRAM IV Rangefinder	8	~2000	<100
AGASEA	Riegl LD90-3800 HiP-LR	15	>2000	25

Table 1.3: Magnetic instrumentation for airborne surveys used in this study

Survey	Make/Model	Measurement Method	Sample Rate (Hz)	Precision (nT)
IRE, BSB, TKD	Geometrics 813	Proton-precession	0.64	1
WMB, AGASEA	Geometrics 823A	Cesium vapor	10	0.1

Table 1.4: GPS receiver instrumentation for timing and navigation on airborne surveys used in this study

Survey	Make/Model	Sampling Rate (Hz)	Navigation Accuracy (m)
IRE, BSB, TKD, WMB, AGASEA	Kinemetrix TrueTime 705-101 Time Code Generator	1	N/A
	Ashtech GG-24 GLONASS/GPS	1	10
IRE, BSB	Trimble TNL-2000 GPS Navigation System	1	5
TKD, WMB, AGASEA	Trimble TrimFlight differential GPS Navigation System	1	5

Table 1.5 GPS receiver instrumentation for positioning of airborne surveys used in this study

Survey	Make/Model	Sampling Rate (Hz)
IRE, BSB, TKD, WMB	Ashtech Z-12	1
IRE, BSB, TKD, WMB, AGASEA	TurboRogue SNR-8000	1
AGASEA	Ashtech Z-Surveyor	1
	Trimble 5700	1

Table 1.6: Gravity instrumentation for airborne surveys used in this study

Survey	System Name	Platform Period (s)	Sampling Rate (Hz)
IRE	ZLS upgraded LaCoste & Romberg S-meter	666 (airborne, Lo-mode)	1
BSB, TKD, WMB (1997-8)	Bell Aerospace BGM-3	666 (airborne, Lo-mode)	1
WMB (1998-9)	Bell Aerospace BGM-3	533 (marine, Hi-mode)	1
AGASEA	Micro-G LaCoste Air/Sea II	240	1
BBAS	ZLS upgraded LaCoste & Romberg S-meter	240	1

Table 1.7: Survey grid line spacing and free-air gravity spatial resolution and RMS error

Survey	Flight Line Spacing (km)	Free-air gravity RMS crossover error (mGals)
IRE, BSB, TKD	5	3
WMB	7.5 (15 just south of Marie Byrd Land)	5
AGASEA	15 (better in areas with drape lines and transits)	2.4
BBAS	30 (15 near coast)	2.8

1.5.2 GRACE Satellite Gravity Data

The Gravity Recovery and Climate Experiment (GRACE) mission was launched through NASA, the Center for Space Research at the University of Texas at Austin, and (GFZ) in Potsdam, Germany in 2002. GRACE is providing the most detailed satellite gravity data ever available. The mission's two satellites are traveling 220 km apart, using microwave range finders to measure small changes in the distance between the satellites [*Adam*, 2002]. The distance changes are due to lateral changes in the gravity field of the Earth, which exerts a different (and measurable) force on each satellite. The result is that GRACE is producing a gravity model of the Earth from high altitude. The resolution is very appropriate for lithospheric studies (of Earth's deeper boundaries between down to 100 km depth) [*National Research Council*, 1997; *Tapley, et al.*, 2004]. One of GRACE's primary purposes is to determine the time-variant part of the gravity field, which is dominated by oceanographic and hydrogeological changes on the Earth. GRACE can resolve temporal anomalies down to a monthly scale because GRACE completely maps the Earth's surface in ~30 days [*Adam*, 2002]. The time-averaged (static) satellite gravity data can be very useful when combined with airborne and terrestrial measurements, especially when the satellite data is used as a guide for determining the regional gravity signals in airborne data [*Müller and Smith*, 1993; *Kern, et al.*, 2003]. The GRACE satellites have a polar orbit and thus a dense polar coverage, making their data particularly appropriate for Antarctic applications.

Chapter 2: First Airborne Gravity Results over the Thwaites Glacier Catchment, West Antarctica

Published in *Geochemistry, Geophysics, and Geosystems* on 5 April 2008. Citation: Diehl, Theresa M., John W. Holt, Donald D. Blankenship, Duncan A. Young, Tom A. Jordan, and Fausto Ferraccioli (2008b), First airborne gravity results over the Thwaites Glacier catchment, West Antarctica, *G-cubed*, 9, Q04011, doi:10.1029/2007GC001878.

ABSTRACT

Recent satellite observations of Thwaites Glacier in the Amundsen Sea Embayment, West Antarctica have shown that the glacier is changing rapidly. The causes of its dynamic behavior are uncertain but are of concern because this glacier has the most negative mass balance of all Antarctic glaciers. To better understand Thwaites Glacier's subglacial setting, we conducted a multi-instrumented aerogeophysical survey of its catchment and present here the first gravity results. We employed a new gravimeter and it performed well despite extreme conditions and an unusual survey design. The unleveled free-air gravity anomalies have a 2.3 mGal RMS error and a 9 km spatial resolution. Despite slightly higher than standard noise levels, the free-air anomalies correlate well with radar-derived subglacial topography. The new airborne gravity data assist in interpreting radar-identified bedrock features and are an ideal basis for future studies of subglacial geology and its control on the dynamics of Thwaites Glacier.

2.1 INTRODUCTION

Thwaites Glacier- in the Amundsen Sea Embayment of West Antarctica- is changing very rapidly over timescales as short as a few years; according to recent satellite measurements it is accelerating [*Rignot, et al.*, 2002], retreating from its grounding line [*Rignot*, 1998], thinning both inland and in the floating sections [*Wingham, et al.*, 1998; *Shepherd, et al.*, 2002; *Thomas, et al.*, 2004], and has a negative mass balance [*Rignot*, 2006]. These satellite measurements have shown over the last decade that Thwaites Glacier has the highest discharge of all West Antarctic glaciers and that its changes are some of the most dramatic on the continent. This behavior is of concern because the Thwaites Glacier catchment contains ~0.6 m of ice-equivalent sea level rise [*Holt, et al.*, 2006a], about 12% of the total ~5 m contained within the West Antarctic Ice Sheet [*Alley and Bindschadler*, 2001]. Even more worrisome is the possibility that Thwaites Glacier's deep topographic connections to the neighboring catchments of Pine Island Glacier and Siple Coast ice streams [*Holt, et al.*, 2006a] would create a path to destabilizing the rest of the West Antarctic Ice Sheet.

Unlike the other embayments of the West Antarctic Ice Sheet, the Amundsen Sea Embayment was not surveyed in any comprehensive way until recently [*Holt, et al.*, 2006a]. Some datasets exist from traverses (mainly from the International Geophysical Year), sparse lines of airborne ice-penetrating radar, and ground-based gravity [e.g. *Bentley and Robertson*, 1982; *Drewry*, 1983]. One aerogeophysical survey in the late 1990s [*Bell, et al.*, 1999; *Morse, et al.,* 2002; *Behrendt, et al.*, 2004] ventured into the southernmost portion of the Thwaites Glacier catchment but did not cover any sizeable area of the catchment. With so little information about Thwaites Glacier, we must construct hypotheses for its behavior based on corollaries from other, better understood areas of the West Antarctic Ice Sheet.

Historically, most field work completed on fast-flowing ice of the West Antarctic Ice Sheet has focused on the Ross Sea Embayment's Siple Coast ice streams (Figure 1A inset, RSE). Many studies- including borehole, seismic, and potential fields- have show

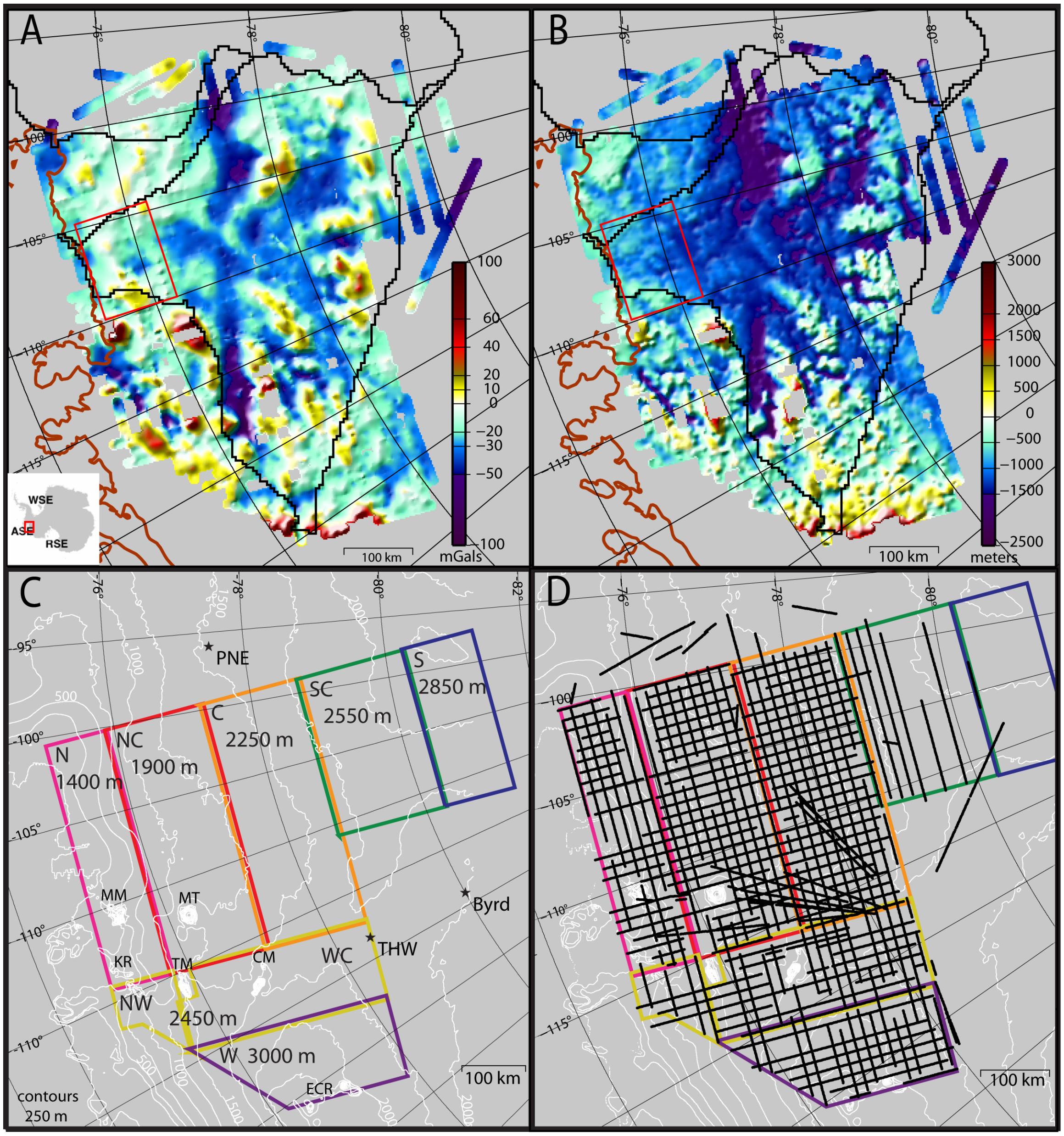

Figure 2.1: A. Free-air gravity anomalies upward continued to 3600m observation level, brown line = coastline [*SCAR*, 2006], black lines = Thwaites and Pine Island Glacier catchments [*Vaughan, et al.,* 1999], red box= location of sill discussed in *Holt et al.* [2006a]; inset: location of the figures with respect to major West Antarctic embayments. B. Subglacial topography from ice-penetrating radar [*Holt, et al.*, 2006a], masked to show areas coincident with gravity data, brown and black lines and red box as in 1A. C. Thwaites Glacier survey plan overlaid on ice surface topography [*Liu, et al.,* 2001] where flight altitudes correspond to block color; exposed volcanic groups

are as follows: MM= Mount Murphy, MT= Mount Takahe, KR= Kohler Range, TM= Toney Mountain, CM= Crary Mountains, ECR= Executive Committee Range; camps and stations are labeled with stars: Byrd Station, PNE and THW = Pine Island Glacier and Thwaites Glacier remote camps. D. Locations of all gravity lines used for the free-air anomaly map.

that these fast-flowing ice streams are predominantly controlled by the distribution of subglacial sediments and water [*Blankenship, et al.*, 1986; *Blankenship, et al.,* 1993; *Blankenship, et al.*, 2001; *Anandakrishnan and Winberry*, 2004; *Peters, et al.*, 2006]. Thus, a reasonable hypothesis is that Thwaites Glacier's recently observed dynamic behavior could be controlled, completely or in part, by its subglacial environment.

Aerogeophysical surveys have a proven history as a useful tool for examining the sub-ice environment [e.g. *Luyendyk, et al.*, 2003; *Ferraccioli, et al.*, 2005]. In the austral summer of 2004-2005, the University of Texas at Austin and the British Antarctic Survey successfully acquired the largest airborne geophysical surveys yet attempted in West Antarctica [*Holt, et al.*, 2006a; *Vaughan, et al.*, 2006] over the neighboring catchments of Thwaites and Pine Island Glaciers in the Amundsen Sea Embayment (ASE; Figure 1B). The ice-penetrating radar results have already provided detailed subglacial topography through a maximum 4.0 km of ice. The subglacial topography shows that Thwaites Glacier mostly lies in a broad, deep basin but that its tributaries appear to exploit deep linear trenches, implying structural control of flow in the distal areas of Thwaites Glacier but not in its trunk [*Holt, et al.*, 2006a]. Here I present the first airborne gravity results of the Thwaites Glacier survey (Figure 2.1A), which are of immediate use in estimating the composition of the new radar-derived bedrock topography.

2.1.1 Survey Location

The Thwaites Glacier catchment covers 290,000 km^2 of a part of the West Antarctic Ice Sheet that is notoriously challenging to study. Cyclonic weather systems in the Southern Ocean consistently make landfall in the Amundsen Sea Embayment [*Kaspari, et al.*, 2004], resulting in a high percentage of cloudy/windy weather and high snow accumulation rates (80 cm/yr on average at the coast [*Monaghan, et al.*, 2006], mostly delivered in bursts from large weather systems [*Kaspari, et al.*, 2004]). Also, Thwaites Glacier and Pine Island Glacier are far enough from major British and American bases– over 2000km from McMurdo Station– that they are operationally difficult to reach. Physical obstacles for the Thwaites Glacier survey included five subaerial volcanic centers in Marie Byrd Land (Figure 2.1C): Mount Murphy (2500m above ice surface, 2705m above sea level), Mount Takahe (2200m, 3460m), Toney Mountain (2600m, 3595m), the Crary Mountains (2 volcanoes; 2200m, 3675m), and the Executive Committee Range (5 volcanoes; 1800m, 4285m) [*LeMasurier and Thompson*, 1990]. As well, the ice surface elevation in the catchment drops to sea level from heights of ~2500m in Marie Byrd Land and similar heights over the Bentley Subglacial Trench to the south (Figure 2.1C) [*Liu, et al.*, 2001].

The rugged terrain of Thwaites Glacier is very difficult to survey, even more so when flying a multi-instrumented platform. Our aerogeophysical platform is mounted in a DeHavilland Twin Otter and includes a coherent ice-penetrating radar, magnetometer, laser altimeter, carrier phase GPS receivers, and a gravimeter. Airborne gravity acquisition produces best results when flying at constant altitude, which minimizes perturbations to the gravimeter. However, the ice surface relief of the Thwaites Glacier catchment is 2500m and our ice-penetrating radar system performs best when operated within ~1000m of the ice surface. The Marie Byrd Land volcanoes also make it impossible to fly a large-scale, constant-altitude survey without exceeding the radar altitude limits. As a result, we adopted an unusual survey design for the AGASEA (Airborne Geophysics of the Amundsen Sea Embayment, Antarctica) survey that represents the best trade-off between radar and gravity requirements. The flight grid was 15 x 15 km, but broken into eight constant-altitude blocks (Figure 2.1C). Given unlimited field time, the survey aircraft would never need to change altitude during data collection by starting and ending recording at every block boundary. In reality we were limited to a 7.5 week field season and could only complete a survey of the glacier if the aircraft continually recorded data from one block to the next, executing altitude changes at block boundaries during data collection. To help limit the expectedly large accelerations, the aircraft performed smooth altitude changes over a 30 km distance centered on the block boundaries. Limitations of the aircraft range relative to the size of the survey precluded overlapping the constant elevation blocks (Figure 2.1C); survey lines that ran along block boundaries were flown at the higher of the two block elevations. Flight altitudes were kept as close to planned altitudes as possible, but inclement weather and turbulence (especially near volcanoes) sometimes caused additional unplanned altitude changes.

2.1.2 Gravimeter Operation

The AGASEA survey design would be impractical with some gravity meters; typical gravimeters lose several minutes of data after the aircraft has finished executing an altitude change (V. Childers, pers. comm., 2006). However, AGASEA was the first application of the new LaCoste & Romberg Air/Sea II gravimeter in an airborne survey. This gravimeter handled survey altitude changes very well and final data loss was much more limited than expected for other gravimeters (see this section's Discussion). The Air/Sea II has been redesigned from the older S-meters to include the most up-to-date technologies, including fiber optic gyros, but the new meter retains the well-proven gyro-stabilized platform, zero-length spring method exhaustively described by others [*LaCoste*, 1967; *Valliant*, 1992]. The Air/Sea II samples at 1 Hz (every ~70m along track at Twin Otter airspeeds) with a precision near 0.1 mGals [*LaCoste and Romberg Corp.*, 2004]. We operated the gravimeter with a 240 s platform period and 0.72 damping (critical is 0.707). The gravimeter ran continuously during the entire 7.5 week field season and took still gravity readings whenever on the ground. The still readings showed that the Air/Sea II experienced negligible measurement drift.

I tied the airborne gravimeter readings to an absolute gravity station at McMurdo Station with a portable LaCoste & Romberg G-meter [*Diehl,* 2008] (Appendix A). The absolute gravity IGSN71 benchmark at McMurdo [Building 146, plaque "Thiel", -77.8490º, 166.6794º, 46.21 m above s.l.] (J. Bucher, unpublished data, 2000) had not been occupied by an absolute gravimeter prior to our season in 2004. The USGS tie to the Building 146 site yielded an absolute gravity value of 982970.52 mGals (J. Bucher, unpublished data, 2000). The United States Geological Survey (USGS) also conducted absolute gravity readings in McMurdo in 1995 [*Sasagawa, et al.*, 2004] and that value, upward continued to the correct elevation, yields an absolute gravity of 982969.7277 mGals. The two absolute gravity values are in good agreement and I used the value derived from *Sasagawa et al.* [2004] for our gravity ties. I also tied the AGASEA survey directly to the British Antarctic Survey's Pine Island Glacier survey (called BBAS) [*Ferraccioli, et al.*, 2007] by taking relative gravity measurements at both the British and American camps with the same portable G-meter. I have included five flights of data collected by the British Antarctic Survey airborne system in my final results.

2.2 Analysis

Airborne gravity data analysis for AGASEA involved several standard corrections and closely followed the methodology laid out by *Holt et al.* [2006b] and *Childers* [1996 and references therein]. The standard reduction for airborne gravity data removes the effects of: theoretical gravity based on an ellipsoid (a_{theo}), accelerations due to the Earth's

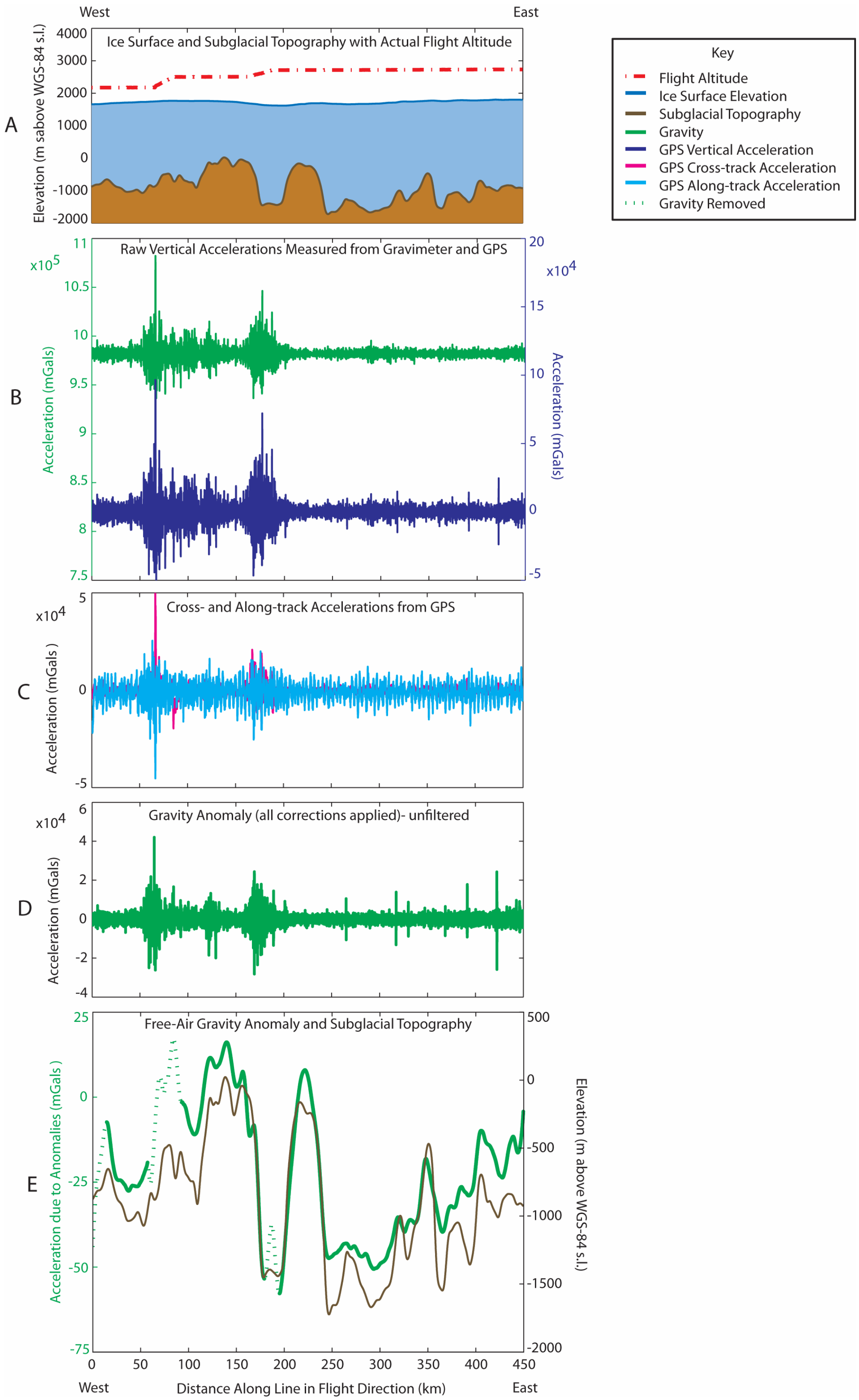

West
East
Ice Surface and Subglacial Topography with Actual Flight Altitude
Elevation (m sabove WGS-84 s.l.)
A
Key
Flight Altitude
Ice Surface Elevation
Subglacial Topography
Gravity
GPS Vertical Acceleration
GPS Cross-track Acceleration
GPS Along-track Acceleration
Gravity Removed
Raw Vertical Accelerations Measured from Gravimeter and GPS
B
Acceleration (mGals)
x10^5
x10^4
Cross- and Along-track Accelerations from GPS
C
Gravity Anomaly (all corrections applied)- unfiltered
D
Free-Air Gravity Anomaly and Subglacial Topography
E
Acceleration due to Anomalies (mGals)
Elevation (m above WGS-84 s.l.)
Distance Along Line in Flight Direction (km)

Figure 2.2: A line of the survey containing two altitude steps. A. Flight altitude, ice thickness, and subglacial topography. B. Raw vertical accelerations measured by the Air/Sea II gravimeter and GPS. C. Cross- and along- track GPS-derived accelerations, which also show large amplitudes correlating to altitude changes. D. Free-air gravity anomaly, corrected but unfiltered. E. Filtered free-air gravity anomaly (before upward continuation) with sections not used in the final grid dashed, compared to subglacial topography.

rotation [*Harlan*, 1968] - called the Eötvös effect (a_{Eotvos}), vertical accelerations due to aircraft motion (a_V), and the free-air correction that accounts for observations' altitudes above sea level (a_{FAC}). All AGASEA gravity anomalies were referenced to the WGS84 ellipsoid.

Accurate GPS positioning plays a critical role in gravity reduction [*Brozena and Jarvis*, 1993; *Bell, et al.*, 1999]. GPS vertical position solutions are double differenced to provide aircraft vertical and horizontal accelerations (Figure 2.2) with magnitudes in the vertical ranging from 10,000 to 100,000 mGals and half that for horizontal accelerations. Position data are also used to calculate the velocity and heading of the aircraft for the Eötvös correction, which can be very large when flying against the rotation of the earth (e.g. 233 to 288 mGals for the data in Figure 2) and is strongly dependent on aircraft velocity. We used differential carrier phase solutions to pinpoint the aircraft's positions to ~10 cm accuracy. We used the K&RS [*Mader*, 1992] and GIPSY/OASIS II [*Lichten, et al.*, 1995] processing packages for our GPS solutions. The major difference between these methods is that K&RS requires static base station GPS measurements, while GIPSY/OASIS II- a precise point positioning (PPP) method- does not. Extensive testing showed that using GIPSY/OASIS II positions consistently provided lower initial noise levels in gravity reduction than K&RS positions, though final gravity anomalies from both position solutions produced equal quality line-by-line anomalies. However, due to the initial reduction in noise, I chose GIPSY/OASIS II solutions almost exclusively in my analyses, substituting carrier-phase K&RS solutions only if GIPSY/OASIS II solutions were unavailable.

The most difficult sources of error to remove from airborne gravity come from horizontal accelerations that tilt the gravity sensor off level. These accelerations are usually due to winds, course corrections, aircraft altitude changes, and flying tracks that are not along great circles (called loxodromes or "rhumb lines") (Figure 2.2). I applied a tilt correction to the AGASEA data because of the survey's non-ideal conditions. The method I used [*Peters and Brozena*, 1995] relies on having measurements of the same accelerations in two 3D reference frames. In this case I have GPS accelerations (ellipsoidal vertical, longitudinal, latitudinal; Figure 2.2) and accelerations measured by the constantly tilting gravity sensor ("vertical", cross-track, along-track). The Air/Sea II gravimeter outputs the cross- and along- track accelerations directly in mGals, without the need for extra calibration. The tilt correction applied calculates three parts to the correction: the two horizontal acceleration vector components measured in the ellipsoidal vertical direction due to sensor tilt and the gravimeter vertical acceleration vector's angle away from the ellipsoidal vertical. I applied a cosine taper filter at the platform period to all GPS and gravimeter-measured accelerations before calculating the tilt correction. Ultimately, the free-air gravity anomaly (g_{FAA}) reduced from the measured vertical acceleration (a_m) such that: $g_{FAA} = a_m - a_{theo} - a_{Eotvos} - a_V - a_{FAC} - a_{tilt}$.

Some airborne gravimeters (BGMs and non-upgraded LaCoste & Romberg S-meters) forward RC-filter the gravity data as it is being collected, necessitating the application of a reverse digitally-equivalent filter to phase-adjust the gravity data at the start of processing [*Holt, et al.*, 2006b]. However, the Air/Sea II gravimeter has negligible internal filtering [*LaCoste and Romberg Corp.*, 2004], so I calculated unfiltered corrections and apply them directly to the unfiltered data. Filtering only took place after all the gravity corrections were applied. I used a 2D spatial, moving-average smoother of 9 km half-width (Figure 2.2) [*Holt, et al.*, 2006b]. When choosing the filter length, I examined the longest overlapping gravity record, which is 86 km in length (Figure 2.3). The 9 km half-width was the shortest to yield an acceptably repeatable gravity signal, with an RMS difference of 3.0 mGals between the overlapping lines (Figure 2.3C).

The free-air gravity time series were then edited by hand to remove spurious signals at the beginning or ends of lines (induced by aircraft turns) and at other times of large acceleration (such as those induced by altitude changes). An additional 2D upward continuation filter brought the final free-air anomalies along each line to a common 3600 m observation level. An additional round of editing removed upward continuation edge effects from the free-air profiles. Five flights of British Antarctic Survey gravity data, flown with a ZLS-modified LaCoste & Romberg S-meter, are included in my final free-air gravity grid (Figure 1A) and all crossover error analyses. The final grid was not leveled, as other surveys have done, because there was not a significant increase in data quality after automated leveling.

2.3 Results

The upward continued free-air anomalies (available digitally) [*Diehl, et al.*, 2008a] have an RMS crossover error of 2.3 mGals (Figure 4) and a 9 km spatial resolution. The expected resolvable "geologic half-wavelength" [*Childers, et al.*, 1999] for the free-air anomalies ranges from 2.5 km to 7.5 km (based on original AGASEA ice thicknesses and flight altitudes before upward continuation), but these estimates are for ideal flight conditions. The chosen 3600 m observation level combined with the closest bedrock sources, gives an expected geologic half-wavelength of ~6.7 km for ideal

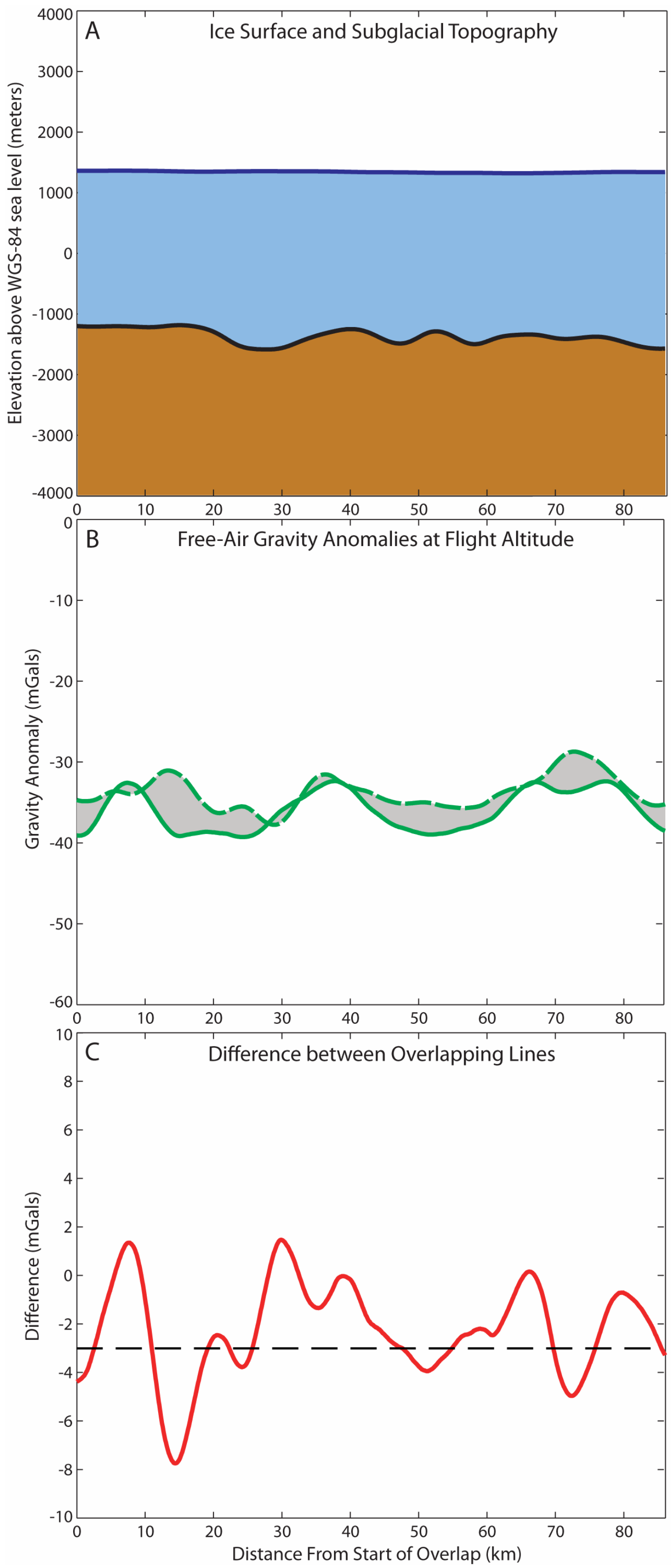

Figure 2.3: A. Ice thickness (blue) and subglacial topography (brown) along the longest section of overlapping profiles. B. Free-air gravity data (not upward continued) from the two overlapping lines, area between them shaded gray. C. Difference between free-air gravity of the overlapping lines; RMS of 3 mGals is represented by the dashed line.

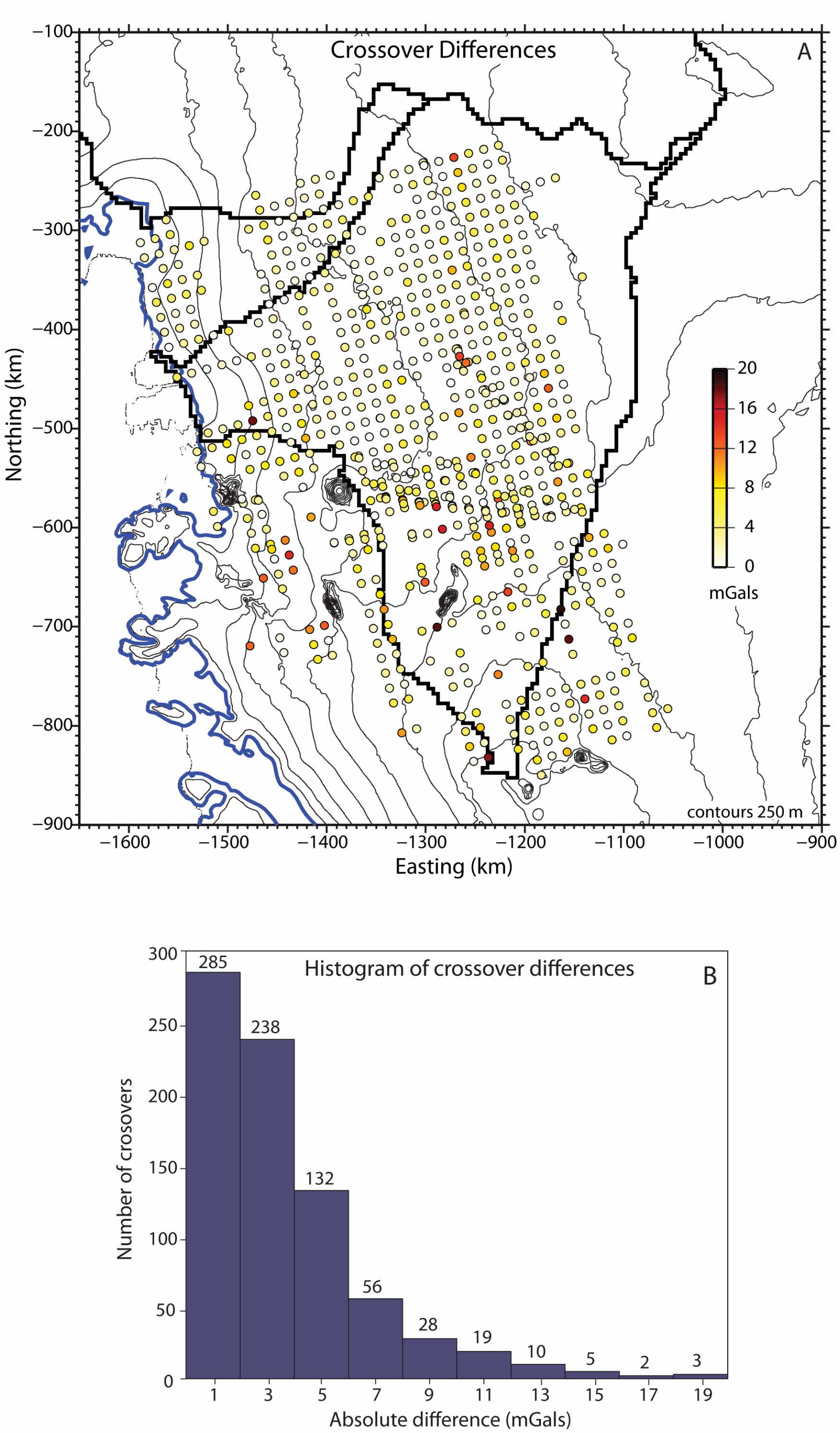

Figure 2.4: A. Map of the absolute value of crossover differences at 744 points across the grid, overlaid on ice surface elevations [*Liu et al.,* 2001]. Glacier catchments [*Vaughan, et al.,* 1999] (in center is Thwaites Glacier and at top is Pine Island Glacier) = black lines; coastline [*SCAR*, 2006] = blue line. B. Histogram of the absolute value of crossover differences, with total number in each bin labeled on the graph

conditions. The 9 km filtering level- chosen to minimize noise- is reasonable considering the survey's prevalent winds and unusual design. As evident in Figure 1, the 9 km resolution free-air anomalies still certainly reflect subglacial topography, as would be expected for good quality free-air gravity results. We acquired gravity data over most of the Marie Byrd Land volcanoes, though much was unusable because of extreme wind shear. The data were, however, able to resolve the flanks of the five major volcanic centers in the area.

2.4 DISCUSSION

The overall gravity coverage of the survey area was excellent (Figure 1D). The Air/Sea II gravimeter's ability to recover from altitude changes was remarkable and data loss was generally limited to the duration of the altitude changes (e.g., a data loss of <430s, or ~30 km at typical ~70 m/s Twin Otter speeds; Figure 2). Often the Air/Sea II recovered quickly enough after a turn that good quality data were recovered at the start of lines. There are a few gaps in the final gravity data, and those exist mostly over the tops of volcanoes and in the grid southwest, coastal part of the survey (near Smith Glacier). The weather in the vicinity of Smith Glacier was particularly unfavorable during the field season and the area has the highest average accumulation rate of any section of the catchment [*Monaghan, et al.*, 2006]. The most poorly resolved volcano is Toney Mountain, while the coverage of the Executive Committee Range is excellent within the survey area.

The much-less-than-ideal survey conditions resulted in a 2.3 mGal RMS error (equivalent to a 4.6 mGal RMS difference) in the free-air anomalies, similar to other Antarctic gravity datasets that have 1-3 mGal RMS errors [*Bell, et al.*, 1999; *Holt, et al.*, 2006b]. These other datasets were collected under much more ideal circumstances, were flown on tighter grid spacings (5 to 7.5 km), and were leveled after data gridding [*Bell,* *et al.*, 1999; *Holt, et al.*, 2006b], underscoring the good quality of the data. Examining error in terms of mean crossover difference, this survey (with its 15 km line spacing) yielded a 3.5 mGal error. I find that this error is reasonable when compared to a gravity dataset in Dronning Maud Land with 10 km line spacing, which yielded a 3.7 mGal error (S. Riedel, pers. comm., 2007).

Crossover differences were calculated- after upward continuation but before gridding- for crossing lines with data points no greater than 140 m distant from each other. A histogram of the crossover differences (Figure 4) shows that 67.2% of them lie within 4 mGals (RMS error of 2 mGals) and 91.4% within +/- 8 mGals (RMS error of 4 mGals). Most of the larger crossover differences are in the grid south portion of the survey, where weather and volcano-induced turbulence were most problematic. Since the differences are a spatially variable but concrete indicator of the minimum reliable signal amplitude, I recommend that features in the free-air data be interpreted in the context of their surrounding crossover errors (available digitally) [*Diehl et al.,* 2008a]. Reanalysis of this dataset upon the development of a better tilt correction algorithm would likely improve the resolution of small-scale features and further eliminate noise.

The range of the free-air anomalies is -92 mGals to 122 mGals. The western branch of the Byrd Subglacial Basin (to the north side of the Crary Mountains) contributes the most negative free-air anomaly and Mount Murphy contributes the most positive anomaly in our available data. Previously published AGASEA subglacial topography [*Holt, et al.*, 2006a] showed that there was a broad "sill" of slightly raised bed near the mouth of Thwaites Glacier (Figure 1a,b; red box). In the free-air gravity, I observe this sill as having four strips of alternating relatively lower and higher free-air gravity, elongated in the grid northwest-southeast direction. Since the pattern is not correlated to topography, I interpret the source as relative changes in density. The gravity trends on the sill parallel trends of alternating driving stress for the ice sheet, indicating that the more dense areas of the sill could be rough spots across the outlet of the glacier and possible pinning points for future grounding line retreat [*Young, et al.*, 2006]. To the grid south of the sill, along the edge of the glacier catchment there is a roughly circular positive free-air anomaly that could indicate sub-ice volcanics, though this remains to be confirmed by further gravity processing and aeromagnetic results.

2.5 Conclusions

The AGASEA aerogeophysical survey over the Thwaites Glacier catchment has proven to be an important tool for investigating the possible controls of the subglacial environment- both geologic and tectonic- on this glacier's dynamic behavior. The initial results of the gravity portion of the AGASEA survey are excellent, despite the unusual survey layout and generally higher than usual noise levels. I followed published data processing schemes, adapted to the new Air/Sea II gravimeter, to produce free-air gravity anomalies. The resulting gravity anomalies correlate very well with subglacial topography, as expected, and show that the sill identified in bedrock topography from radio-echo sounding results corresponds to alternating higher and lower density anomalies, warranting further investigation into the sill's potential "sticky-spot" impact on ice flow. The final 9 km spatial resolution and 2.3 mGal RMS error of the gravity dataset make it ideal for future studies of large-scale subglacial geologic features (such as the coastal sill, potential sedimentary basins, or subglacial lakes) and the deeper crustal and lithospheric structure of the area.

Chapter 3: Crustal Context of Thwaites Glacier in the West Antarctic Rift System and Marie Byrd Land

ABSTRACT

Thwaites Glacier currently has the largest negative mass balance of any glacier in Antarctica (i.e. it is losing more ice into the ocean each year than accumulates at its surface through snowfall). Since little is known about the crust below the bedrock-ice boundary, it is important to understand the glacier's crustal context and its possible influence on the current mass imbalance. Airborne ice-penetrating radar results indicate that Thwaites Glacier flows through a basin ~300 km across and 1-2.5 km below sea level (called the Byrd Subglacial Basin). The glacier's tributaries flow through the lowest areas of the basin and through confined trenches in surrounding higher relief terrain. To characterize the crustal setting in which the deep basin and trenches formed, I present here Bouguer gravity anomalies and crustal structure estimates derived from an airborne survey over Thwaites Glacier. These results support the hypothesis that the West Antarctic Rift System underlies Thwaites Glacier in the Byrd Subglacial Basin. The crust there is more extended (Moho depths 24-20 km b.s.l.) than the crust in the adjacent Rose Subglacial Basin of the Ross Sea Embayment. The rift system's boundary with Marie Byrd Land occurs along a zone that is characterized by the thinnest crust yet observed in West Antarctica (19 km Moho depths) and major subaerial volcanoes. The intact, un-rifted Thurston Island block does not extend beneath Thwaites Glacier. Many of the subglacial highlands and volcanoes in the Thwaites Glacier catchment lack supporting roots, indicating flexural support by a relatively rigid lithosphere and they are thought to postdate wide-scale rifting. However, highlands in Marie Byrd Land seem to be thermally-supported by warm mantle, which may be a melt water source for the fast flow of Thwaites Glacier.

3.1 INTRODUCTION

Thwaites Glacier in the Amundsen Sea Embayment (Figure 3.1 location; Figure 3.2 glacier) is among the fastest-flowing ice on the continent (~2.5 km/yr near its grounding line) [*Rignot*, 2006]. From recent radar-sounding [*Holt, et al.*, 2006a] (Figure 2.1B) and free-air gravity [*Diehl, et al.*, 2008b] (Figure 2.1A) results, we know the glacier's trunk flows through a broad basin called the Byrd Subglacial Basin (Figure 3.3), lying at least 1 km (and sometimes down to 2.5 km) below sea level (b.s.l.). The two tributaries on the eastern side of the catchment (Figure 3.2) flow through wide, 2 km b.s.l segments of the Byrd Subglacial Basin and appear unconstrained by bedrock topography. The other tributaries exploit confined valleys in the Jankowski Subglacial Highlands and eastern Marie Byrd Land (Figure 3.3). Together, the glacier's tributaries provide subglacial connections between Thwaites Glacier and both the Pine Island Glacier catchment (via the Byrd Subglacial Basin and Bentley Subglacial Trench, Figure 3.3) and the Ross Sea Embayment (via the Jankowski Subglacial Highlands, Figure 3.3) [*Holt, et al.*, 2006a].

The bedrock in the Byrd Subglacial Basin is currently depressed to depths below sea level similar to that of mid-ocean ridges because of the weight of the only marine ice sheet on Earth [*LeMasurier*, 2008]. A fundamental instability in the West Antarctic Ice Sheet is suggested by this unique bedrock geometry [*Hughes*, 1975; *Mercer*, 1978; *Oppenheimer*, 1998]. Simple approximations of the geometry and flow of the West Antarctic Ice Sheet have long predicted that runaway grounding line retreat would be possible if the ice sheet thinned to a critical level [*Weertman*, 1974]. More recent models with complex ice flow and realistic bed topography uphold this earlier prediction and suggest that a catastrophic retreat could be sudden [*Schoof*, 2007]. Although the grounding line of Thwaites Glacier is currently fairly stable (though widening)

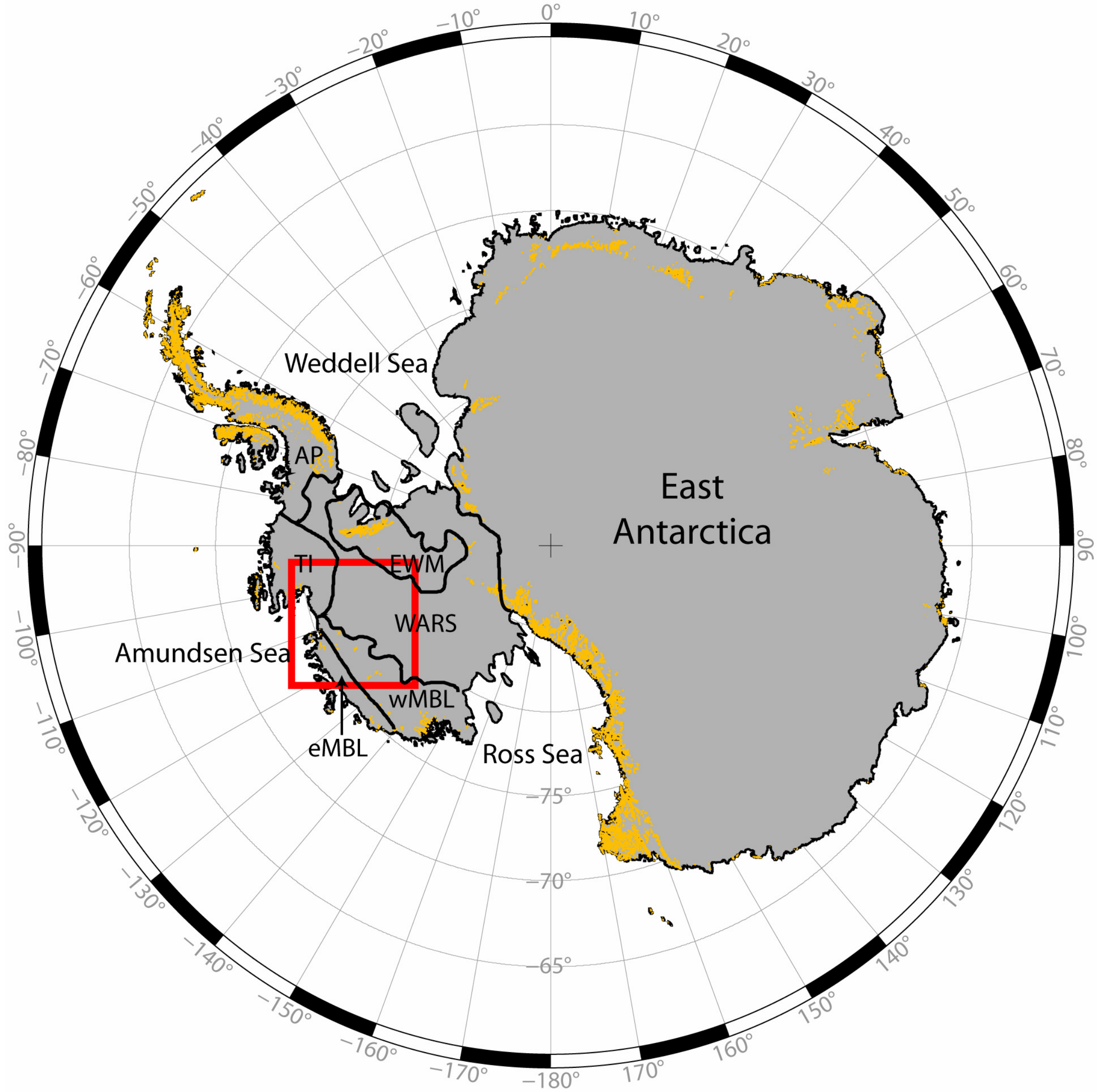

Figure 3.1: Antarctic index map showing the location of all Chapter 3 figures (red box). Also shown: rock outcrop locations (gold lines) [*SCAR*, 2006] and West Antarctic crustal blocks (thick back lines) [*Dalziel and Elliot*, 1982; *Dalziel and Lawver*, 2001]. The area within the red box is shown larger in Figure 3.4. Crustal block names: AP= Antarctic Peninsula; TI= Thurston Island; EWM= Ellsworth-Whitmore Mountains; WARS= West Antarctic Rift System; eMBL and wMBL= eastern and western Marie Byrd Land. Antarctic coastline [*SCAR*, 2006]= thin black line.

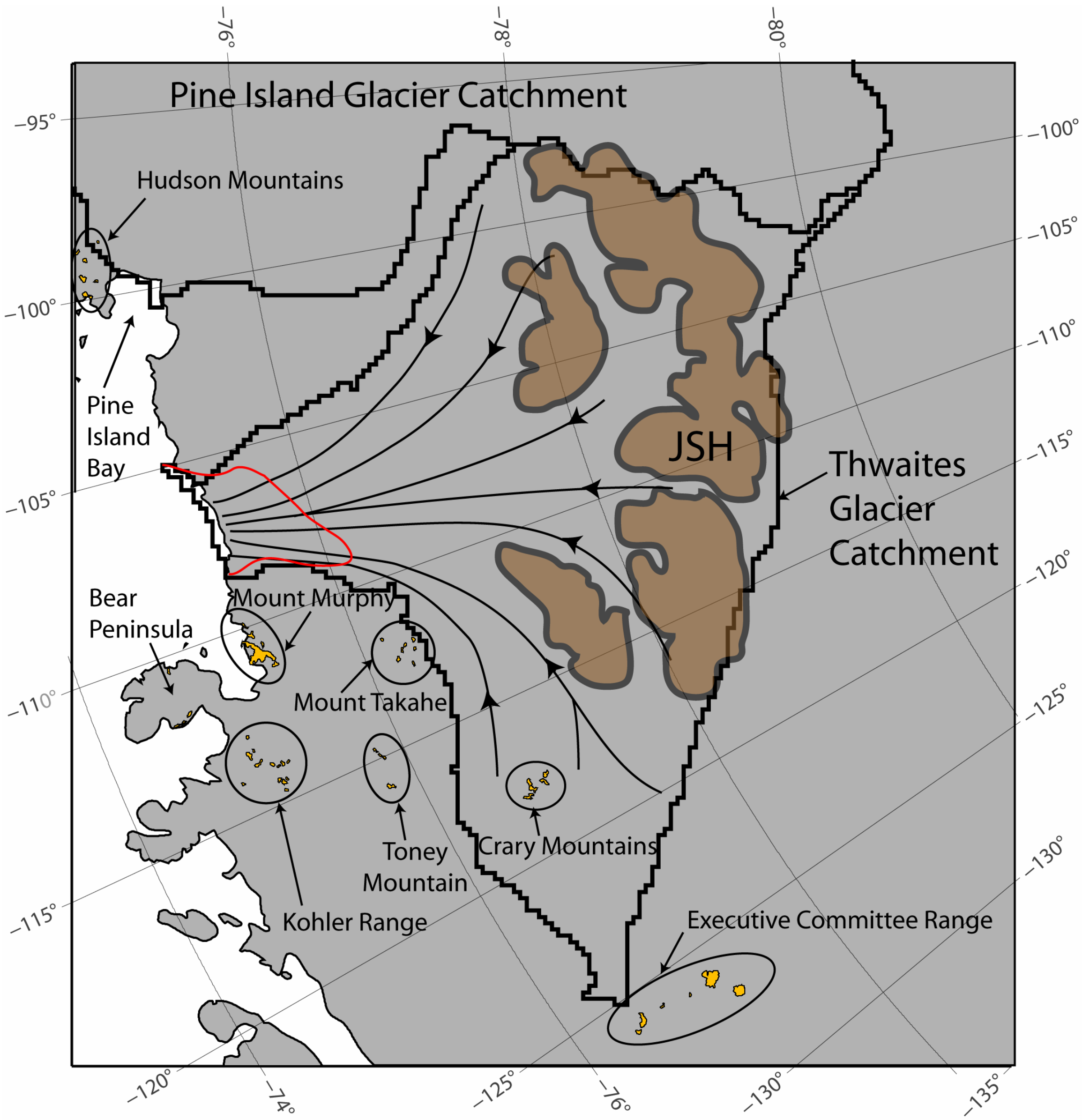

Figure 3.2: Glaciological setting of the Thwaites Glacier area of West Antarctica. Land is colored gray. Shown: rock outcrop locations (thin black lines, gold fill), major glacier catchments (thick black lines) [*Vaughan, et al.,* 1999], generalized ice flow lines for Thwaites Glacier based on InSAR velocities (thin black lines, arrows indicate flow direction), and the area in which InSAR-measured ice flow velocities [*Rignot, et al.*, 2006] for Thwaites Glacier exceed 500 m/yr (thin red line). The Jankowski Subglacial Highlands (JSH) are outlined in black, filled with brown (see Figure 3.3). Circled and labeled areas are volcanic centers.

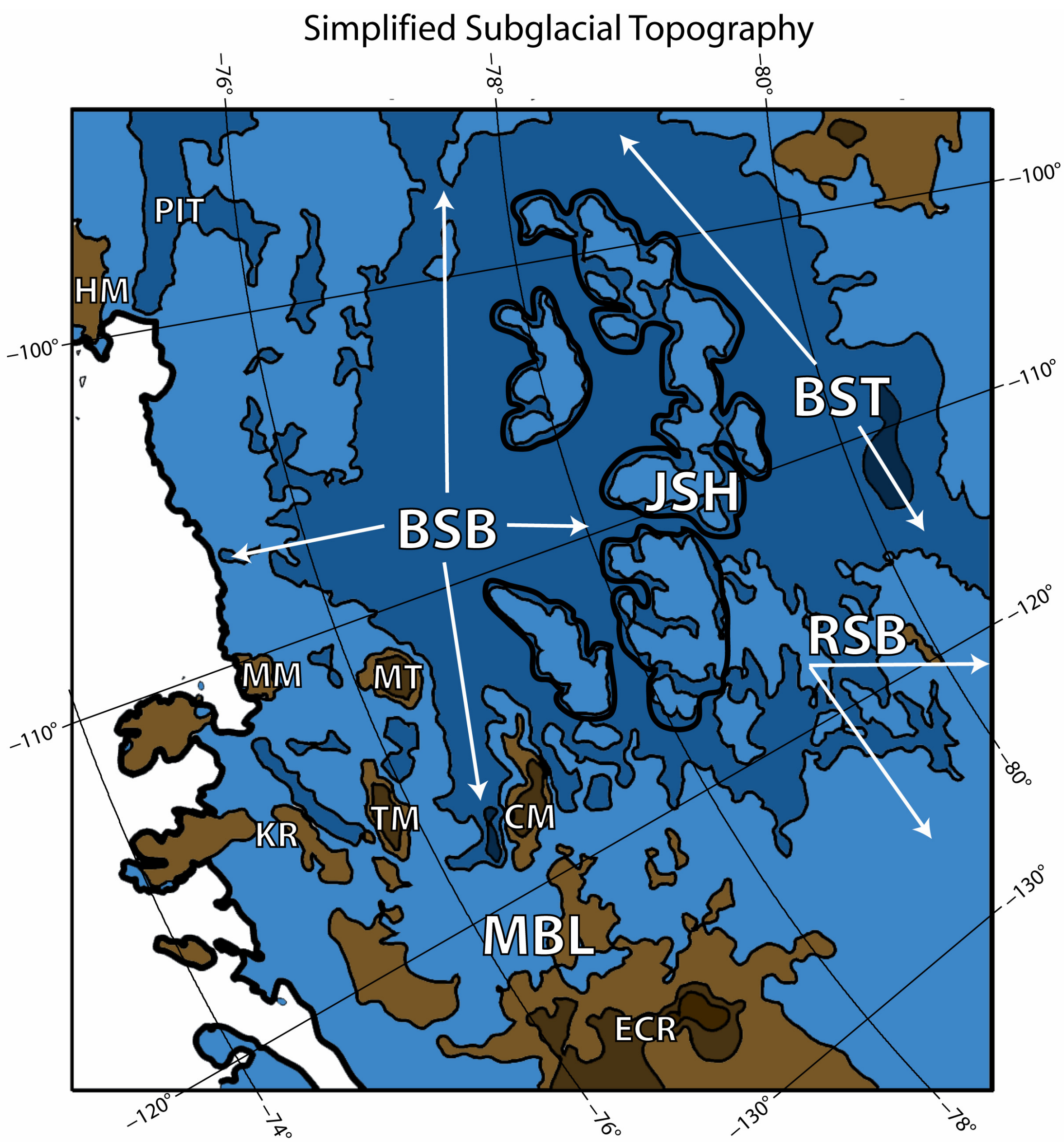

Figure 3.3: Subglacial topography, simplified and colored by elevations deeper than: -2 km (dark blue), -1 km (medium blue), 0 km (light blue), 1 km (light brown), and 2 km (dark brown) contours. Coastline [*SCAR*, 2006] shown in black, figure location with respect to Antarctica shown on Figure 3.1. Major features: BSB= Byrd Subglacial Basin, JSH= Jankowski Subglacial Highlands (outlined in heavy black lines), BST= Bentley Subglacial Trench, RSB= Rose Subglacial Basin, MBL= Marie Byrd Land. Other features: PIT= Pine Island Trench, HM= Hudson Mountains. Marie Byrd Land volcanoes: MM= Mount Murphy, MT= Mount Takahe, KR= Kohler Range, TM= Toney Mountain, CM= Crary Mountains, and ECR= Executive Committee Range. See Figure 1.9 for regional context and details of defining the JSH.

[*Rignot, et al.*, 2002], warm waters from the deep ocean are upwelling offshore of the Amundsen Sea Embayment and threaten future increased melting at the ice-ocean boundary [*Vaughan, et al.*, 2007]. Thus, understanding the genesis of the low-lying Byrd Subglacial Basin below Thwaites Glacier is critical to understanding future (and past) retreats of the West Antarctic Ice Sheet.

The formation of the Byrd Subglacial Basin could be related to the formation of the West Antarctic Rift System [*Dalziel and Lawver*, 2001; *Dalziel*, 2006; *LeMasurier*, 2008], which underlies much of the Ross Sea Embayment (Figures 3.1 and 3.4). The term West Antarctic Rift System is time-ambiguous and here modify the term with a time-specific identifier: Mesozoic West Antarctic Rift System for the large-scale, distributed late Mesozoic activity. Additional localized Cenozoic activity constitutes a second phase of inland West Antarctic activity (see Chapter 1 for details on West Antarctic rifting).

The Mesozoic rift system is thought to be cold and extinct based on seismic results which indicate normal velocity mantle [*Ritzwoller, et al.*, 2001; *Sieminski, et al.*, 2003], magnetotellurics which found high resistivity at mantle depths [*Wannamaker, et al.*, 1996], and topographical comparisons of rift basin depths [*LeMasurier*, 2008]. However, airborne magnetic data in the Rose Subglacial Basin section of the rift system have been interpreted to indicate widespread volcanism, possibly of Cenozoic age [e.g. *Behrendt, et al.*, 1994]. In the Thwaites Glacier area, localized Cenozoic volcanism is visible as six subaerial volcanic centers (Figures 3.2, 3.3, and 3.4) and Cenozoic extension has been invoked to explain the deep sections of the Byrd Subglacial Basin, which may lack significant sedimentary infill [*LeMasurier*, 2008].

Thwaites Glacier has also been hypothesized to overlie the crustal blocks of Marie Byrd Land and Thurston Island (Figure 3.4) [*Dalziel and Elliot*, 1982; *Dalziel and*

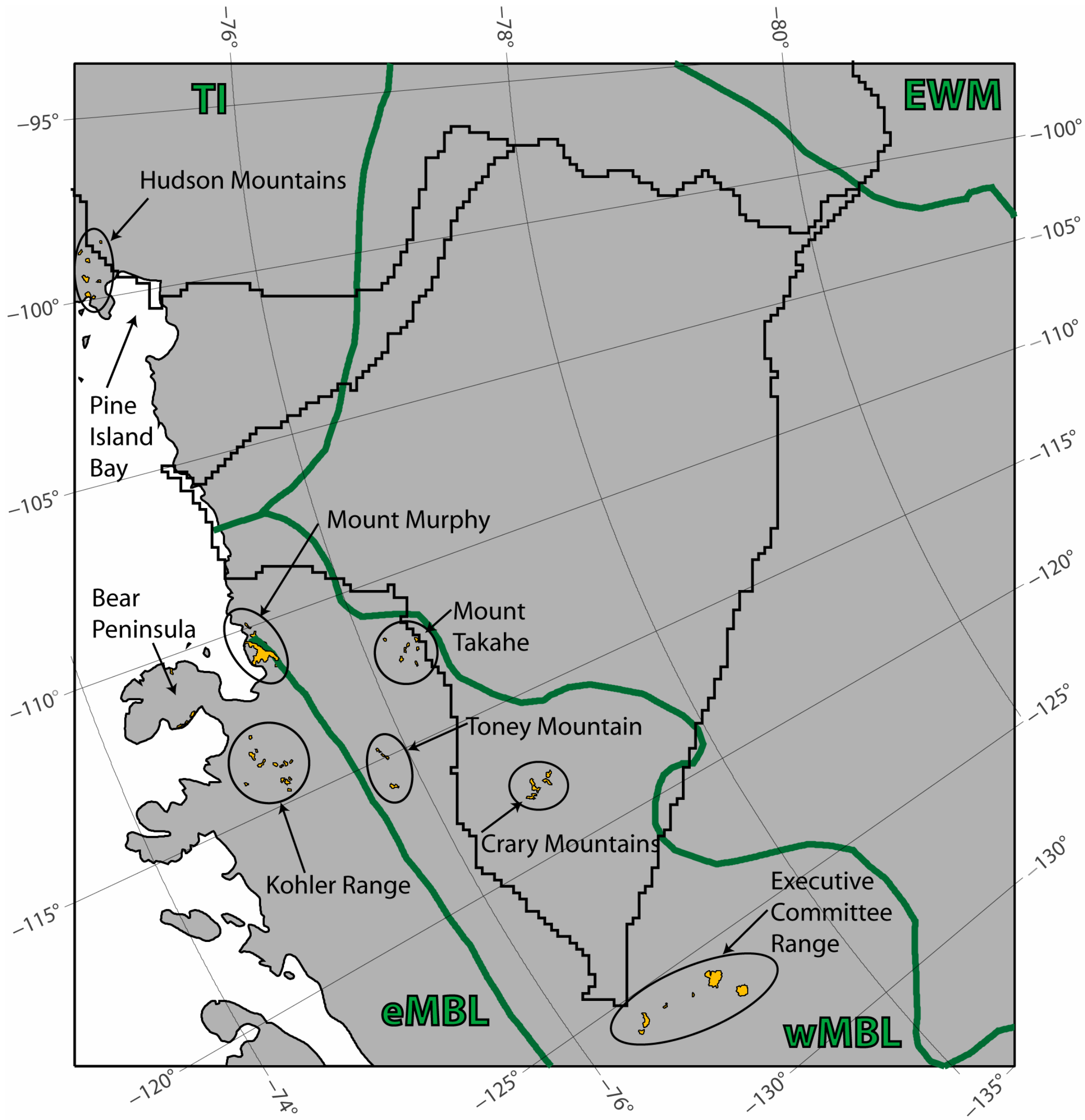

Figure 3.4: The crustal setting (as hypothesized before this study) of the Thwaites Glacier area of West Antarctica. Land is colored gray. Shown: rock outcrop locations (thin black lines, gold fill), Thwaites Glacier and Pine Island Glacier catchments (thicker black lines, see Figure 3.2) [*Vaughan, et al.*, 1999], and West Antarctic crustal blocks (thick green lines) [*Dalziel and Elliot*, 1982; *Dalziel and Lawver*, 2001]. Crustal block names: TI= Thurston Island; EWM= Ellsworth-Whitmore Mountains; eMBL and wMBL= eastern and western Marie Byrd Land. Circled and labeled are volcanic centers.

Lawver, 2001]. The crust in Marie Byrd Land was extended during the Mesozoic and again when New Zealand rifted from its coast [*LeMasurier and Landis*, 1997; *Luyendyk, et al.*, 2003]. A subsequent period of tectonic quiescence ended with Marie Byrd Land uplift within the last ~25 Ma, coincident with Cenozoic West Antarctic Rift System volcanism that may be from a plume source [*LeMasurier and Landis*, 1997] (see Chapter 1 for more details). The results of the recent uplift and volcanism are the distinct Marie Byrd Land Dome, roughly centered upon the crustal block (Figure 1.3), and rock outcrops localized at Cenozoic volcanoes (Figure 3.4).

Commonly, crustal structure is reported in terms of Moho depth or crustal thickness. Both represent the depth to the base of the crust but the former is relative to sea level and the latter is relative to surface topography. In the Byrd Subglacial Basin and eastern Marie Byrd Land, crustal thicknesses are roughly 1.1 and 0.7 km less than Moho depths, respectively. The few crustal thickness and Moho depth estimates near this study area range from 21-31 km (Table 3.1, Figure 3.8 for those closest to the study area). However, the thickest Marie Byrd Land crustal estimates [*Luyendyk, et al.*, 2003] assumed that topography was compensated at the Moho, which may not be the case. The other estimates specify extended crust that is thinner than the 30-38 km Moho depths needed to isostatically compensate Marie Byrd Land topography with Airy assumptions. The crust may instead be thermally-supported by warm mantle or have Pratt-like compensation [*LeMasurier and Landis*, 1997; *Winberry and Anandakrishnan*, 2004]. Surface wave tomography has imaged low-velocity mantle beneath Marie Byrd Land [*Ritzwoller, et al.*, 2001; *Sieminski, et al.*, 2003], consistent with the hypothesis of thermally-supported crust there.

To evaluate the crustal context of Thwaites Glacier and the evolution of the Byrd Subglacial Basin, I first calculated Bouguer gravity anomalies from a new airborne free-air gravity dataset [*Diehl, et al.*, 2008a]. Then, spectral analyses of the free-air and Bouguer gravity anomalies were performed to determine the depths to crustal density boundaries. Finally, forward modeling of a Bouguer anomaly profile across the interior of the glacier catchment is used to evaluate the major crustal hypotheses for the Byrd Subglacial Basin and Marie Byrd Land in light of the new, spectrally-derived Moho depths.

Table 3.1: Crustal thickness and Moho depths near the Byrd Subglacial Basin and Marie Byrd Land

Source	Location	Crustal thickness or Moho depth?	Estimate (km)
Winberry and Anandakrishnan, 2004	Bentley Subglacial Trench (station MTM)	Crustal thickness	21
	Byrd Station, in the Rose Subglacial Basin	Crustal thickness	27
	160 km SE of Marie Byrd Land	Crustal thickness	25
Gohl, et al., 2007	Inner continental shelf, N of Marie Byrd Land	Moho depth	23
	Inner continental shelf, N of Byrd Subglacial Basin	Moho depth	25
Luyendyk, et al., 2003	Western Marie Byrd Land	Moho depth	31-28
	Rose Subglacial Basin, SW of Marie Byrd Land	Moho depth	27-24

3.2 DATA

The AGASEA (Aerogeophysical Survey of the Amundsen Sea Embayment) free-air gravity data were primarily collected by the University of Texas at Austin over Thwaites Glacier in 2004-2005 [*Diehl, et al.*, 2008a; *Diehl, et al.,* 2008b]. A bias in the free-air anomalies was apparent when the data were compared with long-wavelength satellite gravity anomalies from GRACE (Gravity Recovery and Climate Experiment), so the published free-air gravity anomalies [*Diehl, et al.*, 2008a] were shifted +9.7 mGals for the following analyses (see Chapter 4 for more information). Bedrock topography (Figure 3.3) is well-constrained down to 9 km horizontal resolution, primarily by airborne ice-penetrating radar [*Holt, et al.*, 2006; *Vaughan, et al.*, 2006]. Ice sheet surface and sub-aerial volcano elevations are provided by an ERS-1-derived digital elevation model (DEM) for West Antarctica [*Bamber and Gomez-Dans*, 2005].

3.3 METHODS

Complete, terrain-corrected 3D Bouguer gravity anomalies (Figure 3.5) were calculated to enhance the signals of deep crustal anomalies. The calculation assumed typical densities of ice and rock- 915 kg/m^3 and 2670 kg/m^3 respectively- and used a Gaussian-Legendre Quadrature method of calculating the gravity effects of topography [*von Frese, et al.*, 1981]. Ocean bathymetry just offshore of Thwaites Glacier is unknown, so a separate water correction was not included and any Bouguer anomalies over floating ice were removed. The surface elevation DEM used in the correction underestimates the Marie Byrd Land volcano elevations [*Young, et al.,* 2008], thus anomalies over the volcanoes should be interpreted carefully.

Spectral analyses of gravity data provide straightforward estimates of the density structure of the crust [*Fairhead and Okereke*, 1988; *Karner and Watts*, 1983; *Spector and Grant*, 1970]. The radial power spectrum is often plotted as the natural log of power versus wavenumber (k=1/(wavelength)). The spectrum can be fit with a series of straight line segments, where each line's slope (m) is related to the depth (d) of a crustal density boundary such that:

$$d_{Moho} = \frac{m}{2}$$

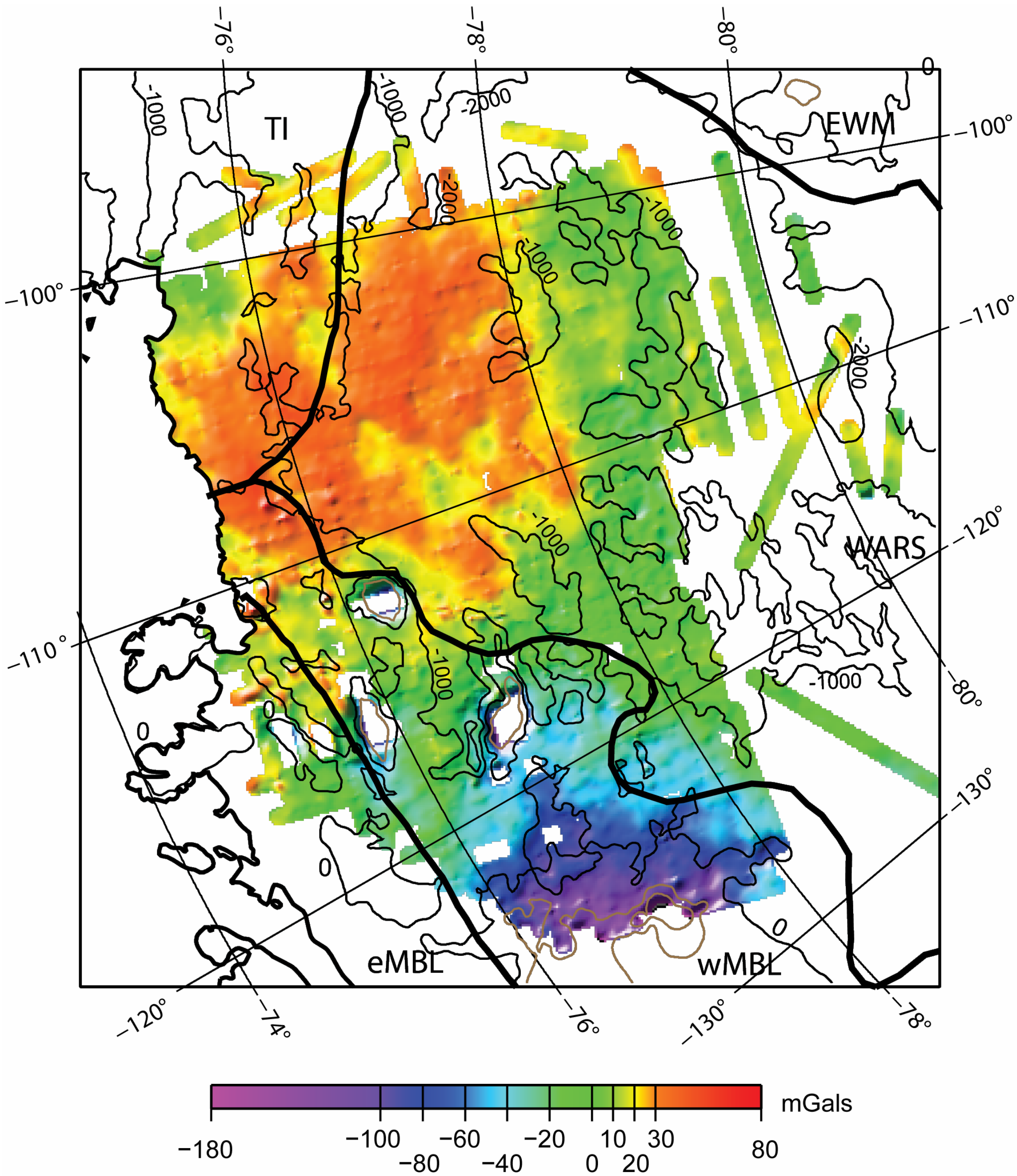

Figure 3.5: Bouguer gravity anomalies for the AGASEA survey. Overlaid: 1000 m subglacial topographic contours (black contours at or below sea level, coastline [*SCAR*, 2006] is medium weight black line, and brown contours above sea level). Heavy black lines= crustal blocks [Dalziel and Elliot, 1982; Dalziel and Lawver, 2001]: TI=Thurston Island; EWM=Ellsworth-Whitmore Mountains; eMBL and wMBL= eastern and western Marie Byrd Land; WARS=West Antarctic Rift System.

for the example of the Moho density boundary between the crust and the mantle [*Fairhead and Okereke*, 1988]. Spectral estimates should be done for areas of relatively homogenous crustal structure so that slope breaks in the spectrum can be easily identified [*Spector and Grant*, 1970]. Each slope break indicates that the spectrum's power above the break results from a different crustal density boundary than the power below the slope break. There are often two major density boundaries found in continental crust (the Moho and a mid-crustal boundary) but detectable near-surface density boundaries could also exist.

Mirroring the data area along two axes (N-S and E-W) improves recovery of long-wavelength signals [*McNutt*, 1983]. For small areas, such as the 200 x 200 km squares used in this study (Figure 3.6), the mirroring process produces an 800 x 800 km area over which to calculate the power spectrum. This greater area allows depth estimates down to 67 km with <10% error [*Regan and Hinze*, 1976]. The spectra for AGASEA data have a lower limit useful information to the 9 km ($k = 0.1111\ km^{-1}$) data resolution and the upper limit of resolution is conservatively constrained by the size of the area ($k = 0.015\ km^{-1}$ for the mirrored 200 x 200 km analysis areas).

Radial power spectra for both free-air and Bouguer gravity anomalies were fit with a series of least-squares, best-fit lines (Figure 3.7). The wavenumbers selected for the endpoints of each regression were chosen at apparent breaks in spectrum slope. The median of the range of depth values that satisfied both the free-air and Bouguer spectral results was the final depth estimate for each boundary. The spectral errors represent the full range of depths that satisfy both spectra.

The spectral analyses were also useful to constrain 2D Bouguer gravity modeling, done with a common iterative forward modeling package called GM-SYS (originally developed by Northwest Geophysical Associates, Inc., now licensed through Geosoft's

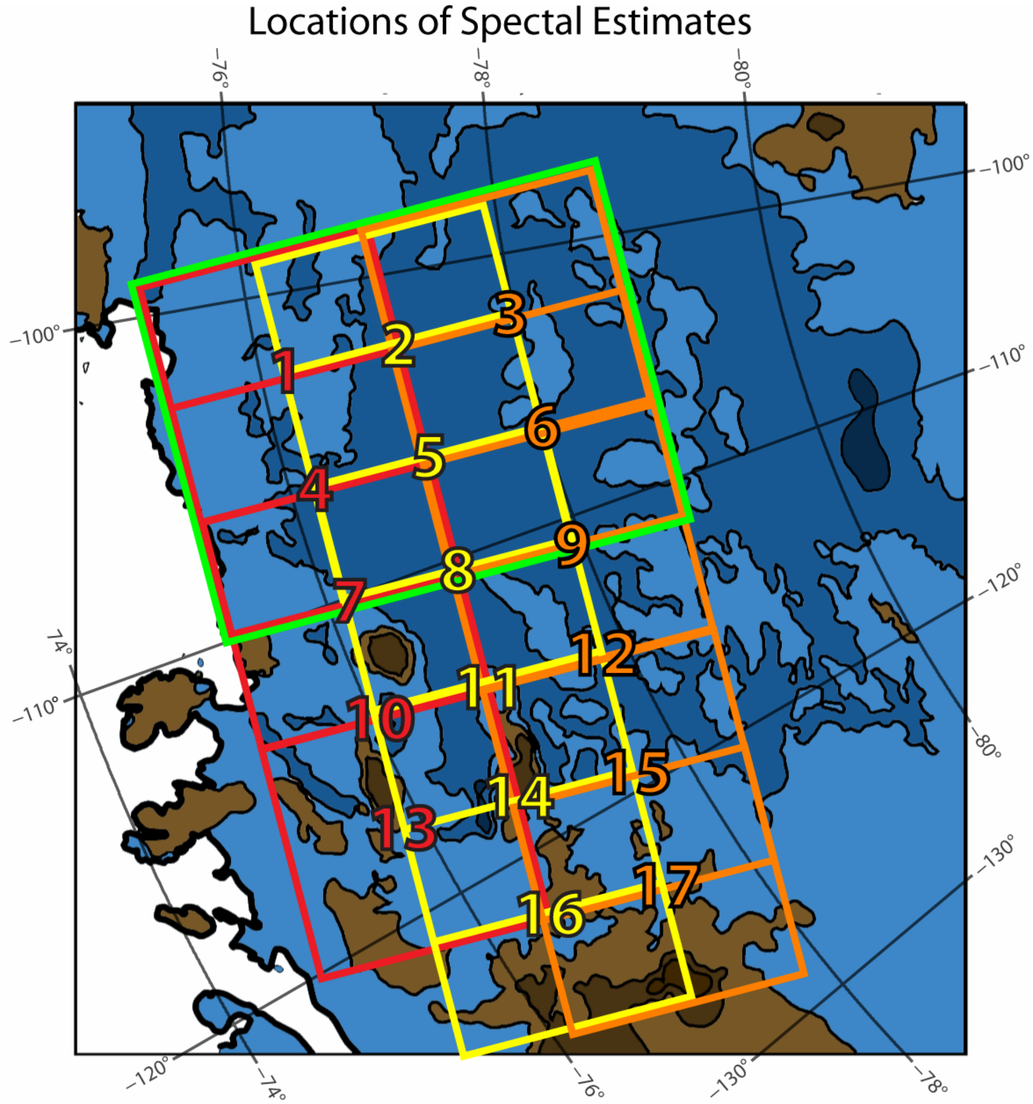

Figure 3.6: Locations of the one 300 x 400 km (green) and seventeen 200 x 200 km radial power spectrum estimates for AGASEA gravity. Background image: Subglacial topography simplified and colored by elevations deeper than: -2 km (dark blue), -1 km (medium blue), 0 km (light blue), 1 km (light brown), and 2 km (dark brown) contours (see Figure 3.3 for feature names). Coastline [*SCAR*, 2006] shown in black, figure location with respect to Antarctica shown on Figure 3.1. The location of the large estimate over the Byrd Subglacial Basin (Figure 3.8) is shown in green. Each small square (Table 3.2) is numbered at its center and color-coded to match the label to the square: all squares along the coast are in red, those in the center of the area (the Byrd Subglacial Basin and Marie Byrd Land) are in yellow, and those furthest into the interior (the Jankowski Subglacial Highlands and Marie Byrd Land) are in orange.

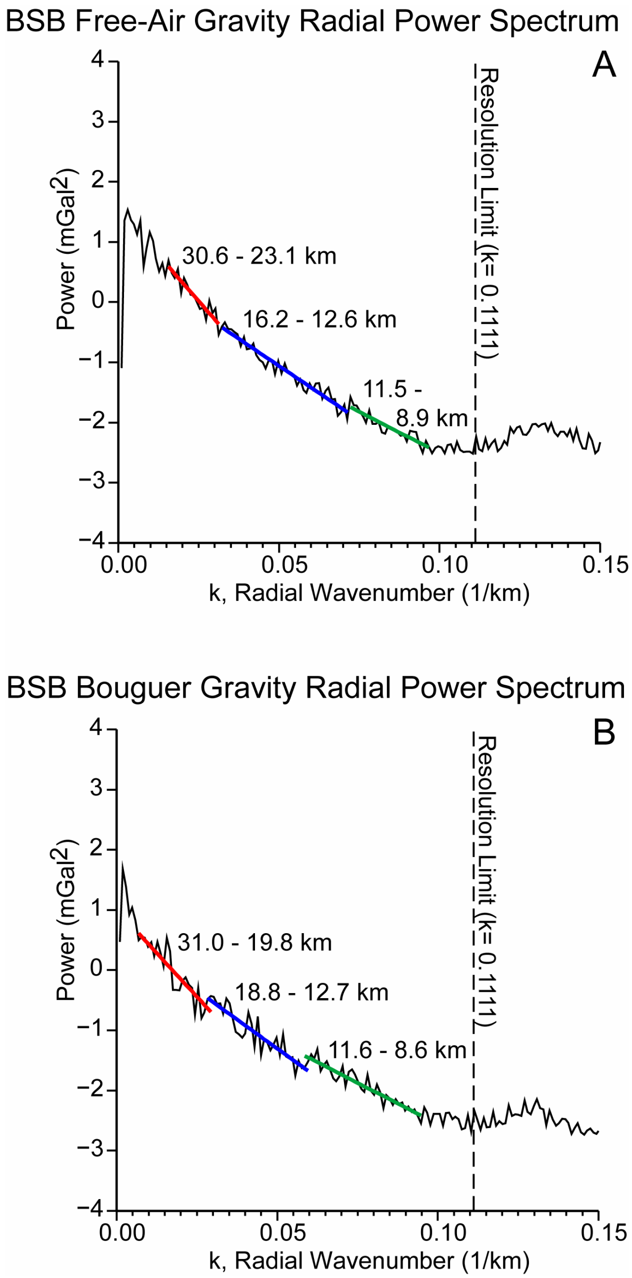

Figure 3.7: Radial power spectra for the 400 x 300 km area within the Byrd Subglacial Basin (BSB, red box on Figure 3.5), A. Free-air gravity; B. Bouguer gravity. Line segments fit to find depths are colored and labeled with depth to boundary: Moho fit = red line; mid-crustal boundary 1 = blue line; and mid-crustal boundary 2 = green line (see text for description of boundaries).

Oasis Montaj software). I used three models to test crustal structure hypotheses: 1. crustal layers solely from spectral results (Figure 3.9); 2. crustal layers from spectral results plus any additional bodies required to test the thermally-supported dome hypothesis (Figure 3.10); and 3. crustal layers loosely guided by spectral results to test the maximum crustal thickness beneath Marie Byrd Land (Figure 3.11). The only crustal density constraints for this modeling come from seismic profiles on the inner continental shelf in the Amundsen Sea Embayment [*Gohl, et al.*, 2007]. The P-wave velocities offshore are equivalent to densities of: 1900-2250 kg/m^3 for sedimentary rocks, 2600-2700 kg/m^3 for the upper crust, 2800-2900 kg/m^3 for the lower crust, and 3200-3300 kg/m^3 for the upper mantle. The gravity forward models thus assume standard, constant layer densities. However, because the modeling is non-unique, the models were kept as simple as possible for each hypothesis being tested.

3.4 RESULTS

Figure 3.5 shows a regional positive Bouguer anomaly (~40 mGals) that coincides with the Byrd Subglacial Basin below Thwaites Glacier, as well as Mt. Murphy and the Kohler Range. Surrounding the regional positive is a zone of near zero-magnitude Bouguer anomalies that includes the Jankowski Subglacial Highlands and surrounds the Crary Mountains, Mount Takahe, and Toney Mountain, though the volcano flanks are more negative. A regional negative Bouguer anomaly west of the Crary Mountains reaches –180 mGals over the Executive Committee Range. This regional negative anomaly may be even more negative than the values we report here because of the DEM height inaccuracies mentioned above.

Spectral analyses of a 400 x 300 km area within the Byrd Subglacial Basin (Figure 3.5, red box) had subtle changes in slope (Figure 3.6), signifying large changes in crustal boundaries. The best-fit Moho and mid-crust boundary depths are 26.85 +/- 3.75

km and 12.55+/- 3.65 from free-air gravity and 25.4 +/- 5.6 km and 13.7 +/- 5.1 km from Bouguer gravity, respectively. To characterize the spatial changes, I divided the data into seventeen 200 x 200 km areas (Figure 3.7) and calculated both the free-air and Bouguer gravity anomaly radial power spectra for each of the seventeen areas (Figure 3.8; Table 3.2). The spatial pattern of these smaller estimates shows shallow Moho depths and under-compensated crust in the interior of the catchment with increasing Moho depth and compensation towards the coast. The average Moho depths across all areas range from 30.6 – 18.6 km and average 24.7 km over the broad basin. The deepest, ~30 km Moho depths areas not continuous, but are separated by pieces of relatively thinner crust. The thinnest crust occurs at the Crary Mountains.

Out of three forward models, only the second two fit the observed regional gravity trends (Figures 3.10 and 3.11). The first model's strict interpretation of the spectral boundary depths (Figure 3.9) cannot reproduce the trends of the observed gravity. The second model adds a lower-density upper mantle body (100 kg/m^3 less than surrounding mantle) beneath Marie Byrd Land. If the body lies adjacent to the lower crust, then it extends down to 42 km depth to fit the observed gravity and there must be body of higher-density crustal material in the adjacent rift area (Figure 3.10). The third model uses the spectral depths only as a rough guide to test how thick the crust beneath Marie Byrd Land could be and, though highly non-unique, obtains a good gravity fit for rift Moho depths of 18-19 km and Marie Byrd Land depths from 20 km to 25 km, deepening westward (Figure 3.11).

3.5 Discussion

The pattern of Bouguer gravity anomalies reveals strong crustal heterogeneity beneath Thwaites Glacier (Figure 3.5) and spectral Moho depth estimates were variable, but relatively shallow throughout (Figure 3.8; Table 3.2). The shallow Moho (19-24 km

Table 3.2: Moho Depth Results for Seventeen Spectral Estimates (200 x 200 km squares) Across the Thwaites Glacier Area (see Figure 3.6 for locations), where 'start k' and 'end k' are the wavenumbers between which the linear regression was performed

Square Number	Gravity Data Type	Start k (km^{-1})	End k (km^{-1})	Distance to Boundary; i.e. Slope/2 (km)	Moho Depth (km)	Error (km)	Combined Moho Depth and Error (km)
1	Free-air	0.01	0.028	36.6	33.0	6.1	30.1 +/- 3.2
	Bouguer	0.01	0.028	31.8	28.2	5.0	
2	Bouguer	0.015	0.034	31.4	27.8	6.4	24.3 +/- 2.9
	Free-air	0.015	0.055	25.4	21.8	5.5	
3	Bouguer	0.015	0.044	23.9	20.3	3.6	19.1 +/- 2.4
	Free-air	0.015	0.047	21.0	17.4	4.1	
4	Free-air	0.015	0.035	31.4	27.8	5.1	23.9 +/- 1.2
	Bouguer	0.013	0.039	24.2	20.6	4.6	
5	Bouguer	0.015	0.037	27.2	23.6	3.7	22.3 +/- 2.4
	Free-air	0.015	0.046	26.4	22.8	2.0	
6	Bouguer	0.017	0.032	28.0	24.4	5.3	21.5 +/- 2.4
	Free-air	0.015	0.037	24.3	20.7	3.2	
7	Bouguer	0.016	0.032	37.3	33.7	4.4	30.6 +/- 1.2
	Free-air	0.015	0.03	31.8	28.2	3.6	
8	Bouguer	0.015	0.037	34.7	31.1	3.1	30.5 +/- 2.5
	Free-air	0.015	0.044	32.9	29.3	3.8	
9	Free-air	0.015	0.054	23.5	19.9	2.9	20.0 +/- 3.0
	Bouguer	0.007	0.037	23.2	19.6	3.4	
10	Free-air	0.022	0.042	24.5	20.9	1.6	20.6 +/- 1.3
	Bouguer	0.015	0.042	23.7	20.1	1.7	
11	Free-air	0.017	0.052	25.0	21.4	3.2	19.3 +/- 1.0
	Bouguer	0.015	0.056	21.3	17.7	2.5	
12	Free-air	0.021	0.053	27.1	23.5	3.3	22.1 +/- 1.9
	Bouguer	0.015	0.03	25.1	21.5	2.5	
13	Bouguer	0.025	0.04	32.9	29.3	2.2	28.4 +/- 1.3
	Free-air	0.015	0.039	30.1	26.5	3.2	
14	Free-air	0.017	0.052	24.8	21.2	3.1	19.0 +/- 0.8
	Bouguer	0.01	0.039	20.9	17.3	2.5	
15	Free-air	0.015	0.053	22.7	19.1	4.3	18.6 +/- 3.7
	Bouguer	0.018	0.054	21.4	17.8	4.5	
16	Free-air	0.015	0.046	29.2	25.6	3.7	22.2 +/- 0.2
	Bouguer	0.024	0.061	23.1	19.5	2.9	
17	Bouguer	0.015	0.045	26.1	22.5	3.8	21.6 +/- 2.9
	Free-air	0.015	0.047	23.9	20.3	4.2	

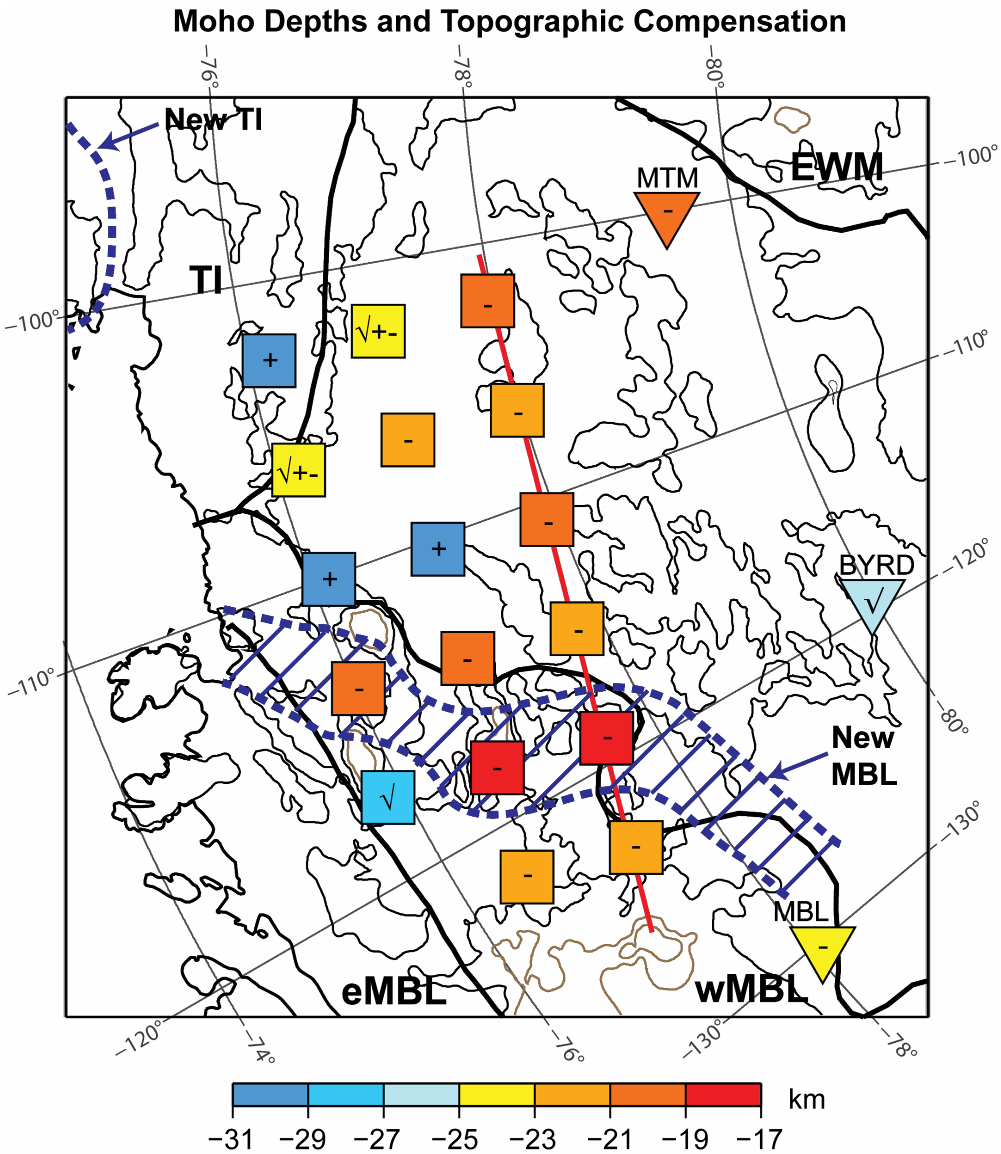

Figure 3.8: Spectrally-defined Moho depth estimates (Table 3.2) centered on the squares over which they were calculated (Figure 3.6). Inverted triangles are Moho depths from *Winberry and Anandakrishnan* [2004], labeled with their station names. Checkmarks indicate Airy isostatic equilibrium, while pluses and minuses indicate over- or under-compensation of topography respectively. Red line = forward models' (Figures 3.9, 3.10, and 3.11) location. Blue dotted lines = revised crustal boundary locations based on these results. Background: Subglacial topography contours as in Figure 3.3. Heavy black lines= crustal blocks [Dalziel and Elliot, 1982; Dalziel and Lawver, 2001]: TI=Thurston Island; EWM=Ellsworth-Whitmore Mountains; eMBL and wMBL= eastern and western Marie Byrd Land.

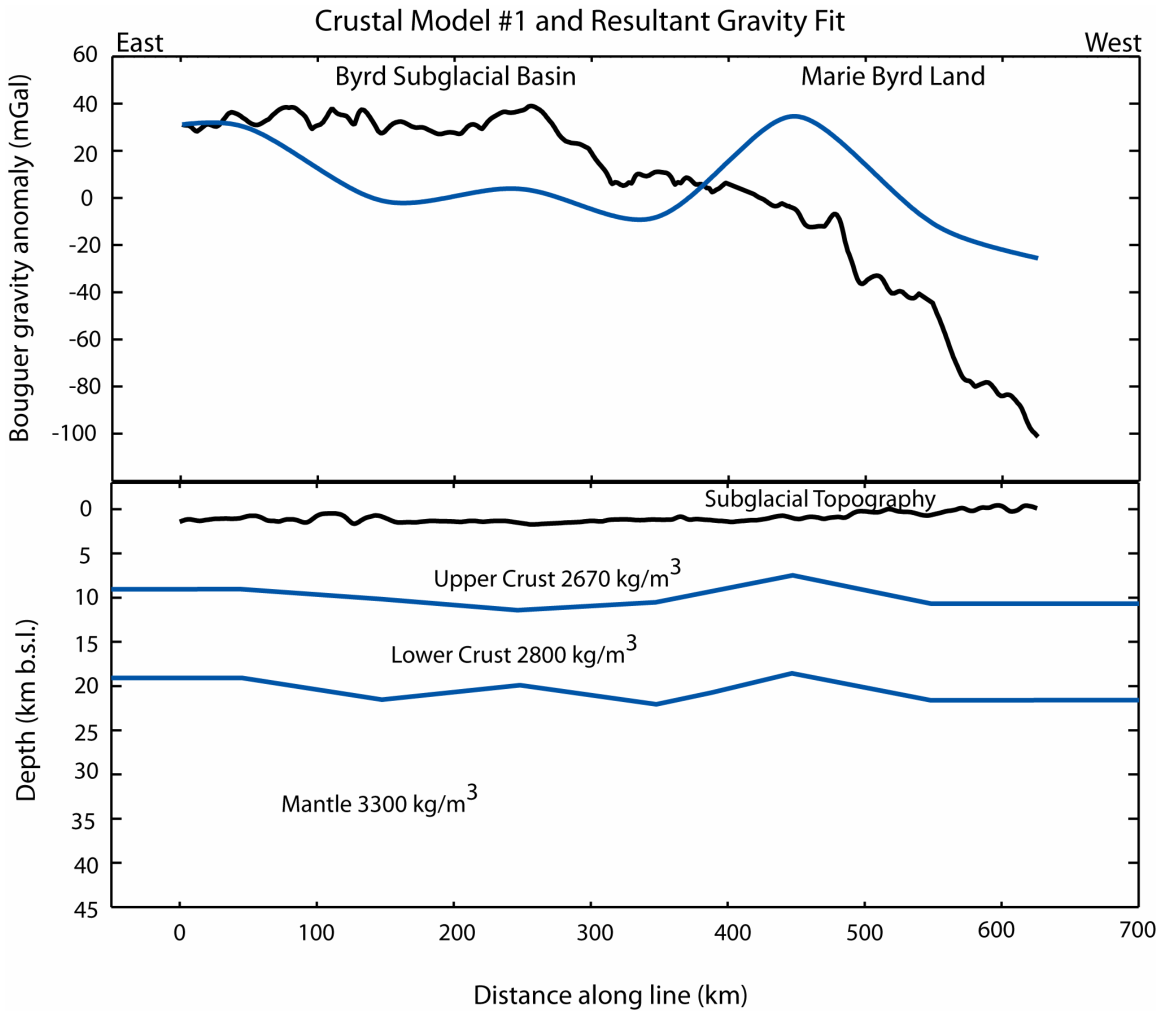

Figure 3.9: Crustal model #1: constrained solely by spectrally-defined boundary depths, in blue on bottom panel. Resulting Bouguer gravity fit (blue line, top panel). Radar-measured subglacial topography on bottom panel in black and Bouguer gravity anomaly sampled from grid (Figure 3.5) on top panel in black. Line location shown in red on Figure 3.8.

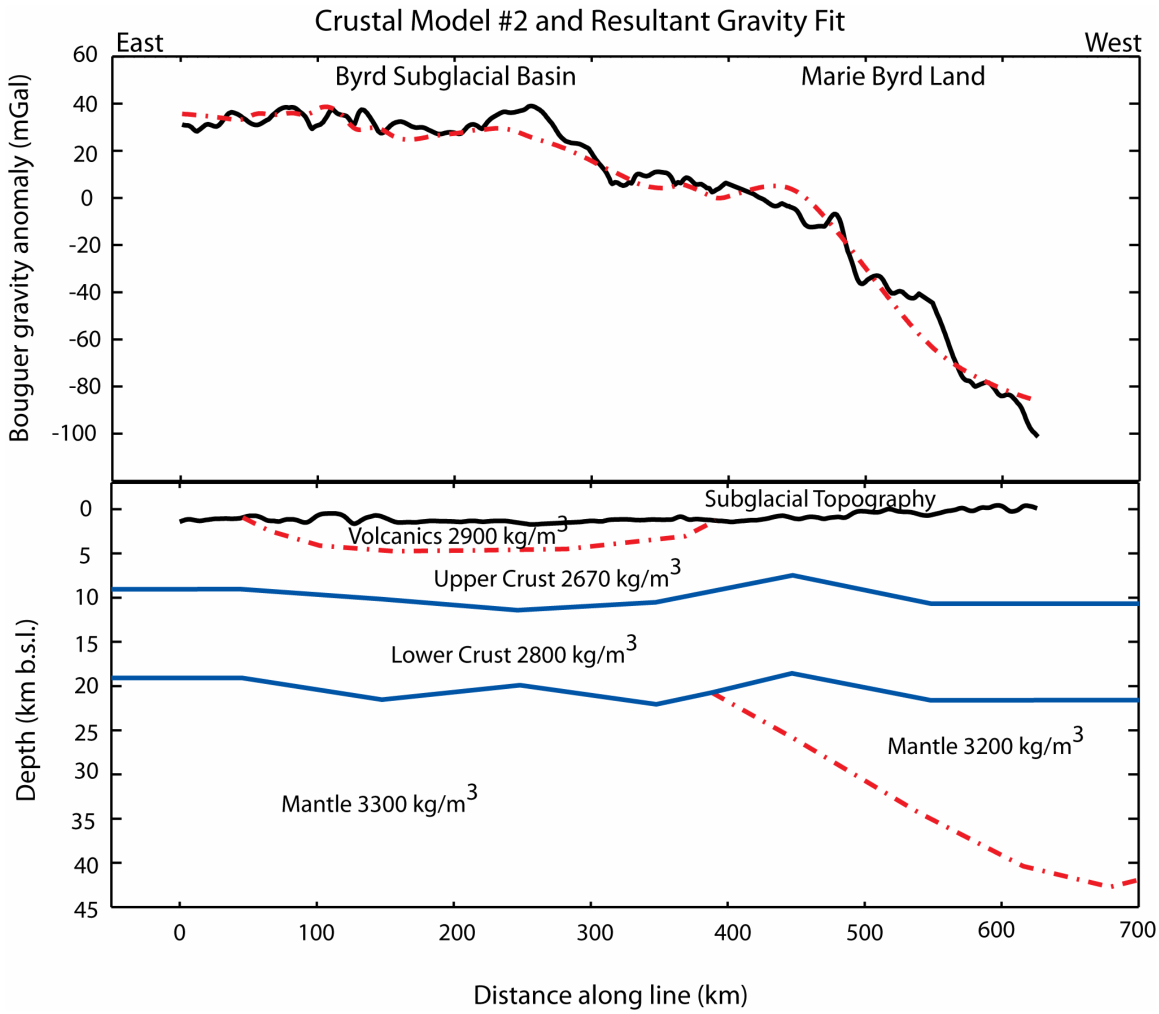

Figure 3.10: Crustal model #2: constrained by 1. spectrally-defined boundary depths as in Figure 3.9's Model #1, in blue on bottom panel and 2. additional volcanics and lower density mantle (red dash-dotted lines, lower panel). Resulting Bouguer gravity fit (red dash-dotted line, top panel). Radar-measured subglacial topography on bottom panel in black and Bouguer gravity anomaly sampled from grid (Figure 3.5) on top panel in black. Line location shown in red on Figure 3.8.

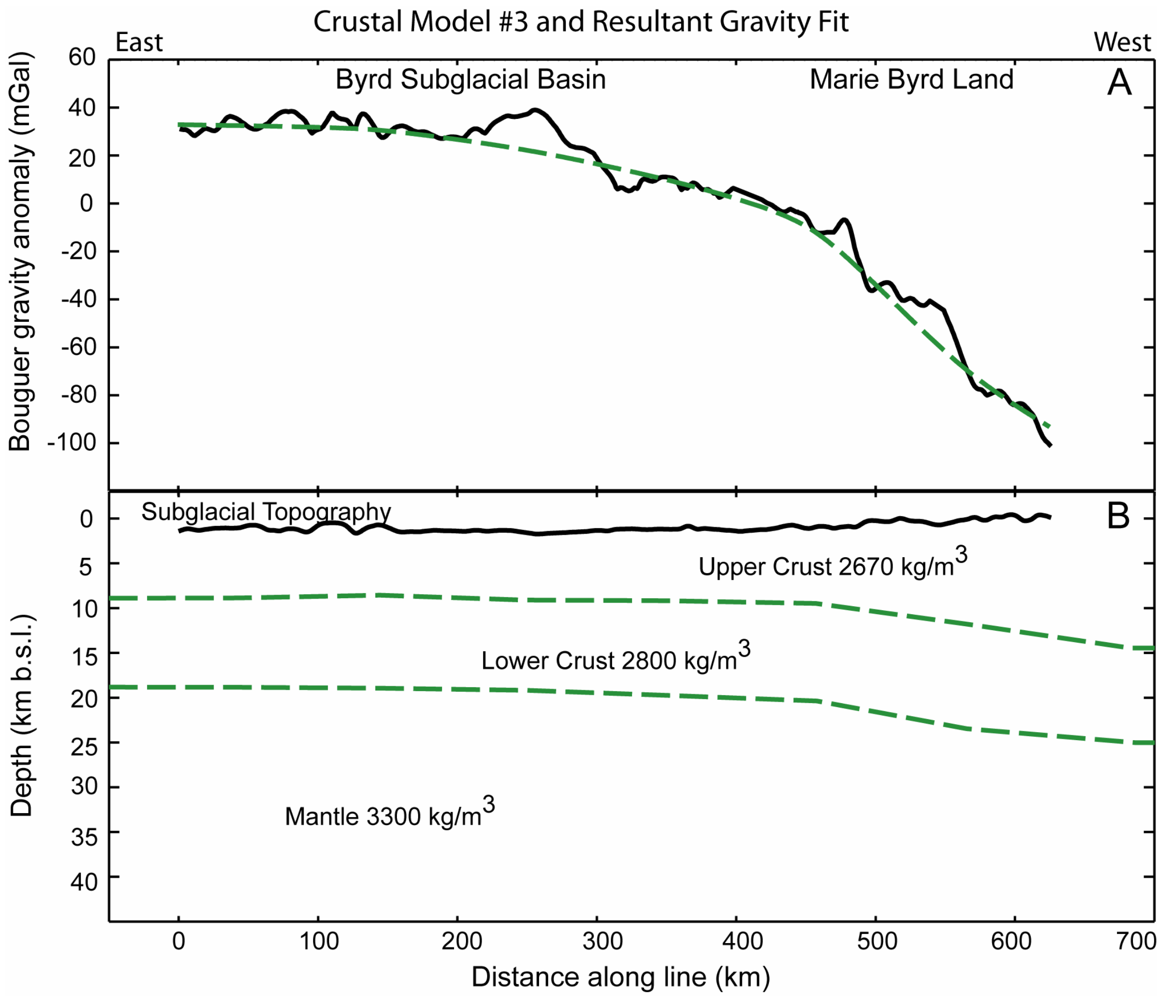

Figure 3.11: Crustal model #3: constrained loosely by spectrally-defined boundary depths (green dashed lines on bottom panel). Resulting Bouguer gravity fit (green dashed line, top panel). Radar-measured subglacial topography on bottom panel in black and Bouguer gravity anomaly sampled from grid (Figure 3.5) on top panel in black. Line location shown in red on Figure 3.8.

deep) underlying Thwaites Glacier's broad basin supports the hypothesis that it is the northern extension of wide-scale Mesozoic rifting. Thus, the Thurston Island block does not extend into this area and the glacier does not flow along a boundary between crustal blocks as previously hypothesized (Figures 3.4). These data also suggest that the West Antarctic Rift System may continue into the western part of the neighboring Pine Island Glacier catchment (Figure 3.4). Moho depths in this rift system sector are shallower than the ~27-28 km that others have estimated in the Ross Sea Embayment sector [*Clarke, et al.*, 1997; *Winberry and Anandakrishnan*, 2004] and imply either more intense Mesozoic rifting or significant additional Cenozoic extension.

The shallowest (18-20 km) Moho depths occur over the Byrd Subglacial Basin, the Jankowski Subglacial Highlands, and the Marie Byrd Land volcanoes (excluding the Executive Committee Range). Interestingly, forward modeling results (Figure 3.10) suggest that the Byrd Subglacial Basin has been intruded by <3 km of higher-density igneous rock in the upper crust, further evidence that the Byrd Subglacial Basin is part of the Mesozoic large-scale rifting. I propose that the boundary between the Mesozoic WARS rifting and Marie Byrd Land occurs within a zone around the two shallowest Moho depths (squares #14 and #15, Figures 3.6 and 3.8) and the 20.5 km Moho depth (square #10, Figures 3.6 and 3.8) between Mount Takahe and Toney Mountain. The thin crust there appears to have been exploited by a zone of volcanism, as evidenced by the Marie Byrd Land subaerial volcanoes. However, since there are no subaerial volcanoes within the most southern piece of thin crust (square #15, Figure 3.6 and 3.8), subglacial volcanoes seem likely to be found there.

Within Marie Byrd Land, forward modeling results show that the regional negative Bouguer anomaly can be interpreted as either thicker crust, or thin crust with a low-density subsurface body (Figure 3.11 and 3.10, respectively). The 21.6-22.2 km spectrally-defined Moho depths clearly suggest thin crust, slightly more so than the 23-25 km crustal thicknesses from nearby seismic results. Even the forward model done to maximize the depth of the Marie Byrd Land Moho (Figure 3.11) still indicates relatively thin crust there (Figure 3.11)- certainly crust that is not thick enough to Airy isostatically compensate the topography. For the spectral results, the crust in Marie Byrd Land and at the West Antarctic Rift System-Marie Byrd Land boundary is 6.3-9.3 km undercompensated. Lithospheric flexural support of high topography over a large area of thin crust is unlikely and provides additional evidence for a thermally-supported crust in Marie Byrd Land.

In addition, the forward modeling results indicate that the spectrally-defined Moho depths alone are inadequate to explain the Bouguer anomaly trends. A low-density mantle body providing thermal support at the base of the crust would explain the negative Bouguer anomaly in Marie Byrd Land. Although forward modeling supports this hypothesis, there are obviously other models that would also fit the data; however the modeling does conclusively show that the crust in Marie Byrd Land is not Airy isostatically-supported.

In contrast to Marie Byrd Land, the zone of undercompensated topography (Moho depths 4.1-6.5 km shallower than predicted by Airy isostasy) around the Jankowski Subglacial Highlands and adjacent to the Byrd Subglacial Basin suggests flexural or Pratt-like support of the subglacial highlands. Speculatively, the Jankowski Subglacial Highlands could be volcanic constructs emplaced in the Cenozoic upon the thin but cooled (and therefore more rigid) Mesozoic rift system crust. Prominent magnetic anomalies in a small section of the highlands have already been identified as subglacial volcanics [*Jankowski and Drewry*, 1981; *Behrendt, et al.*, 2004]. However, more magnetic results for the rest of the highlands are needed to allow this hypothesis to be tested systematically.

3.6 Conclusions

The Bouguer gravity anomalies over Thwaites Glacier from airborne surveying have proven a critical source of information for understanding the glacier's crustal context. The deep, broad Byrd Subglacial Basin through which the glacier flows is part of the same Mesozoic rifting that affected the Rose Subglacial Basin in the Ross Sea Embayment. These results suggest that the Thurston Island crustal block does not exist beneath Thwaites Glacier. In general, the Mesozoic rifting accounts for the Byrd Subglacial Basin extended continental crust lying so far below sea level and, in turn, created a crustal environment on which only an inherently unstable ice sheet could form. The undercompensated crust of the Jankowski Subglacial Highlands suggests that the highlands were emplaced in the Cenozoic upon the relatively rigid, and thus cool, thin Byrd Subglacial Basin crust. The very deepest confined troughs between the highlands are thus also likely to be a result of this Cenozoic activity. The deepest parts of the Byrd Subglacial Basin, however, could have formed either during the initial Mesozoic rifting or during Cenozoic reactivation.

The boundary between Marie Byrd Land and the Byrd Subglacial Basin redefined by this study (blue dotted line, Figure 3.8) is a zone of the thinnest crust (18 km Moho depths) yet found outside the Ross Sea. The zone occurs within the eastern Marie Byrd Land volcanoes, which suggests that the volcanoes are exploiting the crustal boundary there. Marie Byrd Land itself is slightly thicker (~24 km Moho depth) but still thinner than surrounding seismic estimates. The regional negative Bouguer anomaly in Marie Byrd Land is adequately explained by a low-density subsurface body, such as low-density mantle. These results are consistent with the hypothesis that Marie Byrd Land is thin crust, thermally-supported by warm mantle and that Marie Byrd Land is not compensated by a thick crustal root. In this case, we would expect significantly higher subglacial heat fluxes in the Marie Byrd Land area (compared to the surrounding Mesozoic rift system areas) and possibly for an abundance of subglacial melt water to be available for Thwaites Glacier's fast flow.

Chapter 4: West Antarctic Crustal Structure from Airborne and Satellite Gravity

ABSTRACT

The Ross Sea of West Antarctica is volcanically active but rift-related extension there is thought to be dormant or very slow. Beneath the West Antarctic Ice Sheet, however, the status of rifting, the spatial extent of extended continental crust, and the extension's boundaries with Paleozoic crustal blocks are less well-determined. The crustal thickness of West Antarctica is of prime concern because it is an indicator of the tectonic history that led to the formation of crust 1-2 km below sea level. The properties and geometry of that bedrock provided a unique environment for the subsequent formation of the Earth's only marine ice sheet. To examine the crustal structure of West Antarctica, I combined >0.8 million km^2 of free-air gravity data collected during airborne surveys from 1991 to 2005 over West Antarctica with additional GRACE and ERS-1 satellite gravity. Bouguer gravity anomalies calculated from the free-air gravity data then guide crustal structure interpretations both spatially and with depth. In all areas, spectral analyses of the gravity data indicate a 2-layer crust, and- with the exception of Marie Byrd Land- Moho depths similar to those determined from sparse seismic measurements. Inverse modeling of the gravity data proved to be difficult to constrain but yielded results similar to previous forward modeling. Based on these analyses and geologic and geophysical information in the literature, I present a new tectonic sketch map of West Antarctic crustal blocks and rifted areas.

4.1 INTRODUCTION

The subglacial geology of West Antarctica is composed of four crustal blocks and the West Antarctic Rift System (Figures 4.1 and 4.2) [*Dalziel and Elliot*, 1982; *Dalziel and Lawver*, 2001]. The area of interest here covers much of West Antarctica (Figure 4.2) from the Amundsen Sea Embayment to the Ross Sea Embayment, but excludes interpretations into the marine part(s) of the rift. Others have done extensive work in the Ross Sea [e.g., *Davey and Brancolini*, 1995; *Trey, et al.*, 1999; *Luyendyk, et al.*, 2001 and many others], which is why this study focuses on characterizing the inland crust, less well-known since it is covered by the thick ice of the West Antarctic Ice Sheet. As described in Chapters 1 and 3, the West Antarctic Ice Sheet is vulnerable to disintegration from grounding-line retreat [*Weertman*, 1974; *Hughes*, 1975; *Mercer*, 1978; *Oppenheimer,* 1998] because the ice sheet is based well below sea level [*Bentley*, 1964; *Jankowski and Drewry*, 1981; *Drewry*, 1983; *Lythe, et al.*, 2001]. The tectonic history that created this low-lying bedrock also formed isolated highlands above sea level in the Ellsworth-Whitmore Mountains and Marie Byrd Land, which provide the subaerial locations needed to generate the West Antarctic Ice Sheet [e.g., *Pollard and deConto*, 2005]. Thus, the tectonic forces in Antarctica have, over a hundred of million years, not only created appropriate bedrock conditions for the West Antarctic Ice Sheet to periodically and rapidly retreat, but also favorable conditions for the West Antarctic Ice Sheet to have initially formed.

However, the crustal structure of West Antarctica also plays an important role in the current state of the West Antarctic Ice Sheet through interactions at the ice-bedrock boundary. Understanding the source(s) and timing of volcanism, extension, and uplift within the ice sheet's crustal foundation leads to further understanding of the ice sheet's vulnerabilities and subglacial environment. Based on crustal structure interpretations

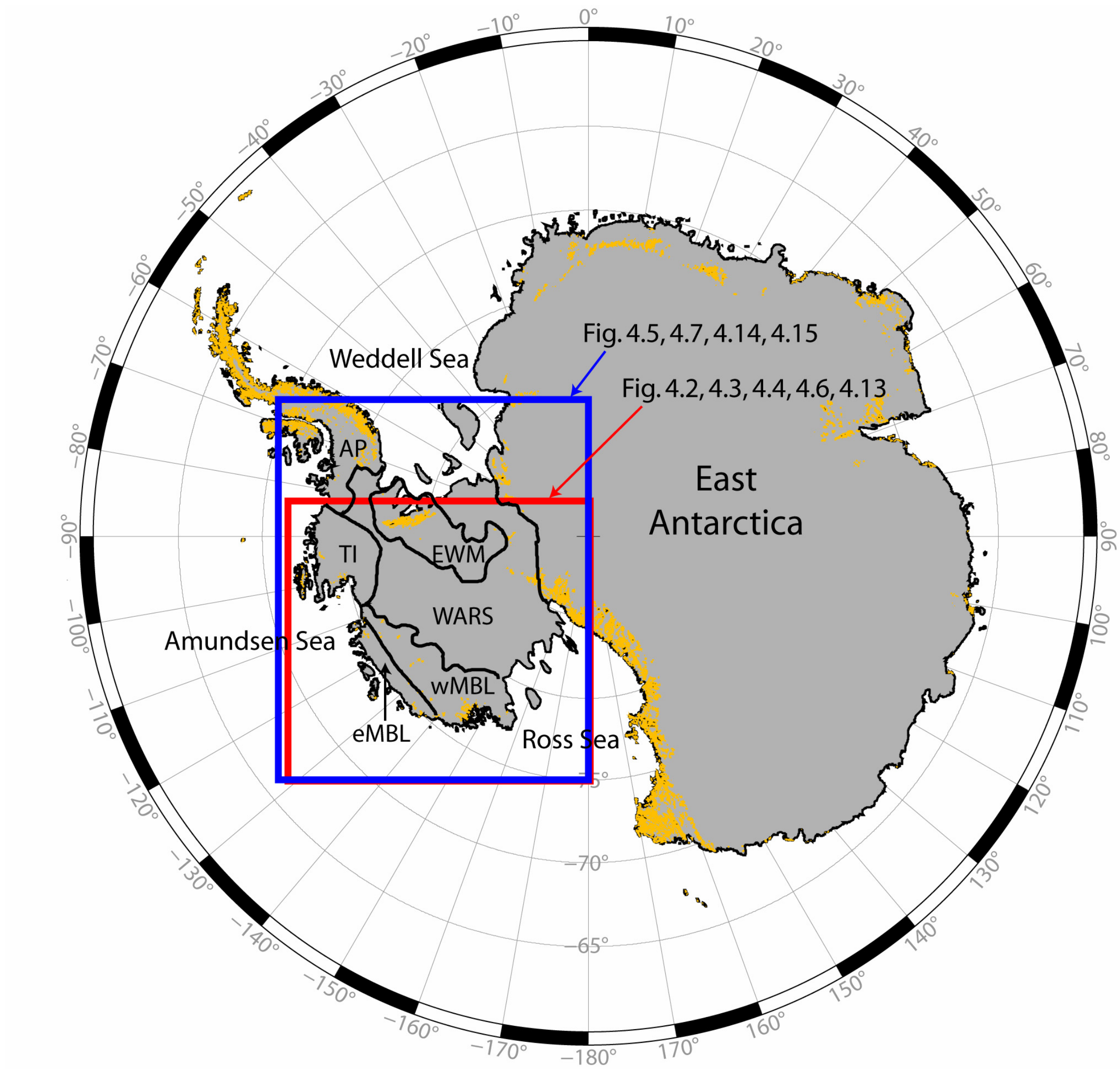

Figure 4.1: Antarctic index map showing the location of some of Chapter 4 figures. A separate index map (Figure 4.8) is used for Figures 4.9 to 4.12. Also shown: rock outcrop locations (gold lines) and coastline from the Antarctic Digital Database [*SCAR*, 2006] and West Antarctic crustal blocks (thick black lines) [*Dalziel and Elliot*, 1982; *Dalziel and Lawver*, 2001]. Crustal block names: AP= Antarctic Peninsula; TI= Thurston Island; EWM= Ellsworth-Whitmore Mountains; WARS= West Antarctic Rift System; eMBL and wMBL= eastern and western Marie Byrd Land.

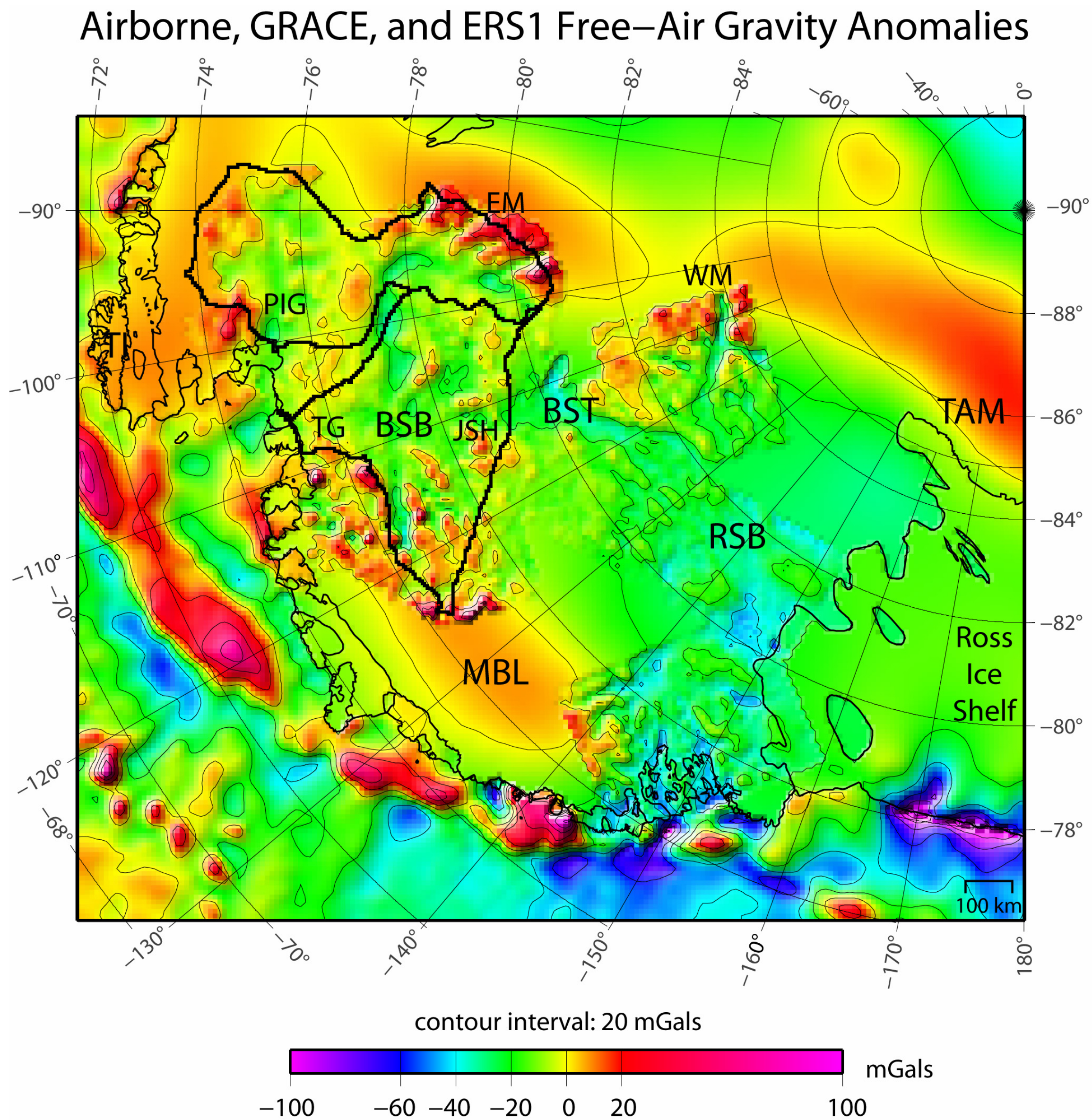

Figure 4.2: Free-air gravity anomaly compilation for West Antarctica, including airborne and GRACE data over land and floating ice and ERS-1 data over open ocean. Thin black line=coastline including ice shelves [*SCAR*, 2006], thick black lines= Pine Island Glacier (PIG) and Thwaites Glacier (TG) catchments [*Vaughan, et al.,* 1999]. Other labels include: BSB= Byrd Subglacial Basin; BST= Bentley Subglacial Trench; RSB= Rose Subglacial Basin; TAM= Transantarctic Mountains; MBL= Marie Byrd Land; EM= Ellsworth Mountains; WM= Whitmore Mountains; JSH= Jankowski Subglacial Highlands.

primarily from gravity data, I introduce here a new sketch map of the West Antarctic crustal blocks, extent of Mesozoic rifting, and areas of known Cenozoic activity. As in Chapter 3, I will use the term Mesozoic West Antarctic Rift System to describe the large-scale, distributed episode of late Mesozoic extension and volcanism.

4.2 DATA

The aerogravity data available in West Antarctica cover over 0.8 million km^2 and were collected over a 15 year time span. These surveys (as introduced in Chapter 1) are: AGASEA [*Holt, et al.*, 2006a; *Diehl, et al.,* 2006a; *Diehl, et al.*, 2008b], BBAS [*Ferraccioli, et al.*, 2007; *Jordan, et al.*, submitted], WMB [*Luyendyk, et al.*, 2003], and CASERTZ [*Blankenship, et al.*, 1993; *Brozena and Jarvis*, 1993; *Behrendt, et al.*, 1994; *Bell, et al.*, 1999; *Studinger, et al.*, 2001] (Figure 1.11). The airborne surveys differ greatly in both the instrumentation and processing utilized, as well as the resolution of their gravity results (see Chapter 1 for a full discussion). Subglacial bedrock [*Holt, et al.*, 2006a; *Vaughan, et al.*, 2006] and ice surface elevations [*Bamber and Gomez-Dans*, 2005] are the same as in Chapter 3.

I also used two satellite-collected datasets to aid my interpretations and fill gaps in the airborne surveys' coverage: 1. the GRACE (Gravity Recovery and Climate Experiment) satellite global static gravity field and 2. ERS-1 radar-altimeter data that was converted to free-air gravity anomalies over the ocean. The University of Texas at Austin, Center for Space Research computed gravity anomalies from the gravity model GGM03s [*Tapley, et al.*, 2007] that are equivalent to airborne free-air anomalies observed at 3600 m above the WGS84 ellipsoid sea level (F. Condi*,* pers. comm., 2007). The gravity anomalies cover the entire Antarctic continent and surrounding Southern Ocean from 60º S to 90ºS with a resolution somewhat better than 140 km half-wavelength, depending on latitude. However, ERS-1 altimeter-derived free-air anomalies are substituted in the following analyses over all ice-free oceanic areas because of their 35-50 km resolution [*McAdoo and Laxon*, 1997]. Note that the ERS-1 free-air anomalies were augmented by Geosat data north of 68°S [*McAdoo and Laxon*, 1997].

4.3 Combining Airborne Surveys and Satellite Data

4.3.1 Methods

First, the airborne free-air gravity anomalies for each survey were upward continued to the same 3600 m observation level of the AGASEA free-air gravity anomalies [*Diehl, et al.*, 2008b] to provide consistent spectral content. Given that only gridded CASERTZ [*Bell, et al.*, 1999] and WMB [*Luyendyk, et al.*, 2003] free-air anomalies were available, grid sections were upward continued with the Generic Mapping Tools (GMT) [*Wessel and Smith*, 1998], using the average altitudes of lines flown within each area of the grid to determine the amount of continuation. The continued grid sections overlapped slightly at the edges so that the sections could be reassembled in GMT, where overlapping edges are weighted with a cosine taper to blend smoothly.

Each survey overlaps slightly with at least one of the others: AGASEA-BBAS, AGASEA-CASERTZ, and CASERTZ-WMB. After upward continuation, the overlapping areas are examined to determine the feasibility of merging the disparate datasets (Table 4.1, columns 1-3). If the difference in the survey levels within the overlap area is above the noise level of the datasets, then the difference is significant enough to be corrected for, before attempting to merge the surveys.

There are two potential ways to correct for offsets between airborne datasets. The first can be used in areas where the airborne datasets lack ground gravity data or other constraints on their absolute levels. For this first method, all surveys are adjusted to match the mean level of a chosen dataset. This method creates locally-consistent datasets but the absolute level of the surveys may not be geologically real. The second method is preferable in all situations where an *a priori* gravity dataset with a trustworthy mean is available. In this method, the airborne surveys are shifted to match the average of the *a priori* dataset. For instance, *Müller and Smith* [1993] performed this type of shifting on a smaller scale using shipborne gravity tracks, matching their data's levels to a combined Seasat, Geosat, and ERS-1 free-air dataset. The GGM03s satellite gravity model (derived solely from GRACE measurements) provides a reliable long-wavelength field for West Antarctica, so the second method of correcting data offsets was applied for this analysis.

After any necessary level shifts are applied to the datasets separately and the overlaps are re-checked for compatibility, the GMT grid blending software [*Wessel and Smith*, 1998] can be used to combine the airborne surveys by applying cosine tapers to their overlapping areas. In addition, areas without airborne free-air gravity anomalies can be patched (with the same GMT blending software) with anomalies from GRACE (on land and over ice shelves) and ERS-1 (over open ocean).

4.3.2 Results

When the airborne free-air gravity anomalies for each survey were compared in their overlapping areas, significant differences were found in two out of three overlapping areas (Table 4.1). The one overlapping area without a significant difference was the AGASEA-BBAS area. Since the BBAS survey was collected collaboratively with the AGASEA survey, data sharing ensured that the differences between the datasets in their overlapping areas were within data error [*Diehl, et al.*, 2008b]. However, the differences between the other surveys' means within the overlap areas were very large (Table 4.1) and needed to be addressed before the surveys could be merged.

Thus, all the airborne free-air gravity datasets were DC shifted separately to match free-air gravity anomalies derived from the GRACE global field (Table 4.2). The shifts applied maintained the negligible difference between AGASEA and BBAS surveys (Table 4.1). In addition, the mean free-air gravity difference within the large area of overlap between the AGASEA and CASERTZ surveys dropped from 34.6 mGals to only 2.7 mGals (within data error). However, there did remain a significant (though small) difference of -6.4 mGals between the mean free-air gravity anomalies within the CASERTZ and WMB overlap area.

Table 4.1: Average gravity in survey overlap areas, before and after leveling to GRACE

Overlapping Surveys	Area of Overlap (sq. km)	Mean Free-air gravity difference in overlap area (mGals)	Mean Free-air gravity difference in overlap area after leveling to GRACE (mGals)
AGASEA-BBAS	73,120	-0.8	0.6
AGASEA - CASERTZ	13,550	34.6	2.7
CASERTZ - WMB	1,250	17.9	-6.4

Table 4.2: Average gravity and shifts applied to airborne survey areas based on GRACE

Survey	Area Used for Average (sq. km)	Airborne Free-air gravity mean (mGals)	GRACE Free-air gravity mean (mGals)	Shift applied to Airborne Free-air gravity (mGals)
AGASEA	600,000	-15.9	-6.2	9.7
BBAS	434,500	-11.5	-3.2	8.3
CASERTZ	855,000	8.5	-13.7	-22.2
WMB	200,000	-12.5	-36.7	24.2

The GRACE and ERS-1 datasets showed a slight difference in their levels that was left intact in the final grid; GRACE is an average of 4.9 mGals higher than ERS-1 over the ocean. The final map combines all available airborne and satellite free-air anomalies together into an on-shore and off-shore West Antarctic free-air gravity anomaly map (Figure 4.2). The merged data are sampled at 10 km throughout, though the resolution is much lower over areas with the satellite data.

4.3.3 Discussion

The method of leveling airborne free-air gravity datasets to the GRACE-derived free-air anomalies works well, as illustrated by improvements in the match of the surveys' overlapping areas after applying the method. Similar GRACE free-air anomalies can be calculated for anywhere in the world (and at any observation height), so this method can also be used on airborne datasets elsewhere in the world. One caveat, as shown by the lesser improvement of the CASERTZ-WMB overlap difference, is that the airborne surveys' overlapping areas must be fairly large. The exact amount of survey overlap needed will likely depend on the resolution of the GRACE free-air anomalies in the area of interest.

4.4 Bouguer Gravity Anomalies

4.4.1 Methods

Bouguer gravity anomalies are more useful for examining crustal geology, so updated complete 3D Bouguer gravity anomalies were then calculated for the older CASERTZ and WMB datasets. Complete Bouguer anomalies have been previously published for these older surveys [*Studinger, et al.,* 2001; *Luyendyk, et al.,* 2003; *Bell, et al.,* 2006] but reprocessing was warranted in light of the newest subglacial topography *[Lythe, et al.*, 2001; *Holt, et al.*, 2006a; *Vaughan, et al.*, 2006] and ice surface topography

[*Bamber and Gomez-Dans*, 2005] data available. The new Bouguer anomalies were calculated with a Gaussian-Legendre Quadrature method [*von Frese, et al.*, 1981].

The new CASERTZ and WMB Bouguer anomalies were then merged with the AGASEA (Chapter 3) and BBAS [*Jordan, et al.*, submitted] Bouguer anomalies, which were both calculated using the same Gaussian-Legendre Quadrature method and topography datasets. Dataset merging was accomplished with the GMT blending tool, as was done with the free-air anomalies (see section 4.3.1). The final Bouguer gravity anomalies were masked to remove data over floating ice, since water depth is either unconstrained or not accurately incorporated into the topography datasets used in these calculations.

4.4.2 Results

The Bouguer anomalies in West Antarctica (Figure 4.3) are characterized by several regional signals whose magnitudes are, for the first time, directly comparable. The regional negative anomalies in western Marie Byrd Land [*Luyendyk, et al.,* 2003] and the Whitmore Mountains [*Studinger, et al.,* 2001] are of generally smaller amplitude than the negative Bouguer signals in eastern Marie Byrd Land (Chapter 3) and the Ellsworth Mountains [*Jordan, et al.,* submitted]. The most striking and well-defined boundary in the Bouguer anomalies occurs in the BBAS survey between the Ellsworth Subglacial Highlands (-80 mGals) and the Bentley Subglacial Trench (40 mGals) [*Jordan, et al.*, submitted]. The transitions between regional positive and negative anomalies are more gradual elsewhere.

The regional positive Bouguer anomalies in the AGASEA and BBAS data are connected across the glacier catchment boundaries and are located in areas of the Byrd Subglacial Basin (BSB, Figure 1.2) with thinner crust, especially the deepest topographic

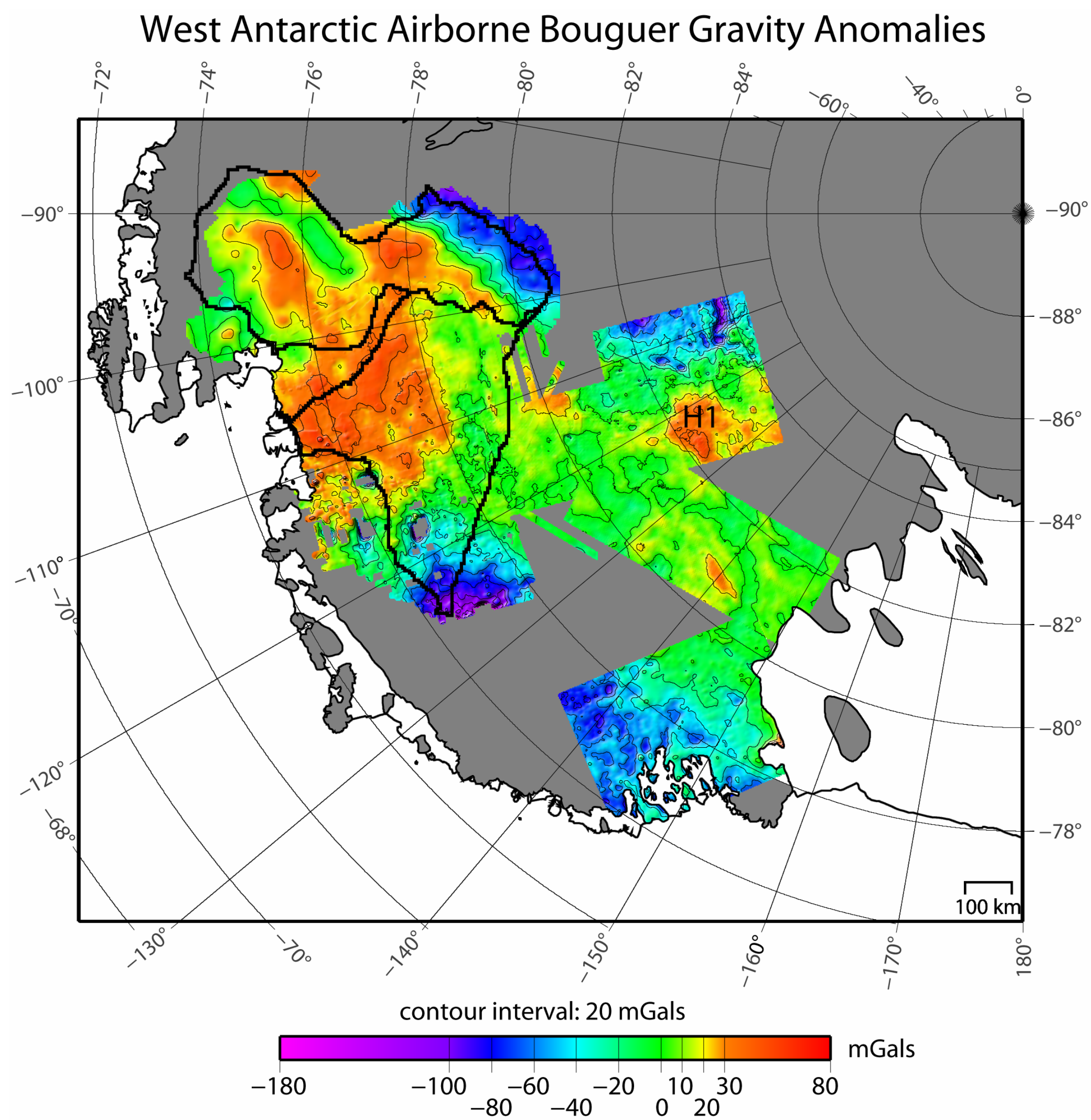

Figure 4.3: Airborne 3D complete Bouguer anomalies across West Antarctica. H1 marks a positive Bouguer anomaly discussed in the text. Thin black line=coastline including ice shelves [*SCAR*, 2006], thick black lines= Pine Island Glacier (PIG) and Thwaites Glacier (TG) catchments [*Vaughan, et al.,* 1999], as in Figure 4.2. Grey areas are ice sheet-covered areas without data.

basins (interpreted as Cenozoic rift troughs in *Jordan, et al.* [submitted]). In the Rose Subglacial Basin (RSB, Figure 1.2), positive Bouguer anomalies of this amplitude are only observed at a few local features (Figure 4.3, e.g. H1).

4.4.3 Discussion

The large regional positive and negative values of the Bouguer anomalies across West Antarctica are indicative of crustal sources. The regional positive anomalies occur in areas where wide-spread Mesozoic rifting has been suggested, while regional negative anomalies occur in areas where crustal blocks have been suggested [*Dalziel and Elliot*, 1982; *Dalziel and Lawver*; 2001]. The gradual changes in the Bouguer anomalies from positive to negative (except the fairly abrupt change at the Ellsworth Mountains-Bentley Subglacial Trench boundary) suggest that West Antarctica is generally characterized by broad zones of crustal change rather than abrupt crustal boundaries. These zones, which occur along the flanks of suggested crustal blocks, are possibly transitional crust, i.e. crust that is partially-rifted, but less so than the area considered to be part of the rift system. The zones are likely the result of heating and thinning of the edges of crustal blocks during the several West Antarctic rifting events. Further classification of the West Antarctic crust can only be attained by calculating crustal thicknesses (or Moho depths, see section 4.5).

The Bouguer anomalies' magnitudes and patterns also suggest that the crust in the Rose Subglacial Basin is fundamentally different (either thicker and/or with more sedimentary infill) than the crust of the Byrd Subglacial Basin. The Bouguer anomalies in the Rose Subglacial Basin are significantly less positive than the Bouguer anomalies within the Byrd Subglacial Basin (anomalies that underlie both major Amundsen Sea Embayment glacier catchments). This difference underscores the need to consider these two basins as separate subglacial features, beyond the topographic observations that they are separated by the Jankowski Subglacial Highlands and that the Byrd Subglacial Basin is generally much deeper.

4.5 Spectral Crustal Structure Estimates

4.5.1 Methods

Although free-air and Bouguer gravity anomalies may be modeled to determine crustal structure, such models are often non-unique. Another method for examining the crust involves calculating the radial power spectrum of gravity data (either free-air or Bouguer anomalies). The power spectrum is calculated by taking the Fourier transform of the dataset (one done in the radial direction may be calculated with the Generic Mapping Tools (GMT) [*Wessel and Smith*, 1998]) and is simply a measure of how much of the gravity signal (i.e. the power in the gravity signal) can be explained by sine waves of a given wavenumber. The wavenumber is similar to frequency, except that wavenumber (k) is [cycles/km] and frequency (f) is [cycles/s] (i.e. the former is for spatial data and the latter is for timeseries).

The radial power spectrum becomes useful for examining crustal structure when it is plotted as the natural log of power (on the y-axis) versus wavenumber (on the x-axis) [*Spector and Grant*, 1970; *Karner and Watts*, 1983; *Fairhead and Okereke*, 1988]. The resulting power spectrum will have decreasing logarithmic power with increasing wavenumber, and the curve can be approximated with several line segments. Each line segment's slope (m) reveals the average depth to a crustal density boundary (d) such that:

$$d_{Moho} = \frac{m}{2}$$

for the example of the Moho density boundary between the crust and the mantle [*Fairhead and Okereke*, 1988] (see Chapter 3 for details, including error estimation). Mirroring gravity datasets across N-S and E-W boundaries enhances the recovery of long-wavelength features [*McNutt*, 1983] for small datasets (such as those 300 x 300 km or smaller) but are not necessary for large data areas purposefully taken for determining the average crustal structure.

Spectral analyses were done over five areas of West Antarctica (Figure 4.4) to determine their average crustal structures. The areas were chosen to: 1. compare the two large subglacial basins (the Byrd and the Rose), both of which were potentially part of wide-scale rifting based on occurrence of positive Bouguer gravity anomalies in each; 2. compare the two surveyed edges of Marie Byrd Land and determine whether the crust there is thin and mantle less dense or the crust there is thick; and 3. compare the crustal thickness numbers from the subglacial basins and Marie Byrd Land to the thicker crustal block containing the Whitmore Mountains.

4.5.2 Results

All power spectra were fit with at least two line segments. The free-air gravity anomalies' spectra showed higher power at shorter wavelengths, suggesting an additional near-surface density boundary. No such power was discernible in the Bouguer gravity anomalies' power spectra. The average actual depths of the ice-bedrock boundaries in each area, from radio-echo sounding are always shallower than the shallowest density boundary from the spectral results (Table 4.3).

The spectral depth estimates indicate a two layer crust, with a mid-crustal boundary varying greatly in depth across West Antarctica, from 6.7 to 13.3 km (Table 4.4). The mid-crustal boundary mimics changes in Moho depth (Table 4.5), generally being deeper in areas of thick crust and shallower in thin crust. Marie Byrd Land has the shallowest mid-crustal boundary of all these estimates and western Marie Byrd Land is the shallowest of all. The two Marie Byrd Land mid-crustal depths are significantly less than the other three estimates, which are similar despite being in different types of crust.

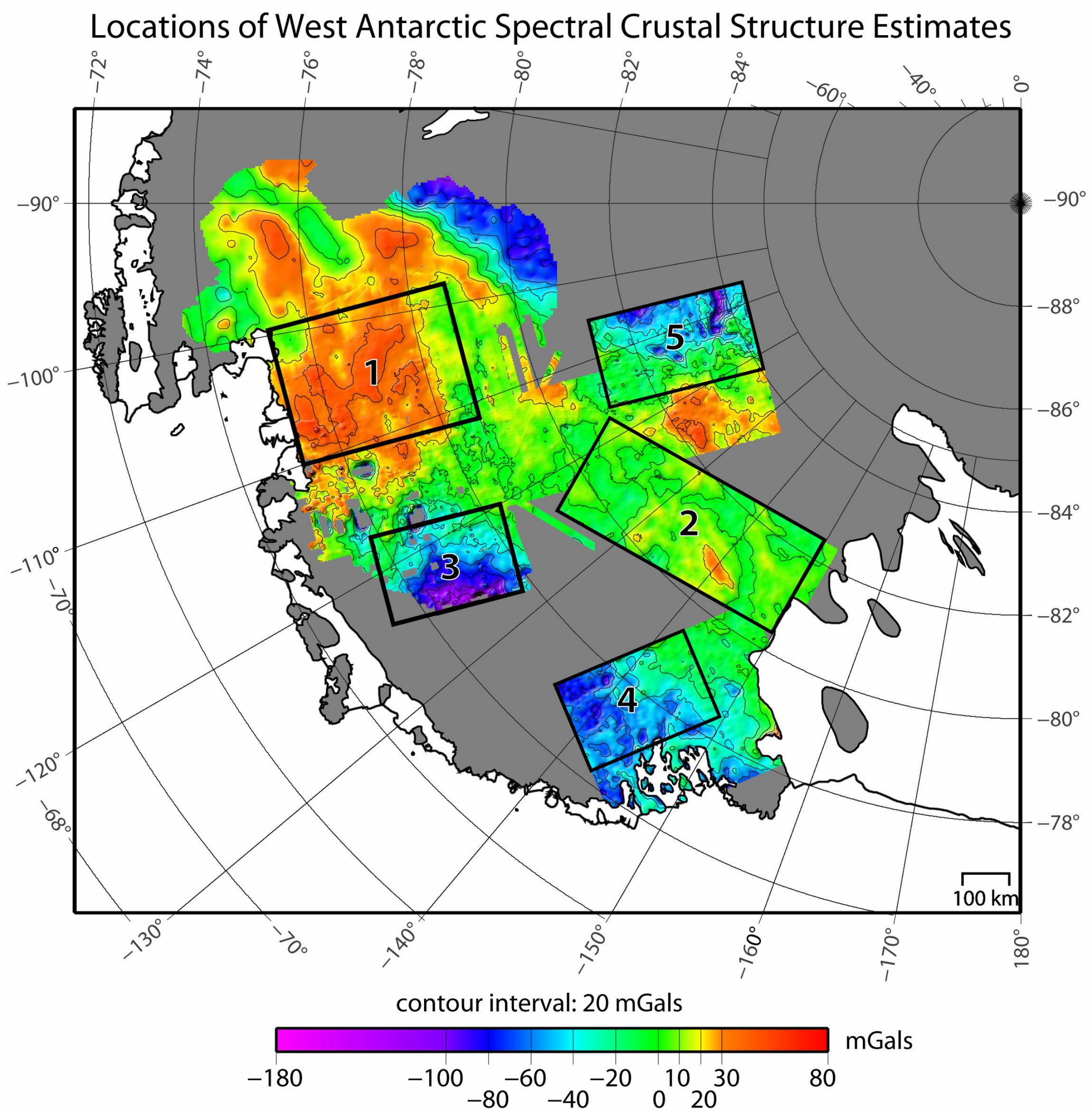

Figure 4.4: Locations of West Antarctic spectral analyses (results listed in Tables 4.3-4.5). Black boxes are numbered according to the areas as listed in the data tables: 1: Byrd Subglacial Basin; 2. Rose Subglacial Basin; 3. Eastern Marie Byrd Land; 4. Western Marie Byrd Land; and 5. Whitmore Mountains. Background image: Airborne Bouguer gravity anomalies for West Antarctica. Ice sheet-covered areas lacking data are grey.

Table 4.3: Shallowest density boundary depths from spectral gravity analyses, compared to actual bedrock elevations

Area name	Area dimensions (East km x North km)	Boundary depths from free-air anomalies (km b.s.l)	Average bedrock depth from radar sounding (km b.s.l.)	Average difference in depth (m)
1. Byrd Subglacial Basin	400 x 300	1.6 +/- 0.1	1.11 $\sigma = 0.37$	490
2. Rose Subglacial Basin	480 x 230	1.9 +/- 0.3	0.71 $\sigma = 0.18$	1190
3. Eastern Marie Byrd Land	Two areas ea. 200 x 200 (Figure 3.6, #16 & 17)	0.4 +/- 0.2 0.7 +/- 0.2 Ave: 0.5 +/- 0.1	0.08 $\sigma = 0.69$	420
4. Western Marie Byrd Land	250 x 300	1.6 +/- 0.1	0.34 $\sigma = 0.42$	1260
5. Whitmore Mountains	200 x 330	0.5 +/- 0.3	0.14 $\sigma = 0.52$	360

Table 4.4: Mid-crustal boundary depths from spectral gravity analyses

Area name	Area dimensions (East km x North km)	Boundary depths from free-air anomalies (km b.s.l)	Boundary depths from Bouguer anomalies (km b.s.l)	Final depth estimates (km b.s.l.)
1. Byrd Subglacial Basin	400 x 300	12.5 +/- 3.7	13.7 +/- 5.1	12.5 +/- 3.7
2. Rose Subglacial Basin	480 x 230	13.1 +/- 1.7	12.7 +/- 1.9	13.0 +/- 1.6
3. Eastern Marie Byrd Land	Two areas ea. 200 x 200 (Figure 3.6, #16 & 17)	7.4 +/- 1.7 11.1 +/- 1.8	7.3 +/- 1.4 10.1 +/- 1.9	7.2 +/- 1.4 10.7 +/- 1.4 Ave: 8.9
4. Western Marie Byrd Land	250 x 300	7.0 +/- 0.5	6.1 +/- 0.7	6.7 +/- 0.2
5. Whitmore Mountains	200 x 330	12.2 +/- 1.0	13.9 +/- 0.6	13.3 +/- 0.1

Table 4.5: Moho depths and crustal thicknesses from spectral gravity analyses

Area name	Area dimensions (East km x North km)	Boundary depths from free-air anomalies (km b.s.l)	Boundary depths from Bouguer anomalies (km b.s.l)	Final depth estimates (km b.s.l.)	Crustal thickness* (km)
1. Byrd Subglacial Basin	400 x 300	26.9 +/- 3.8	25.4 +/- 5.6	26.9 +/- 3.8	25.8 +/- 3.8
2. Rose Subglacial Basin	480 x 230	24.5 +/- 3.7	29.8 +/- 2.9	27.5 +/- 0.7	26.8 +/- 0.7
3. Eastern Marie Byrd Land	Two areas ea. 200 x 200 (Figure 3.6, #16 & 17)	25.6 +/- 3.7 20.3 +/- 4.2	19.5 +/- 2.9 22.5 +/- 3.8	22.2 +/- 0.2 21.6 +/- 2.9 Ave: 21.9	21.8
4. Western Marie Byrd Land	250 x 300	27.1 +/- 3.0	21.9 +/-1.2	23.0 +/- 0.2	22.7 +/- 0.2
5. Whitmore Mountains	200 x 330	30.3 +/- 1.3	31.7 +/- 0.6	31.4 +/- 0.3	31.3 +/- 0.3

* Crustal thickness is Moho depth (Table 4.5, col. 5) minus the depth of ice-bedrock boundary (Table 4.3, col. 4)

The average crustal thicknesses estimated with this method for the Byrd Subglacial Basin and for the Rose Subglacial Basin are similar, within error, and approximately 26-27 km. The Whitmore Mountains crust is thicker, at ~31 km, and the crust in Marie Byrd Land (east and west) is thinnest at 22-23 km. These last three estimates have fairly small errors associated with them, while the Byrd Subglacial Basin estimate has a large error.

4.5.3 Discussion

The shallowest spectrally-defined density boundary, which is always deeper than the ice-rock boundary, could potentially be due to the combination of near-surface density contrasts between: ice, bedrock, sedimentary basins, and water. Since the density contrast between ice and water is much lower than the contrast between ice and sedimentary rock, any disparity between the depth of the shallow density contrast and actual bedrock depths could be indicating changes in the thickness of subglacial sediment. If this is indeed the case, then the crust-ice boundary in the Whitmore Mountains, eastern Marie Byrd Land, and Byrd Subglacial Basin is a fairly clean surface (i.e. only small amounts of subglacial sediment) while the Rose Subglacial Basin and western Marie Byrd Land would have the most subglacial sediment.

The spectrally-defined crustal thickness estimates for the two major basins (the Byrd Subglacial Basin and Rose Subglacial Basin) are very similar to nearby receiver function estimates of crustal thickness (25-28 km) [*Winberry and Anandakrishnan*, 2004]. These two methods of estimating crustal thickness are not easily comparable however, since the spectral method returns the average crustal thickness over a large area while the receiver function estimates return crustal thickness for a single location. The low variation in crustal thickness estimates in the Rose Subglacial Basin from *Winberry and Anandakrishnan* [2004] could either result from the fortuitous placement of the seismic sites, or it could be reflecting a true homogeneity of the crust within that basin. Comparatively, the error for the spectrally-estimated crustal thickness in the Rose Subglacial Basin is low (+/- 0.7 km) and that for the Byrd Subglacial Basin is high (+/- 3.8 km). In fact, the more detailed analyses of the Byrd Subglacial Basin in Chapter 3 have already shown that the basin is characterized by both very thin (~19 km) and thicker (~28 km) crust. One interpretation is that the seismic and spectral estimates are indicating significantly more heterogeneity in the crust of the Byrd Subglacial Basin compared to the relative homogeneity in the crust of the Rose Subglacial Basin. Either way, both basins are part of the large-scale Mesozoic rifting that occurred in West Antarctica.

The Whitmore Mountains' ~31 km spectrally-defined Moho depth estimate is reasonable given the adjacent 28-30 km depth transitional crust [*Clarke, et al.*, 1997] and given that my estimate was taken over both the transitional crust and the edge of the mountains. Here, transitional crust is defined as partially-rifted crust, with a composition and thickness between those of continental and oceanic crust (L. Lawver, pers. comm, 2008). This transitional crust is more rifted than the crustal blocks and less rifted than the basin floors of the West Antarctic Rift System. The Ellsworth Mountains (Figure 4.2), to the northeast of the Whitmore Mountains, are part of the same crustal block [*Dalziel and Elliot*, 1982; *Dalziel and Lawver*, 2001] and have an average Moho depth that is 4 km deeper [*Jordan, et al.*, submitted] than that for the Whitmore Mountains. Slightly thicker crust in the Ellsworth Mountains is not surprising since 1. the Bouguer anomalies of the Ellsworth Mountains are more negative than those in the Whitmore Mountains and 2. the Ellsworth Mountains are topographically higher, necessitating a thicker Airy isostatic root to maintain equilibrium.

In contrast, the Moho depth estimates for both portions of Marie Byrd Land are very shallow, as shown previously for eastern Marie Byrd Land (Chapter 3) but contradictory to the only existing Moho depth estimate (31 km) in western Marie Byrd Land [*Luyendyk, et al.*, 2003]. The *Luyendyk, et al.* [2003] estimate assumed that the crust there was Airy isostatically compensated with a deep Moho; whereas this study's Moho depth estimate was done independently of any isostatic assumptions. If the topography in Marie Byrd Land were Airy isostatically compensated, the Moho depth would be 30-31 km in the west [*Luyendyk, et al.*, 2003] and >38 km in the east (Chapter 3). The new spectral estimates imply that the Moho in western Marie Byrd Land is of very similar depth to that in eastern Marie Byrd Land. Both sets of mountains are thus significantly undercompensated (by 6.3-9.3 km in the east (Chapter 3) and 7-8 km in the west) and their heights must be explained by a method of support other than Airy isostasy. Thermal support by warm mantle, as previously suggested for eastern Marie Byrd Land (Chapter 3) and the flank of central Marie Byrd Land [*Winberry and Anandakrishnan*, 2004], is also a possible method of compensation for western Marie Byrd Land.

No matter the type of compensation, these spectral estimates clearly show that the crust in Marie Byrd Land (both east and west) is very thin despite its high elevation; in fact, it is thinner than the crust in the rift basins. Perhaps labeling Marie Byrd Land as a crustal block was appropriate for describing its crustal thickness prior to the Cretaceous (see Chapter 1), but labeling it as transitional crust is currently more appropriate given its thin, highly rifted crust. The history of events in Marie Byrd Land could be laid out in terms of crustal effects: 1. exploited by arc magmatism from subduction outboard until the Mesozoic; 2. thinned in the wide-spread early Cretaceous rifting associated with the opening of the Ross Sea and creation of the Byrd and Rose Subglacial Basins; 3. rifted in late Cretaceous when New Zealand broke away; 4. overprinted in the Oligocene (and into at least the Pleistocene) by additional volcanism and uplifted into its current domal shape, possibly by plume-induced, thermal uplift. Such a history of thinning and volcanic exploitation could easily produce the 22-23 km thick transitional crust found in Marie Byrd Land.

4.6 Crustal Boundary Interpretation Map

4.6.1 Methods

A commonly-used sketch map of the West Antarctic crustal blocks was created by *Dalziel and Elliot* [1982] (modified by *Dalziel and Lawver* [2001]). Given the amount of new geophysical data available (both gravity and radar-derived subglacial topography; Figures 4.5 - 4.7), it is now possible to significantly update their crustal boundary interpretations. Re-interpreting crustal boundaries involves both locating the position of boundaries and defining the type of boundary that occurs.

Here, crustal boundaries are re-located first by using airborne gravity interpretations and then by applying the topographical/morphological constraints first set out by *Dalziel and Elliot* [1982]. In order of importance (most to least), the detailed criteria for defining boundaries in this study are:

a. A regional gradient in the Bouguer gravity anomalies, generally from positive to negative.

b. Significant changes in crustal thickness numbers from spectral analyses of free-air and Bouguer gravity anomalies.

c. Information from exposed rock outcrops (Figures 4.9 - 4.12, Index Figure 4.8) or other geophysical datasets (such as magnetic anomalies) that place the area within a given crustal block or rifted area.

d. Continuations of similar bedrock topography that extend from already-interpreted boundaries, as found in the newest radar-derived subglacial topography datasets.

e. Breaks in the morphology of subglacial topography, as found in the newest radar-derived subglacial topography datasets.

f. When no new data exist for an onshore area, the previously-interpreted boundaries [*Dalziel and* Elliot, 1982; *Dalziel and* Lawver, 2001] are left unchanged.

g. Trend changes in the satellite free-air gravity anomalies (which reflect changes in sub-ice and submarine topography), mostly for offshore areas.

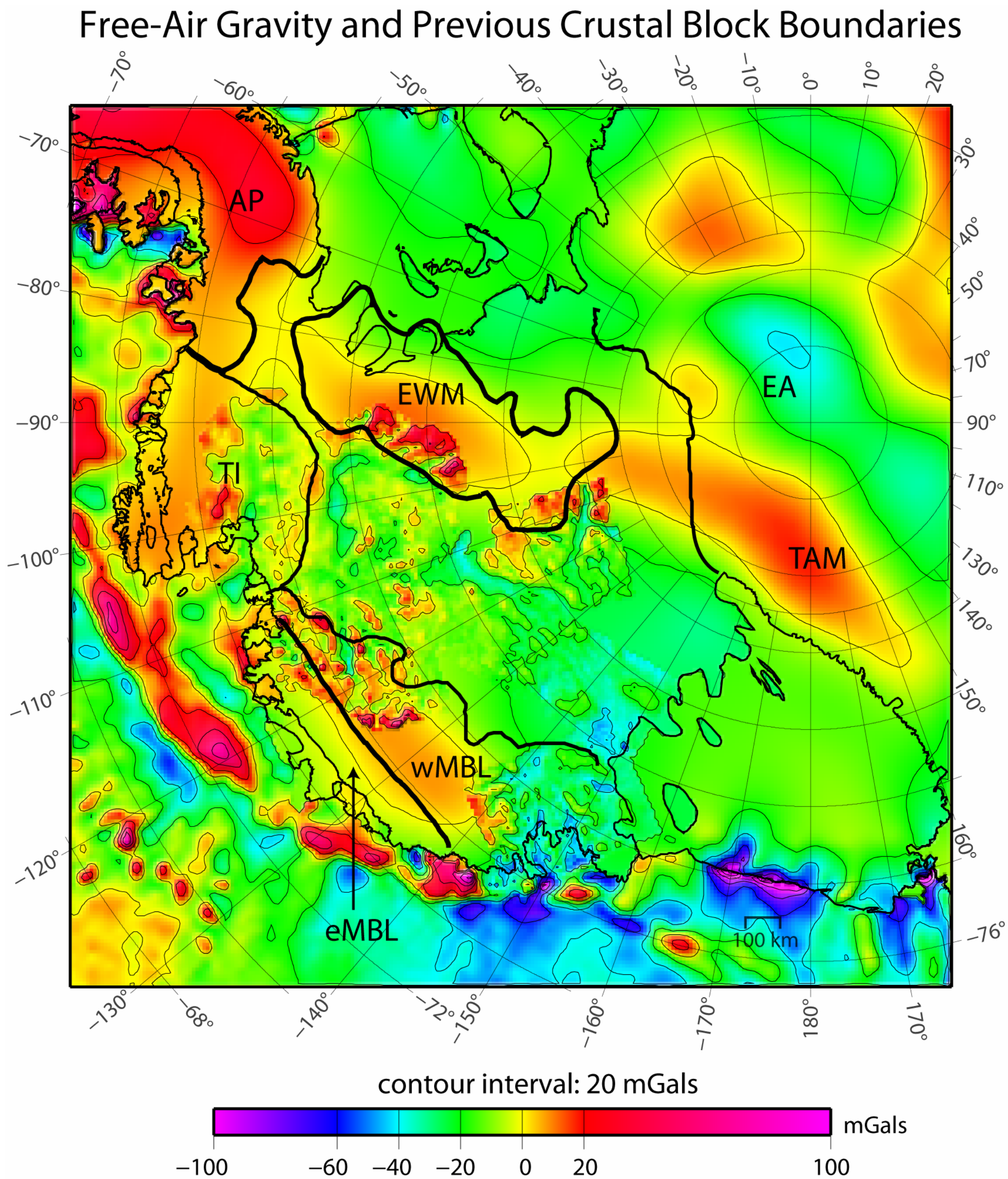

Figure 4.5: Free-air gravity compilation overlaid with hypothesized crustal block boundaries (thick black lines) from *Dalziel and Elliot* [1982] (modified by *Dalziel and Lawver* [2001]). Thin black line=coastline including ice shelves [*SCAR*, 2006]; AP=Antarctic Peninsula; EWM-Ellsworth-Whitmore Mountains; TI=Thurston Island; EA=East Antarctica; eMBL = eastern Marie Byrd Land; wMBL = western Marie Byrd Land; TAM=Transantarctic Mountains.

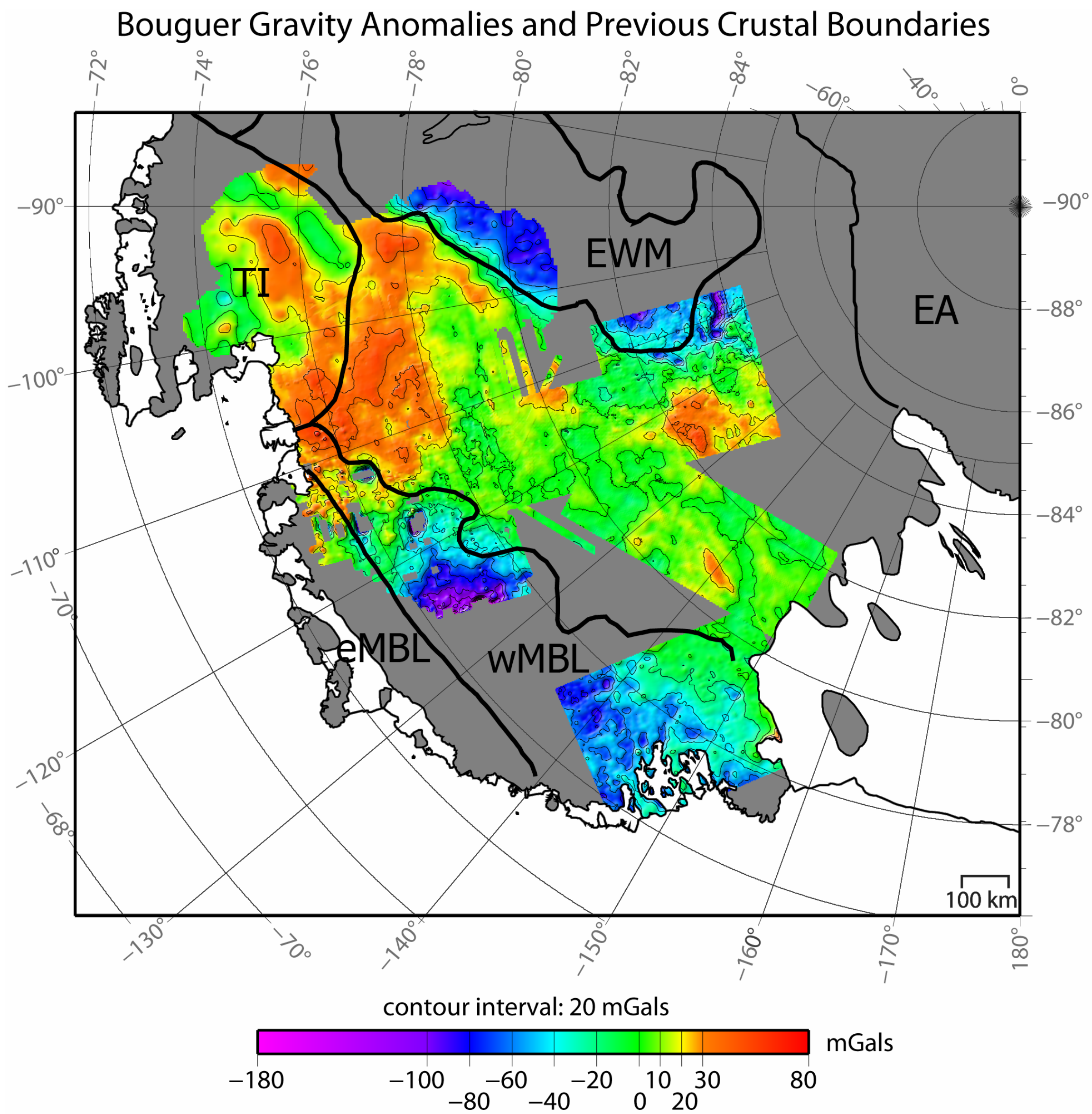

Figure 4.6: Airborne Bouguer anomalies compilation overlaid with hypothesized crustal block boundaries (thick black lines) from *Dalziel and Elliot* [1982](modified by *Dalziel and Lawver* [2001]). Thin black line=coastline including ice shelves [*SCAR*, 2006]; EWM-Ellsworth-Whitmore Mountains; TI=Thurston Island; EA=East Antarctica; eMBL = eastern Marie Byrd Land; wMBL = western Marie Byrd Land. Ice sheet-covered areas with no data are grey.

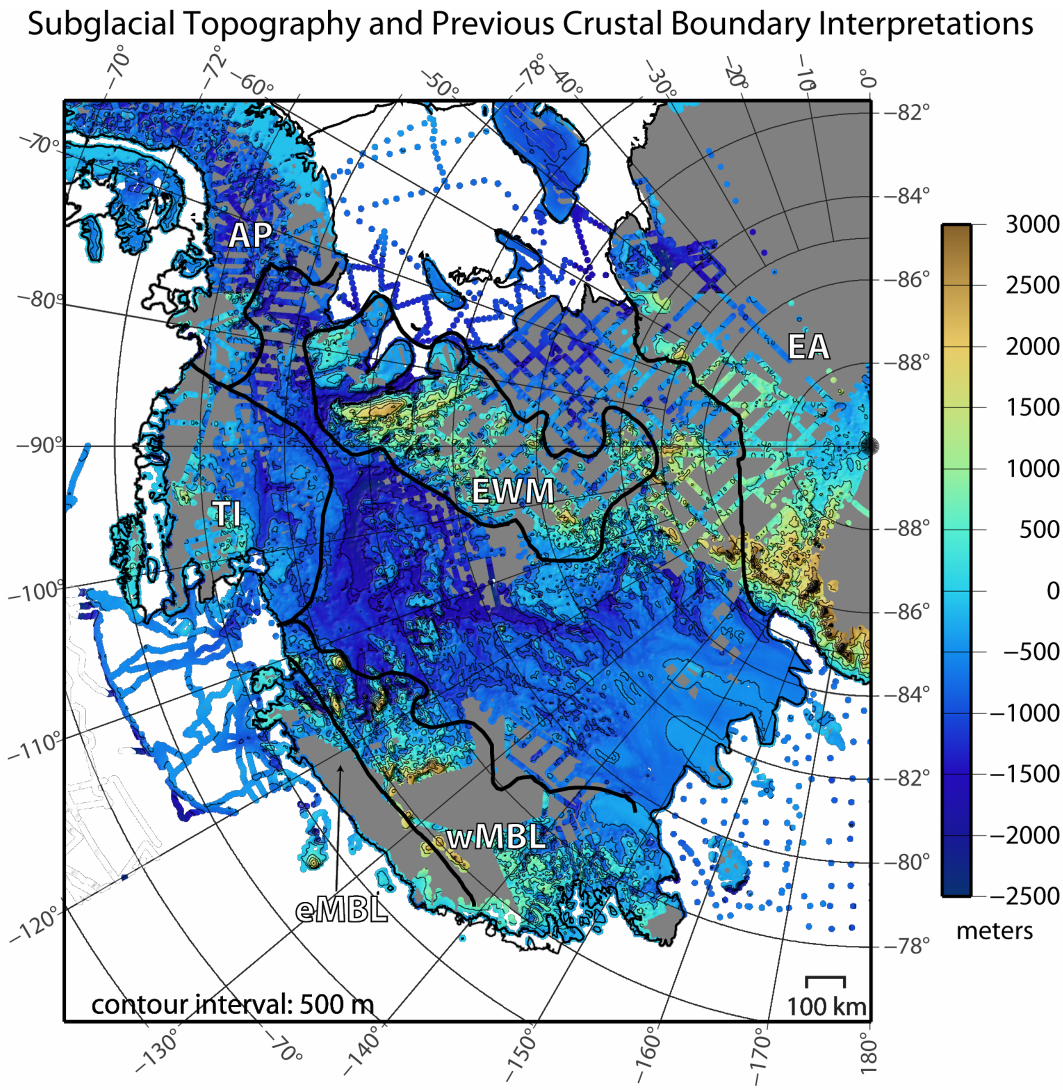

Figure 4.7: Bedrock topography, primarily from radar, overlaid with hypothesized crustal block boundaries (thick black lines) from *Dalziel and Elliot* [1982](modified by *Dalziel and Lawver* [2001]). Thin black line=coastline including ice shelves [*SCAR*, 2006]; AP = Antarctic Peninsula; EWM-Ellsworth-Whitmore Mountains; TI=Thurston Island; EA=East Antarctica; eMBL = eastern Marie Byrd Land; wMBL = western Marie Byrd Land. Ice sheet-covered areas with no data are grey.

Re-defining crustal boundaries also involves defining the type of boundary observed. Data is limited in West Antarctica, but crustal boundaries can generally be grouped into: a. transitional zone boundaries or b. distinct boundaries. Transitional zones are defined mostly by the wide gradient of the regional Bouguer gravity anomalies along a crustal boundary, which is indicative of partially-rifted edges along the crustal blocks. Crustal thickness estimates from gravity (Chapter 3 and Section 4.5) and seismic [e.g. *Clarke et al.,* 1997] show that these pieces of transitional crust separate crustal elements where at least one side is (and sometimes both sides are) thicker than the transitional crust. Distinct boundaries are either areas where regional Bouguer gravity anomalies have a steep gradient or areas in which topographically-defined boundaries occur in space-limited areas between crustal blocks. From this definition, distinct boundaries are most likely to be characterized by crustal-scale faulting and abrupt changes in rock lithology on either side of the boundary. All other boundaries occur in areas where there is limited subglacial information. These remaining boundaries are simply of 'unknown' type, until enough data is collected along their lengths to warrant classifying them as either transitional zones or distinct boundaries.

4.6.2 Results/Discussion

Application of Criteria (a) through (c)

First, crustal block boundaries are interpreted from the Bouguer gravity anomaly map of West Antarctica (Figure 4.13). This step takes into account criteria (a) through (c) for each of the several boundaries located in the Bouguer gravity data area. Since certain criteria (and sources of information) were weighted differently for each boundary decision, a brief overview of the boundary placements is necessary.

Boundary section #1 (Figure 4.13) falls between the Ellsworth Mountains

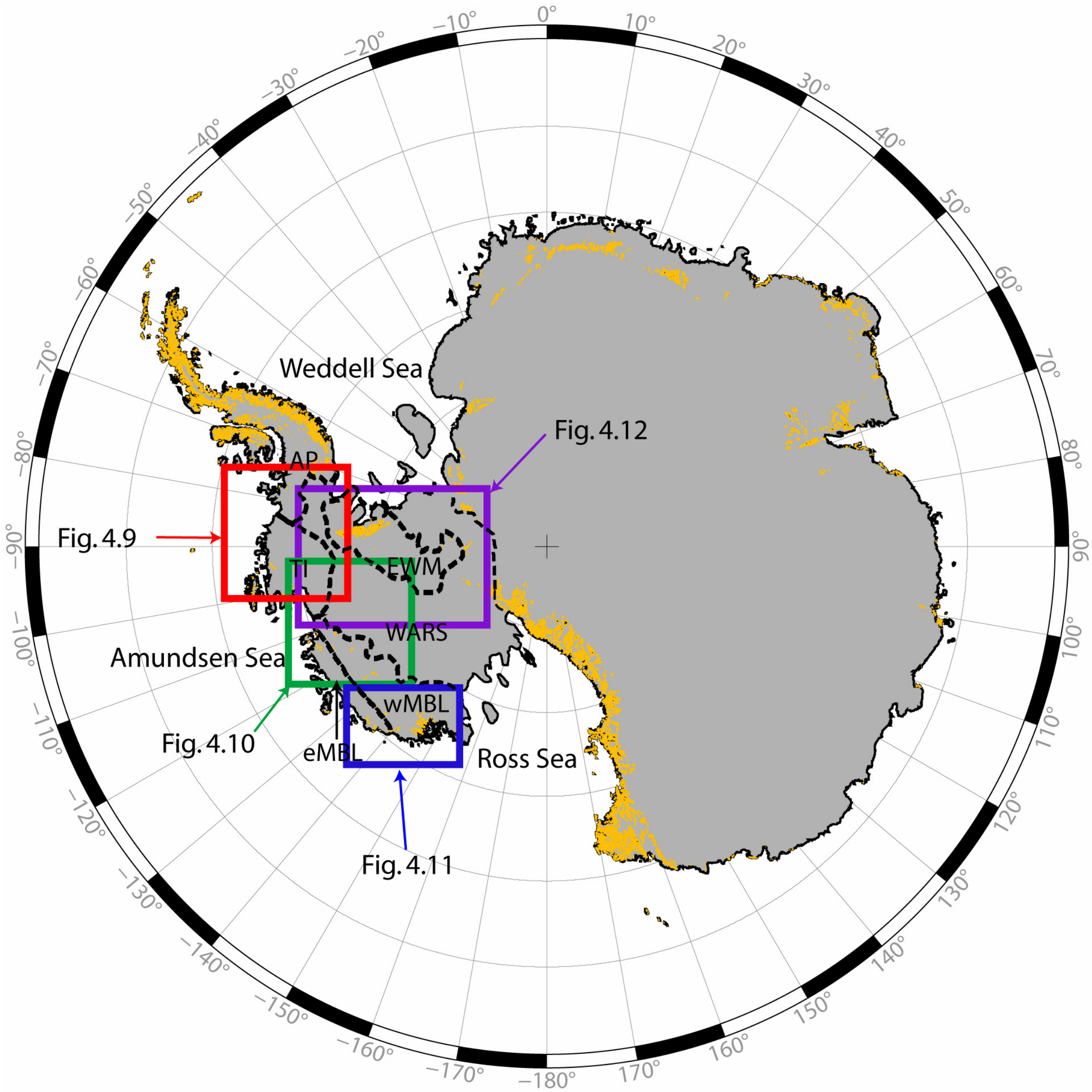

Figure 4.8: Antarctic Index Map for Figures 4.9 through 4.12. Also shown: rock outcrop locations (gold lines) from the Antarctic Digital Database [*SCAR*, 2006] and West Antarctic crustal blocks (dashed, thick back lines) [*Dalziel and Elliot*, 1982; *Dalziel and Lawver*, 2001]. Crustal block names: AP= Antarctic Peninsula; TI= Thurston Island; EWM= Ellsworth-Whitmore Mountains; WARS= West Antarctic Rift System; eMBL and wMBL= eastern and western Marie Byrd Land.

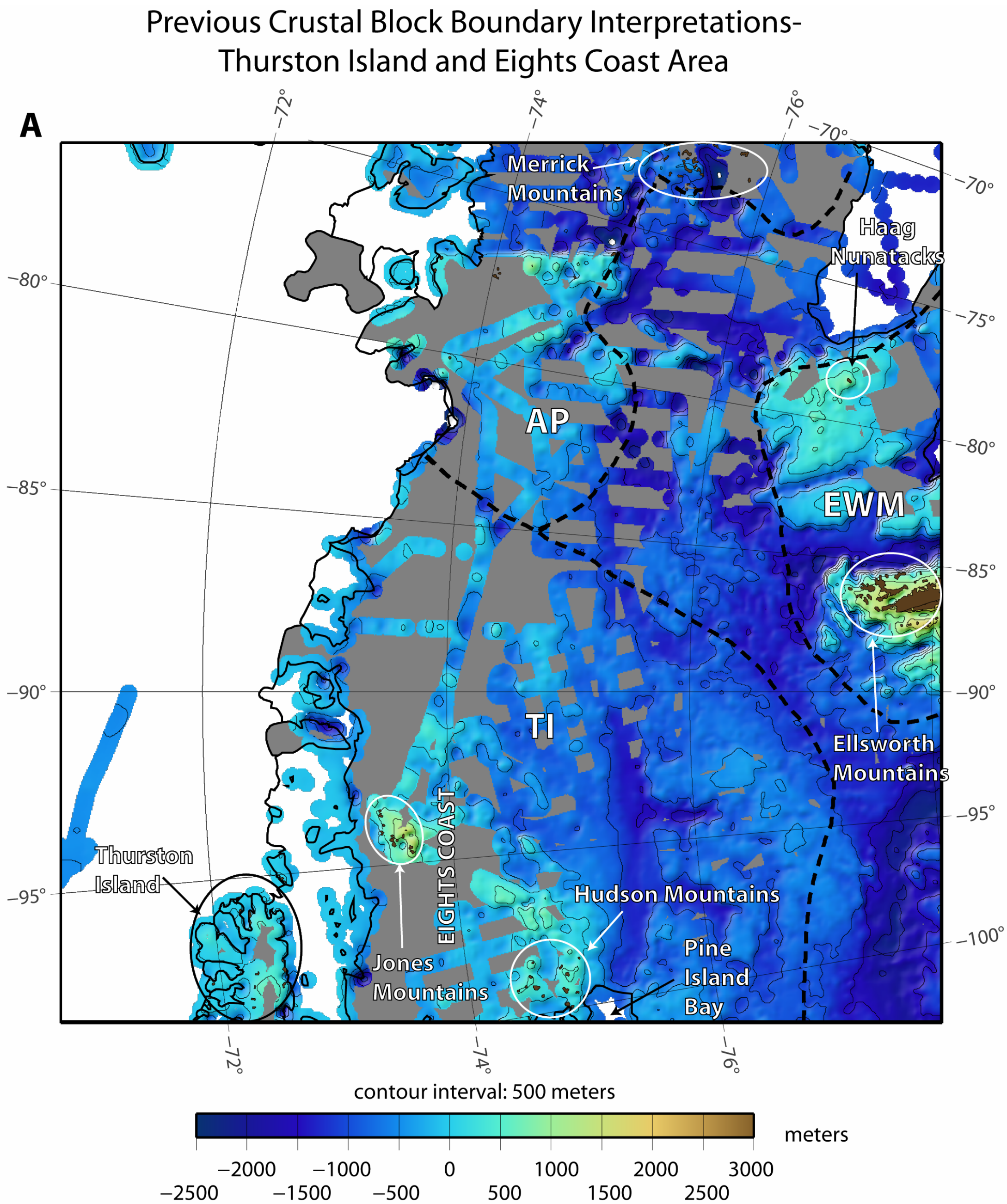

Figure 4.9A: Thurston Island – Eights Coast rock outcrop locations (brown-filled lines) from the Antarctic Digital Database [*SCAR*, 2006] and West Antarctic crustal blocks (dashed, thick black lines) [*Dalziel and Elliot*, 1982; *Dalziel and Lawver*, 2001]. Outcrops are overlain on subglacial topography, primarily from radar sounding [*Lythe, et al.,* 2001] (D. Young, unpub., data, 2008). Crustal block names: AP= Antarctic Peninsula; TI= Thurston Island; EWM= Ellsworth-Whitmore Mountains. Outcrop locations mentioned in the text are circled and labeled, as well as the Merrick Mountains for reference.

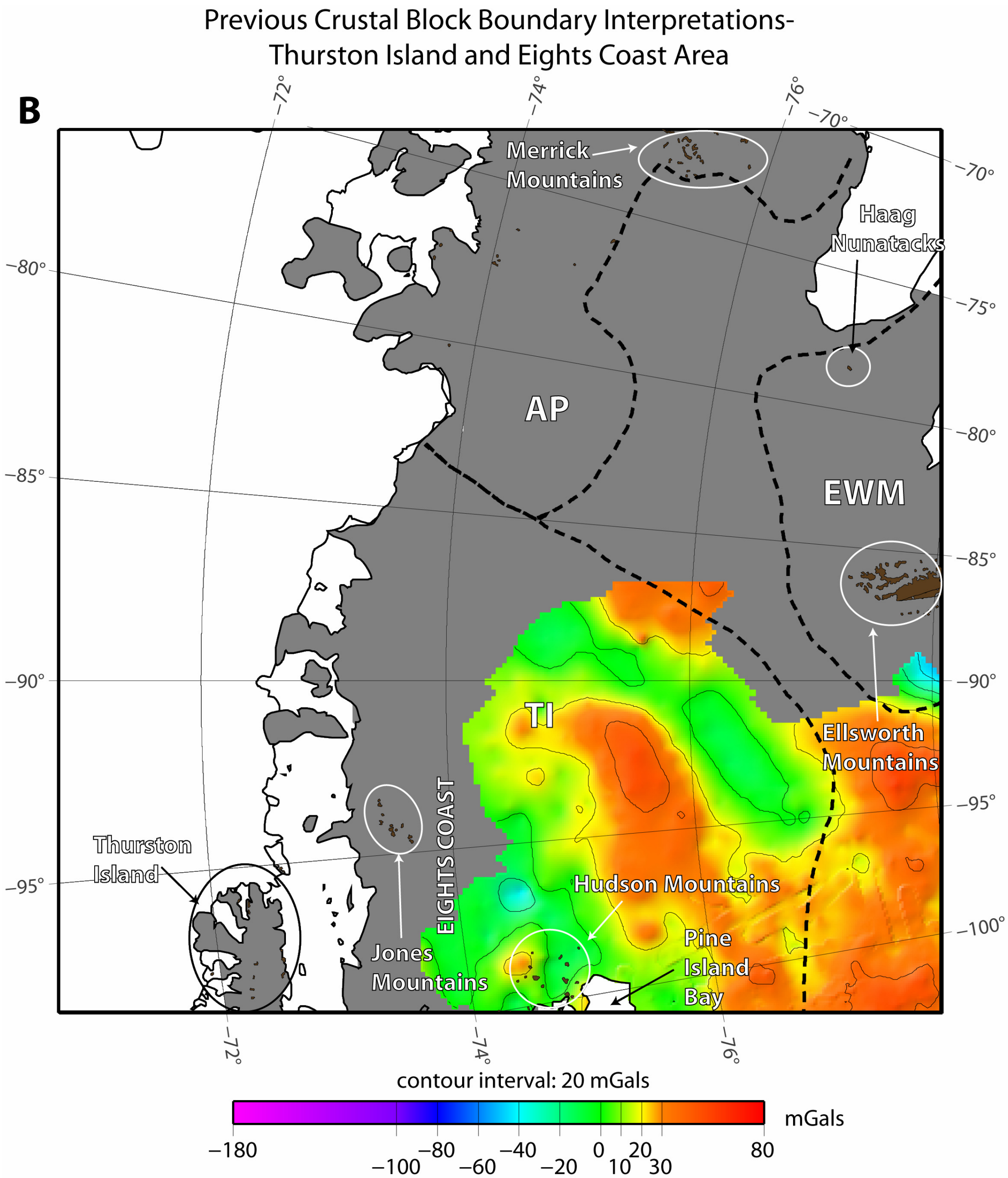

Figure 4.9A: Thurston Island – Eights Coast rock outcrop locations (brown-filled lines) from the Antarctic Digital Database [*SCAR*, 2006] and West Antarctic crustal blocks (dashed, thick black lines) [*Dalziel and Elliot*, 1982; *Dalziel and Lawver*, 2001]. Outcrops are overlain on the airborne Bouguer gravity anomaly compilation from this study (Figure 4.3). Crustal block names: AP= Antarctic Peninsula; TI= Thurston Island; EWM= Ellsworth-Whitmore Mountains. Outcrop locations mentioned in the text are circled and labeled, as well as the Merrick Mountains for reference.

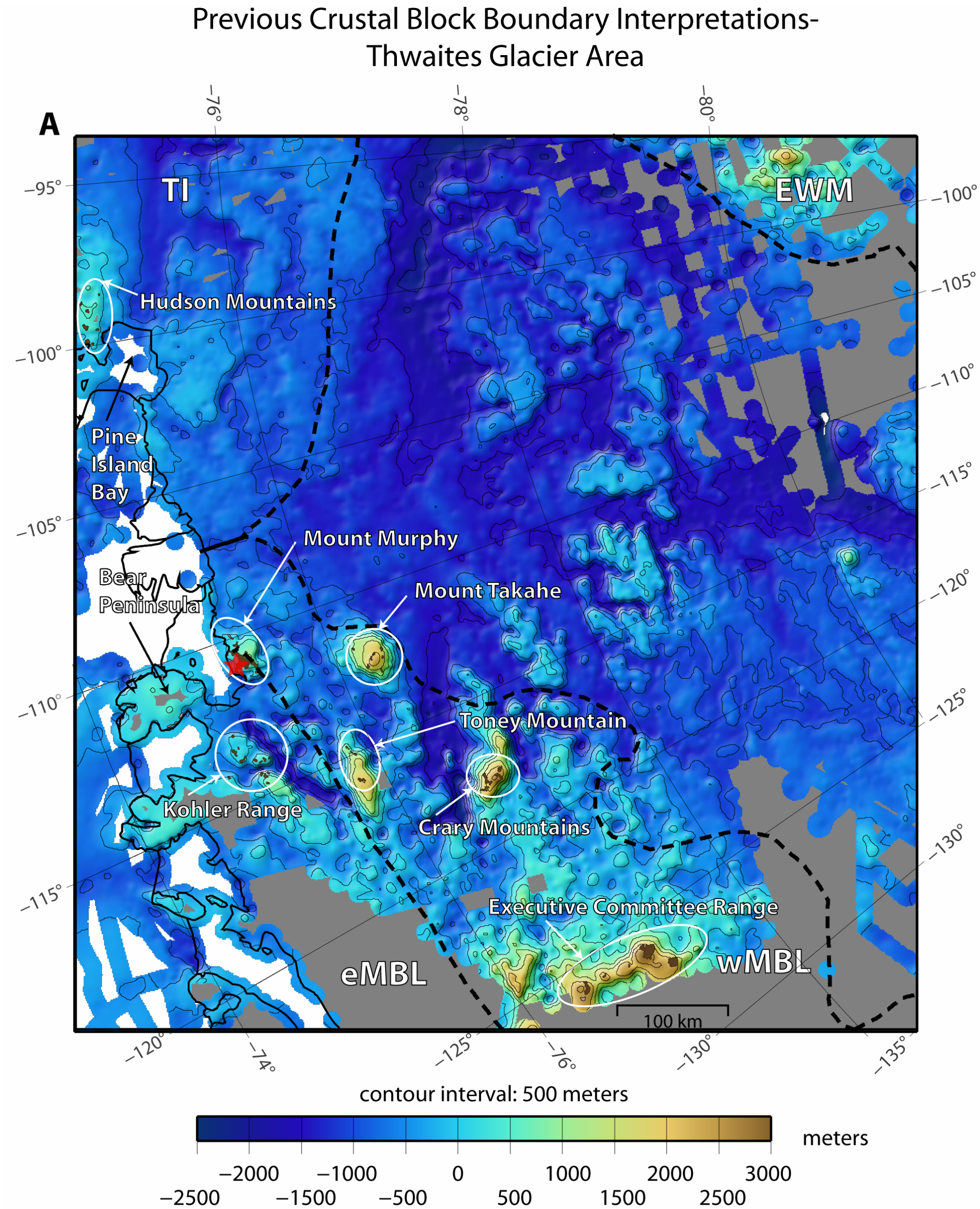

Figure 4.10A: Thwaites Glacier area rock outcrop locations (brown-filled lines) from the Antarctic Digital Database [*SCAR*, 2006] and West Antarctic crustal blocks (dashed, thick black lines) [*Dalziel and Elliot*, 1982; *Dalziel and Lawver*, 2001]. Outcrops are overlain on subglacial topography, primarily from radar sounding [*Lythe, et al.,* 2001] (D. Young, unpub., data, 2008). Crustal block names: TI= Thurston Island; EWM= Ellsworth-Whitmore Mountains; eMBL and wMBL= eastern and western Marie Byrd Land. Outcrop locations mentioned in the text are circled and labeled, as well others for reference. The red star on Mount Murphy marks the location of Kay Peak.

Previous Crustal Block Boundary Interpretations-
Thwaites Glacier Area

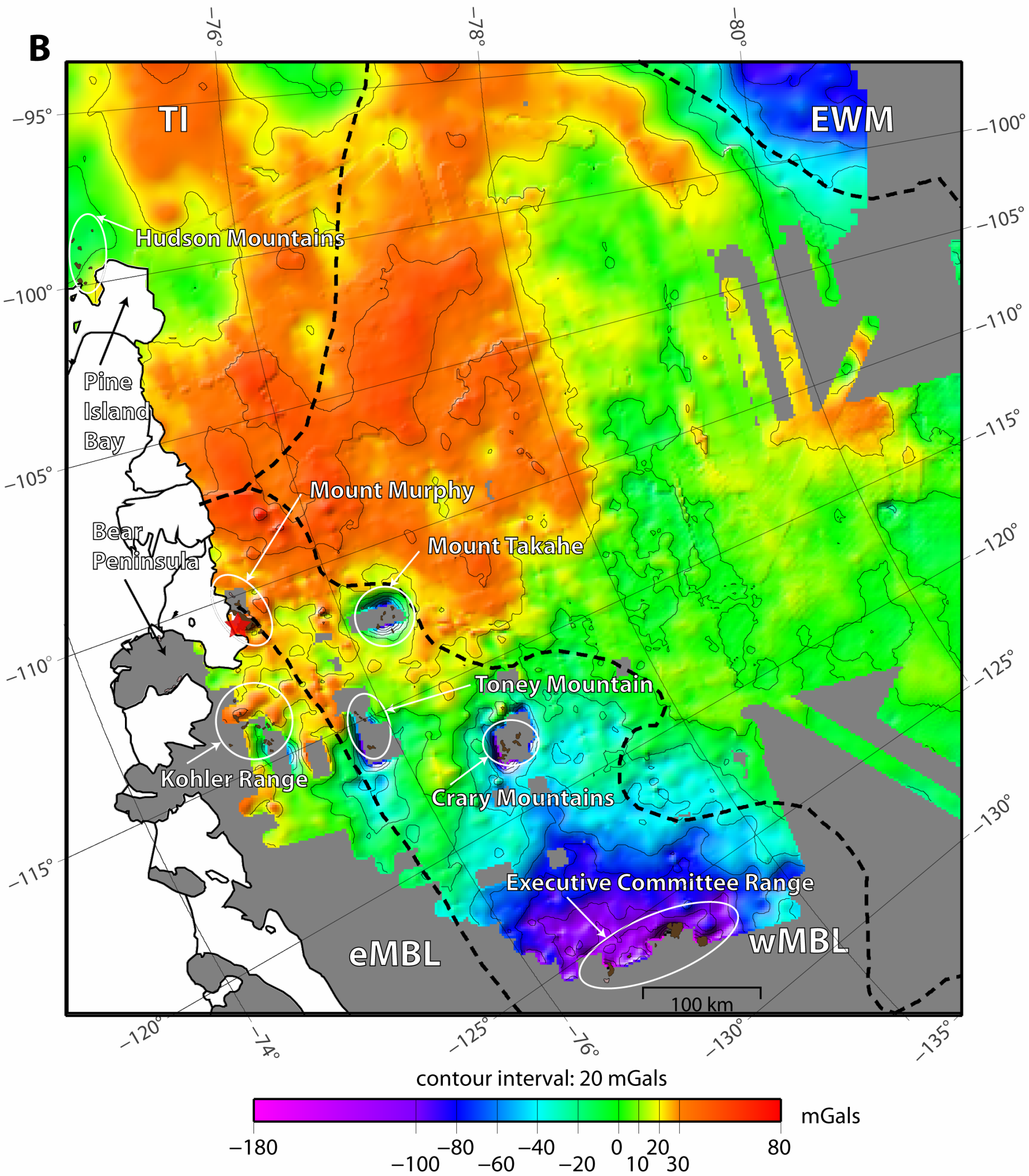

Figure 4.10B: Thwaites Glacier area rock outcrop locations (brown-filled lines) from the Antarctic Digital Database [*SCAR*, 2006] and West Antarctic crustal blocks (dashed, thick black lines) [*Dalziel and Elliot*, 1982; *Dalziel and Lawver*, 2001]. Outcrops are overlain on the airborne Bouguer gravity anomaly compilation from this study (Figure 4.3). Crustal block names: TI= Thurston Island; EWM= Ellsworth-Whitmore Mountains; eMBL and wMBL= eastern and western Marie Byrd Land. Outcrop locations mentioned in the text are circled and labeled, as well others for reference. The red star on Mount Murphy marks the location of Kay Peak.

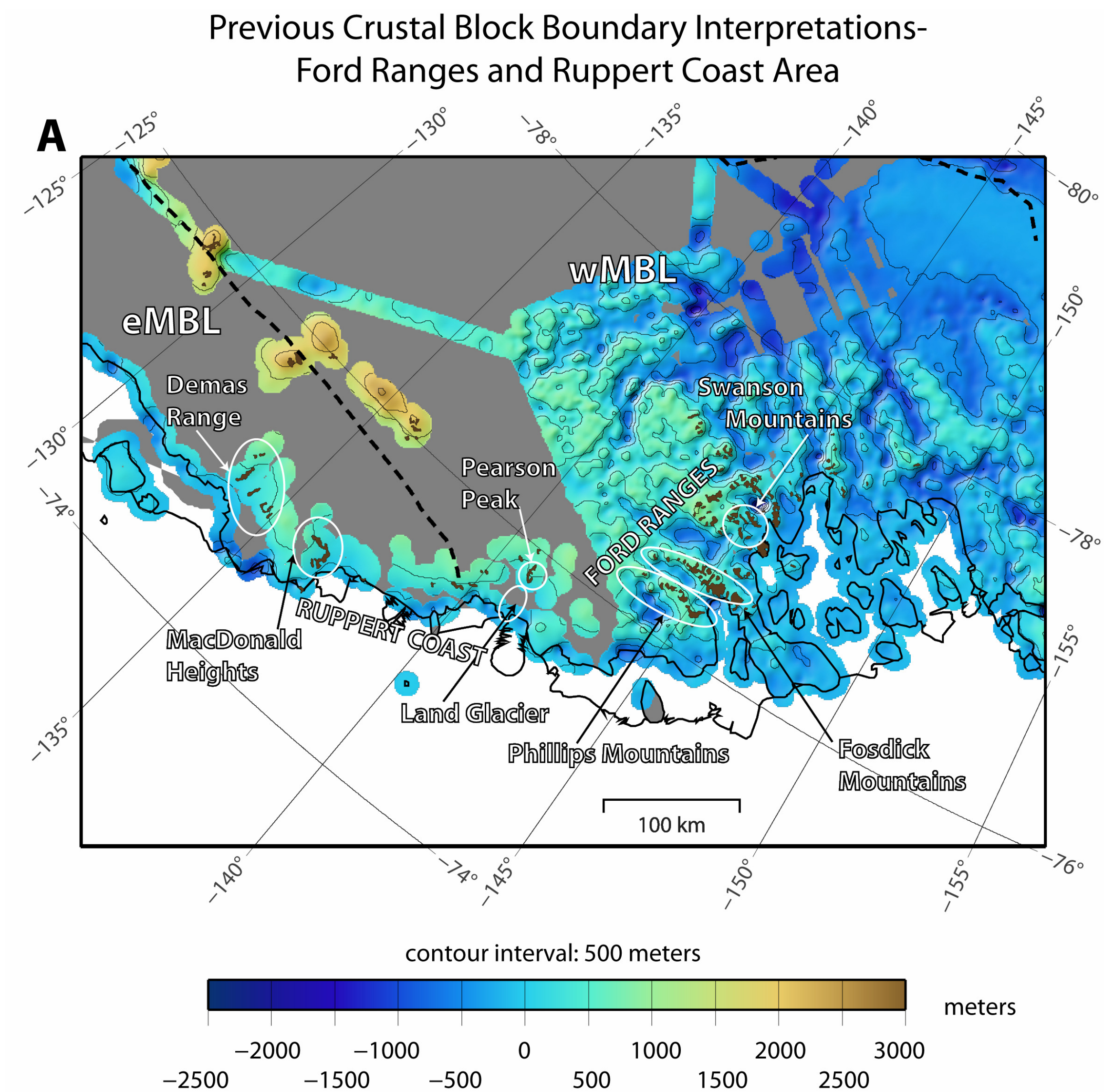

Figure 4.11A: Western Marie Byrd Land (Ford Ranges – Ruppert Coast) rock outcrop locations (brown-filled lines) from the Antarctic Digital Database [*SCAR*, 2006] and West Antarctic crustal blocks (dashed, thick black lines) [*Dalziel and Elliot*, 1982; *Dalziel and Lawver*, 2001]. Outcrops are overlain on subglacial topography, primarily from radar sounding [*Lythe, et al.,* 2001] (D. Young, unpub., data, 2008). Crustal block names: eMBL and wMBL= eastern and western Marie Byrd Land. Outcrop locations mentioned in the text are circled and labeled, as well as a few others for reference.

Previous Crustal Block Boundary Interpretations-
Ford Ranges and Ruppert Coast Area

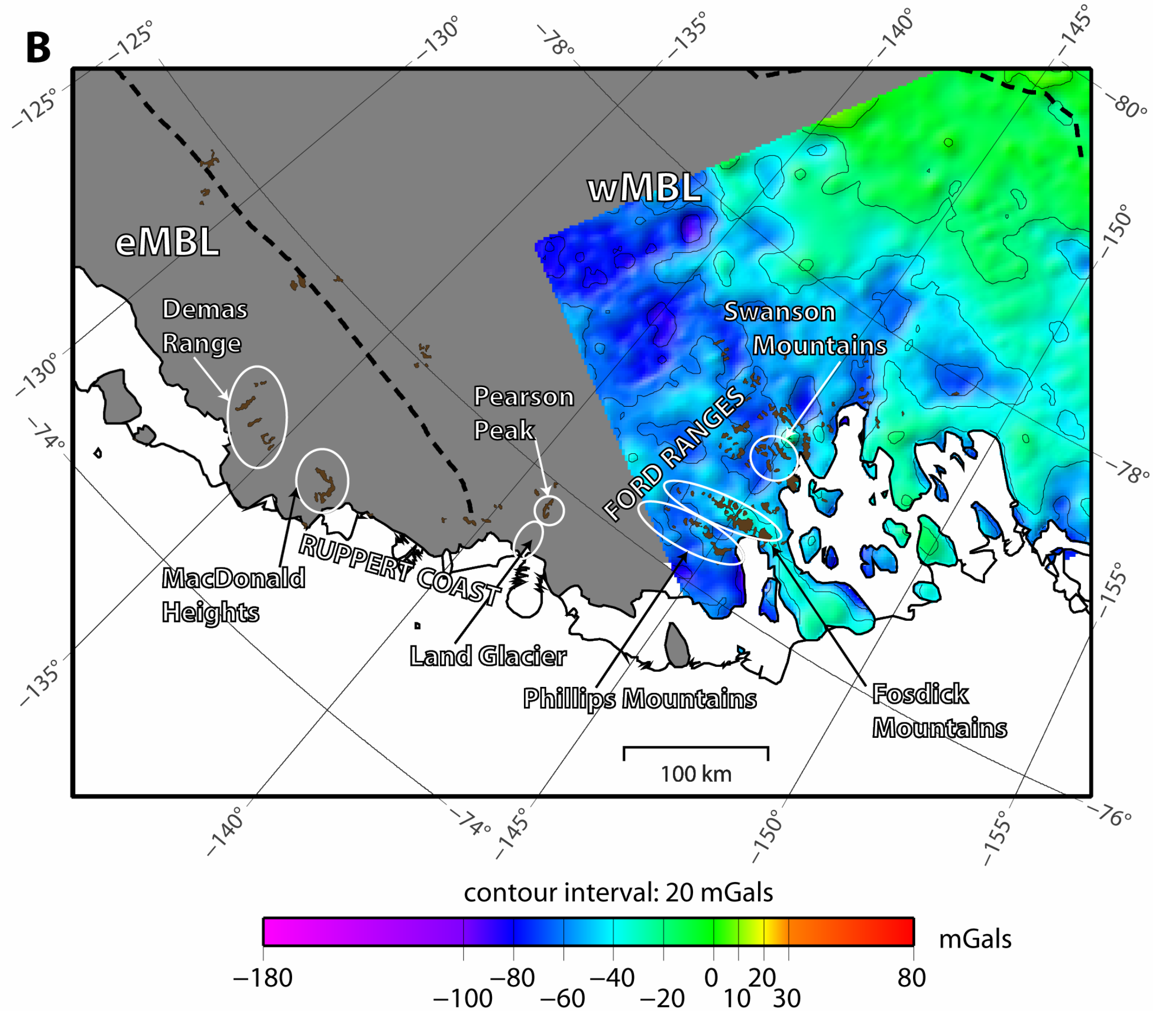

Figure 4.11B: Western Marie Byrd Land (Ford Ranges – Ruppert Coast) rock outcrop locations (brown-filled lines) from the Antarctic Digital Database [*SCAR*, 2006] and West Antarctic crustal blocks (dashed, thick black lines) [*Dalziel and Elliot*, 1982; *Dalziel and Lawver*, 2001]. Outcrops are overlain on the airborne Bouguer gravity anomaly compilation from this study (Figure 4.3). Crustal block names: eMBL and wMBL= eastern and western Marie Byrd Land. Outcrop locations mentioned in the text are circled and labeled, as well as a few others for reference.

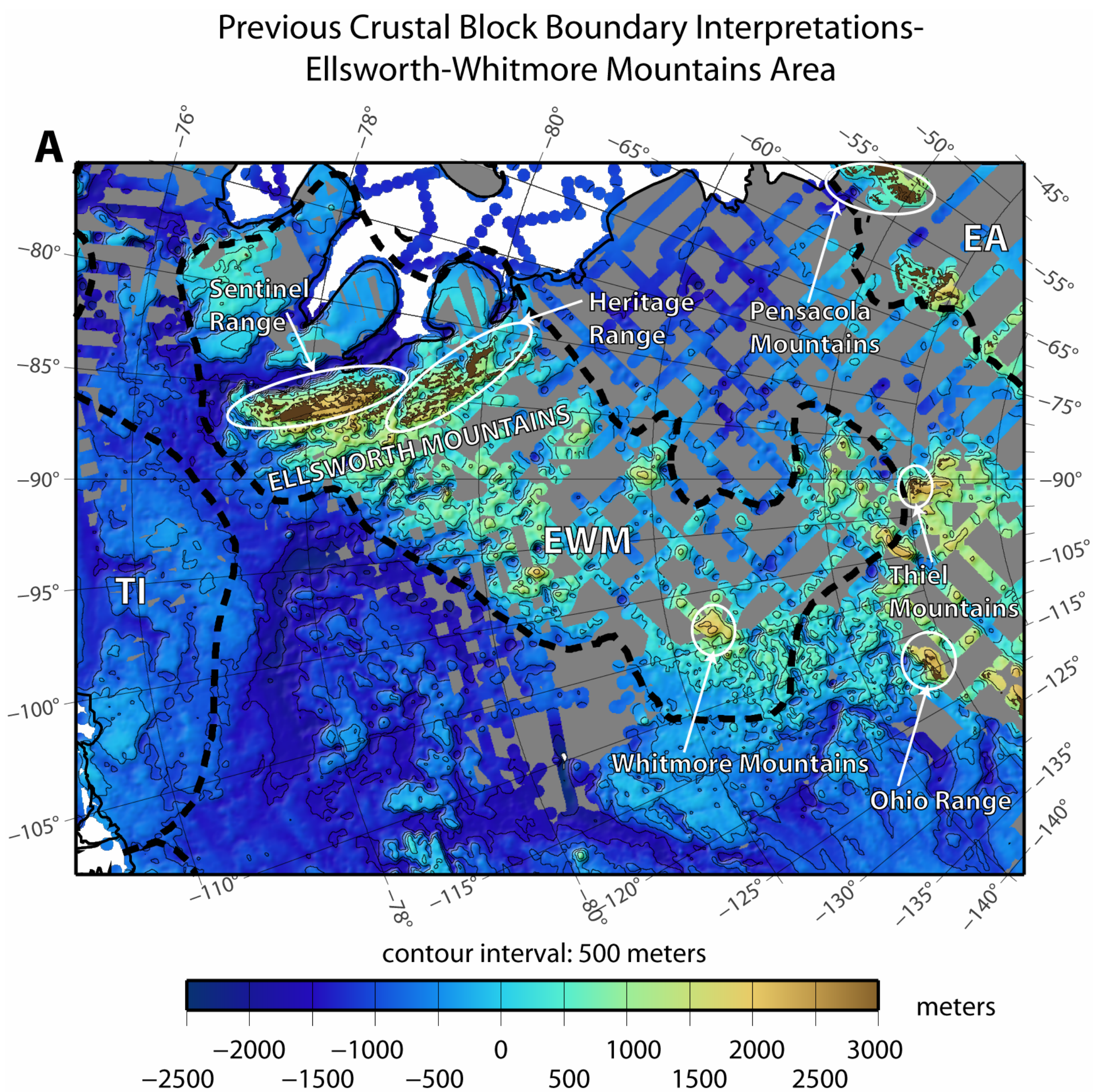

Figure 4.12A: Ellsworth-Whitmore Mountains area rock outcrop locations (brown-filled lines) from the Antarctic Digital Database [*SCAR*, 2006] and West Antarctic crustal blocks (dashed, thick black lines) [*Dalziel and Elliot*, 1982; *Dalziel and Lawver*, 2001]. Outcrops are overlain on subglacial topography, primarily from radar sounding [*Lythe, et al.,* 2001] (D. Young, unpub., data, 2008). Crustal block names: AP= Antarctic Peninsula; TI= Thurston Island; EWM= Ellsworth-Whitmore Mountains. Outcrop locations mentioned in the text are circled and labeled, as well as others for reference.

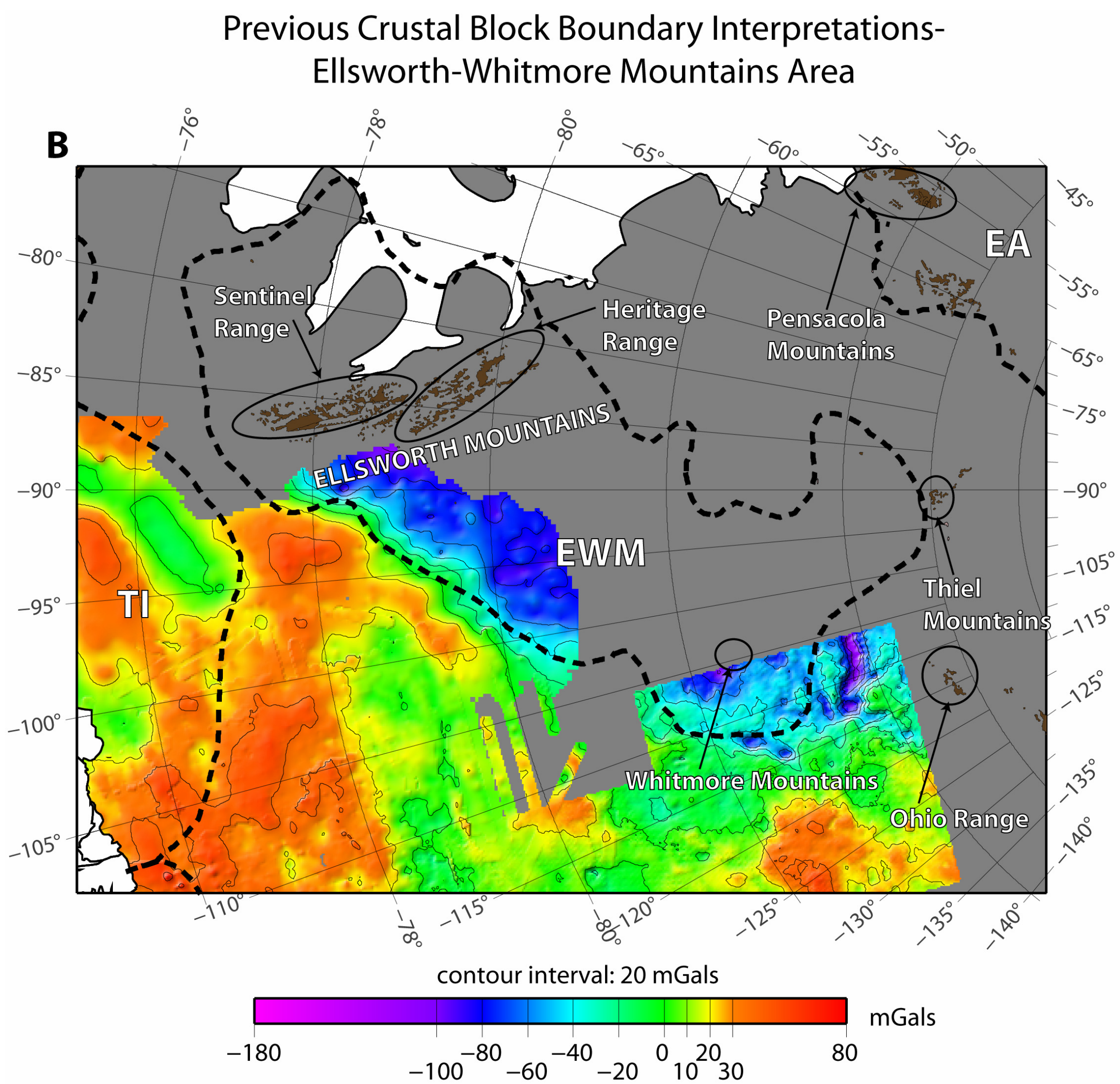

Figure 4.12B: Ellsworth-Whitmore Mountains area rock outcrop locations (brown-filled lines) from the Antarctic Digital Database [*SCAR*, 2006] and West Antarctic crustal blocks (dashed, thick black lines) [*Dalziel and Elliot*, 1982; *Dalziel and Lawver*, 2001]. Outcrops are overlain on the airborne Bouguer gravity anomaly compilation from this study (Figure 4.3). Crustal block names: AP= Antarctic Peninsula; TI= Thurston Island; EWM= Ellsworth-Whitmore Mountains. Outcrop locations mentioned in the text are circled and labeled, as well as others for reference.

(Figures 4.9 and 4.12B) and the Bentley Subglacial Trench (Figure 4.2) [*Jordan, et al.,* submitted]. The Bouguer gravity anomaly gradient along the boundary is strikingly steep and the Moho deepens by ~6 km across the only ~50 km distance between the trench and the mountains [*Jordan, et al.,* submitted]. This section of the Ellsworth-Whitmore block boundary is certainly a distinct section, with no geophysical evidence for transitional crust between the block and the trench.

Boundary section #2 (Figure 4.13) lies between the Whitmore Mountains (Figure 4.12B) and the Rose Subglacial Basin (Figures 4.2 and 1.9). The Bouguer gravity anomalies, alone, are adequate to place the southern edge of the boundary against the mountains (Figure 4.13), roughly continuing from boundary section #1 across the data gap. Contrary to the case of boundary segment #1, there is a wide area of crust just north of the mountain front that is characterized by a very low Bouguer gravity gradient, indicating a transitional rather than a distinct crustal boundary here. The existence of transitional crust there was identified by *Clarke, et al.* [1997], whose wide-angle refraction seismic study showed crustal thicknesses of 28-30 km in this area. Therefore, this boundary is taken as a transitional zone that extends from the mountain front north, to the edge of steeper gradient Bouguer anomalies (Figure 4.13).

The boundary (#3, Figure 4.13) between the Rose Subglacial Basin (Figure 4.2) and the western edge of Marie Byrd Land (Figure 4.11B) is characterized by an area of low-gradient Bouguer anomalies. The gradual nature of the Bouguer anomalies makes them alone insufficient to place the location of the crustal boundary, but does indicate that the boundary is a transitional zone and not distinct. Studies of the rock outcrops in the Ford Ranges (Figure 4.11B) suggest that they are associated with the Marie Byrd Land block [*Siddoway*, 2008] and the crustal boundary must be south of there. Airborne

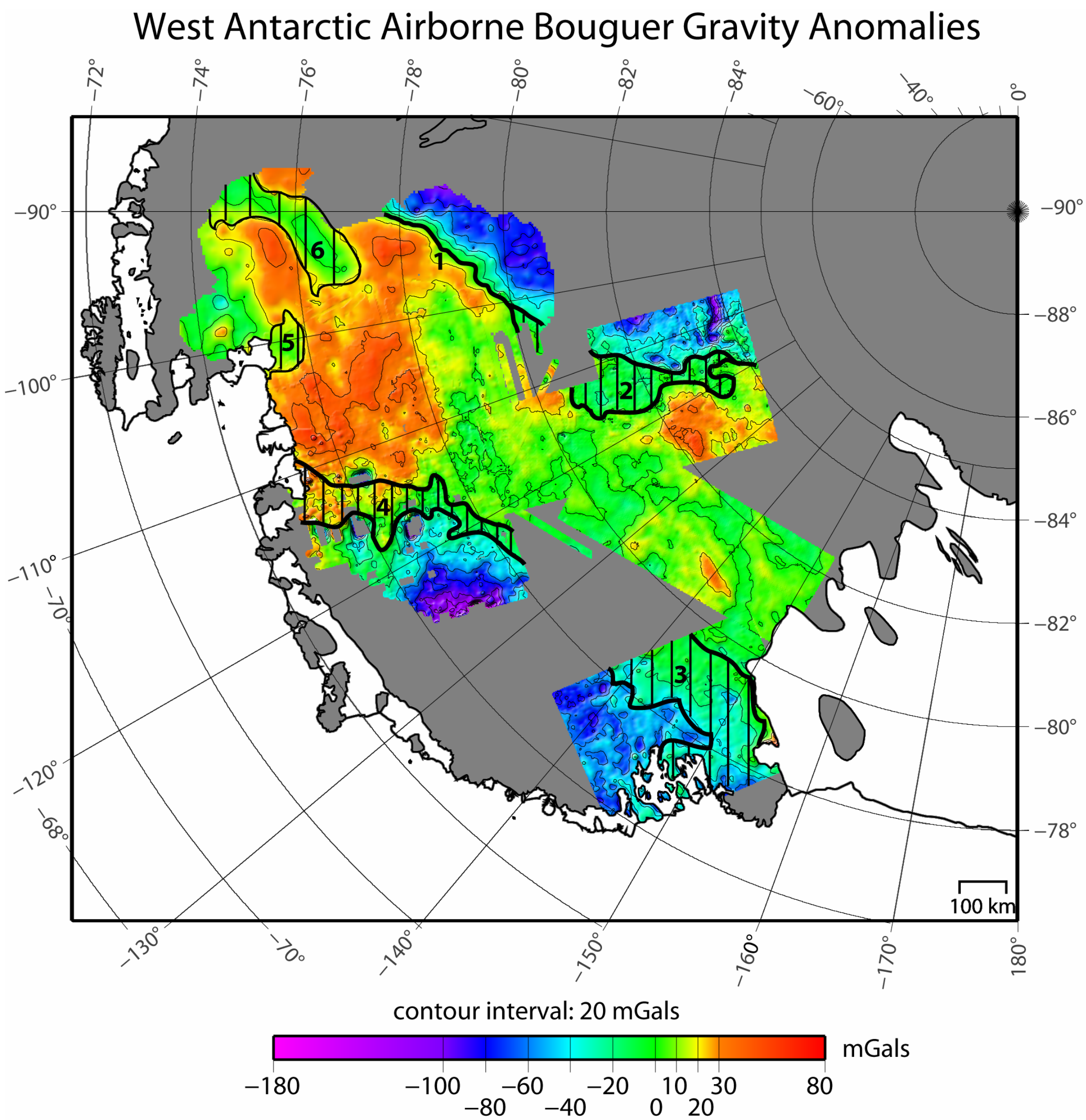

Figure 4.13: The first portion of this study's new crustal block boundary interpretations, which fall within the area covered by airborne Bouguer gravity anomalies. Boundaries were identified based on criteria (a) through (c) and are marked by boundary type: transitional crust zone= two heavy black lines separated by an area of vertical hatches; distinct boundary= single heavy black line. Boundary sections labeled with numbers are discussed in the text. Background image: airborne Bouguer gravity anomalies for West Antarctica, compiled by this study (see Section 4.4). Thin black line= coastline, including ice shelves [*SCAR*, 2006]. Ice sheet-covered areas lacking data are in grey.

magnetic results for the area [*Luyendyk, et al., 2003*] revealed a subglacial volcanic field (characterized by high-amplitude magnetic anomalies) extending southward to approximately 79.5°. The initial interpretation of boundary #3 thus places the northern side of the Marie Byrd Land boundary (Figure 4.13) along the steeper-gradient Bouguer anomalies to the north of the area with the high-amplitude magnetic anomalies, also satisfying the geological evidence [*Siddoway*, 2008].

Boundary section #4 (Figure 4.13) has already been discussed in Chapter 3, though we define the boundary further here as a transitional zone. Lines of evidence for its location include the character of the Bouguer anomalies along its southern half (Chapter 3 and Figure 4.13), shallow Moho depths along the boundary's length from spectrally-analyzed gravity anomalies (Chapter 3), and a zone of high-amplitude magnetic anomalies running through the area [*Holt, et al., 2007*] that are similar to those along the western Marie Byrd Land boundary (discussed above). An additional constraint is that Mount Takahe (Figure 4.10B) is different from the other surrounding volcanoes because it appears to have been emplaced entirely in the Cenozoic, within the last 0.5 million years [*LeMasurier and Thompson*, 1990]. Interestingly, the Bouguer anomalies surrounding Mount Takahe are more related to the Byrd Subglacial Basin (Figure 4.2) regional Bouguer positive anomaly than the Marie Byrd Land regional negative anomaly (Figure 4.10B). Thus, the volcano appears to have erupted on the Byrd Subglacial Basin side of the transitional crustal boundary zone and so is not interpreted as part of the Marie Byrd Land crustal block (Figure 4.13).

The transitional crust piece labeled as #5 (Figure 4.13) represents the roughly zero-magnitude Bouguer anomaly area to the south of Pine Island Glacier, partly within that glacier's catchment and partly within the adjacent unnamed catchment (Figure 4.2). The area is characterized by an anomalously deep (~30 km) Moho, as found from spectral gravity analyses (Table 3.2, Figure 3.8). A larger piece of transitional crust, labeled as #6 in Figure 4.13 and fully within in the Pine Island Glacier catchment (Figure 4.2), has been identified here on the similar grounds as piece #5. The crustal thickness in that area is 24-26 km [*Jordan, et al.,* submitted], which is deeper than the surrounding thin crust of the Byrd Subglacial Basin (Figure 4.2). Both areas, however, contain no rock outcrop data and so their boundaries could be subject to further refinement in the next interpretation step, by applying boundary location criteria (d) through (f).

As is already apparent from interpreting the new Bouguer gravity anomaly compilation (Figure 4.13), the *Dalziel and Elliot* [2001] (modified by *Dalziel and Lawver* [2001]) boundary of the Thurston Island crustal block (Figures 4.6B, 4.9B, and 4.10B) is the least concordant with the new gravity data. The Thurston Island block is much smaller than previously identified [*Dalziel and Elliot*, 1982; *Dalziel and Lawver*, 2001] and it is questionable whether the Hudson Mountains (Figure 4.9B) are located on that crustal block, based on boundary location criteria (a) through (c). The Hudson Mountains have only Cenozoic volcanics exposed [*LeMasurier and Thompson*, 1990]. The easterly neighboring Jones Mountains' (Figure 4.9B) oldest exposed volcanics date to only 200 Ma (early Jurassic) [*Pankhurst, et al.*, 1993]. Neither set of mountains can be used to place the current boundary of the Thurston Island crustal block (Figure 4.13).

Application of Criteria (d) through (f)

The next three criteria for placing the West Antarctic crustal boundaries are based mostly on the character of the subglacial topography. The second set of interpreted boundaries was therefore created by overlaying the first set of new boundaries on the subglacial topography and then modifying and extending those boundaries according to the new criteria (Figure 4.14). Criterion (c) was also re-visited in many places to account for rock outcrops now represented with the subglacial topography that were not within the Bouguer gravity anomaly data area. Again, systematic consideration of boundary changes is necessary because of the varying types and quality of information available in each area. The boundaries numbered in Figure 4.14 are different from those numbered in Figure 4.13.

Boundary section #1 (Figure 4.14) occurs at the northeastern end of the Ellsworth-Whitmore crustal block. The Ellsworth Mountains (Figure 4.12A) are bounded there by a steep topographic break represented by a narrow, incised valley (Figure 4.14). However, there is evidence from rock outcrops that the Haag Nunataks, to the northeast of that valley, (Figure 4.9A) are related to the Ellsworth Mountains [*Dalziel and Elliot*, 1982] and so should be within the outermost boundary of the crustal block. The nunataks and adjacent subglacial topographic highs are also separated from each other by deep, narrow valleys, indicating extension between the more rigid crustal pieces. Thus, this boundary is a transitional zone, though its topographic expression of extension is different from the other transitional zone boundaries already interpreted (Figure 4.13).

Boundary segment #2 represents the boundary between the Ellsworth-Whitmore block and East Antarctica. First, geologic investigations of the rock outcrops in the Thiel Mountains (Figure 4.12A), Pensacola Mountains (Figure 4.12A), and Berkner Island (Figure 4.14) place each of these within East Antarctica [*Dalziel and Elliot*, 1982]. Second, there is a morphological break (narrow valley) within the Whitmore Mountains area (Figure 4.14, where the East Antarctic boundary meets the Ellsworth-Whitmore boundary in the north), which is the only indication of a crustal boundary there since the topography is similarly mountainous on both sides of the break. From there, the East Antarctic boundary (of unknown type because of the scarcity of topographic data there) roughly follows the edge of higher terrain, relative to the low-lying extended crust of the

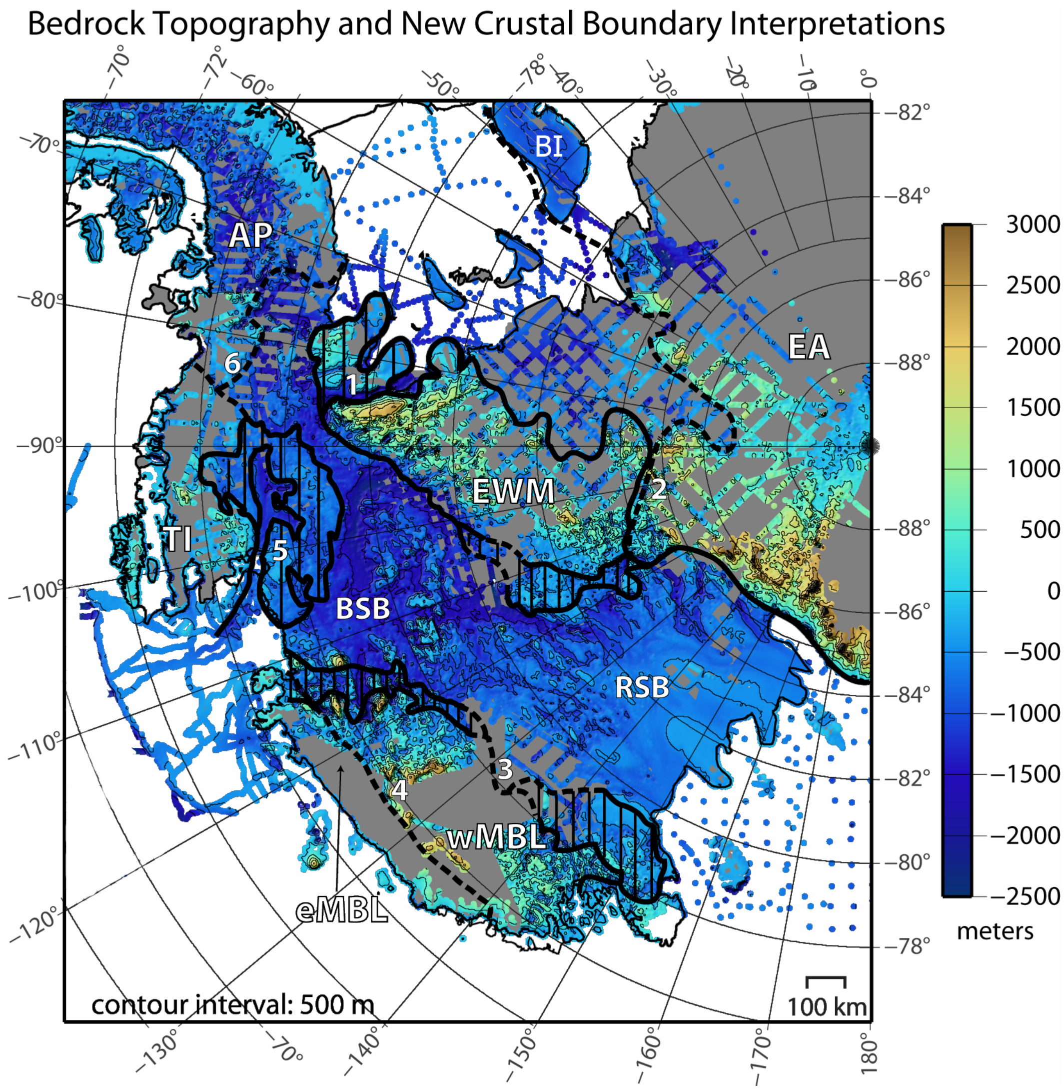

Figure 4.14: The second portion of this study's crustal block boundary interpretations. Boundaries are marked by type: transitional crust zone= two heavy black lines separated by and area of vertical hatches; distinct boundary= single heavy black line; unknown= dashed heavy black line. Boundary sections labeled with numbers are discussed in the text. Background image: Subglacial topography for West Antarctica [*Lythe, et al.,* 2001] (D. Young, unpub. data, 2008). Thin black line= coastline, including ice shelves [*SCAR*, 2006]. Ice sheet-covered areas lacking data are in grey. AP= Antarctic Peninsula; EWM-Ellsworth-Whitmore Mountains; TI=Thurston Island; EA=East Antarctica; eMBL & wMBL = eastern & western Marie Byrd Land; RSB= Rose Subglacial Basin; BSB= Byrd Subglacial Basin; BI= Berkner Island.

Weddell Sea Embayment, and encompasses Berkner Island (Figure 4.14). On the southern side of the Ellsworth-Whitmore crustal block, the boundary is very similar to the *Dalziel and Elliot* [1982] (modified by *Dalziel and Lawver* [2001]) interpreted boundary there, though the new one is adjusted slightly to follow the new subglacial topography more closely.

The boundary segment (#3, Figure 4.14) between the central area of the Marie Byrd Land crustal block and the Rose Subglacial Basin (Figure 4.14) is an unknown crustal boundary type. There is no data available for this segment, so the boundary was left unaltered from the *Dalziel and Elliot* [1982] (modified by *Dalziel and Lawver* [2001]) interpreted boundary in this small section, which joins up nicely with the new interpretations on either side of the data gap.

The crustal boundary that separates the eastern and western Marie Byrd Land crustal blocks [*Pankhurst, et al.*, 1998; *Siddoway*, 2008] (#4, Figure 4.14) is mostly unconstrained by topography or any other data. Therefore, most of its length follows the *Dalziel and Elliot* [1982] (modified by *Dalziel and Lawver* [2001]) interpreted boundary. However, new constraints at each end of the boundary have slightly altered its placement. At the northeast end, geochemical data and Paleozoic ages of volcanism place the Bear Peninsula and Kohler Range (Figure 4.12A) in eastern Marie Byrd Land [*DiVenere, et al.*, 1995; *Pankhurst, et al.*, 1998]. Neighboring Mt. Murphy (Figure 4.12A), however, is thought to be part of western Marie Byrd Land, based on a small basement outcrop on its flank at Kay Peak [*Pankhurst, et al.*, 1998]. Although no basement outcrops exist on the other Marie Byrd Land volcanoes along the boundary with the Byrd Subglacial Basin (Figure 4.14), they are volcanically similar enough to Mount Murphy (except Mount Takahe, as discussed in the previous set of interpretations) [*LeMasurier and Thompson*, 1990] that they more likely lie in western Marie Byrd Land (Figure 4.14). At the northwestern end of the boundary, the suture may end in the Ruppert Coast (Figure 4.12A), possibly east of Land Glacier (Figure 4.12A) [*DiVenere, et al.*, 1995; *Pankhurst, et al.*, 1998]. Given the lack of data along most of its length, the boundary is classified as an unknown type.

The boundary labeled #5 (Figure 4.14) is an updated version of the two transitional crust areas previously interpreted here as separate, based on the Bouguer gravity anomalies (#5 and #6 in Figure 4.13). Inspection of the subglacial topography shows that the two pieces of transitional crust are topographically similar and connected without a break. In fact, this area of crust is the same area that *Dalziel and Elliot* [1982] (modified by *Dalziel and Lawver* [2001]) originally interpreted as the edge of the Thurston Island crustal block. However, based on its crustal thicknesses and Bouguer gravity anomalies, it is now classified as a transitional crustal boundary zone. This zone wraps around the southern, eastern, and northeastern sides of the narrow rift valley through which Pine Island Glacier (Figure 4.2) flows. Their morphological relationship suggests that the rift valley post-dates creation of the transitional crust zone. Erring on the conservative side of boundary placement, the Thurston Island block boundary now occurs just north of Pine Island Glacier and just south of the Hudson Mountains (Figure 4.12A).

The last boundary (#6, Figure 4.14) remains completely unaltered from the one interpreted by *Dalziel and Elliot* [1982] (modified by *Dalziel and Lawver* [2001]). This boundary, at the southern edge of the Antarctic Peninsula (Figure 4.9A) has an unknown classification (as does the adjacent, unaltered segment of the Thurston Island block crustal boundary) because of the poor resolution of the subglacial topography in this area.

Application of Criterion (g)

The last step in redrawing the crustal block boundaries of West Antarctica involves extending the onshore boundaries into the offshore. This is done by utilizing criterion (g) and overlaying the already-interpreted boundaries on this study's West Antarctic free-air gravity anomaly compilation. The final interpretations (Figure 4.15) are only different from those already accomplished (Figure 4.14) in that the offshore boundary extensions have been added.

The only two crustal blocks with offshore extensions are the Marie Byrd Land block and the Thurston Island block. For each, the free-air gravity anomalies are a relatively good indicator of submarine topography. In particular, the blocks likely extend out to the continental shelf, which is represented as the land-ward side of the ring of positive anomalies around the continent (Figure 4.15). The boundary types for these marine extensions are unknown and their exact position uncertain due to a lack of data. The result is a Thurston Island crustal block that is approximately half the size of the previously interpreted block [*Dalziel and Elliot*, 1982; *Dalziel and Lawver*, 2001].

4.7 CONCLUSIONS

GRACE satellite free-air gravity anomalies provided a long-wavelength reference dataset, with which four large West Antarctic airborne gravity surveys were successfully combined. The GRACE free-air gravity anomalies then augmented the merged airborne data, along with ERS-1 free-air anomalies, to provide free-air gravity data coverage over ~6 million km^2 of West Antarctica and surrounding areas. The resulting map illustrates the changes in subglacial topography across the continent and is useful as both a guide and base map for tectonic and crustal structure interpretations. The Bouguer anomalies calculated for the merged airborne surveys suggested that most of the old crustal boundaries in West Antarctica are now diffuse, likely from heating & thinning of the margins by the various phases of rifting and magmatism that have affected the continent since ~200 Ma- the breakup of Gondwana. The one exception to this observation is the

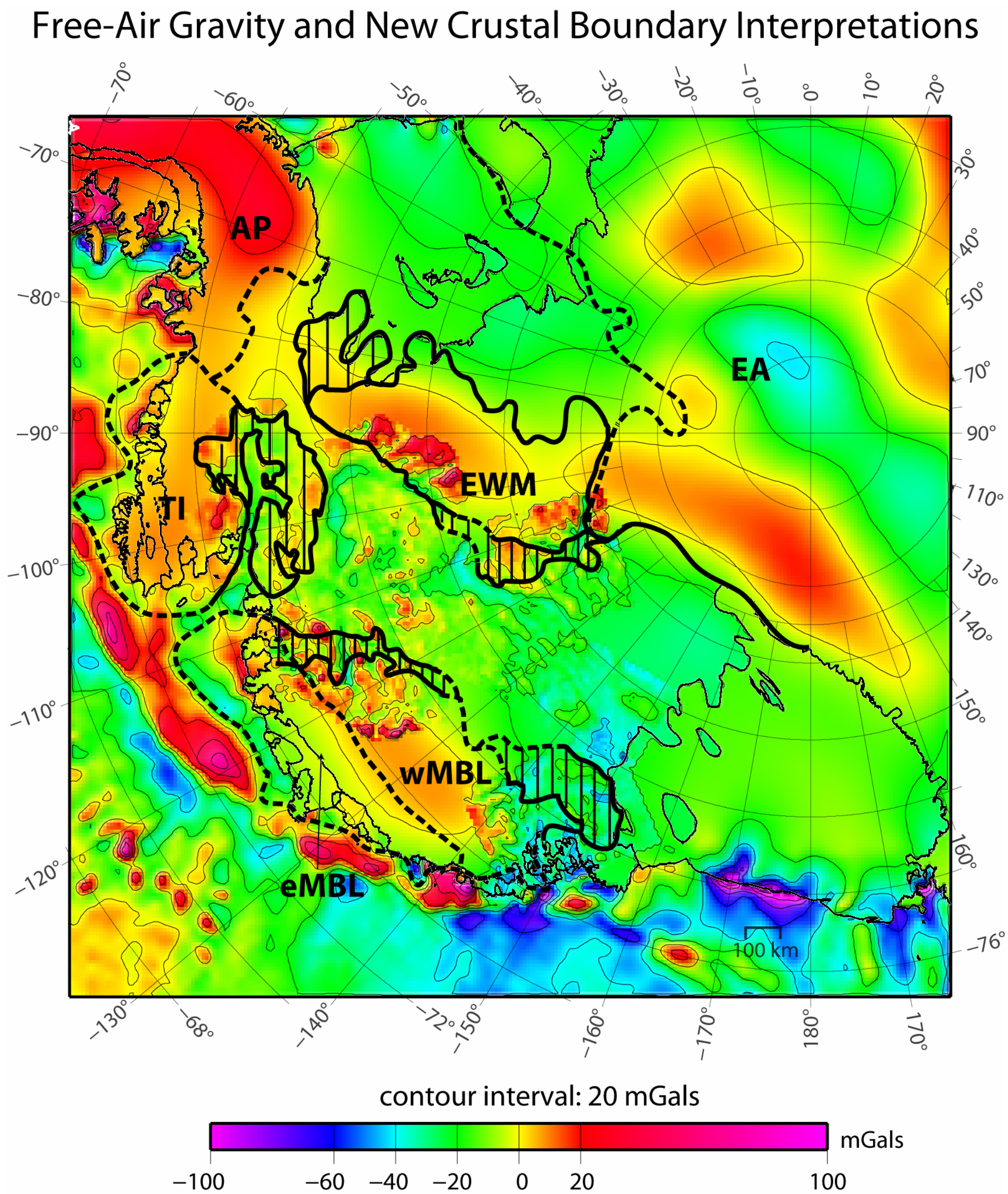

Figure 4.15: Final new crustal block boundary interpretations, after applying criterion (g). Boundaries are marked by type: transitional crust zone= two heavy black lines separated by and area of vertical hatches; distinct boundary= single heavy black line; unknown= dashed heavy black line. Background image: this study's compilation of West Antarctic free-air anomalies. Thin white line= coastline, including ice shelves [*SCAR*, 2006]. Ice sheet-covered areas lacking data are in grey. AP= Antarctic Peninsula; EWM-Ellsworth-Whitmore Mountains; TI=Thurston Island; EA=East Antarctica; eMBL & wMBL = eastern & western Marie Byrd Land.

distinct, abrupt Bouguer anomaly transition at the boundary between the Ellsworth Subglacial Highlands and the Bentley Subglacial Trench.

Spectral analyses of both free-air and Bouguer gravity anomalies from the airborne data indicated a 2-layer crust across West Antarctica. The Moho depths from spectral estimates agreed well with seismic estimates in the Whitmore Mountains (31 km) and the Byrd Subglacial Basin and Rose Subglacial Basin (~27 km). The Marie Byrd Land Moho depths agreed with the few surrounding estimates that suggested thin crust there and support the hypothesis that the crust is not Airy isostatically compensated, but possibly thermally uplifted. Inverse modeling results from the Byrd Subglacial Basin and juxtaposed edge of Marie Byrd Land were difficult to accomplish but suggest that the mantle below the Byrd Subglacial Basin is of normal temperature since the Moho depths there are well-fit by a normal density contrast between the lower crust and upper mantle. The inversion results also agree well with previous forward modeling results (Chapter 3).

Based on the newest gravity anomalies and subglacial topography maps, I created an updated crustal and tectonic sketch map of West Antarctica. The interpretation process was accomplished by systematically applying seven criteria (a through g) to interpret new crustal boundaries starting with the airborne gravity data and then moving to subglacial topography and satellite gravity. The new interpretations greatly decrease the size of the Thurston Island block but underscore that our understanding of its extent is still very limited. The crust in Marie Byrd Land is better understood with the new results but the area's complexity and series of overprinting events makes interpretation of its crustal boundaries difficult. This study is also able to more generally conclude that, except for the boundary segment separating the Bentley Subglacial Trench and the Ellsworth Mountains, there is little evidence for well-defined, crustal-scale fault zones at crustal boundaries in West Antarctica. Most boundaries are instead transitional crust zones (partially-extended pieces of crust) that complicate the crustal structure of West Antarctica by providing wide zones over which to accomplish gradual crustal changes.

Chapter 5: West Antarctic Near-Surface Subglacial Geology, Especially Sedimentary Basin Distribution, Using Airy Isostatic Gravity Anomalies

Abstract

Subglacial sediments are an important control on fast flowing ice in West Antarctica but their spatial distribution over catchment-wide areas is still largely unknown. Previously, airborne gravity anomalies could not clearly image sub-ice sedimentary basins (long-lived potential sources of subglacial sediment) because broad, crustal-scale gravity signals masked the near-surface anomalies. I show that Airy isostatic anomalies can be used to better locate near-surface bodies of anomalous density in West Antarctica. I use a set of merged airborne gravity surveys to compare sedimentary basin distribution between the Rose Subglacial Basin in the Ross Sea Embayment and the Byrd Subglacial Basin in the Thwaites Glacier catchment. The results of this research indicate that known sedimentary basins in the Rose Subglacial Basin coincide with negative isostatic anomalies and that the Rose Subglacial Basin is much more sediment rich than the Byrd Subglacial Basin. The Byrd Subglacial Basin beneath Thwaites Glacier has confined depocenters that underlie the onset of fast flow in the glacier's tributaries. From the isostatic gravity anomalies, I construct a likelihood template of the distribution of long-lived sedimentary basins beneath the ice sheet. The results suggest that if the fast flow of Thwaites Glacier is created due to basal sliding through the mobilization of subglacial sediment, then that sediment is being transported down-flow from the tributaries and Thwaites Glacier has eroded much of its long term sediment supply. Alternatively, a different mechanism may be causing the glacier's high ice velocities. Also, positive isostatic anomalies indicate a ~120 km wide swath of crystalline rock that runs parallel to the coastline at the mouth of Thwaites Glacier, which may influence the stability of the glacier's grounding line.

5.1 INTRODUCTION

Determining the distribution of subglacial sediments beneath the West Antarctic Ice Sheet is necessary for understanding the dynamic behavior of the ice sheet's glaciers and ice streams. In the Ross Sea Embayment, fast flow of the ice streams is controlled by the co-existence of sediment and water [*Alley, et al.*, 1986; *Blankenship, et al.*, 1986; *Anandakrishnan, et al.*, 1998; *Blankenship, et al.*, 2001; *Studinger, et al.*, 2001]. Drill sites [*Engelhardt and Kamb*, 1998], active source seismic experiments [*Blankenship, et al.*, 1987b], and passive seismic stations [*Blankenship, et al.*, 1987a; *Anandakrishnan and Winberry*, 2004] provide local verification of the existence of sediment below fast flowing ice in the Ross Sea Embayment. However, in order to have a better understanding of ice sheet response, long-lived and easily eroded sources of sediment (such as deep sedimentary basins) must be located across subglacial catchments. Only airborne geophysics currently provides sufficient information about the subglacial environment on such a large scale. This capability has already been exercised on a local scale; airborne potential fields data in the Ross Sea Embayment have been forward modeled for the locations of potential sedimentary basins and thickness of sedimentary infill [e.g. *Bell, et al.*, 1998; *Studinger, et al.*, 2001; *Bell, et al.*, 2006].

The technique of using isostatic anomalies in areas with large crustal signals to interpret near-surface geology has not, until now, been applied in West Antarctica. Here I present a processing scheme and isostatic gravity anomaly results from two overlapping surveys (Figure 1.11 for survey shapes; Figure 5.1 for location): Thwaites Glacier (called AGASEA) and Ross Sea Embayment (called CASERTZ). With verification of isostatic anomalies along profiles and the creation of a sedimentary basin template, I aim to delineate potential long-lived sources of subglacial sediment and other subglacial geologic features, such as volcanics, more regionally than has been previously attempted.

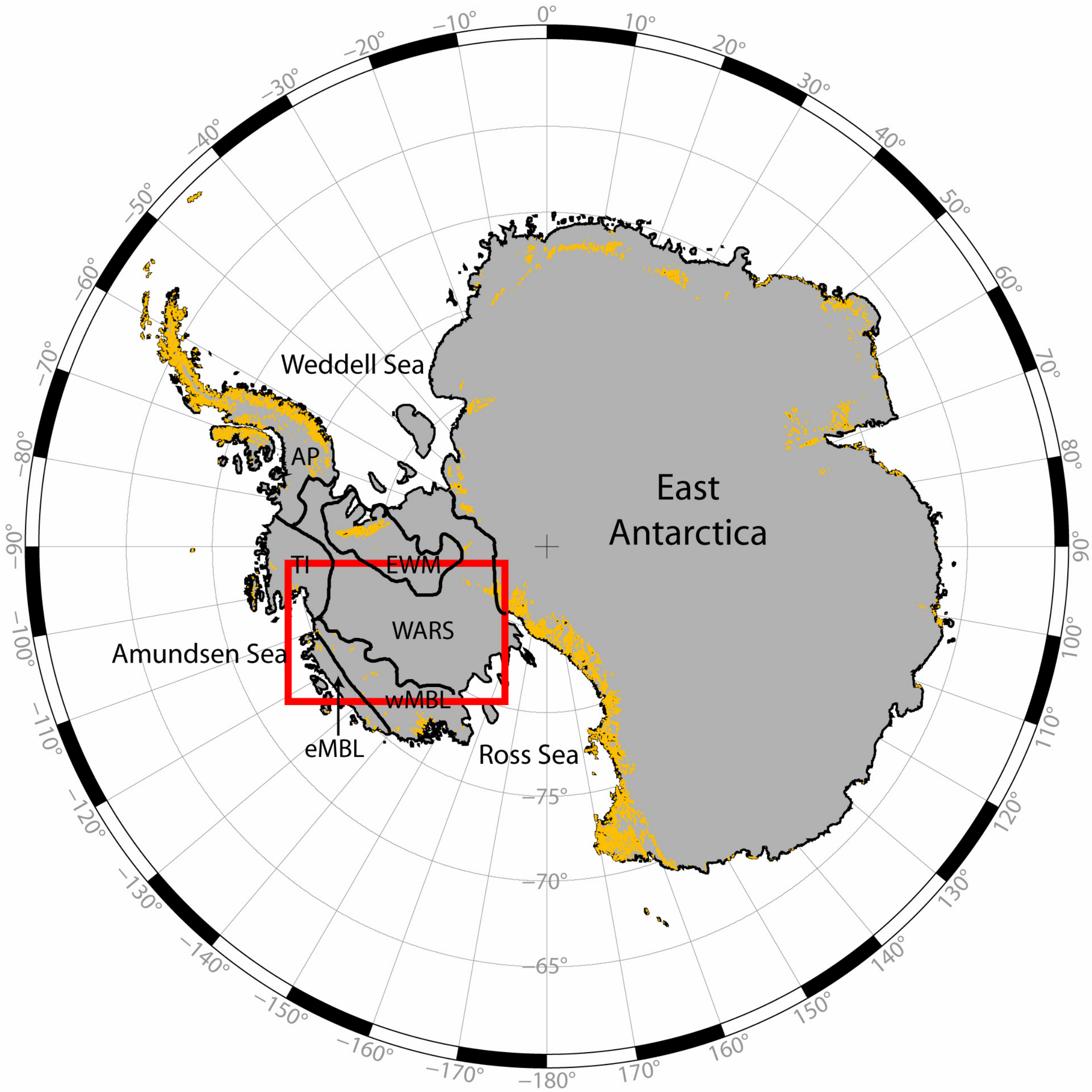

Figure 5.1: Antarctic index map showing the location of Figures 5.2, 5.3, and 5.7 (red box). Also shown: rock outcrop locations (gold lines) and Antarctic coastline (thin black line) [*SCAR*, 2006], and West Antarctic crustal blocks (heavy black lines) [*Dalziel and Elliot*, 1982; *Dalziel and Lawver*, 2001]. Crustal block names: AP= Antarctic Peninsula; TI= Thurston Island; EWM= Ellsworth-Whitmore Mountains; WARS= West Antarctic Rift System; eMBL and wMBL= eastern and western Marie Byrd Land.

5.2 ANALYSIS

Bouguer gravity anomalies in West Antarctica are difficult to interpret for the locations of near-surface density anomalies [*Studinger, et al.*, 2001; *Studinger, et al.*, 2002; *Karner, et al.*, 2005; *Bell, et al.*, 2006]. Changes in the Moho and mid-crustal boundaries produce broad Bouguer signals that obscure signals from spatially-extensive sedimentary basins [*Karner, et al.*, 2005]. In addition, the timing of sedimentation is disjointed with respect to the original creation of accommodation space in the basins and results in anti-correlated gravity anomalies [*Karner, et al.*, 2005]. So, further gravity analysis is needed to separate the regional gravity signals due to crustal changes from residual gravity signals due to near-surface density changes.

To do so, an Airy isostatic correction is employed [*Jachens and Griscom*, 1985]. The correction calculates the compensation needed at depth to support all of the topography (including the ice sheet) in Airy isostatic equilibrium. Airy isostasy is a simple mode of compensation that assumes zero lithospheric rigidity, i.e. an elastic thickness (Te) of zero. This assumption will not be appropriate in all of the surveys' areas, particularly those that have already been identified as being significantly out of Airy isostatic equilibrium (Chapter 3, Jankowski Subglacial Highlands and Marie Byrd Land). Since the rift basins are the lowest-lying areas and the Rose Subglacial Basin is already known to be a major depocenter for sediment [e.g. *Blankenship, et al.*, 2001; *Studinger, et al.*, 2001; *Peters, et al.*, 2006], the isostatic anomalies should be calculated to fit the assumed crustal structure of these areas. And, in fact, the assumption of Airy Isostasy is relatively accurate for the Rose Subglacial Basin, which had low lithospheric flexural strength during extension and subsequently higher strength during sedimentation [*Karner, et al.*, 2005].

The isostatic anomaly method is sensitive to the amount of root or anti-root needed to compensate topography relative to a given depth of compensation. Here topographic compensation at the Moho, a common compensation depth, is assumed. The isostatic anomaly is calculated for an "equivalent topography" that represents the entire crustal load- both rock and ice. The equivalent topography is sometimes also called effective topography. First, a thickness of rock (t_r) that is gravitationally-equivalent to the thickness of the ice sheet (t_i) at any location (x,y), is calculated such that:

$$t_i(x,y) = z_s(x,y) - z_b(x,y) \qquad [5.1]$$

$$t_r(x,y) = \frac{\rho_i * t_i(x,y)}{\rho_r} \qquad [5.2]$$

where z_s is the ice sheet surface elevation from satellite laser altimetry, z_b is the bedrock elevation from airborne radar, ρ_i is the density of ice, ρ_r is the density of the desired equivalent rock unit. The density of the rock unit should be the same as that used for the Bouguer correction and was 2670 kg/m^3 in this study. The amount of equivalent topography (z_e) is then:

$$z_e(x,y) = z_b(x,y) + t_r(x,y) \qquad [5.3]$$

The compensating surface's (i.e. Moho's) depths needed to isostatically support the equivalent topography are easily calculated using the Generic Mapping Tools (GMT) [*Wessel and Smith*, 1998]. The calculation produces relative changes in depth along the compensating surface, so the zero Moho change was pinned to (i.e. set equal to) the average Moho depths for the Byrd and Rose Subglacial Basins derived from gravity spectra (Chapters 3 and 4). Since the spectral analyses of the gravity data indicate a 2-layer crust here, relief on the mid-crustal boundary is assumed to parallel to the calculated Moho depth changes, similar to results from forward and inverse modeling (Chapters 3 and 4). The Airy isostatic correction is then obtained by calculating the gravity effect of the 2-layer crustal models needed to compensate the equivalent topography (Table 5.1) with the same 3D Gaussian-Legendre Quadrature method [*von*

Frese, et al., 1981] already used to calculate Bouguer anomalies (Chapters 3 and 4).

Table 5.1: Crustal Structure Density Model Used for Airy Isostatic Correction

Survey	Crustal Boundary	Pinning Depth	Density Difference Across Boundary
AGASEA	Moho	27 km	500 kg/m^3
CASERTZ	Moho	27.5 km	500 kg/m^3
AGASEA	Mid-crust	10 km	130 kg/m^3
CASERTZ	Mid-crust	13 km	130 kg/m^3

The cumulative assumptions involved in this correction make error estimation difficult. As a result, interpretation of anomalies <10 mGals in amplitude or modeling of the isostatic anomalies is not recommended. However, the anomalies are very useful as a relative indicator of differences in near-surface geology across the subglacial basins. By treating the magnitudes of the isostatic anomalies as a “likelihood” indicator, I instead create a template of the most likely places to find sedimentary basins based on the gravity anomalies. In other words, my template identifies a -10 mGal isostatic anomaly as more likely to represent a sedimentary basin than a zero-magnitude or positive isostatic anomaly and a < -30 mGal anomaly as a location where a sedimentary basin is much more likely to exist. The one caveat to this template is that it marks all near-surface bodies of < 2670 kg/m^3 density- sedimentary rocks, water, hyaloclastites, etc.- and here I interpret all bodies as sediment unless there is direct evidence to the contrary.

5.3 RESULTS

5.3.1 Description of Isostatic Anomalies

The Airy isostatic gravity anomalies (Figure 5.2) do not exceed +/- 50 mGals, and most of their dynamic range is from +20 to -40 mGals. Since the original Bouguer signals were +100 to -180 mGals with most of their dynamic range from +40 to -120 mGals, the isostatic correction accounted for nearly two-thirds of the Bouguer gravity signal. The

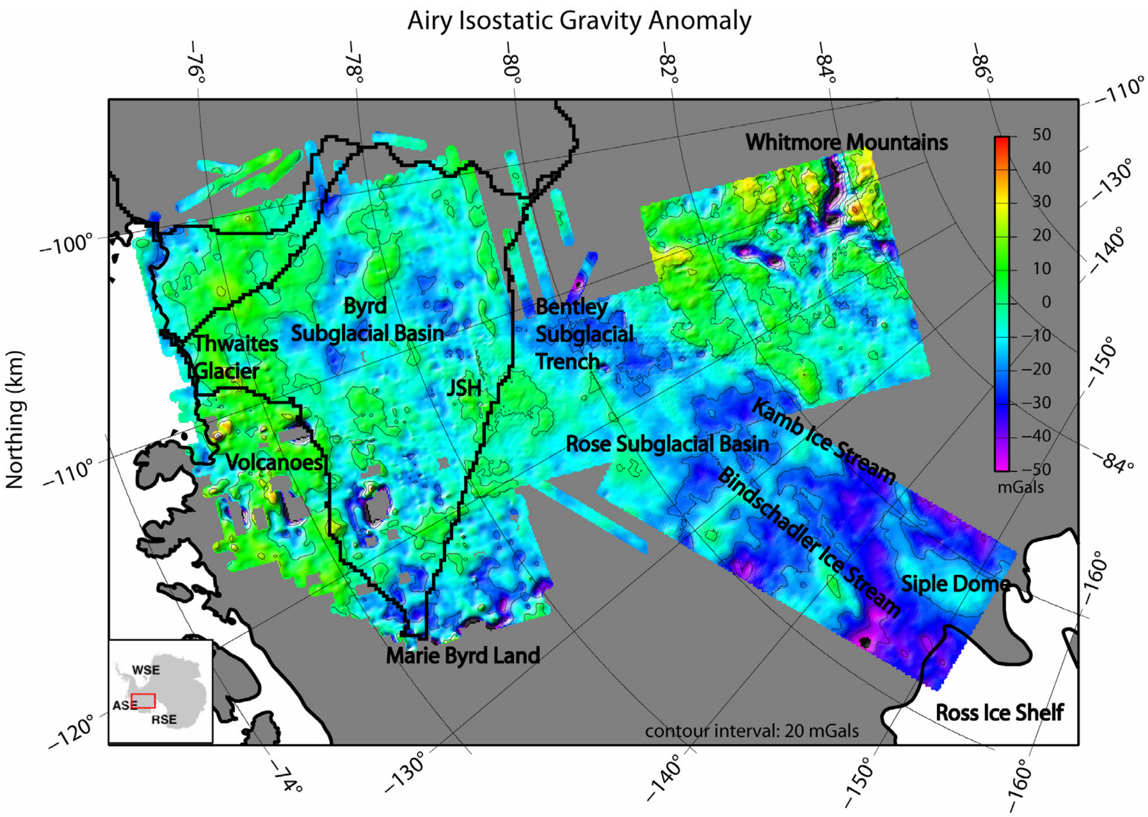

Figure 5.2: Airy Isostatic Anomalies for the AGASEA (northeastern) and CASERTZ (southwestern) surveys, major features labeled. JSH=Jankowski Subglacial Highlands; smooth black line=coastline [*SCAR*, 2006]; thick, jagged black lines=glacier catchments [*Vaughan, et al.,* 1999]. Inset: Location of figure in West Antarctica (red box), RSE=Ross Sea Embayment, ASE=Amundsen Sea Embayment, WSE=Weddell Sea Embayment. Location of this figure is shown larger on Figure 5.1. Gray shading indicates ice sheet-covered areas with no data.

isostatic anomalies in the AGASEA survey have more high frequency noise, especially in the western portion (over Marie Byrd Land), giving the anomalies a stippled look. The higher noise there is a reflection of the higher noise levels in the original free-air data (Chapter 2). The most positive anomalies occur at the Whitmore Mountains and the Marie Byrd Land volcanoes (Figure 5.2). The most negative anomalies occur in the

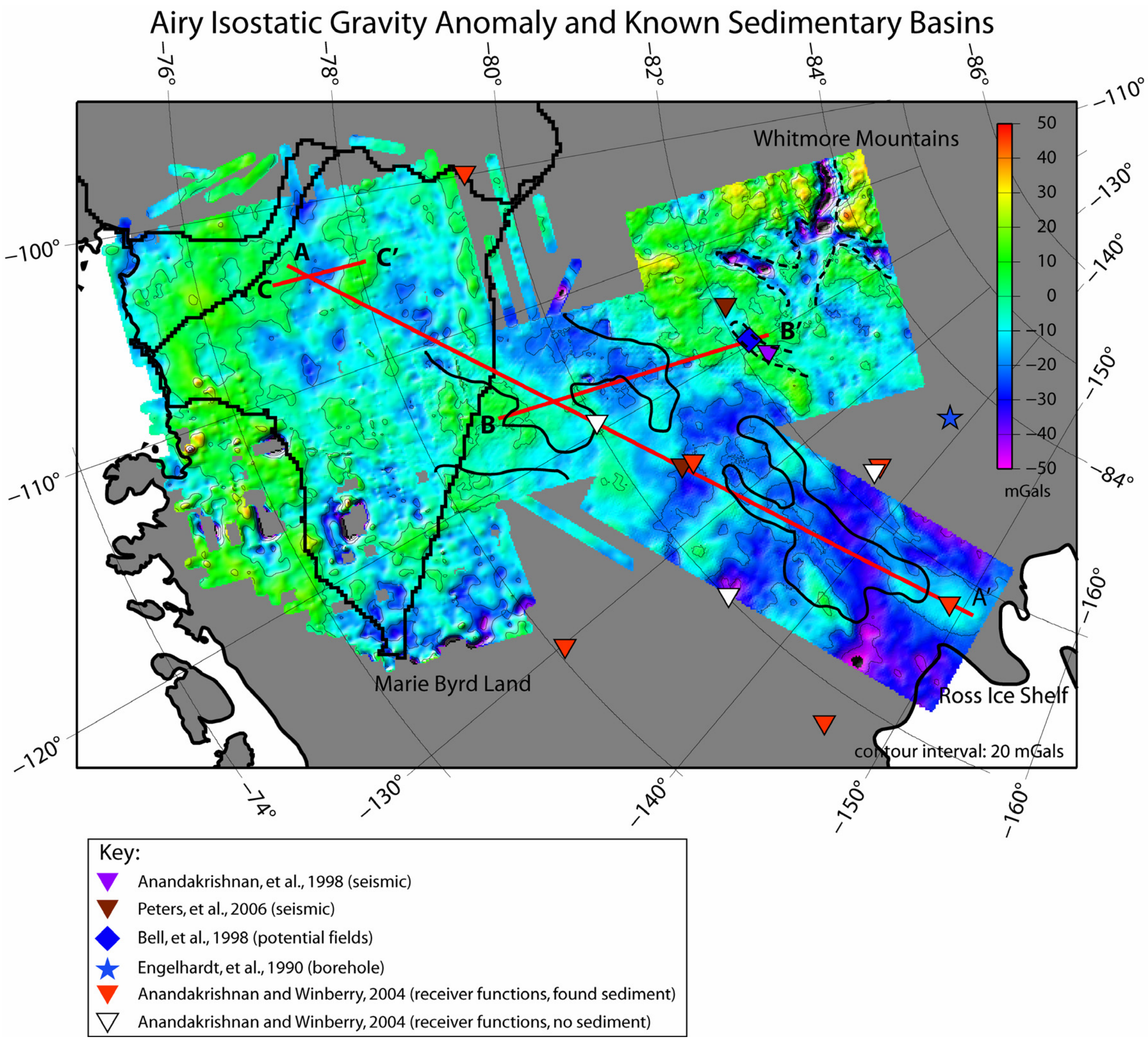

Figure 5.3: Airy Isostatic Anomalies overlaid with locations of known sedimentary basins, heavy black lines as in Figure 5.2; red lines are the locations of Figures 5.4-5.6; triangles are seismic studies (red for sediment present and white for no sediment [*Anandakrishnan and Winberry*, 2004]; brown [*Peters, et al.*, 2006]; purple [*Anandakrishnan, et al.*, 1998]), blue diamond is potential fields [*Bell, et al.*, 1998], blue star is borehole [*Engelhardt, et al.*, 1990], solid thin black lines are magnetically-defined basins [*Bell, et al.*, 2006], thin dashed lines are others' gravity-defined basins [*Studinger, et al.*, 2001]. Gray shading indicates ice sheet-covered areas with no data.

Bentley Subglacial Trench, the three trenches (fault-bounded rift basins) [*Studinger, et al.*, 2001] in the Whitmore Mountains, and around Siple Dome (Figure 5.7, e.g. yellow circles 1 & 2).

The positive gravity anomalies (Figure 5.2) mostly occur in two areas: 1. a continuous E-W band 80-200 km wide, running the whole length of the surveyed Amundsen Sea coastline and 2. the Whitmore Mountains and its associated transitional crust. Additional positive anomalies occur over parts of the Jankowski Subglacial Highlands, though the highlands are almost equally characterized by negative gravity anomalies. Negative anomalies cover a greater area of the Rose Subglacial Basin (conversely, less area with positive anomalies) than the Byrd Subglacial Basin. The largest area of continuous anomaly is the negative swath running the length of Bindschadler Ice Stream (Figure 5.2).

5.3.2 Isostatic Anomaly Verification

Since this was the first application of an isostatic correction to a West Antarctic gravity dataset, the anomalies needed to be verified 1. against the locations of known sedimentary basins (Figure 5.3) and/or 2. against other datasets that are also indicators of subglacial sedimentary basins. I used both methods of verification: the first in the Rose Subglacial Basin where some sedimentary basins have already been identified and the second in the Byrd Subglacial Basin where no sedimentary basins had been previously identified.

The first line of isostatic anomalies to be examined crosses the West Antarctic Ice Sheet divide into both basins (Figure 5.4; A to A' on Figure 5.3)- starting from a deep portion of the Byrd Subglacial Basin, crossing the Jankowski Subglacial Highlands, running roughly parallel to flow in the Bindschadler Ice Stream, and ending at Siple Dome. The negative isostatic anomalies correlate in location and relative magnitude with

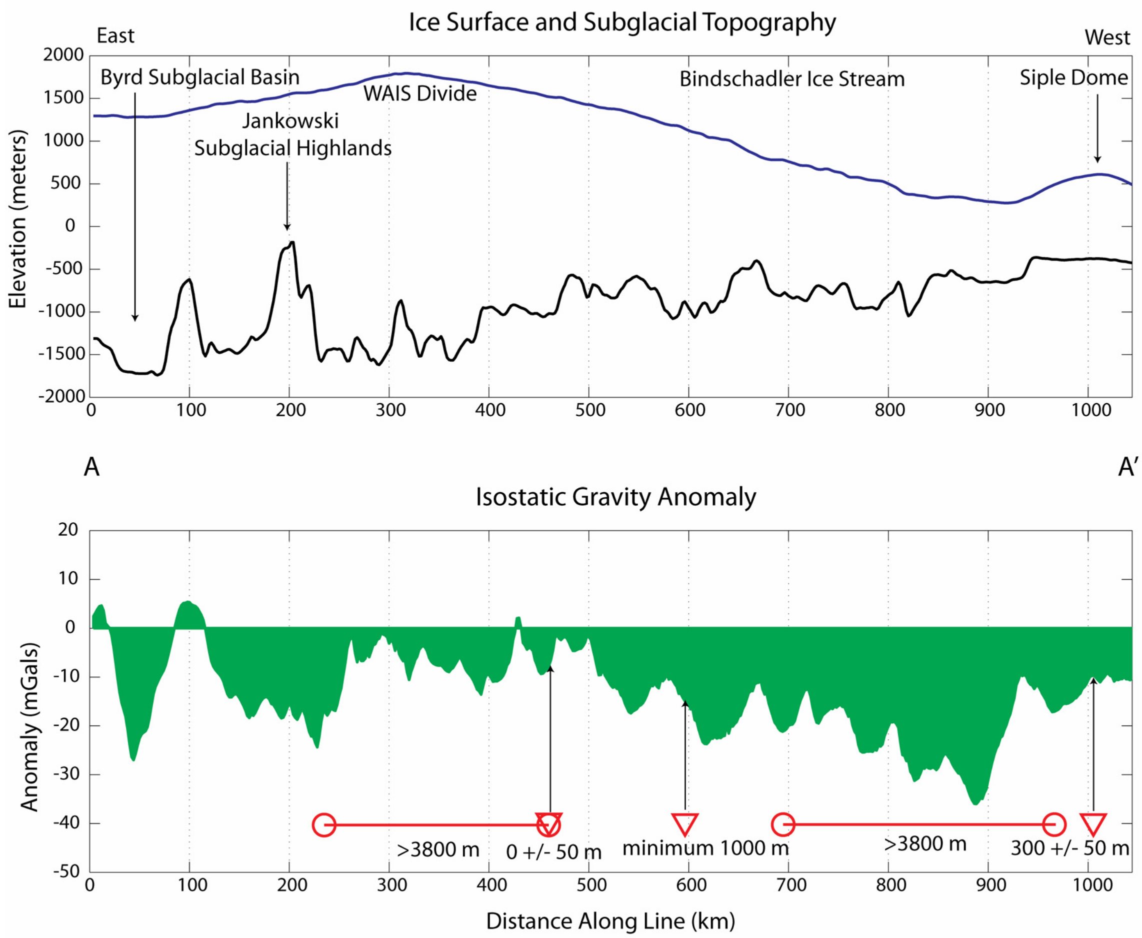

Figure 5.4: Profile #1 running east to west (A-A' in Figure 5.3). Top: Ice sheet surface (blue) and subglacial bedrock topography (black) with major features labeled. Bottom: Coinciding Airy isostatic gravity anomalies (green), filled to emphasize the sign of the anomaly; labeled in red are the locations of others' sedimentary basins and their depths (references in Figure 5.3) where seismic results are inverted triangles and magnetically-defined basins are indicated with circles at each end connected by a red line (to show the extent of the basin).

seismically-defined sediment infill [*Anandakrishnan and Winberry*, 2004; *Peters, et al.*, 2006]: 0 +/- 50m and -8 mGals; 300 +/- 50 m and -10 mGals; >1000 m and -15 mGals (seismic sediment depth and isostatic gravity anomaly, respectively). This correlation

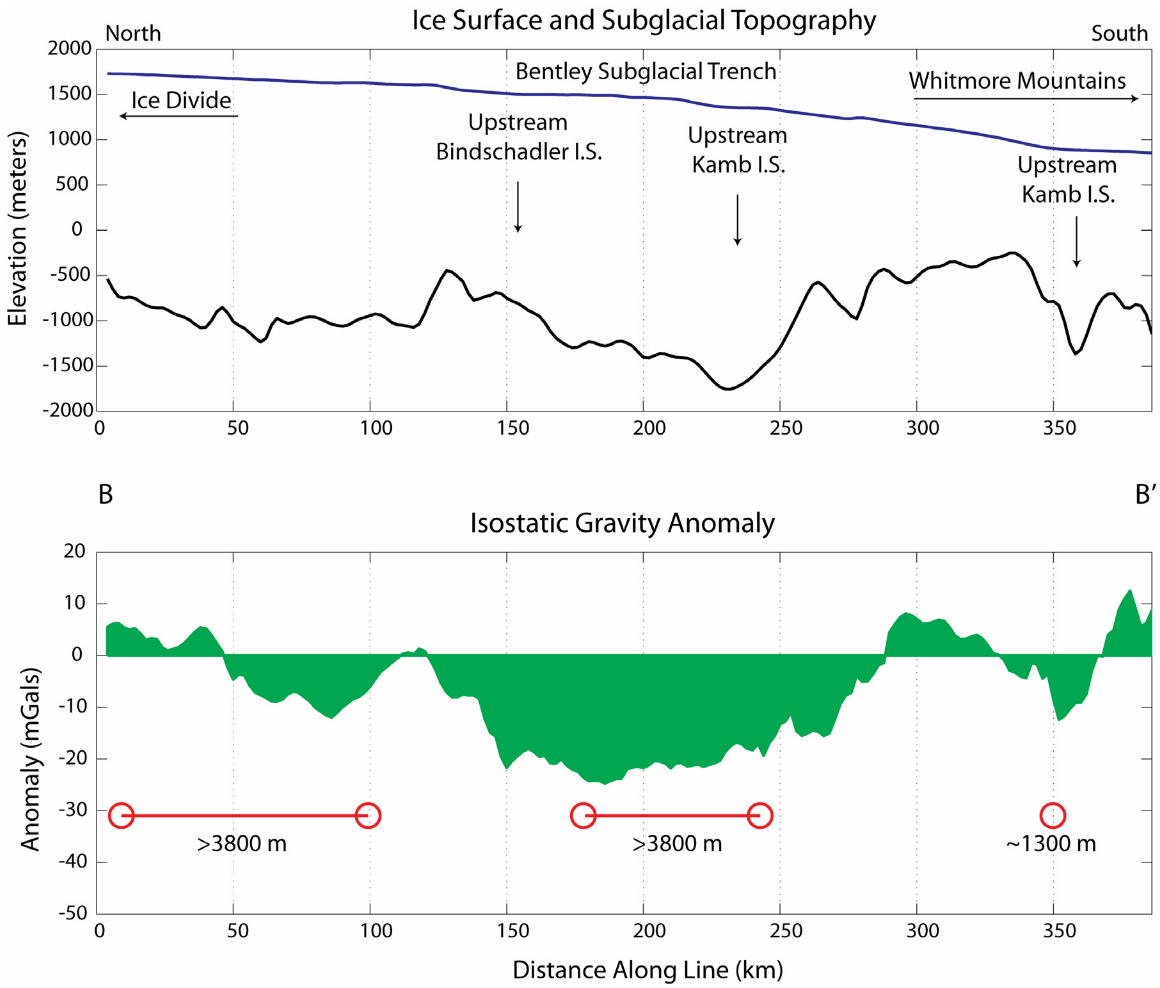

Figure 5.5: Profile #2 running north to south (B-B' in Figure 5.3). Top and Bottom labeled as in Figure 5.4.

suggests that the isostatic anomalies are a fairly good indicator of sedimentary basins.

The magnetic depth-to-basement estimates along this line [*Bell, et al.*, 2006], however, do not correlate well with either the isostatic anomalies or the seismic results. Where a magnetically-defined basin indicates > 3800 m sediment infill under the West Antarctic Ice Sheet divide, isostatic anomalies are only 2 to -13 mGals and a receiver function analysis indicates negligible sedimentary infill (0 +/- 50 m). The magnetically-defined basin beneath Bindschadler Ice Stream indicates a relatively consistent thickness

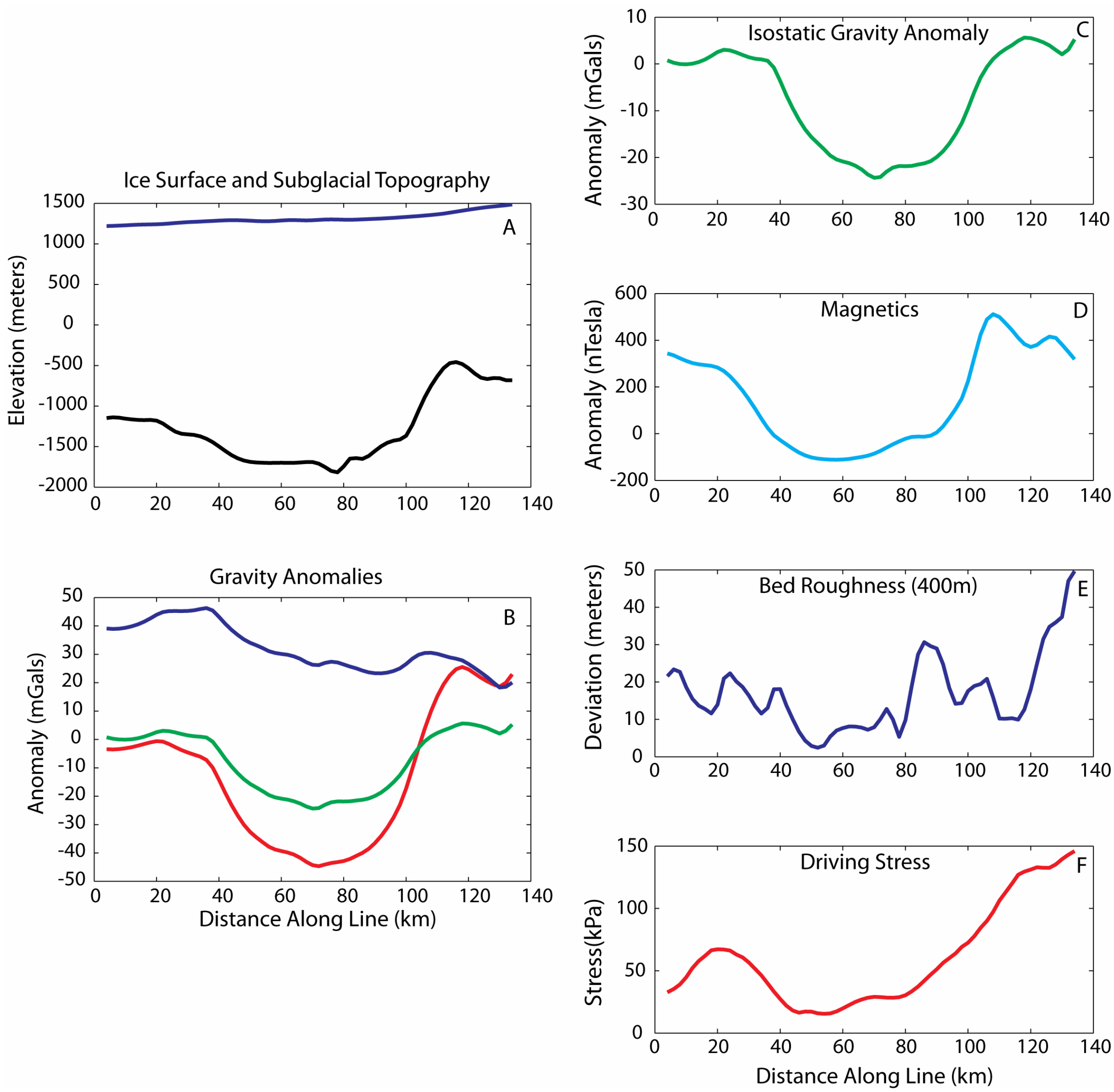

Figure 5.6: Profile #3 across the Byrd Subglacial Basin, perpendicular to ice flow (C-C' in Figure 5.3). A: Ice sheet surface (blue) and subglacial bedrock topography (black). B: All gravity anomalies: free-air (red), Bouguer (blue), and Airy isostatic (green). C: Again, the Airy isostatic gravity anomaly, aligned for comparison purposes. D: Magnetic anomaly. E: Subglacial bed roughness, averaged along 400 m horizontally (D. Young, pers. comm., 2007). F: Ice driving stress.

of > 3800 m infill across its length, but the isostatic anomalies registered to the seismic results suggest that the basin infill is significantly thinner (only several hundred meters) near Siple Dome, thickens dramatically just east, and then thins up-flow to only ~1000 m. Based on these comparisons, I suggest that the magnetic depth-to-basement estimates are significantly overestimating sedimentary basin thickness and may be biased downward by the fact that the basement in the Rose Subglacial Basin is fairly non-magnetic (C. Finn, pers. comm., 2008).

As an additional test of the isostatic anomalies, a second line was examined; this line is perpendicular to ice flow in the Bentley Subglacial Trench and Rose Subglacial Basin (Figure 5.5), near the upstream onsets of tributary ice stream flow. The isostatic anomalies agree well with interpretations of 800-1300 m of sediment infill in the Whitmore Mountains fault-bounded basin [*Anandakrishnan, et al.*, 1998; *Bell, et al.*, 1998], though the examined profile only runs through the *Bell, et al.* [1998] 1300 m estimate. The magnetically-defined basin beneath upstream Kamb Ice Stream and Bindschadler Ice Stream, in the Bentley Subglacial Trench, agrees spatially with the isostatic anomalies, but the relative depth indicated by the isostatic anomalies is less than that reported by the magnetic analysis. The northern magnetically-defined basin (close to the ice divide) does not generally agree with the isostatic anomalies, though there may be a shallow basin over part of its length.

The good correlations with others' seismic and gravity locations of sedimentary infill (though not with the magnetic depth-to-basement results) in the Rose Subglacial Basin are evidence that the isostatic anomaly method is working well. However, the Byrd Subglacial Basin lacks *a priori* sedimentary basin locations or depths against which to test the validity of the isostatic anomalies there. To counter this, a distinct negative isostatic anomaly in the Byrd Subglacial Basin (Figure 5.4) is compared to other

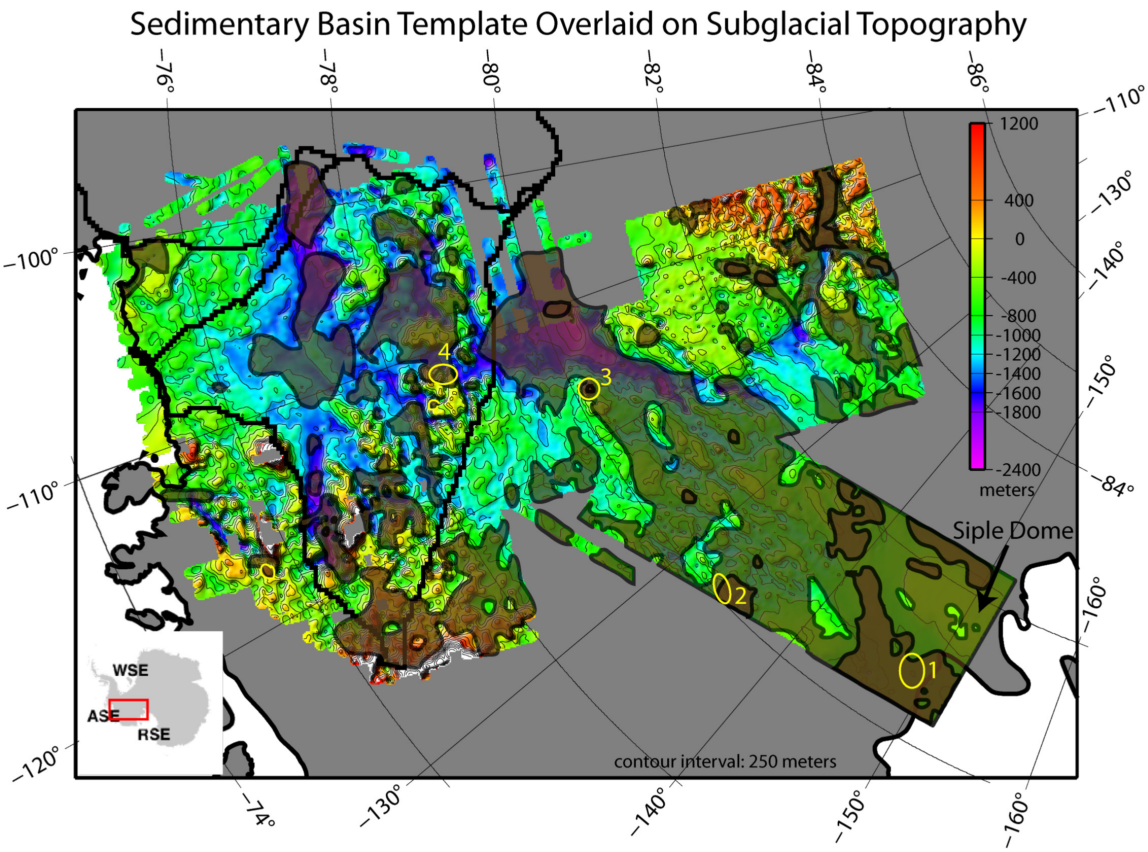

Figure 5.7: Subglacial Topography overlaid with the sediment template interpreted from Airy isostatic gravity anomalies; light brown for "moderate likelihood" of <-10 mGals; dark brown for "high likelihood" of <-30 mGals; yellow numbered circles correspond to both negative isostatic and negative magnetic anomalies over subglacial volcanoes or constructs [*Behrendt, et al.*, 2004]. Black lines (glacier catchments [*Vaughan, et al.,* 1999] and coastline [*SCAR*, 2006]) and inset as in Figure 5.2. Gray shading indicates ice sheet-covered areas with no data.

coincident datasets: magnetics [*Holt, et al.,* 2007], subglacial bed roughness (D. Young, pers. comm., 2007), and ice driving stress (D. Young, pers. comm., 2007). When compared (Figure 5.6), they show a direct correlation such that: the magnetic anomaly is 400 nT more negative than its surroundings, the sub-ice bedrock roughness is very low

(<40 m height change over a 400m horizontal distance), and the ice's driving stress indicates basal sliding (< 50 kPa, [*Blankenship, et al.*, 2001]). These are all indications that the ice is flowing over the top of a sedimentary basin and the comparison, by extension, supports the interpretation of other negative isostatic anomalies in the Byrd Subglacial Basin as sediment-filled basins.

5.4 Discussion

The Airy isostatic anomalies highlight those near-surface features that were difficult to identify in the Bouguer gravity anomalies by removing the nearly two-thirds of the Bouguer signal that was due to changes in deep crustal boundary depths. The method appears to work well, based on correlations of negative isostatic anomalies with seismically-determined sedimentary basins in the Rose Subglacial Basin. Thus, I interpret negative isostatic anomalies as sedimentary basins (Figure 5.7), with likely exceptions to that general interpretation as discussed below. The positive isostatic anomalies (Figure 5.2) represent bodies with relatively higher densities (>2670 kg/m^3) and are tentatively interpreted here as metamorphic or crystalline igneous rocks.

However, caution is warranted when interpreting the very negative anomalies in the Bentley Subglacial trench and the Whitmore trenches because the subglacial topography in these deep areas is not yet well-constrained. The coherent radar used in the AGASEA survey was not flown extensively over the Bentley Subglacial Trench (which is >2.5 km below sea level and was ~4.5 km from the airborne radar system) and advanced SAR (synthetic aperture radar) processing is underway for the data that was collected to image the bottom of the Bentley Subglacial trench (D. Young, pers. comm., 2008). In addition, the incoherent radar used in the CASERTZ survey could not image the bottom of the Whitmore trenches or the Bentley Subglacial Trench.

5.4.1 Positive Isostatic Anomalies

A prominent positive isostatic anomaly runs parallel to the Amundsen Sea coastline (Figure 5.4), including beneath Thwaites Glacier's mouth. It coincides with an interpreted piece of transitional crust that was part of the "Weddellia" crustal blocks that make up West Antarctica, either as a section of Thurston Island or eastern Marie Byrd Land (Chapters 3, 4). The Moho beneath this area is slightly deeper than predicted by Airy isostasy (30 km, as compared to 26 km predicted by Airy isostasy; Chapter 3) and so the positive isostatic anomaly should actually be more positive in this area due to an incomplete correction of the crustal thickness. The anomaly potentially represents a crystalline rock "sill" (Chapter 2) [*Holt, et al.*, 2006a] that has been mostly or completely denuded by ice flow. The pattern of ice driving stresses over the sill looks very similar to the isostatic anomalies' pattern (D. Young, pers. comm., 2007) and shows that the area has relatively high driving stresses. Thus, this sill of interpreted transitional crust could be providing Thwaites Glacier with a wide grounding zone over which to accommodate future glacier grounding line retreat. To retreat off of the sill, the glacier's grounding line would have to move about 100 km inland, where the ice would encounter deepening bedrock topography and sedimentary basins. The existence of a denuded sill that slows the flow of Thwaites Glacier at its mouth is critical because the sill would as the only stabilizing impediment (at least for ~120 km of retreat) for a glacier rooted mostly 1-2.5 km below sea level over much of its several hundred thousand km^2 catchment.

The large area of positive isostatic anomalies in the Whitmore Mountains is certainly due to near-surface density anomalies. The Moho beneath the mountains is at ~31 km, essentially in Airy isostatic equilibrium (Chapter 4), and would not produce a positive isostatic anomaly. Yet, the exposed rocks in the Whitmore Mountains are granite and feldspar-rich metasedimentary rocks [*Flowerdew, et al.*, 2007] and would have densities too close to 2670 kg/m^3 to cause the large anomalies observed. Hypothetically, if Whitmore Mountains have a similar Paleozoic geology to the adjoining Ellsworth Mountains, then a corollary to the 3000 m of volcaniclastic rocks at the base of the Cambrian-age Union Formation in the Ellsworth Mountains [*Curtis*, 2001; *Flowerdew, et al.*, 2007] could exist in the Whitmore Mountains and be causing the positive isostatic anomalies.

5.4.2 Negative Isostatic Anomalies

5.4.2.1 Thwaites Glacier and the Byrd Subglacial Basin

A sediment template, overlaid on subglacial topography, illustrates where negative isostatic anomalies < -10 mGals indicate a moderate likelihood of sedimentary basins (Figure 5.7, light brown) and < -30 mGals indicate a high likelihood of sedimentary basins (Figure 5.7, dark brown). Comparing the spatial extent of the negative isostatic anomalies in the major basins shows a lack of negative anomalies in the Byrd Subglacial Basin. In fact, on close inspection, over half of the limited negative anomalies there lie over the Jankowski Subglacial Highlands and in Marie Byrd Land. These anomalies are not sedimentary basins because they lie on high topography and occur where the assumption of Airy isostasy is most likely to be incorrect.

Thus, Thwaites Glacier's subglacial environment appears to very sediment poor, especially in comparison to the extensive isostatic anomalies in the Rose Subglacial Basin beneath the Ross ice streams and in the Bentley Subglacial Trench. The Byrd Subglacial Basin's sedimentary infill lies directly under Thwaites Glacier's tributaries (compare Figure 1.9 to Figure 5.7) and in the confluence of their flow at the center of the Byrd Subglacial Basin, suggesting that tributary flow is not only structurally-controlled, but geologically-controlled as well. The lack of sedimentary basins beneath the fastest glacier flow- towards the coast, particularly on the western side- suggests that the glacier has probably exhausted its sediment supply there. If the fast flow occurs by the same mechanisms as observed in the Ross Sea ice streams, the main trunk of Thwaites Glacier must be lubricated at the bed with sediment transported tens to hundreds of kilometers down-flow from the tributaries. More likely, a different mechanism for creating sustained fast ice flow is causing Thwaites Glacier's high velocities.

Note that the suggested higher heat flow of Marie Byrd Land could provide a source for substantial melt water that would drain off the highlands into the low-lying topography of the Byrd Subglacial Basin (Chapter 3). A favorable pathway for such melt water drainage has already been identified in the deep trough between the Crary Mountains and Mount Takahe based on lithostatic head calculations (*S. Carter, pers. comm.,* 2007). When Thwaites glacier's ice flow velocities are examined in detail, it is evident that the only section of Thwaites Glacier to reach velocities above 0.6 m/yr is confined to the western half of its trunk. This western half of the glacier is the section of the catchment that would be most strongly influenced by influx of subglacial melt from Marie Byrd Land since it is directly downstream of the suggested melt water pathway. This correlation strongly suggests that Thwaites Glacier's fastest flow (in the western section of the glacier trunk) is underlain with significant amounts of subglacial melt water as a direct result of warm mantle temperatures in Marie Byrd Land. The water would provide basal lubrication in an area where fast flow would otherwise be difficult to sustain because of thin to negligible subglacial sediment thickness.

5.4.2.2 The Ross Sea Ice Streams and the Rose Subglacial Basin

The very negative isostatic anomalies around Siple Dome (and moderately negative anomalies extending well northeast from there) are well-constrained. Surprisingly, two of these very negative anomalies correlate with prominent magnetic anomalies (Figure 5.7, yellow circles 1 & 2) that have been interpreted as the remains of subglacially-erupted and glacially-smoothed volcanic edifices [*Behrendt, et al.*, 2004, no. 8 & 9]. The magnetic anomalies are negative because the volcanoes were erupted during the time of a reversed magnetic field. Quick quenching of the erupting material by ice and melt water would have produced relatively non-magnetic hyaloclastites, pillow breccias, and fragmented volcanics [*Behrendt, et al.*, 2004] that would have been easily eroded away, leaving behind only a negatively magnetized intrusion within the crust. The correlation of these magnetic anomalies with broad areas of negative isostatic anomalies (rather than correlating to localized positive isostatic anomalies, which would have expected given the higher density of intrusive rock) suggests that the eruptions occurred within sediment basin depocenters. Cenozoic volcanic exploitation of this rifted crust (that was subjected to wide-scale thinning in the late Mesozoic and subsequently filled with sediment) is not surprising. One example of a similar rift basin, in the nearby Ross Sea (the Victoria Land Basin, which is underlain with thinner crust than its surroundings [*Trey, et al.*, 1999]) is associated with prominent Cenozoic subaerial volcanoes on Ross Island [*LeMasurier and Thompson*, 1990]. Volcanic exploitation of sediment in-filled rift basins has also been suggested for other sections of the rift [*LeMasurier*, 2008].

Two other negative isostatic anomalies also correlate to negative magnetic anomalies in the Rose Subglacial Basin (Figure 5.7, yellow circles 3 & 4), although these negative isostatic anomalies are not as spatially-extensive as the anomalies discussed above. The localized, circular negative isostatic anomaly labeled #3 is located over Mount Resnik, a circular and subaerially erupted- now subglacial- volcano that has not been significantly eroded by the ice sheet [*Behrendt, et al.*, 2007]. Anomaly #4 is located in the Jankowski Subglacial Highlands [*Behrendt, et al.*, 2004]. The correlation for isostatic anomaly #4 is tenuous because our isostatic method is circumspect in the highlands, as noted previously. The correlation over Mount Resnik, however, is striking. Mount Resnik cannot be made of hyaloclastites because it would certainly have been eroded away quickly [*Behrendt, et al.*, 2007] and yet it is characterized by a negative isostatic anomaly. The volcano is also located along the edge of a sedimentary basin, not in the middle of a depocenter, as with the anomalies discussed above. A possible explanation for its gravity signature is that it was erupted along a basin-bounding fault or fracture onto the cold, rigid crust and, not unlike my proposed explanation for volcanics interpreted in the Jankowski Subglacial Highlands (Chapter 3), is flexurally supported by the crust and has little to no crustal root. In this case, the isostatic correction would have over-corrected for the volcano by assuming a deep, locally-compensating root and created the negative isostatic anomaly over the volcano. My hypothesis is consistent with the suggestion that Mount Resnik is <15 m.y. old [*Behrendt, et al.*, 2007] and that the interior West Antarctic Rift System crust is generally cool. Therefore, the negative isostatic anomalies appear to be detecting low-density bodies of a range of compositions.

5.5 Conclusions

I have presented the first application in West Antarctica of an Airy isostatic correction to airborne Bouguer gravity anomalies and it successfully enhanced the gravity signals of near-surface changes in geology. The isostatic correction removed nearly two-thirds of the Bouguer signal, resulting negative isostatic anomalies that agree well with seismically-determined sedimentary basin thicknesses in the Rose Subglacial Basin. A sediment template can be derived by treating the -10 and -30 mGal isostatic anomalies as relative “likelihoods” of finding subglacial sedimentary basins. Negative isostatic anomalies over areas of high topography in the Jankowski Subglacial Highlands and Marie Byrd Land reflect undercompensated crust (i.e. lack of supporting Airy isostatic roots) rather than sedimentary basins. The pattern of the other isostatic anomalies, however, suggests that the Byrd Subglacial Basin is very sediment poor and that the Rose Subglacial Basin is sediment rich. The numerous borehole, seismic, and potential fields studies done in the Rose Subglacial Basin had previously suggested that the basin has been a long-lived depocenter for sedimentation and support my conclusion. In stark contrast, long-lived sedimentary basins are mostly limited to the structurally-controlled deep parts of the Byrd Subglacial Basin beneath Thwaites Glacier's tributaries. The lack of evidence for sedimentary basins near the fastest flowing ice at the coast suggests either long-distance, down-flow transport of sediment- or that a different mechanism is sustaining the glacier trunk's fast flow in the absence of basal lubricating sediment. Possible increased crustal heat flux in Marie Byrd Land could be providing substantial subglacial melt water to the fast flow in the western portion of the glacier trunk. A hydraulically-favorable flow path from Marie Byrd Land intersects Thwaites Glacier just upstream of its fastest flow velocities and is the most likely conduit for the hypothesized, lubricating subglacial melt water (*S. Carter, pers. comm.,* 2007).

Interesting correlations exist in the Ross Sea Embayment between previous studies of airborne magnetic anomalies [*Behrendt, et al.*, 2004] and this study's negative isostatic anomalies. Two isostatic anomalies that are here interpreted as deep sedimentary basins (labeled #1 and #2) correlate to magnetic anomalies interpreted by others as the intrusive remains of eroded volcanoes [*Behrendt, et al.*, 2004]. Based on the well-studied sedimentary basins in the Ross Sea section of this rift, thin crust probably underlies these thick interior basins and the volcanoes would have exploited that thin crust. A third magnetic anomaly and negative isostatic anomaly correlation, at subglacial volcano Mount Resnik, indicates lack of a compensating root for the volcano. Thus the volcano is not Airy isostatically compensated and would have erupted (hypothetically within the last 15 My [*Behrendt, et al.*, 2007]) after the rifted crust there became cool and rigid enough to flexurally support its topography.

Finally, positive isostatic anomalies indicate that there is a continuous “sill” running the length of the Amundsen Sea coastline that I interpret as crystalline basement. The area is underlain by thicker crust, now slightly thinned, that was once related to the Thurston Island or eastern Marie Byrd Land crustal blocks (Chapter 3). The sill underlies areas of high ice driving stress and thus is providing a wide grounding area for Thwaites Glacier. The sill will impede future grounding line retreat by providing stabilizing pinning points for the grounding line. If the glacier were to retreat ~100 km inland, sedimentary basins and deepening topography there would likely destabilize the glacier and induce runaway grounding line retreat [*Weertman*, 1974]. Thwaites Glacier is currently loosing substantially more mass than it is accumulating [*Rignot*, 2006]. This mass imbalance is causing significant widening of Thwaites Glacier’s trunk along the sill [*Rignot, et al.*, 2002], although there are few indications the grounding line is currently retreating across the sill.

This new information about the subglacial geology beneath Thwaites Glacier, from the lack of long-lived sedimentary basins to a crystalline sill at the coast beneath the grounding line, shows that this glacier’s subglacial setting is very different from the better-studied Ross ice streams in the Rose Subglacial Basin. The newly-gained knowledge of Moho depths across both basins (Chapters 3 and 4) led to better understanding of the causes of isostatic anomalies within the Jankowski Subglacial Highlands, Marie Byrd Land, the Whitmore Mountains, and at Mount Resnik. This study shows that carefully evaluated potential field studies can be used to provide a reliable geologic framework for the response of the West Antarctic ice sheet to current subglacial conditions and future climatic change.

Chapter 6: Conclusions

6.1 Renaming Subglacial Features

Based on recent subglacial topography results and this study's analyses of free-air, Bouguer, and Airy isostatic gravity anomalies, I suggest that two prominent subglacial features (actually three) be renamed. Throughout the text, I refer to the features as the Jankowski Subglacial Highlands (formerly the Sinuous Ridge), which separates the Byrd Subglacial Basin in the Amundsen Sea Embayment from the Rose Subglacial Basin in the Ross Sea Embayment (Figure 1.9). These names are appropriate because they honor the scientists who first discovered the features and also reflect our knowledge of the features' characteristics. These names are currently only suggested, but will be submitted for approval by the US Board on Geographic Names to become permanent name changes.

6.2 AGASEA Free-air Gravity Anomalies

This study's main technique was airborne gravity, and the main dataset from the AGASEA (Airborne Geophysics of the Amundsen Sea Embayment, Antarctica) survey from 2004-2005, in which I participated. I processed the raw gravity data from AGASEA into free-air anomalies and published a paper on the results [*Diehl, et al.*, 2008b].

Advances in gravimeter engineering evident in the Micro-G LaCoste Air/Sea II, which was used in the AGASEA survey, now allow more freedom in survey flight design. Planned and unplanned altitude changes did not contaminate as much of the recorded gravity signals with this new meter as would have been contaminated when using older meters, such as the BGM-3. The altitude changes induced little to no decrease in the overall quality of the dataset, as illustrated by the reasonable crossover errors for AGASEA. Having the capability to perform altitude changes in mid-flight (without extensive data loss) improves the competence of lower altitude gravity surveying in areas of rugged topography.

The tilt correction in free-air gravity processing is a limiting factor for final data quality. An accurate method for removing horizontal accelerations from the vertical gravity component does not yet exist in the literature. In the future, accurate modeling of the behavior of a gravimeter's platform (especially taking into account its platform period and damping) and horizontal accelerations recorded in two reference frames would probably yield the best tilt corrections.

Collecting concurrent surveys that significantly overlap their flight lines and share gravity ties, reduces final crossover errors between the surveys to within the limit of data quality- as seen with the AGASEA and BBAS overlapping data. This was particularly important because information was difficult to obtain about the histories, locations of, and gravity values at the McMurdo and South Pole gravity stations. Therefore, I also assembled a field guide [*Diehl*, 2008] (Appendix A) to the sites we visited during the 2004-2005 season. The field guide is also available online, on the UTIG website, so that these gravity sites are easier to locate for others' future Antarctic gravity research.

6.3 AGASEA Bouguer Gravity Anomalies

A paper based on the results presented in Chapter 3 is in preparation for submission to *Earth and Planetary Science Letters*. The first of several important findings was that the wide-scale Mesozoic rifting observed in the Rose Subglacial Basin continues into the Amundsen Sea Embayment and underlies Thwaites Glacier- topographically corresponding with the Byrd Subglacial Basin. Evidence for this interpretation includes a regional Bouguer gravity high over the basin, spectrally-derived Moho depths equivalent to or slightly shallower than those in the Ross Sea Embayment's Rose Subglacial Basin, and forward modeling results that suggest both ~3 km of intrusive rock in the upper crust and normal mantle temperatures within the Byrd Subglacial Basin. The interpretation of this area as thin, cool, rifted crust is consistent with off-shore, continental shelf seismic profiles [*Gohl, et al.*, 2007] as well as other previous work (see Chapter 1).

The boundary between the Byrd Subglacial Basin and Marie Byrd Land is not clearly defined in the Bouguer gravity anomalies. Rather, the smooth transition from regional positive to regional negative Bouguer anomalies indicates a diffuse crustal boundary rather than an abrupt change in crustal thickness or properties. The spectrally-derived Moho depths for the AGASEA survey indicate a zone of thin crust running through the center of the eastern Marie Byrd Land volcanoes, with Moho depths as shallow as 19 km. This is the thinnest crust yet identified in the ice-covered part of West Antarctica and I have interpreted this zone of thin crust as center of the transitional crust boundary between the Byrd Subglacial Basin and Marie Byrd Land.

Eastern Marie Byrd Land is characterized by spectrally-determined shallow Moho depths (~24 km) and the topography there cannot be Airy-isostatically compensated with this Moho depth. Therefore, the regional Bouguer negative anomaly observed in Marie Byrd Land is due to a different sub-surface, lower-density body, possibly located in the mantle. Forward modeling suggests that a warm mantle body adjacent to the base of the thin Marie Byrd Land crust fits the observed Bouguer gravity anomalies. If such a low-density body exists, it could be providing heat to thermally-support the high topography of the Marie Byrd Land volcanoes, as has been previously suggested [*LeMasurier and Landis*, 1997; *Winberry and Anandakrishnan*, 2004].

The Thurston Island crustal block is much smaller in extent than previously suspected and is not located in the AGASEA area. The only sections of thicker crust (~30 km Moho depths) in the surveyed area, interpreted as transitional crust, are located along the coast of the Amundsen Sea Embayment.

The Jankowski Subglacial Highlands lack crustal roots and thus are not Airy-isostatically compensated. The highlands, based on others' interpretations of negative magnetic anomalies over a small area of the chain, may have been volcanically-emplaced. To account for their lack of a crustal root, they must have been emplaced on cool, thin crust in the Byrd Subglacial Basin part of the rift system and their height must be flexurally-supported.

6.4 Free-air and Bouguer Gravity Anomalies Across West Antarctica

The work presented in Chapter 4 is in preparation for submission to the *Journal of Geophysical Research*. The scope of this study section was broad and major conclusions range from the feasibility of merging airborne gravity surveys to interpretations of the crustal structure of West Antarctica.

The disparities between overlapping sections of West Antarctic airborne free-air anomalies, from surveys collected over the span of 15 years, were up to 35 mGals even after accounting for flight altitude differences. GRACE (Gravity Recovery and Climate Experiment) satellite gravity anomalies proved to be an excellent long-wavelength dataset for correcting the offsets between the West Antarctic airborne datasets. Correcting the datasets with GRACE reduced offsets in the surveys' overlapping areas to within or just above the surveys' error thresholds. This method of leveling airborne gravity data to GRACE should be applicable anywhere else in the world with reliable GRACE free-air anomalies. Using this method to correct the airborne datasets allowed me to compare the relative magnitudes of Bouguer anomalies across West Antarctic for the first time.

The Thurston Island block must be reduced to at least half its previously hypothesized size [*Dalziel and* Elliot, 1982; *Dalziel and* Lawver, 2001] and is confined to the area north of Pine Island Glacier. However, several spectral estimates identified a ~30 km deep Moho along the coast of the Amundsen Sea Embayment. This deep Moho could represent a partially-rifted piece of transitional crust and/or could speculatively be the continuation of New Zealand's Median Batholith into Antarctica.

The character of the West Antarctic Rift System is different in the Byrd Subglacial Basin than in the Rose Subglacial Basin. The difference between the basins is immediately evident by the higher magnitude positive Bouguer anomalies in the Byrd Subglacial Basin. Yet, the average crustal thickness in the Byrd Subglacial Basin is not dissimilar from that in the Rose Subglacial Basin. Receiver function analyses of crustal thickness in the Rose Subglacial Basin [*Winberry and Anandakrishnan*, 2004] show little heterogeneity in the crust there, which is significantly different from my spectral analyses in the Byrd Subglacial Basin (Chapter 3) that revealed a large range in crustal thicknesses. Thus the heterogeneity of the Byrd Subglacial Basin crust suggests that the rifting history of the Byrd Subglacial Basin is more alike to that of the Ross Sea rift section than that of the Rose Subglacial Basin rift section. However, this may be a premature assessment based on the sparse sampling of Rose Subglacial Basin receiver function analyses and the coarse, averaging nature of my gravity spectral analyses.

The thin crust previously identified by this study (Chapter 3) in eastern Marie Byrd Land also exists on the western side of Marie Byrd Land, contrary to others' results that assumed a deep Moho there [*Luyendyk, et al.*, 2003]. This study's hypotheses of thin, thermally-supported crust in eastern Marie Byrd Land can then be broadened to include the western edge of Marie Byrd Land as well. However, a large data gap in central Marie Byrd Land precludes linking these two interpretations and further data is needed to assess whether the whole of Marie Byrd Land is thin, possibly thermally-supported crust. At very least, the crust in Marie Byrd Land is thinner than that in the large rift basins (the Rose and the Byrd) and can accurately be called transitional crust.

The edges of crustal blocks in West Antarctica (with the exception of the relatively sharp boundary between the Bentley Subglacial Trench and the Ellsworth Mountains) are generally diffuse zones of crustal change. The edges of the blocks are not likely to be characterized by a distinct crustal-scale fault. Instead, the character of the Bouguer anomalies shows that the boundaries are more gradual, possibly the product of heating and extension during the formation of the rift system and subsequent exploitation by Cenozoic volcanism (as is evident in eastern Marie Byrd Land, Chapter 3).

When combined, the West Antarctic free-air gravity anomalies from satellite and airborne data, the Bouguer gravity anomalies of the airborne datasets, and spectral Moho depth analyses of the airborne datasets have allowed new interpretations of crustal boundaries across > 1 million km^2 of West Antarctica. The pre-existing crustal block interpretations [*Dalziel and Elliot*, 1982; *Dalziel and Lawver*, 2001] were proven to be discordant with the new geophysical datasets in several places, especially in the Thurston Island block and Marie Byrd Land areas. This study redefined the locations and type of crustal boundaries across West Antarctic using a series of criteria, based on the geophysical compilation maps constructed here, as well as geologic information in the literature. The process of assembling a new interpretation map served to underscore two things: a. that our knowledge of subglacial geology is still very limited over many areas of West Antarctica and b. that identification of clear crustal boundaries is complicated by several stages of overprinting magmatism (subduction and rift-related) and extension.

6.5 Near-Surface Geology of West Antarctica, Particularly Sedimentary Basins and Volcanics

The work done as part of Chapter 5 is in preparation for publication, possibly to be sent to *Geology* or *Geophysical Research Letters*. This body of work shows that Airy isostatic anomalies, which have been used successfully elsewhere in the world to locate changes in near-surface geology, can also be successfully applied to West Antarctic airborne gravity datasets. Treating the West Antarctic Airy isostatic anomalies as relative "likelihoods" is much more appropriate than interpreting their magnitudes directly. Doing so, I created a sediment template of the areas most likely to contain long-lived, sediment-filled basins, based on gravity data alone.

The Airy isostatic anomalies generated for the AGASEA and CASERTZ airborne gravity datasets (Chapter 5) compare well with seismically-identified sedimentary basins and their relative thicknesses in the Rose Subglacial Basin. In the Byrd Subglacial Basin, where no sedimentary basins have yet been identified, the isostatic anomalies correlate well to other datasets that are potential indicators of subglacial sediment and sedimentary basins.

There are several areas where the assumption of Airy isostatic compensation is invalid (as suggested in Chapters 3 and 4). Thus the isostatic anomalies in the Jankowski Subglacial Highlands and Marie Byrd Land should not be interpreted for near-surface subglacial geology since they also reflect departures of the Moho from Airy isostatic equilibrium. Further studies that calculate isostatic anomalies over the Jankowski Subglacial Highlands due to flexural support of the highland topography may obtain a better result for near-surface geologic interpretations.

Positive Airy isostatic gravity anomalies along the coastline of the Amundsen Sea Embayment correlate to the same area that I previously suggested could be thicker transitional crust. Also, the pattern of the isostatic anomalies matches that of ice driving stresses and suggest a "sill" of rough, denuded bedrock that will impede future Thwaites Glacier grounding line retreat of up to ~100 km, providing a stabilizing force for a glacier catchment grounded significantly below sea level.

The pattern of isostatic anomalies across the two subglacial basins reveals previously unknown patterns of subglacial infill. Thwaites Glacier is situated over the very sediment poor, rifted crust of the Byrd Subglacial Basin while the Ross Sea ice streams are positioned over a sediment rich, also rifted crust of the Rose Subglacial Basin. The isostatic anomalies in the Rose Subglacial Basin indicate that the sedimentary basins there are both spatially more extensive and deeper (based on the relative magnitudes of the isostatic anomalies). The differences between the subglacial conditions of these two basins, suggests that Thwaites Glacier is either transporting sediment down-flow from where it underlies its tributaries (unlikely given the distanced necessary for transport) or that a different subglacial mechanism is sustaining Thwaites Glacier's fastest flow (in the western half of its trunk). I suggest that substantial melt water flow from Marie Byrd Land (which may have higher heat flux, according to results in Chapter 3) is lubricating the base of the ice in the absence of subglacial sediment.

6.2.2 DELIVERABLES FROM THIS STUDY

The AGASEA free-air gravity processing produced line-based and gridded free-air gravity anomalies. I released to the public in April 2008 both a free-air anomaly grid and a map of flight line crossover errors, permanently housed at the National Geophysical Data Center [*Diehl, et al.*, 2008a]. I also modified the in-house free-air gravity processing codes (written in Matlab by Tom Richter [*Holt, et al.*, 2006b], based on the original codes by Vicki Childers [*Childers*, 1996]) to be general enough to handle surveys flown at angles to projected straight Northing and Easting lines and to include a tilt correction.

At the start of this study, no in-house programs existed for calculating a complete 3D Bouguer correction of gravity data. A program acquired to do a complete Bouguer correction had to be general enough to allow: 1. calculations at flight altitudes, not assuming sea level as the observation height; 2. topography below sea level; 3. a correction for the ice sheet; and 4. input topography over very large areas (over 800 x 800 km) at 2-10 km resolution. Bouguer correction codes from Geosoft's Oasis Montaj software (for the PC) and the University of British Columbia's GRAV3D software (for MS-DOS) were not general enough to accommodate the airborne gravity from West Antarctica. However, a Gaussian-Legendre Quadrature (GLQ) gravity calculation code (for UNIX/LINUX, obtained from the British Antarctic Survey) [*von Frese, et al.*, 1981] was appropriately flexible. The GLQ code was applied it to this study in Chapters 3 and 4 and resulted in a new grid of 3D complete Bouguer gravity anomalies over Thwaites Glacier, as well as updated Bouguer anomalies for the Ross Sea Embayment and western Marie Byrd Land.

Additionally, I created Linux shell scripts to implement spectral depth calculations (Chapters 3 and 4) on both the free-air and Bouguer gravity data, making use of existing functions in the Generic Mapping Tools (GMT) software [*Wessel and Smith*, 1998]. The program is general enough to apply to any gridded gravity dataset and can iterate over any number of user-defined sub-sets of the input gridded data and subsets of wavenumbers over which to fit linear segments. The spectral depth estimates yielded a map of small-scale Moho depth changes in the Thwaites Glacier area (Chapter 3) and regional changes in Moho depth across West Antarctica (Chapter 4).

In order to successfully merge airborne gravity anomalies across several disparate datasets (Chapter 4), I used a method for leveling the airborne gravity datasets that utilized a GRACE gravity dataset. Close collaboration with the University of Texas at Austin, Center for Space Research was necessary to produce the satellite equivalent free-air anomalies at 3600 m altitude, based on the GGM03s global static model. In exchange, this study's airborne free-air anomaly compilation for West Antarctica is being used to verify the small-scale features of GRACE "combined" global gravity model (GGM03c, satellite plus ground data from all over the world).

Forward modeling codes were created to calculate gravity based on a published method [*Talwani, et al.*, 1959] and used as the 2D forward problem in Chapter 4's inversions. I also wrote the codes to perform the simulated annealing inversions, which were based on the methods of *Roy, et al.* [2005] and *Sen and Stoffa* [1995]. These codes were both accomplished in Matlab.

The major data and interpretation-based deliverables from Chapter 4 of this study included compilation maps of: a. free-air gravity of West Antarctica and the surrounding oceans from airborne and satellite datasets, b. Bouguer gravity anomalies from overlapping airborne datasets in West Antarctica, and c. a new interpretation sketch map of West Antarctic crustal blocks and rifted areas. The interpretation map includes boundaries for those crustal blocks that were once part of Gondwana in the Paleozoic, overlaid with the extent of the late Mesozoic rift system and more localized Cenozoic activity.

The British Antarctic Survey kindly provided codes to calculate an Airy isostatic correction, which I then modified to calculate a correction for the 2-layer crust in West Antarctica (Chapter 5). The code utilizes GMT tools, as well as the GLQ gravity calculation program described above. The major product of this section's work is a sediment template, which identifies the most likely areas to find sedimentary basins in West Antarctica, assuming Airy isostatic equilibrium and that all negative anomalies indicate sedimentary basins. The template is readily testable by future seismic work and drilling and will be useful for further cross-catchment studies of the West Antarctic subglacial environment.

Appendices

Appendix A: Details of AGASEA Campaign Field Work

A version of this appendix was also published as (reproduced with permission):

Diehl, Theresa M. 2008. "Field Guide to Antarctic Gravity Stations Visited During the 2004-2005 AGASEA Airborne Campaign." UTIG Technical Report No. 194. 23 pp. Available online: http://www.ig.utexas.edu/library/tech_reports/utig_tech_rep_194.pdf

A1. Handheld G-meter Gravity Readings

Over the course of the 2004-2005 AGASEA field season, three main operators (Theresa M. Diehl (TMD), Irina Y. Filina (IYF), and Erick Leuro (EL)) took gravity readings with a hand-held LaCoste & Romberg G-meter borrowed from the USGS. Janessa M. Link (JML) performed only one reading at the Thiel Station in McMurdo for the purpose of training her on the gravimeter. There were a total of 90 "average" readings taken over an 80 day span at a variety of station locations (Table A1.2). An "average" reading usually consists of three readings taken by a single operator at a location, where between each reading the gravimeter was clamped, un-leveled, re-leveled, and then re-read. This procedure provides an estimate of operator errors involved in the leveling and reading process. The operators established this procedure after Julian Day 320 and consistently followed it throughout the rest of the season. A complete field guide to the locations used for these gravity ties, as well as other historical gravity tie information, is included in Appendix A.2. Gravimeter readings in counter units were transformed into mGals using the information in Table A1.1. For example, a meter reading of 5732.7 CU (and thus, a base reading of 5700 CU) yields a gravity reading of 5973.67 such that: 5939.59 mGal + (1.04210 * (5732.7 CU - 5700 CU) = 5973.67 mGal.

Table A1.1: Conversions from counter units (CU) to milliGal (mGal)

Base Reading (CU)	Base Reading (mGal)	Interval Factor
5700	5939.59	1.04210
5800	6043.80	1.04190
6300	6564.57	1.04085

Table A1.2: Gravity Tie Data

Location	Year	Julian Day	Operator	Julian Day & Time	Average Reading (CU)	Gravity (mGal)	Reading Precision (mGal)
Thiel	2004	319	IYF	319.251	6351.75	6618.43	-
Thiel	2004	319	TMD	319.256	6351.85	6618.54	-
Seismic	2004	319	IYF	319.270	6351.52	6618.19	-
Seismic	2004	319	TMD	319.274	6351.59	6618.27	-
Hut Pt BC-4	2004	320	IYF	320.271	6356.68	6623.57	-
Hut Pt BC-4	2004	320	TMD	320.274	6356.88	6623.77	-
Thiel	2004	323	IYF	323.256	6351.75	6618.43	0.03
Thiel	2004	323	TMD	323.261	6351.78	6618.46	0.01
Seismic	2004	323	IYF	323.269	6351.51	6618.18	0.01
Seismic	2004	323	TMD	323.275	6351.45	6618.13	0.02
Thiel	2004	323	IYF	323.281	6351.79	6618.48	0.02
Thiel	2004	323	TMD	323.285	6351.77	6618.45	0.01
Hut Pt BC-4	2004	323	TMD	323.304	6356.85	6623.75	0.02
Hut Pt BC-4	2004	323	IYF	323.309	6356.90	6623.80	0.01
Thiel	2004	323	TMD	323.328	6351.87	6618.55	0.01
Thiel	2004	323	IYF	323.333	6351.82	6618.50	0.02
SJB ZCM	2004	323	TMD	323.379	6332.96	6598.88	0.16
SJB ZCM	2004	323	IYF	323.384	6332.87	6598.78	0.05
Thiel	2004	323	IYF	323.422	6351.87	6618.56	0.01
Thiel	2004	323	TMD	323.427	6351.87	6618.56	0.01
Thiel	2004	323	IYF	323.748	6351.85	6618.54	0.00
Thiel	2004	323	TMD	323.752	6351.84	6618.53	0.02
Old S. Pole	2004	324	TMD	324.026	5721.00	5961.48	0.01
Old S. Pole	2004	324	IYF	324.030	5721.01	5961.48	0.01
New S. Pole	2004	324	TMD	324.052	5722.56	5963.10	0.00
New S. Pole	2004	324	IYF	324.055	5722.60	5963.14	0.00
Thiel	2004	324	IYF	324.231	6351.83	6618.52	0.03
Thiel	2004	324	TMD	324.237	6351.85	6618.54	0.02
Thiel	2004	328	TMD	328.025	6351.75	6618.44	0.02
Thiel	2004	328	EL	328.034	6351.75	6618.43	0.03
Seismic	2004	328	EL	328.046	6351.45	6618.13	0.03
Seismic	2004	328	TMD	328.050	6351.49	6618.16	0.01
Thiel	2004	328	EL	328.058	6351.61	6618.28	0.29

Location	Year	Julian Day	Operator	Julian Day & Time	Average Reading (CU)	Gravity (mGal)	Reading Precision (mGal)
Thiel	2004	328	TMD	328.061	6351.79	6618.48	0.02
Hut Pt BC-4	2004	328	TMD	328.075	6356.72	6623.61	0.01
Hut Pt BC-4	2004	328	EL	328.084	6356.73	6623.61	0.03
Thiel	2004	328	TMD	328.095	6351.74	6618.43	0.04
Thiel	2004	328	EL	328.105	6351.73	6618.41	0.03
SJB ZCM	2004	328	TMD	328.148	6332.86	6598.77	0.06
SJB ZCM	2004	328	EL	328.154	6332.95	6598.87	0.09
Thiel	2004	328	EL	328.179	6351.72	6618.40	0.02
Thiel	2004	328	TMD	328.183	6351.77	6618.46	0.01
Thiel	2004	331	TMD	331.237	6351.69	6618.37	0.01
Thiel	2004	331	EL	331.241	6351.71	6618.39	0.01
SJB ZCM	2004	331	EL	331.261	6332.12	6598.00	0.68
SJB ZCM	2004	331	TMD	331.266	6332.73	6598.64	0.05
Thiel	2004	331	TMD	331.289	6351.73	6618.41	0.01
Thiel	2004	331	EL	331.293	6351.70	6618.38	0.00
Thiel	2004	336	EL	336.210	6351.68	6618.36	0.02
Thiel	2004	336	TMD	336.214	6351.74	6618.42	0.00
Thiel	2004	337	EL	337.872	6351.74	6618.42	0.03
Thiel	2004	337	TMD	337.876	6351.78	6618.47	0.01
Seismic	2004	337	TMD	337.881	6351.37	6618.04	0.01
Seismic	2004	337	EL	337.892	6351.37	6618.04	0.01
Thiel	2004	337	EL	337.898	6351.72	6618.40	0.02
Thiel	2004	337	TMD	337.902	6351.78	6618.47	0.01
Hut Pt BC-4	2004	337	EL	337.921	6356.75	6623.64	0.01
Hut Pt BC-4	2004	337	TMD	337.926	6356.77	6623.66	0.01
Thiel	2004	337	TMD	337.938	6351.77	6618.46	0.01
Thiel	2004	337	EL	337.942	6351.77	6618.45	0.00
Thiel	2004	338	JML	338.081	6351.73	6618.42	0.03
Thiel	2004	338	TMD	338.084	6351.77	6618.46	0.01
Thiel	2004	338	EL	338.088	6351.73	6618.41	0.02
SJB ZCM	2004	338	TMD	338.109	6332.67	6598.57	0.09
SJB ZCM	2004	338	EL	338.117	6332.73	6598.63	0.02
Thiel	2004	338	EL	338.134	6351.73	6618.41	0.01
Thiel	2004	338	TMD	338.145	6351.75	6618.44	0.01
Thiel	2004	344	EL	344.845	6351.50	6618.17	0.27
Thiel	2004	344	TMD	344.850	6351.70	6618.38	0.01
SJB Willy	2004	344	TMD	344.889	6310.24	6575.23	0.12
SJB Willy	2004	344	EL	344.905	6310.35	6575.34	0.09
Thiel	2004	344	TMD	344.959	6351.70	6618.39	0.01
Thiel	2004	344	EL	344.968	6351.72	6618.40	0.03
SJB THW	2004	347	EL	347.451	5883.76	6131.07	0.06
SJB THW	2004	347	TMD	347.456	5883.85	6131.16	0.02
SJB THW	2004	354	TMD	354.984	5883.76	6131.07	0.03

Location	Year	Julian Day	Operator	Julian Day & Time	Average Reading (CU)	Gravity (mGal)	Reading Precision (mGal)
SJB THW	2004	354	EL	354.986	5883.81	6131.12	0.02
PNE	2004	355	TMD	355.164	5849.54	6095.42	0.02
SJB THW	2004	355	TMD	355.347	5883.80	6131.11	0.01
SJB THW	2004	365	TMD	365.025	5883.61	6130.91	0.01
SJB THW	2004	365	EL	365.284	5883.79	6131.10	0.05
PNE	2005	2	TMD	2.994	5849.40	6095.27	0.01
SJB THW	2005	8	TMD	8.081	5883.51	6130.81	0.01
SJB THW	2005	8	EL	8.085	5883.65	6130.95	0.01
PNE	2005	19	TMD	19.982	5849.53	6095.41	0.01
SJB THW	2005	21	EL	21.190	5883.73	6131.04	0.01
SJB THW	2005	22	TMD	22.910	5883.52	6130.82	0.01
SJB THW	2005	32	EL	32.862	5883.52	6130.82	0.02
SJB THW	2005	32	TMD	32.867	5883.53	6130.83	0.02
Thiel	2005	33	EL	33.978	6351.69	6618.38	0.02
Thiel	2005	33	TMD	33.984	6351.73	6618.42	0.01

A.2. Gravimeter Drift Calculations, Absolute Gravity Determination, and Ties

Since the handheld and airborne gravity meters for this survey were relative instruments (measuring changes in gravity, not the absolute value of gravity), they were calibrated by tying their counter values to a base station of known absolute gravity value. At McMurdo the only station with a "known" gravity value was the Thiel station, which was tied to the IGSN71 network (see Appendix A.2. and Chapter 2 for discussions of the marker's history and absolute gravity value). Therefore, the three main G-meter operators took 44 readings at the Thiel station, with 42 of those readings occurring before the put-in to THW remote field camp and two occurring in the limited three days the field party had at McMurdo post-season.

The total length of each timeseries at Thiel varies by operator, but all three operators' readings cluster within a rage of only 0.5 mGal, including both pre- and post-field operations (Figure A1.1). Therefore, there were no tares in the G-meter data during the four-month field season. Using all the Thiel data points and assuming a linear fit, the drift rate would be 0.0016 mGal/dy and would produce a total 0.128 mGal drift over the 80 days of measurement (Figure A1.2). I also calculated a G-meter drift rate for the TMD timeseries at the THW field camp. At 0.0073 mGal/dy, the total drift would be 0.3723 mGal over the 51 days of G-meter measurements at THW field camp (Figure Al.3). Both calculated drift rates are too small to be significant and are thus negligible considering the accuracy of airborne surveys is generally several (1-4) mGal. So, no G-meter drift correction was needed. I performed a similar analysis with the Micro-g LaCoste Air/Sea II average still readings taken throughout field operations and also found a negligible drift rate for that meter.

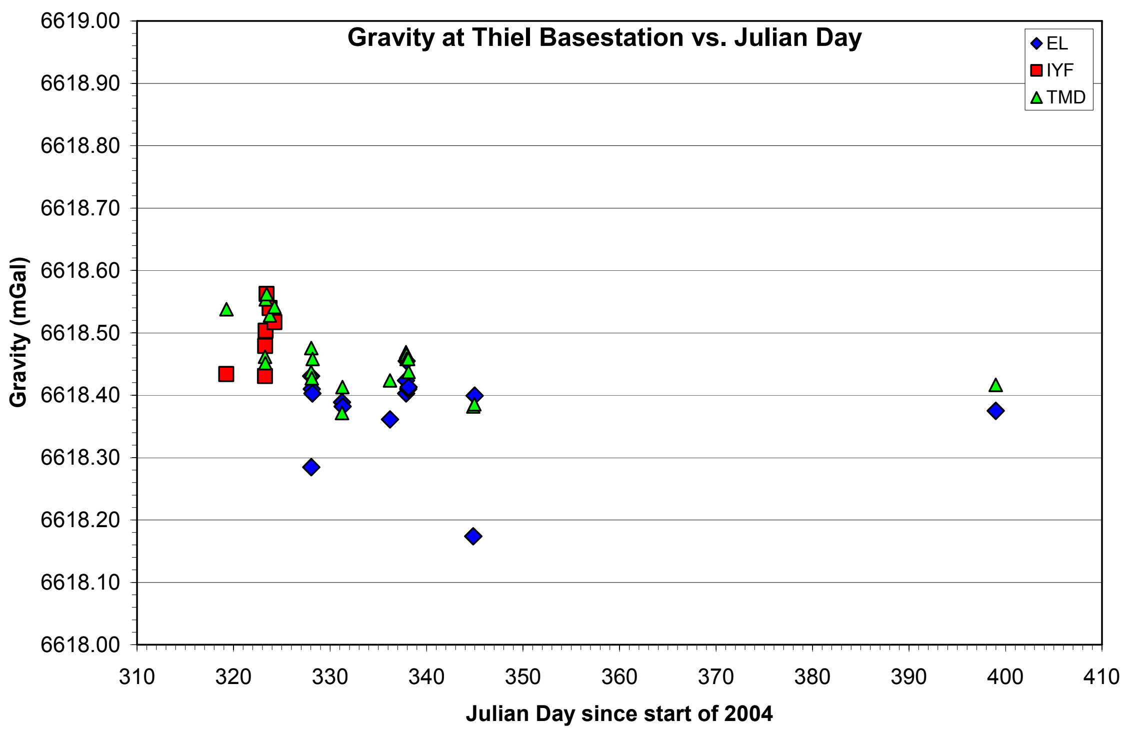

Figure A1.1: Gravity readings in mGals at the Thiel basestation in McMurdo over the course of the 2004-2005 AGASEA season, for three operators.

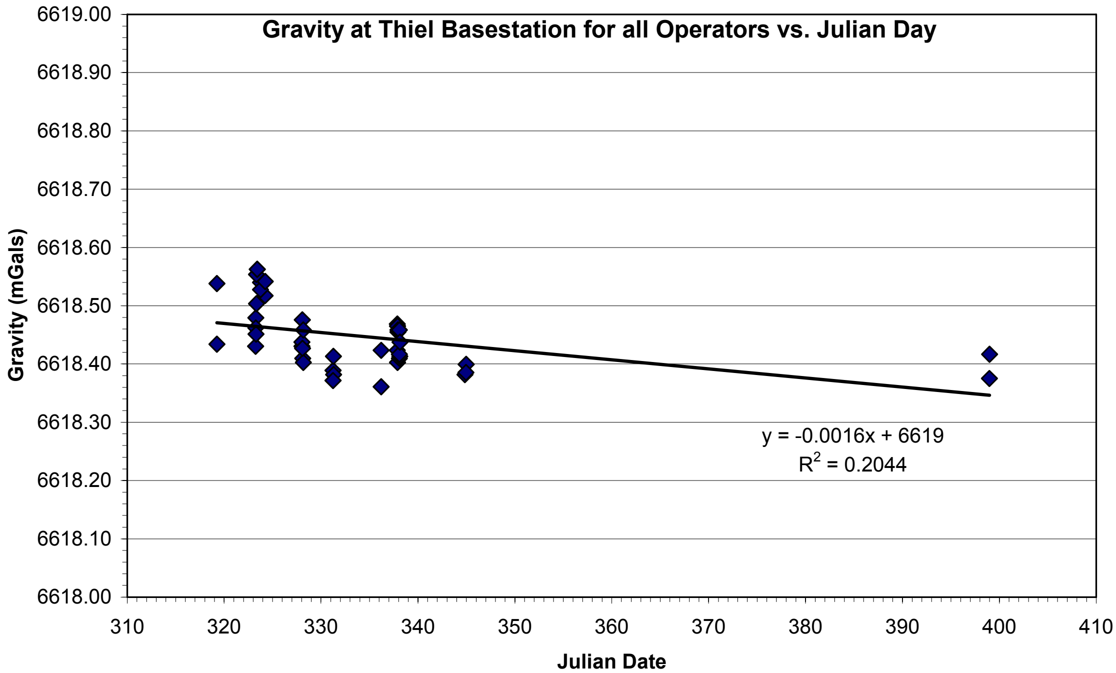

Figure A1.2: Same as figure A1.2 but with best-fit drift rate.

Of the three series available at McMurdo's Thiel station, those from TMD and EL have readings both before and after field operations. But TMD's series is the longest, therefore I used the average of the TMD data points at Thiel station to calculate the offset between the G-meter gravity reading and absolute gravity (Table A1.3, column 1): 976351.27 mGals. I then applied this offset to the average TMD readings at THW and PNE temporary field camp stations in order to tie the still reading of the Micro-g LaCoste Air/Sea II gravimeter (at THW, Figure A1.4) and the gravimeters used during the British Antarctic Survey's field season (at PNE) (Table A1.3). The offsets I calculated from the UTIG ties are being used for the British Antarctic Survey's datasets preferentially over their own ties due to UTIG's slightly shorter time between Thiel base station measurements and access to a more recent absolute gravity value reading in McMurdo than those available for Rothera's gravity station (T. A. Jordan, pers. comm., 2007); [*Jordan, et al.*, submitted].

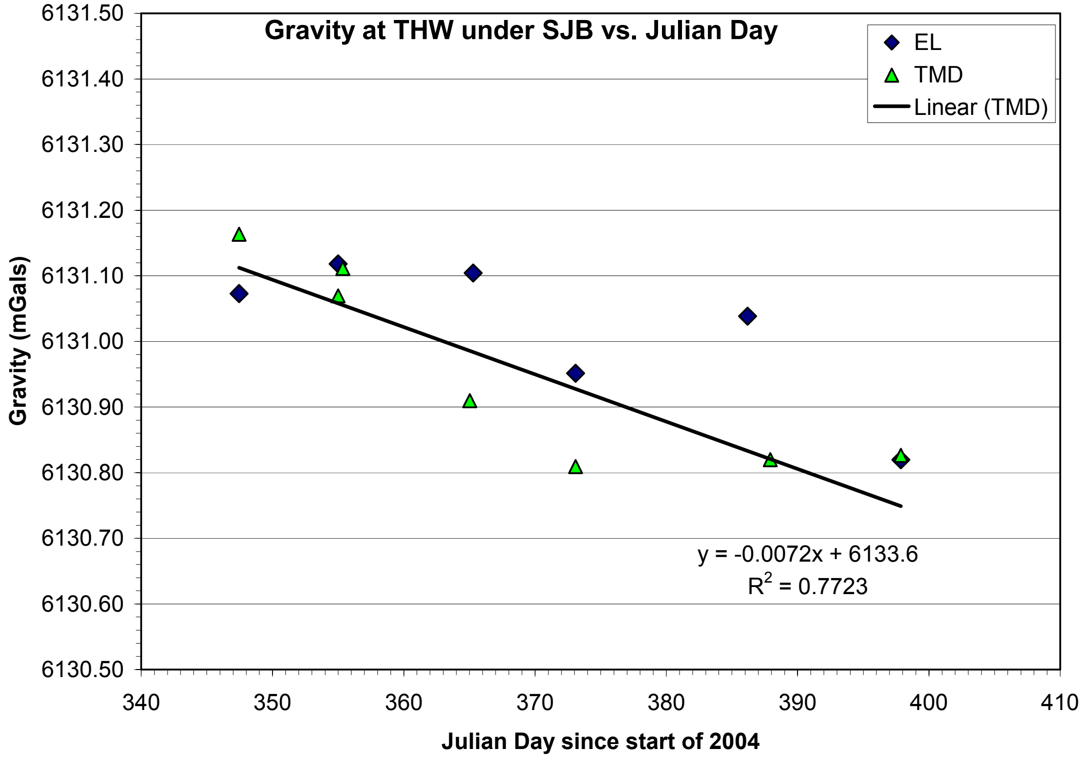

Figure A1.3: Handheld gravimeter readings at the Thwaites remote field camp.

Table A1.3: Absolute gravity at three stations, tied to IGSN71

	Thiel (McMurdo) TMD Average	THW TMD Average	PNE TMD Average
G-meter Gravity Reading (mGals)	6618.46	6130.96	6095.41
IGSN71 Absolute Gravity (m/s2)	9.829697277	9.824822263	9.824466819
IGSN71 Absolute Gravity (mGals)	982969.7277	982482.2263	982446.6819
Air/Sea II Still Gravity Reading (mGals)	-	13914.16	-

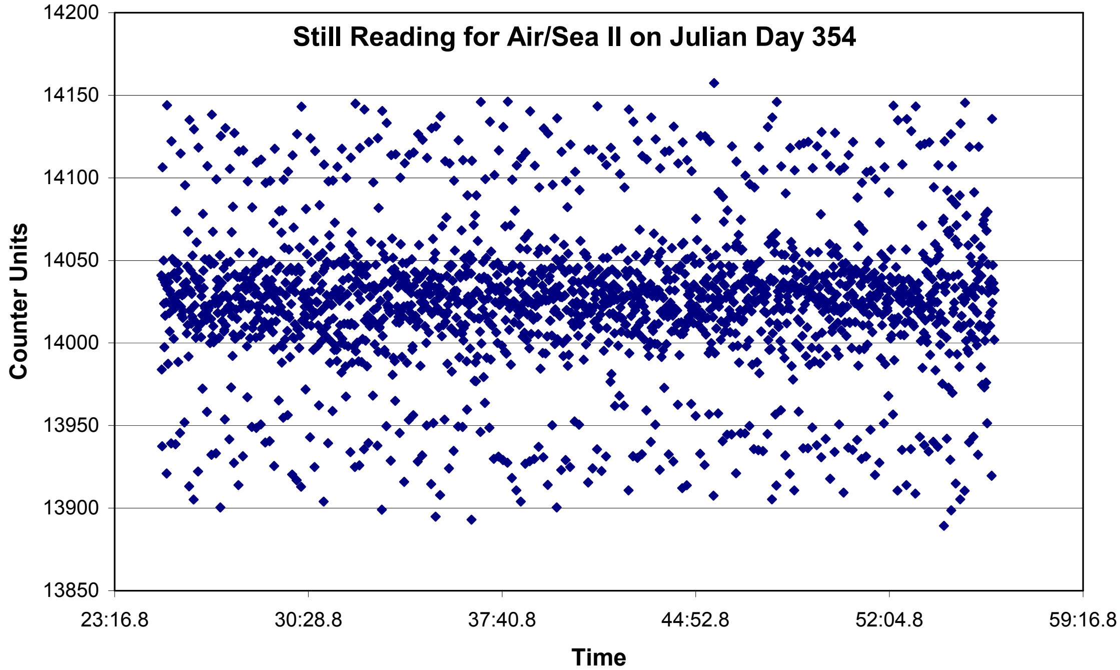

Figure A1.4: Still reading for the Air/Sea II airborne gravimeter (raw counter units sampled at 1 Hz) over 30 min on Julian Day 354 (coincident in time and location with handheld gravimeter readings), the average 14026.37 CU from this still reading equates to 13914.16 mGals when adjusted for the gravimeter's scaling factor.

A2. Field Guide to Major McMurdo Gravity Station Locations

Bldg 146: Gravity Benchmark Shack, USGS brass plaque labeled "THIEL"

The USGS THIEL gravity benchmark (Figure A2.1) was located in the Thiel Science Building until 2001- when the building was demolished to make way for the Crary Lab). At that time, the benchmark was moved to Bldg 146, a shack up the hill from Science Cargo but set back on the right side (Figure A2.2). The shack was originally used as a water pump house but was converted to a small, heated office with the installation of the benchmark. A description of the location (and the gravity reading there) is as follows from a compilation posted (as of Feb. 2005) on the wall inside Bldg. 146 (see Figure A2.8 for photograph of whole compilation) (J. Bucher, unpublished data, 2003):

> "Pier inside old Water Transfer Pump House Building
> USGS Brass Disk "Thiel Gravity Base Station" 2001-2002
> Lat: -77˚ 50' 55.9068" / -77.8490˚
> Long: 166˚ 40' 45.9629" / 166.6794˚
> Elev: 46.21 m above MSL
> Absolute Gravity (mGals): 982970.52"

As of 2007, no absolute gravity readings had been done in Bldg. 146 and Thiel had only been tied to absolute gravity by hand or by upward continuation of an old value to its current location (see Chapter 2 for the upward continued value, which was used for the AGASEA survey). There are plans to demolish this marker in the 2007-2008 season and establish a new gravity benchmark elsewhere in McMurdo.

Figure A2.1: THIEL Gravity Benchmark in Bldg 146

Figure A2.2: The Gravity Shack (Building 146), uphill from Science Cargo and the BFC.

Hut Point: USGS brass plaque labeled BC-4

There are two USGS satellite triangulation benchmarks on Hut Point but only one has a record of gravity measurements associated with it. The benchmark on top of the concrete pillar (visible in Figure A2.3 and featured in Figure A2.4) is named "Astro Pier" and there are no gravity measurements associated with this benchmark. The second benchmark is mounted on a weather-beaten concrete block in the ground a few meters from the "Astro Pier" and the brass plaque reads "BC-4" (Figure A2.5). A description of the location and the gravity reading there is as follows (J. Bucher, unpublished data, 2003):

> "International Satellite Triangulation Station
> Brass Disk "Station Number 053 B-04" 1969
> Lat: -77° 50' 41.1720" / -77.8448°
> Long: 166° 38' 30.6278" / 166.6418°
> Elev: 17.58 m above sea level
> NIMA Station ID: 0-185-6
> Absolute Gravity (mGals): 982976.62"

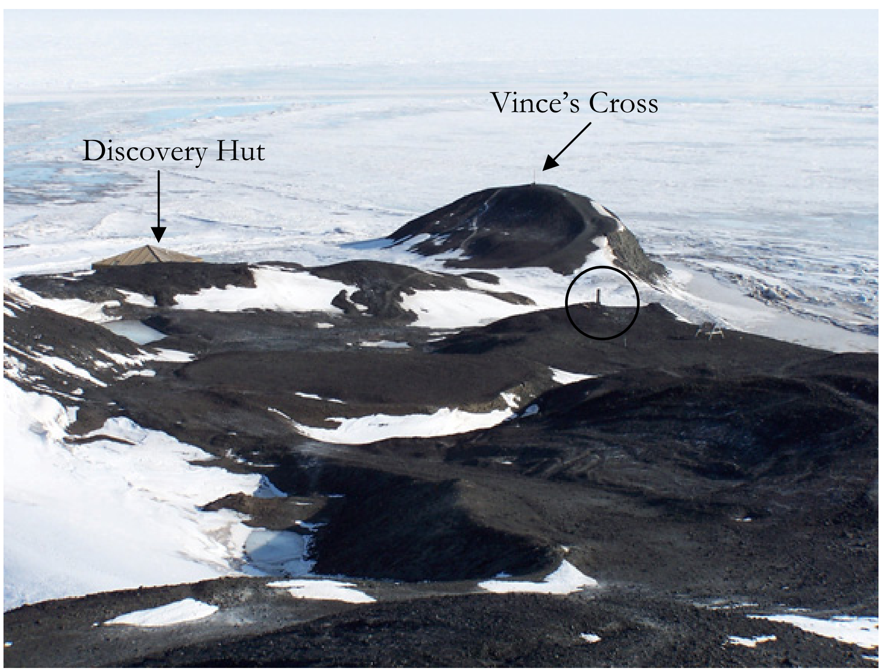

Figure A2.3: Location of USGS benchmarks (black circle) on Hut Point, McMurdo.

Figure A2.4: Satellite Triangulation Marker “Astro Pier”

Figure A2.5: Satellite Triangulation and Gravity Marker labeled “BC-4”

Bldg 139(Abandoned FSTOP office in 2005)- SEISMIC plaque

A metal pin (Figure A2.6) is located in a concrete pad at this location but lacks any other distinguishing markers. Based on description of the site (Figure A2.7) that follows (J. Bucher, unpublished data, 2003), this is the assumed location of the SEISMIC plaque:

"SE corner of building on concrete pad
USGS Brass Disk "SEISMIC" 1966-67
Lat: -77 deg 50' 55.15" / -77.8487 deg
Long: 166 deg 40' 47.93" / 166.6800 deg
Elev: 49.29 m above MSL
NIMA Station ID: 0-185-4
Absolute Gravity (mGals): 982970.18"

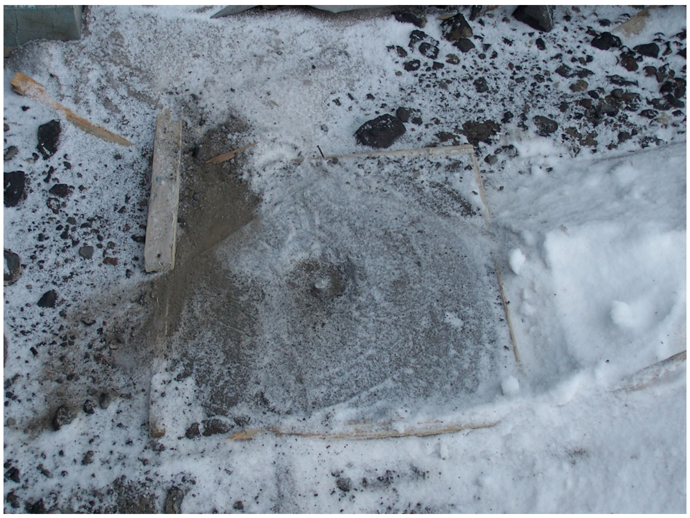

Figure A2.6: Metal pin in concrete slab on ground- assumed location of SEISMIC

Figures A2.7: SE corner of Bldg. 139

SATGRAV a.k.a. HUGO marker near old Building 57

This marker was moved from Building 57 (old MEC) to the ground northeast of Bldg 602 when Bldg 57 was demolished to make way for Building 4 (SSC). Building 602 was subsequently also demolished in 2003 to make room for an extension to Building 4 and the marker was also demolished in 2003. A description of the location is as follows (J. Bucher, unpublished data, 2003):

> "Building 57 demolished, marker in ground NE of Bldg 602
> USGS Brass Disk "SATGRAV" 1991-1992
> Lat: -77 deg 50' 51.66" / -77.8487 deg
> Long: 166 deg 40' 27.78" / 166.6744
> Elev: 35.07 m above MSL
> NIMA Station ID: 0-185-7
> Absolute Gravity (mGal): 982972.95"

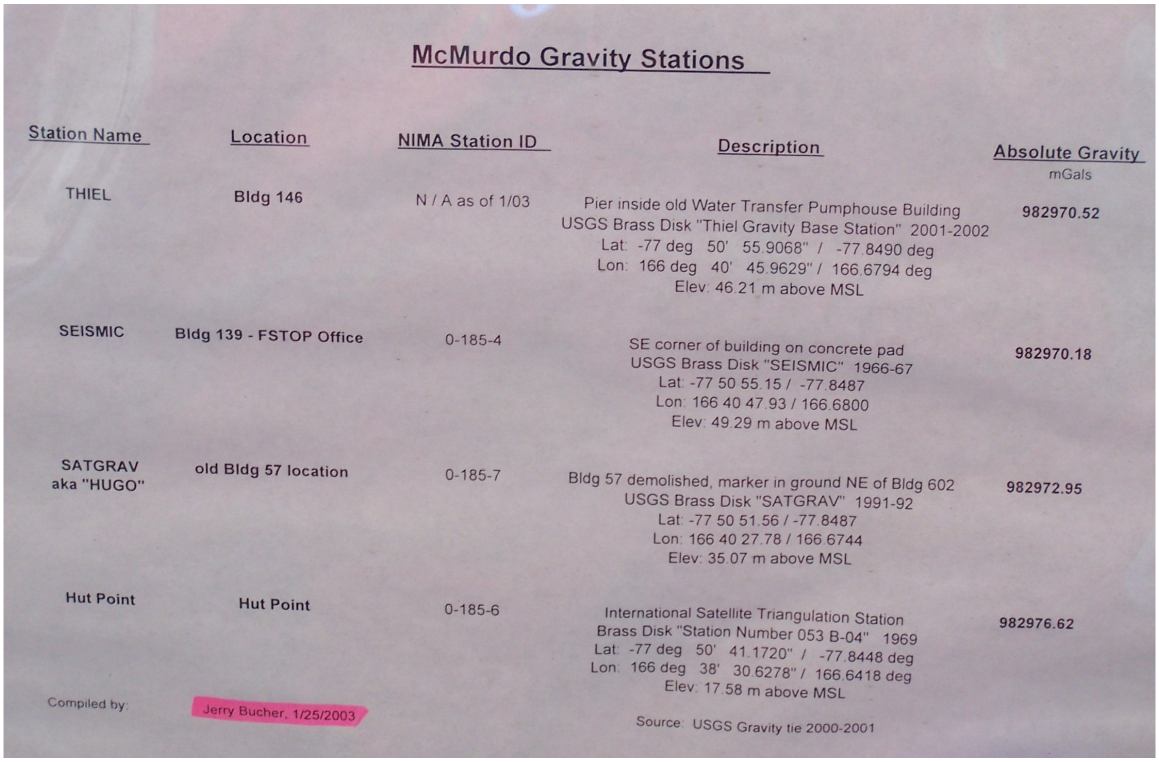

McMurdo Gravity Stations

Station Name	Location	NIMA Station ID	Description	Absolute Gravity mGals
THIEL	Bldg 146	N / A as of 1/03	Pier inside old Water Transfer Pumphouse Building USGS Brass Disk "Thiel Gravity Base Station" 2001-2002 Lat: -77 deg 50' 55.9068" / -77.8490 deg Lon: 166 deg 40' 45.9629" / 166.6794 deg Elev: 46.21 m above MSL	982970.52
SEISMIC	Bldg 139 - FSTOP Office	0-185-4	SE corner of building on concrete pad USGS Brass Disk "SEISMIC" 1966-67 Lat: -77 50 55.15 / -77.8487 Lon: 166 40 47.93 / 166.6800 Elev: 49.29 m above MSL	982970.18
SATGRAV aka "HUGO"	old Bldg 57 location	0-185-7	Bldg 57 demolished, marker in ground NE of Bldg 602 USGS Brass Disk "SATGRAV" 1991-92 Lat: -77 50 51.56 / -77.8487 Lon: 166 40 27.78 / 166.6744 Elev: 35.07 m above MSL	982972.95
Hut Point	Hut Point	0-185-6	International Satellite Triangulation Station Brass Disk "Station Number 053 B-04" 1969 Lat: -77 deg 50' 41.1720" / -77.8448 deg Lon: 166 deg 38' 30.6278" / 166.6418 deg Elev: 17.58 m above MSL	982976.62

Compiled by: Jerry Bucher, 1/25/2003

Source: USGS Gravity tie 2000-2001

Figure A2.8: The "McMurdo Gravity Stations" compilation done by J. Bucher (unpublished data, 2003), hanging in Bldg. 146 in 2004-2005.

A3. Field Guide to South Pole Gravity Station Locations

Old South Pole Marker: In dome, metal pier in ice

The Old South Pole marker was established by researchers from the University of Wisconsin, Madison (possibly in 1989?). It is a cylindrical metal pier embedded in the ice beneath the Dome (Figure A3.1) and accessed through a hatch in the floor of one of the storage buildings (being used for computer parts storage in 2004). The location was marked with a paper on the ceiling indicating the gravity station and we had to unroll a floor mat to reveal the hatch (A3.2). Two sheets of field notebook paper stapled to the floor beneath the hatch reveal the following visitors and readings:

Neal Lord (UW Madison) 1/21/89 to 1/26/89		
1/26/89	G1	5808.76
	G19	5703.92
T. Clarke		
1/22/92	G1	5812.49
	G19	5790.32
Peter Buckholder & Chen Liu		
1/25/94	G1	5813.72
(~1300 hrs)	G19	5779.41
Carol Finn (USGS) & Vicki Langenheim (USC)		
	G161	5743.36
	C191	5772.65
Marcy Davis & Vicki Langenheim (SOAR)		
12/18/98 08:54	G-64	5717.43

We added Theresa Diehl and Irina Filina to the list in 2004 (see values in Table A1.2).

However, this marker was decommissioned during the demolition of the old station, which started in the winter after the 2004-2005 season (P. Sullivan, pers. comm., 2008).

Figure A3.1: Metal pier gravity station below floor hatch in the South Pole Dome

Figure A3.2: Metal pier gravity station with handheld gravimeter for scale.

New South Pole Marker: Recessed wooden in snow tunnels

The new gravity station at South Pole is located at the end of one of the snow utility tunnels at the pole (Figures A3.3 and A3.4, labeled “Gravity vault”). The tunnel is accessed through a door and the vault is down a long, narrow passageway that is wide enough for only one person abreast because of utility pipes running through the tunnel. The station is clearly marked with a hanging sign (Figure A3.5), but is in a dark corner. I recommend bringing a flashlight or other light source in addition to the built-in lights on the gravimeter in order to easily see the readings. This station is awkward to access (Figure A3.6) since it is recessed into the snow of the tunnel floor. Layers of thick clothing and -50°F temperatures in the snow tunnel make kneeling/laying in the snow for any amount of time an uncomfortable experience. However, this new station is exceptionally quiet and yields very accurate readings.

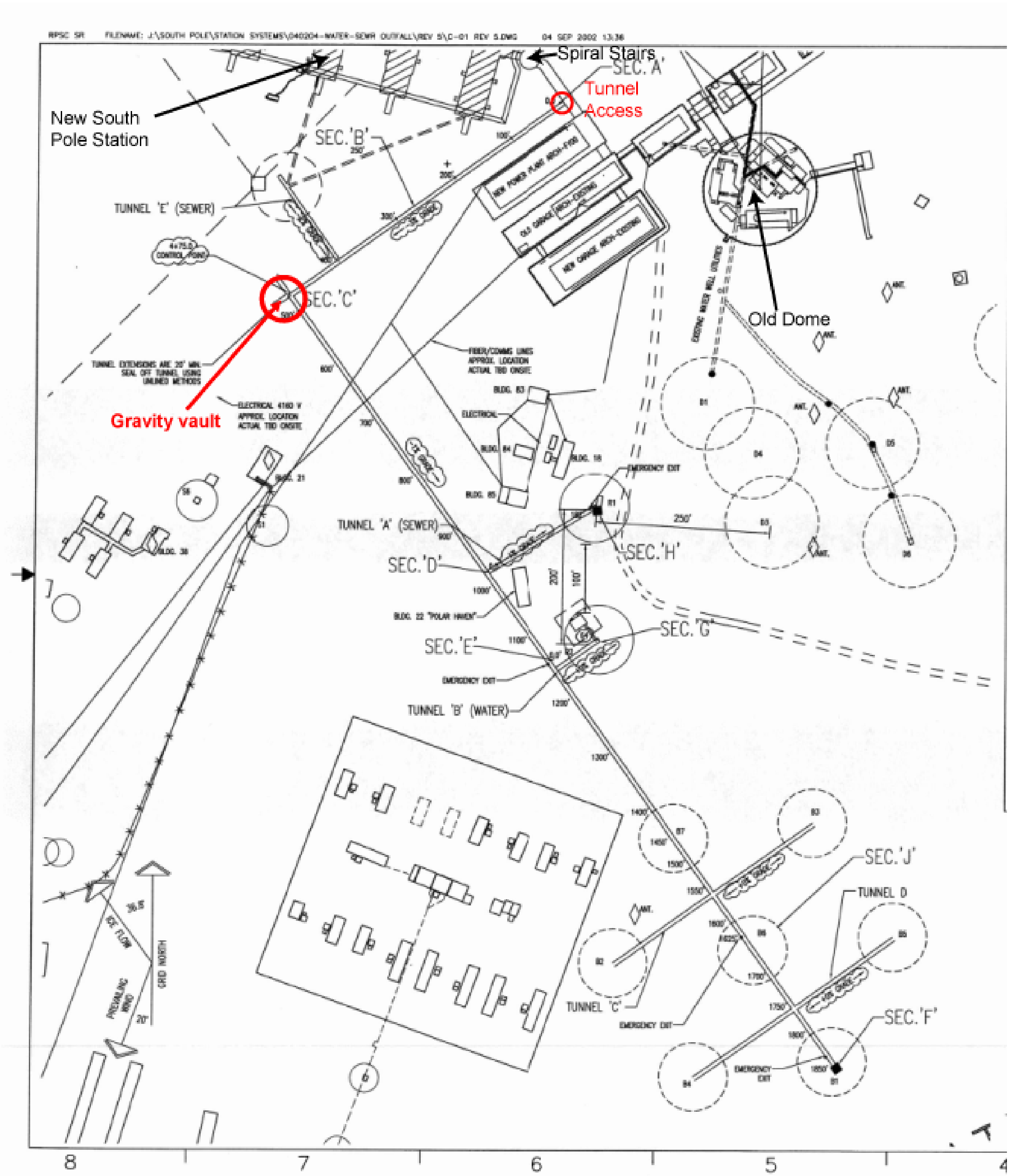

Figure A3.3: Raytheon Polar Services Sewer/Water Tunnel Plan at South Pole, sheet 2 of 25, drawn by C. Rock on 09/15/98. Labels added for the current location of the new gravity vault, old dome, new station, and spiral stairs (modified, image courtesy of P. Sullivan, pers. comm., 2008).

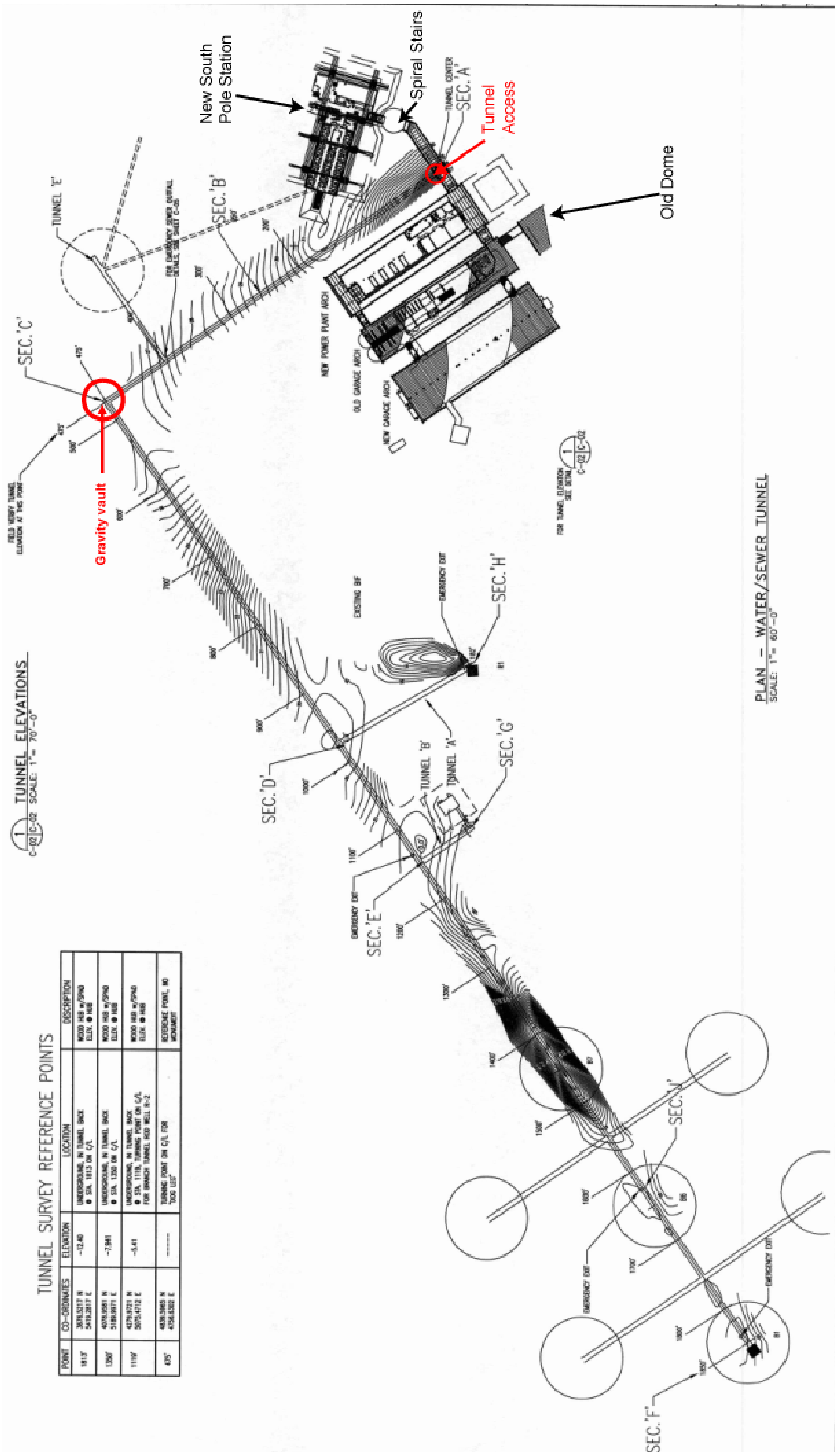
New South Pole Station
Spiral Stairs
Tunnel Access
Old Dome
Gravity vault
SEC.'A'
SEC.'B'
SEC.'C'
SEC.'D'
SEC.'E'
SEC.'F'
SEC.'G'
SEC.'H'
TUNNEL 'A'
TUNNEL 'B'
TUNNEL 'E'
NEW POWER PLANT ARCH
OLD GARAGE ARCH
NEW GARAGE ARCH
EMERGENCY EXIT
TUNNEL ELEVATIONS
PLAN – WATER/SEWER TUNNEL
TUNNEL SURVEY REFERENCE POINTS

Figure A3.4: (previous page) Raytheon Polar Services Sewer/Water Tunnel Profiles and Elevations at South Pole, sheet 3 of 25, drawn by C. Rock on 07/13/98. Labels added for the current location of the new gravity vault, old dome, new station, and spiral stairs (modified, image courtesy of P. Sullivan, pers. comm., 2008).

Figure A3.5: New South Pole gravity station in the snow tunnels; the Science Support Supervisor in 2004, Paul Sullivan, showed us the location.

Figure A3.6: The author taking a gravity reading at the New South Pole station.

A.5. Field Guide to Other Gravity Station Locations used in 2004-2005

SJB ZCM and SJB Willy: McMurdo Airport Locations

These two gravity locations were on floating ice, the first (ZCM) at the sea-ice runway at the beginning of the season and the second (Willy) at Williams Field on the ice shelf. Both were temporary locations and measurements were taken beneath the airplane in line with the airborne gravimeter. Both sites were difficult to take measurements at, especially ZCM) because the floating ice flexed due to nearby loads and readily transferred vibrations from other parts of the runway. These are the least trust-worthy gravity readings of the field season.

SJB THW: Thwaites Glacier Remote Field Camp 2004-2005

This gravity site was located at the remote field camp, though the exact position changed within a half-dozen meters in any direction depending on the where the plane was parked. Measurements were always taken under the plane, in line with the airborne meter. Since the metal plate used for leveling was kept inside a jamesway and was warmer than the ice, we had to put a flat piece of wood or cardboard beneath it to keep it from melting into the ice and becoming unleveled.

PNE: Pine Island Glacier Remote Field Camp 2004-2005

The Pine Island Glacier field camp station was well-located and stationary. The station consisted of a square, shallow trench in the snow with a "pier" of snow left in the center, about half the height of trench, on which to level the gravimeter. The trench was covered by a piece of wood to protect it from drifting and was located several meters away from the area where our Twin Otter parked for refueling. Establishing a semi-permanent base station like this one is preferable at field camps, compared to the method of measurements at Thwaites Glacier field camp.

APPENDIX B: GRAVITY CALCULATION FORWARD MODEL

My 2D forward problem used a common geometrical approximation to calculate gravity anomalies for bodies of a known density and shape, which was derived by *Grant and West* [1965] from *Talwani, et al.* [1959]. The *Grant and West* [1965] equation is as follows:

$$\Delta g(l_m) = 2G\Delta\rho \sum_{k=1}^{N} (b_k /(1+a_k)) \left[\tfrac{1}{2}\ln\left(\frac{x_{k+1}^2 + z_{k+1}^2}{x_k^2 + z_k^2}\right) + a_k \left(\tan^{-1}\left(\frac{x_{k+1}}{z_{k+1}}\right) - \tan^{-1}\left(\frac{x_k}{z_k}\right)\right)\right] \quad (1)$$

where:

$$a_k = \left(\frac{x_{k+1} - x_k}{z_{k+1} - z_k}\right)$$

$$b_k = \left(\frac{x_k z_{k+1} - x_{k+1} z_k}{z_{k+1} - z_k}\right)$$

G is the gravitational constant (6.6732 x 10^{-11} Nm^2/kg^2),

$\Delta\rho$ is the density contrast between the perturbing body and its surroundings in kg/m^3,

x is the horizontal distance between any corner point (k=1:N) and the observation point (l_m; m=1:M) in meters,

z is the locally-defined depth of the body's corner point in meters, positive downward,

M is the number of observation points,

and N is the number of corner points.

For any given geometry, the number of calculations performed to calculate gravity at one observation point is N and the total number for M observation points is M*N. The perturbing body is represented by a closed polygon, where the first corner and the last corner points coincide i.e. $(x_{N+1},z_{N+1})=(x_1,z_1)$, as noted in *Grant and West* [1965].

Equation 1 works in the locally-defined coordinate system of x-z (distance-depth). Zero distance is defined as the position of the m=1 observation point. Zero depth is defined as the elevation of your measurements, which are assumed to all be at the same elevation. In practice, defining the model's local coordinates is straight-forward. First, create a vector of the distances along a profile that represent the gravity observation points. Although the observation points have been observed at some real elevation, they do not require an associated depth vector since they are defined as having zero depth. Then, create two vectors- one distance and one depth- to represent the corner points of the disturbing body. The depth vector should simply be the real estimated depth to the body plus the elevation of the observation points. This process preserves the distance between the observation points and the corner points of the body and allows Equation 1 to remain general. Finally, define the density contrast between the perturbing body and surrounding material based on *a priori* information and assume it to be constant across the entire body.

A few mathematical complications arise when using Equation 1 because it is very general. A simple evaluation reveals that division-by-zero errors occur when any corner point's depth is equal to zero and when any two consecutive corner points' depths are equal. It is necessary to add very small fractions of a number (~.00001 m) to any depths that may cause division by zero errors. As well, calculating the gravity effects of subsurface layers (e.g. the crust)- where gravity changes are essentially due to an undulating lower surface- must be modeled to appear "infinite" in the x direction to eliminate edge effects. This involves setting the end corner points at very large distances from the center. The actual distance needed to eliminate edge effects can be determined by trial and error with synthetic models, and from experience is sufficient at > 10,000 km on either side of the first and last observation points.

There is a correction factor associated with Equation 1 that is used to obtain gravity anomalies rather than the full gravity effect of a subsurface layer. For example, Equation 1 would calculate the full gravity effect of the crust in Figure B.1 (red outline). The correction factor removes the effect of a constant-thickness portion of the layer (here called a “slab”) so that only the changes in gravity across the layer (i.e. gravity anomalies) are calculated for the remaining mass (Figure B.1, blue outline). The correction factor (C) is a constant for a slab of a given thickness (t), according to *Grant and West* [1965]:

$$C = 2\pi G \Delta\rho t \qquad (2)$$

The correction assumes that the slab’s top boundary is at zero depth.

Even in the case where a body can be approximated as a slab, a correction factor may not be necessary if the forward problem is parameterized differently. For instance, Figure B.1 shows two representations of Moho undulations for the same piece of theoretical crust. Both representations result in the same observed gravity anomaly when a correction for t = 20,000 m is used on the approximate slab model. Thus, the t-factor may be avoided in the forward model completely, if carefully approached.

Synthetic Tests of Forward Problem

To test the accuracy of my forward problem with synthetic data, I calculated gravity anomalies for examples given in *Telford, et al.* [1990] (Figures B.2, B.3, and B.4) and compared my gravity anomalies with those given. The forward problem using Equation 1 performed as expected when all the aforementioned corrections and considerations were applied. The forward problem replicated the gravity results exactly for the examples for each scenario of: a displaced rod, a faulted horizontal bed, and a semi-infinite sheet. The Matlab codes used to generate these test models and then perform the forward problem are listed in Appendix F4.

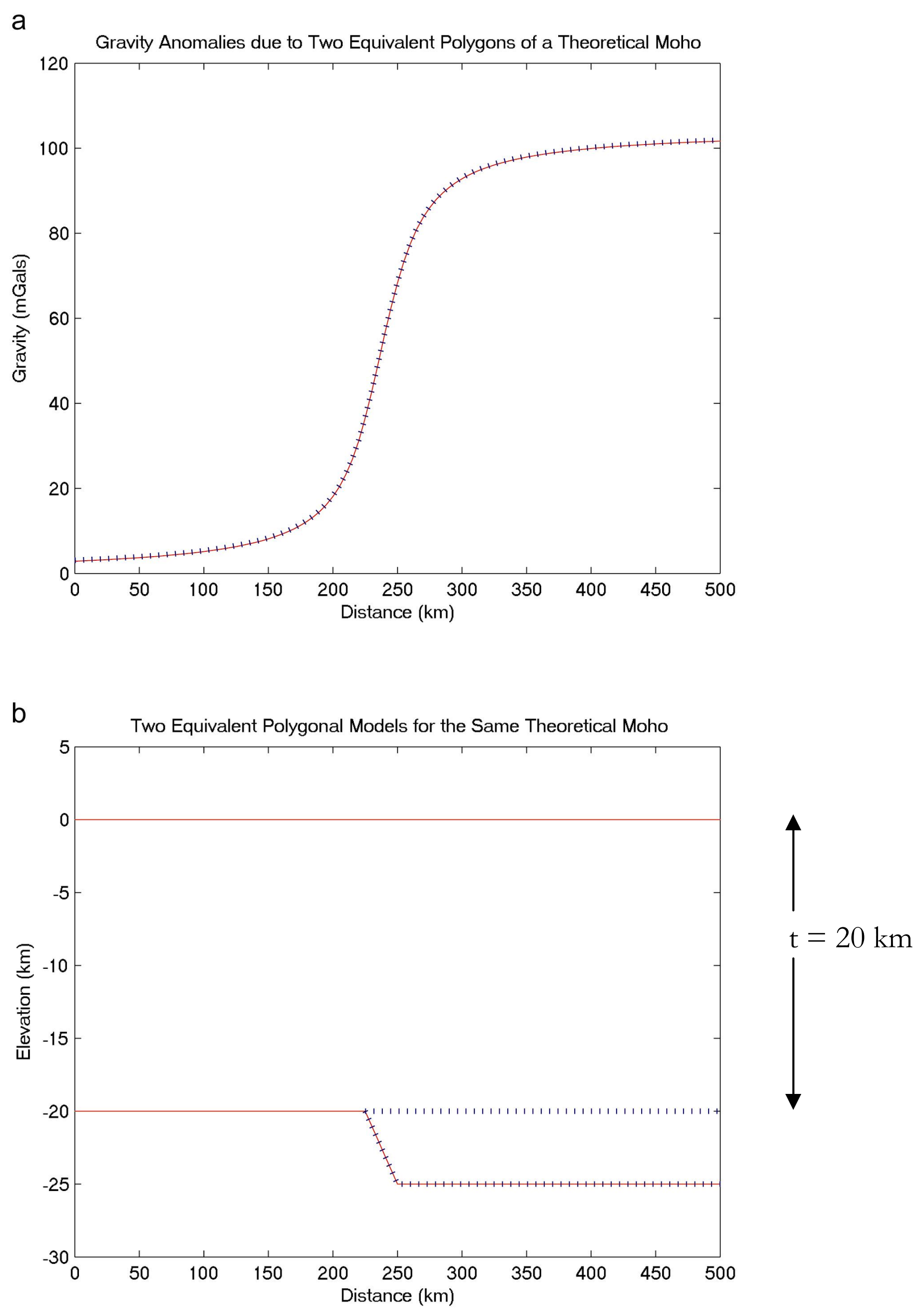

Figure B.1: a. Equivalent gravity effects of two ways to parameterize a theoretical crust. For the red-line model: calculated with Equation 1 and corrected for a 20 km thick slab using Equation 2. For the blue-line model: calculated using only Equation 1 for the semi-infinite 5 km thick body; b. Polygonal models used to approximate the crust, color-coded to match the results in (a).

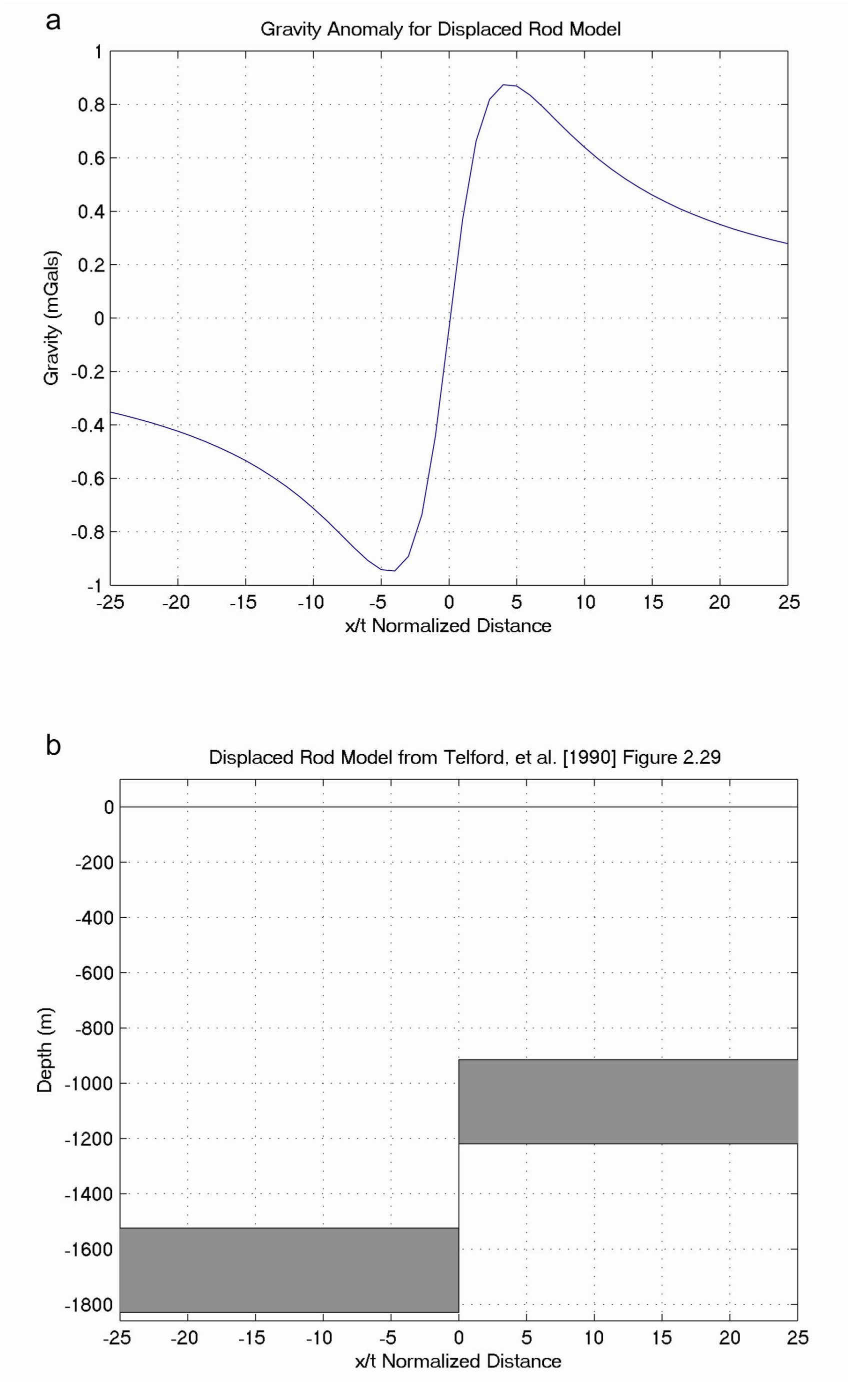

Figure B.2: a. Gravity anomaly calculated by forward problem (Equation 1) for the displaced rod model of *Telford, et al.* [1990] Figure 2.29, displacement angle of 90°; b. Displaced rod polygon input to the forward model.

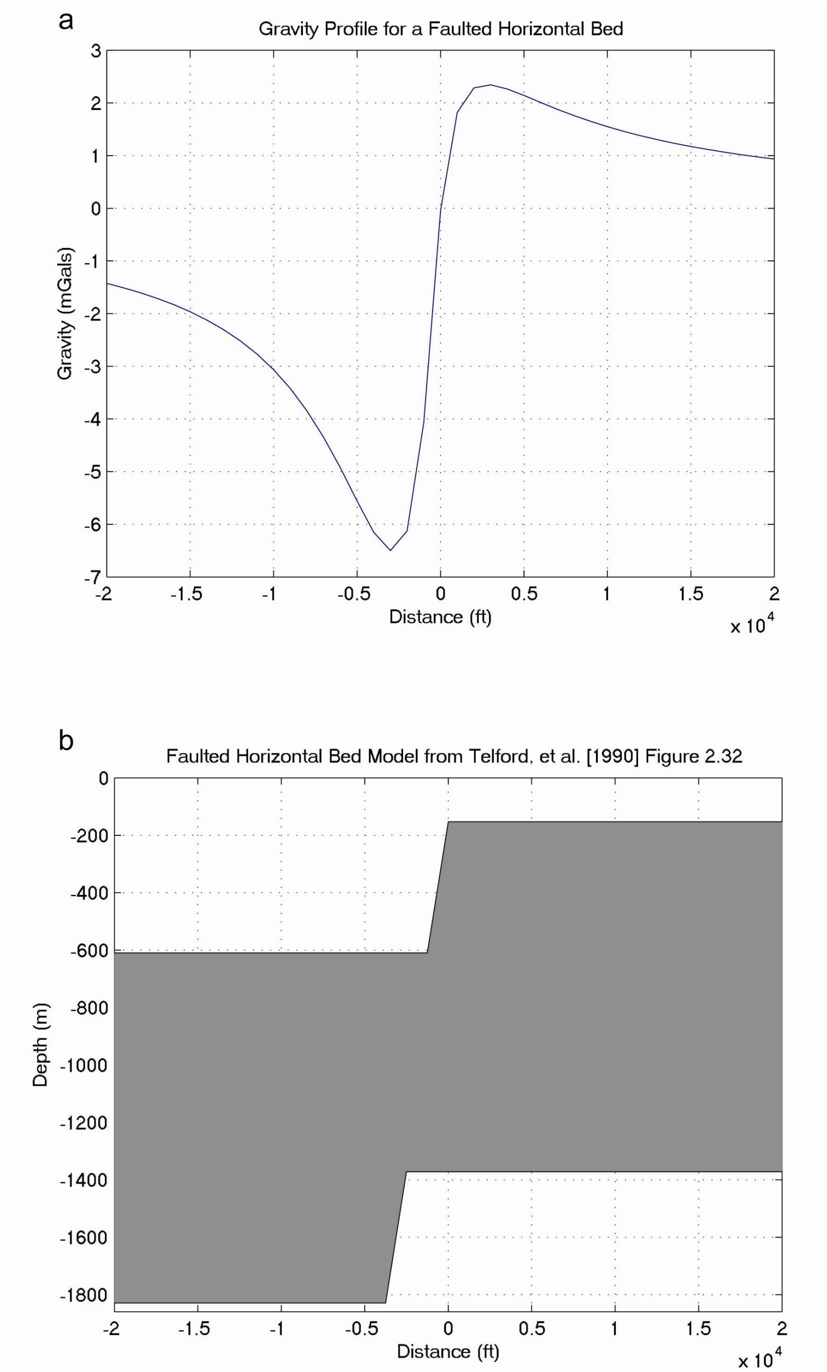

Figure B.3: a. Gravity anomaly calculated by forward problem (Equation 1) for the faulted slab model from *Telford, et al.* [1990] figure 2.31; b. Faulted slab polygon input to the forward model, dip angle = 60°.

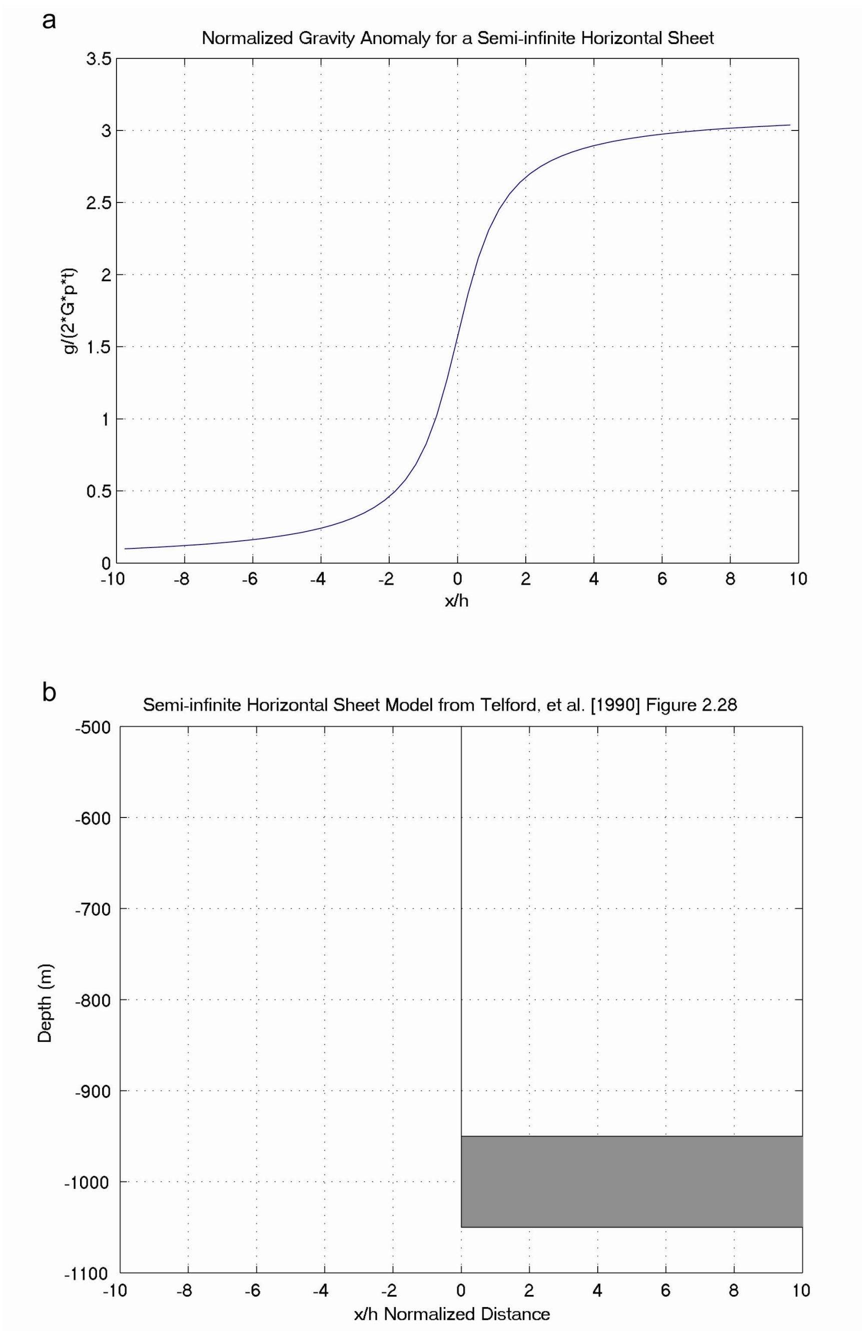

Figure B.4: a. Gravity anomaly calculated by forward problem (Equation 1) for the semi-infinite horizontal sheet model from *Telford, et al.* [1990] figure 2.28; b. Semi-infinite sheet polygon input to the forward model.

APPENDIX C: VERY FAST SIMULATED ANNEALING GRAVITY INVERSION

Inversion Theory

Gravity data modeling can be approached with either iterative forward modeling- in which the user dictates changes to the input physical model in order to fit observed data- or with inverse modeling where a mathematical routine controls the changes made the physical model and fits the data as closely as statistically appropriate. The former method is very straight-forward to accomplish once a forward model has been coded and can be made very complicated based on *a priori* geologic and geophysical information on the densities and shapes of sub-surface bodies. The latter method, however, is more appropriate for areas where less is know about the structures causing gravity anomalies and where there are a number of possible, non-unique physical models, as is common with gravity. Inversion also provides a statistically rigorous data fit that accounts for error.

Two general types of inversions exist: local and global methods. Local inversions, such as the conjugate gradient algorithm, are appropriate for modeling problems that are well-constrained by borehole, seismic, or other datasets. These constraints limit the number of possible physical models that provide a close fit to the gravity data and provide a good initial guess of the physical situation at hand. Global methods could potentially be useful in gravity modeling situations where there is little to no other constraining information available and thus there is not an accurate guess of the physical situation to be modeled (e.g. no seismically-determined crustal thickness estimates available to guide a gravity model of crustal thickness). Global methods have an advantage in this situation since they search a range of physical models for the global minimum error and do not require initial knowledge of the body creating the gravity anomaly.

I used a global inverse method called very fast simulated annealing (vfsa). All simulated annealing methods (of which there are several others, including Metropolis, Heat Bath, Fast SA, and Mean Field SA [*Sen and Stoffa*, 1995]) share similar traits in their algorithms. They are based on physical process of slowly crystallizing a high-energy liquid by decreasing its temperature slowly enough to allow the particles to organize themselves into a low energy state. According to *Sen and Stoffa* [1995], annealing occurs when a solid is heated to liquid state in a heat bath so that all the particles in the bath are randomly distributed before the temperature is slowly decreased toward crystallization. In the parallel sense, the inverse method considers the particles to be the physical model parameters, the energy to be the amount of error in a model's fit to the data, the state to be the lowest-error physical model at a given level of random perturbation (i.e. higher temperature = higher excitability = higher randomness), and crystallization to be the convergence of the inversion at lowest randomness to a lowest error model fit to the data.

Cooling is analogous to randomly perturbing the physical model at each step, but generally with less and less departure from the previous model at every step. The cooling process is step-wise because the particles must be allowed to remain in each temperature state for enough time to obtain the lowest energy possible at that temperature. If temperatures are decreased too fast, the particles may retain too much energy in their current states and never organize into an orderly crystal. Likewise, if the temperature is not decreased to a sufficiently low level, then there will be too much energy remaining in that state for the particles to crystallize. However, one advantage of the vfsa algorithm is that a global minimum error (i.e. energy state) can be reached given a statistically-proven cooling schedule [*Sen and Stoffa*, 1995]:

$$T_i(k) = T_{0i} \exp\left(-c_i k^{1/NM}\right) \qquad (1)$$

where $T_i(k)$ is temperature of the model parameter (i) at any iteration (k), T_{0i} is the initial temperature for the model parameter, c_i is a tuning coefficient, k is the iteration number, N is the total number of model parameters, and M is the number of possible values for each model parameter. In practice, the cooling schedule is often treated as the same for each model parameter, so that all are governed by one cooling schedule:

$$T(k) = T_0 \exp\left(-ck^{1/NM}\right) \qquad (2)$$

Vfsa has this advantage over other simulated annealing algorithms because the amount that any model parameter is perturbed is based on a non-Cauchy probability distribution [*Sen and Stoffa*, 1995]. Using a Cauchy distribution is slow, so *Ingber* [1989] identified a different distribution (Eqns. 4.38 and 4.39 in *Sen and Stoffa* [1995]) that increases the speed with which a model can converge (i.e. crystallize). *Sen and Stoffa* [1995] concisely and clearly outline the inversion process (which I present below) and show that any given model parameter (m_i) at any given step in cooling (k) will always lie within the model space dictated by the parameter's maximum and minimum values:

$$m_i^{\min} \le m_i^k \le m_i^{\max} \qquad (2)$$

and can be perturbed at the next cooling iteration (k+1) such that:

$$m_i^{k+1} = m_i^k + y_i\left(m_i^{\max} - m_i^{\min}\right) \qquad (3)$$

where $y_i \in$ [-1,1] (i.e. in a uniform distribution) and satisfies the non-Cauchy distribution from *Ingber* [1989] when written as:

$$y_i = \mathrm{sgn}\left(u_i - \tfrac{1}{2}\right)T_i\left[\left(1 + \frac{1}{T_i}\right)^{|2u_i - 1|} - 1\right] \qquad (4)$$

where $u_i \in$ [0,1] and is a randomly drawn number.

These equations control the random process of perturbing the model parameters during cooling, with the perturbations becoming less with increasing iterations (since they are dependent on an exponentially decreasing temperature), and the model eventually converging using the cooling schedule in Equation 1.

However, the equations above require additional criteria to determine whether any set of model perturbations are acceptable and should be applied to the model before the next iteration. First, an error is calculated for both the existing model's fit to the data and for the randomly perturbed- but not yet accepted- model. There are many possible error criteria available with which to evaluate the model fit and I chose an error derived from *Sen and Stoffa*'s [1995] Equation 6.4 normalized measure of fitness:

$$E = \frac{2\sum |g_{mi} - g_{oi}|^{\alpha}}{\sum |g_{mi} + g_{oi}|^{\alpha} + \sum |g_{mi} - g_{oi}|^{\alpha}} \qquad (5)$$

where g_{oi} is the gravity observed at a location (i) and g_{mi} is the gravity calculated for the model such that the sums are taken over the number locations of gravity points. The constant α is a method of tuning, usually set to 1 or 0.5, and I set it to the latter value.

At any temperature iteration, the model parameters are updated with the new, randomly perturbed parameters if and only if the error (as calculated above) for the new model is less than that of the old model. However, there is one critical exception. An additional layer of randomness is built into vfsa to ensure that the algorithm arrives at the global minimum error model. Sometimes a model with errors worse than the previous model is accepted as an update, to ensure that the algorithm does not fall into a local error minimum. The criteria for accepting a worse model is random such that if the probability (P):

$$P = \exp\left(-\frac{\Delta E}{T_i}\right) \qquad (6)$$

is greater than a randomly generated number, r, such that $r \in [0,1]$, then the worse model is accepted as an update for that temperature iteration of the algorithm. It is very important to note that using a normalized error (as in Equation 5) also allows $P \in [0,1]$. Thus, normalizing the error calculation allows P to be directly compared to the randomly drawn number, without the use of an additional tuning factor to scale the random number as would be the case if a non-normalized error calculation were used. A very illustrative flow chart/pseudocode of the vfsa algorithm described here is given in *Sen and Stoffa* [1995] (pg. 109).

Executing the vfsa algorithm for any particular physical problem requires, as mentioned above, an amount of tuning for choosing the values of constants. Particularly, the extent of the model space (maximum and minimum values for the model parameters) and the constants governing the cooling schedule are subject to change. Adequate tuning is absolutely critical for the convergence of the inversion and usually becomes easier with experience. Geophysical problems, for instance, rarely need more than 1-2 possible model updates calculated at any given temperature within the cooling schedule (i.e. the particles do not need many iterations at that temperature to obtain a low-energy state) (M. Sen, pers. comm., 2007).

Inverse Modeling of Thwaites Glacier Bouguer Anomalies for Crustal Structure

A 2D gravity inversion scheme was implemented in an attempt to more rigorously quantifying the crustal heterogeneity of West Antarctica. The inversion utilized a geometrically-parameterized 2D forward problem (Appendix B) [*Talwani, et al.*, 1959; *Grant and West*, 1965], which fed into a very fast simulated annealing method of optimization (Appendix C, above) [*Sen and Stoffa*, 1995; *Roy, et al.*, 2005]. The inversion was tested on the AGASEA dataset so that the results could be compared to previous forward modeling (see Chapter 3).

Method

First, a heavy filter (200 km half-width 3D Gaussian) was applied to the AGASEA Bouguer anomalies to remove signals from near-surface geology (such as large sedimentary basins). This filter length yielded filtered gravity anomalies that were uncorrelated with topography (Figure C.1A), leaving the higher frequency gravity signals as the un-modeled residual (Figure C.1B). As a result, inversion with these data provides only regional variations in the depth to density boundaries. Future improvements in the inversion scheme- such as regularizing the inversion to produce a smooth crustal model- would allow the use unfiltered Bouguer gravity data in the inversion and avoid any assumptions made during the filtering process.

The inversion was used to model a two-layer crust, as indicated by the spectral results, and densities were initially fixed to standard values (such that upper crust was 2670 kg/m3, lower crust was 2800 kg/m3, and mantle was 3300 kg/m3) that agree with densities derived from nearby seismic velocities [*Gohl, et al.*, 2007]. Note that seismic tomography of the Marie Byrd Land mantle from surface waves (which cannot image the crust) indicate a sizable body of slow velocity (possibly warmer and lower density) mantle at ~60 km depth extending downward to ~200 km depth [Ritzwoller, et al., 2001] underlying Marie Byrd Land and the thin crust of the Marie Byrd Land volcanoes (Chapter 3).

The inversion's model parameters included: the depths of the two crustal boundaries at ~12 points each along the line, as well as two scaling parameters (t1 and t2) that result from parameterizing the 2D forward problem as slabs (Appendix B). In theory, a simulated annealing inversion should be able to search a very wide model space and arrive at a global minimum in error for a model fit to the data. In practice, the inversion was increasingly unstable for large model spaces, so the possible ranges of the boundaries' depths were constrained to within +/- 20% of the spectrally-derived depths for the area. Even with this constraint and careful tuning of the temperatures controlling the inversion, often the models had difficulty converging. Thus a threshold on the "acceptable" normalized error (0.35-0.2, subjectively chosen based on the performance of

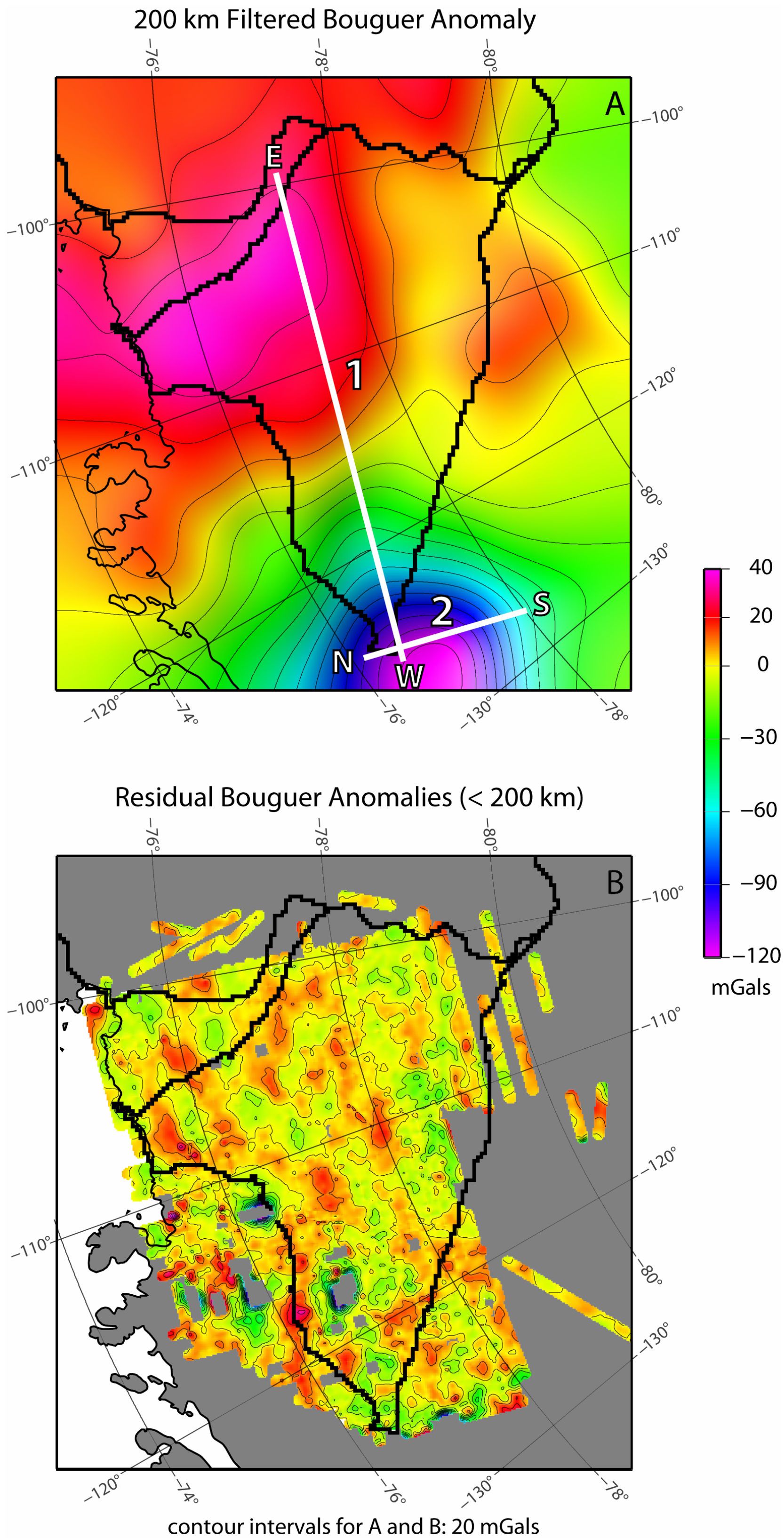

Figure C.1: A. Filtered Bouguer gravity anomalies used for inversion; white lines are the locations of profile #1 (long line, running roughly E-W) and #2 (short line, running roughly N-S). B. Residual Bouguer anomalies, which are highly correlated with topography. Both: thin black line = coastline [*SCAR*, 2006]; thick black lines = glacier catchments [*Vaughan, et al.,* 1999]. Grey areas are ice sheet-covered areas without data. See Figure 4.1 for this figure location.

a particular line of data & model space) was used to determine model convergence. The inversion was run to convergence five times for each line of gravity data and the average of the five models' depth results was used as the final model. Although one standard deviation of the depths was calculated as the final error, the small number of models over which it was calculated means that it is not a robust estimate of true model error.

Results

Two lines of data were used for inversion (Figure C.1A): line #1 running E-W as a cross-section of major crustal features (the Byrd Subglacial Basin and Marie Byrd Land) very near to a line used in previous forward modeling (Figure 3.1) and line #2 running N-S within Marie Byrd Land and crossing line #1. One inversions was performed on line #1 and two on line #2. For standard density contrasts at the crustal boundaries, inversion #1 (Figure C.2) places the Byrd Subglacial Basin Moho at ~28 km depth with a gradual transition to deeper Moho depths (near 34 km) in Marie Byrd Land. The mid-crustal boundary slopes from 12 km depth in the Byrd Subglacial Basin to 15 km depth in Marie Byrd Land- generally mimicking the Moho changes. Line #2 was more difficult to invert with standard density contrasts and so there are two solutions: a. where "t" was a model parameter as in inversion #1a, and b. where "t" was a boundary condition I imposed, using the "t" values determined from inversion #1. For inversion #2a (Figure C.3), the final model places the Moho at 28-30 km depth under the Executive Committee Range and at 26 km depth on the southern flank. For inversion #2b (Figure C.4), the Moho is constrained to be deeper based on the prescribed "t" values and is placed at 35-38 km depth under the volcanoes and at 34 km on the southern flank.

Despite instabilities, the inversions show some interesting features. First, inversion #1 places the Moho depth very close to the spectrally-derived depths for a standard density contrast in the Byrd Subglacial Basin. This means that the upper mantle

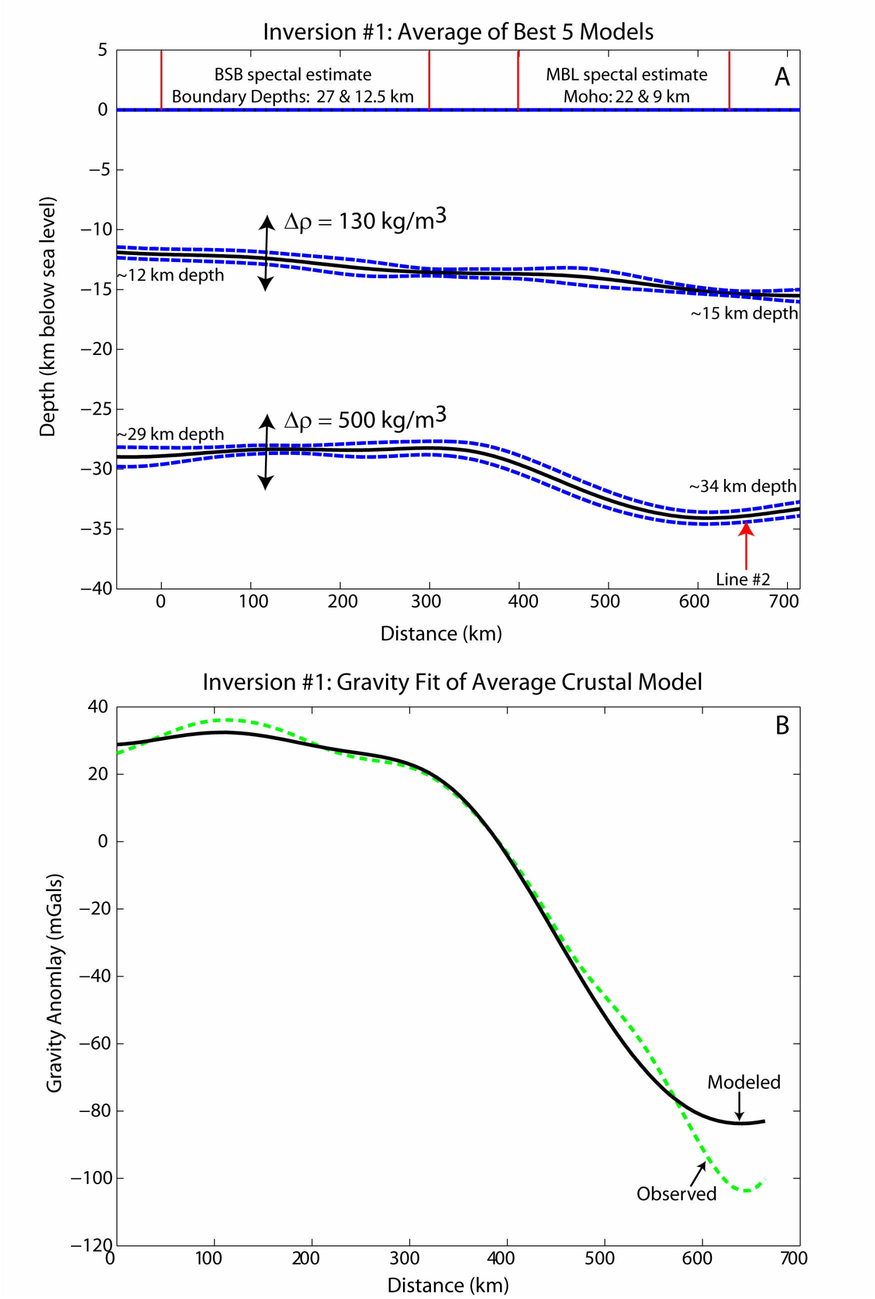

Figure C.2: Inversion #1 results. Fixed standard crustal densities, inverting for layer depth. A. Final 2-layer crustal model, labeled with density contrasts used and depth results; red arrow indicates location at which Line #2 crosses this one. B. Gravity fit achieved by the inversion.

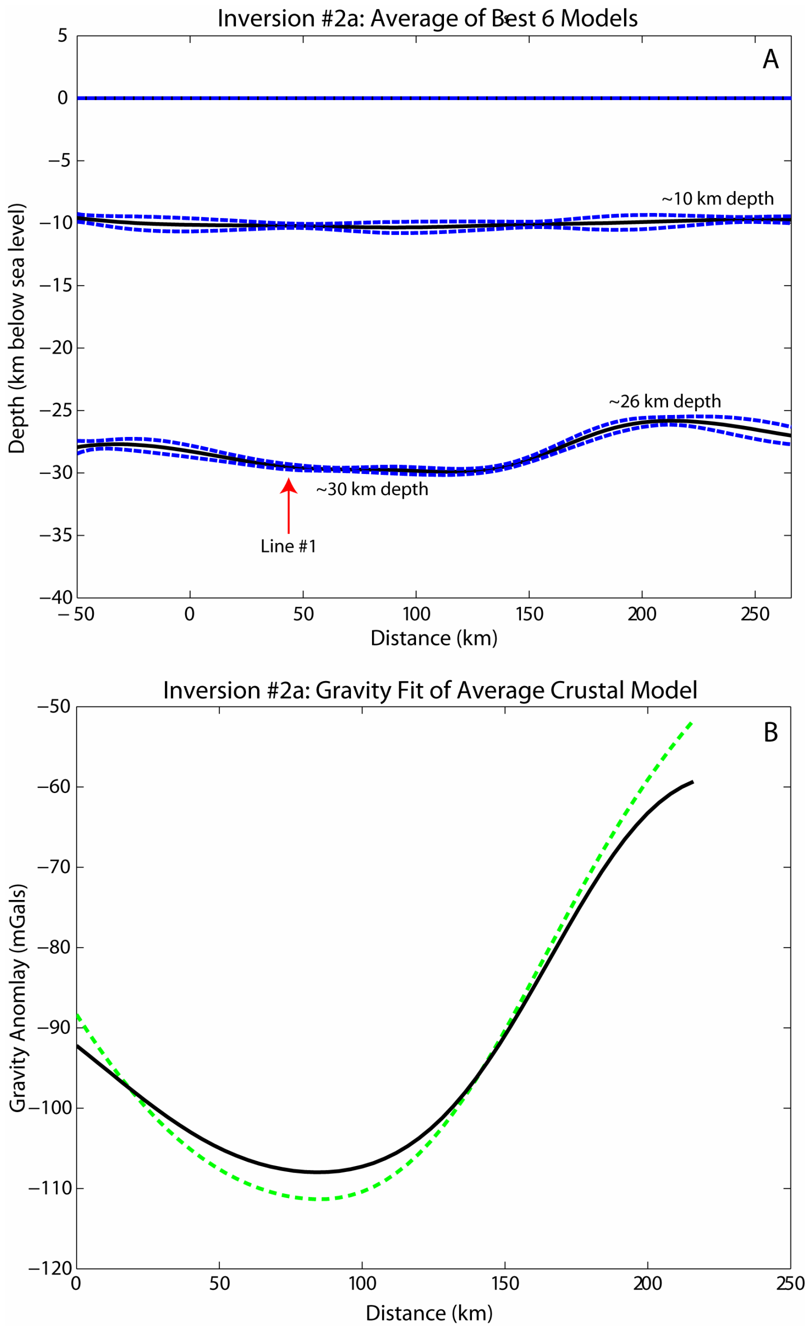

Figure C.3: Inversion #2a Results. Fixed standard crustal densities, inverting for layer depth. A and B. Description same as Figure 4.5.

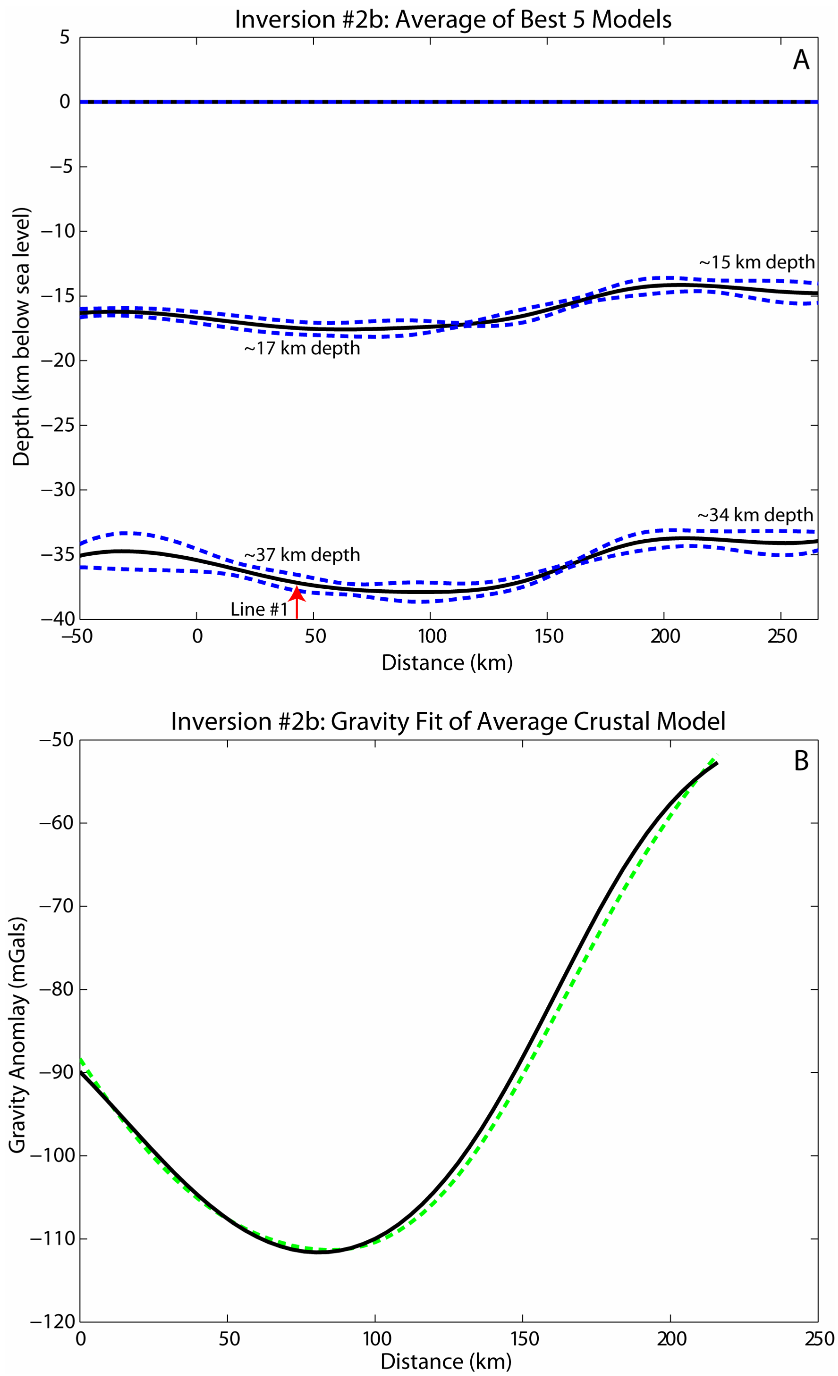

Figure C.4: Inversion #2b Results. Fixed standard crustal densities and t-values, inverting for layer depth. A and B. Description same as Figure 4.5.

beneath the Byrd Subglacial Basin is relatively cool. However, the depths for the Marie Byrd Land Moho in inversion #1 are significantly different from the spectrally-derived depths and suggest that a standard density contrast at the Moho is not appropriate for Marie Byrd Land. Still, all inversions for Marie Byrd Land suggest shallow Moho depths and thus topography that is not Airy isostatically compensated. Inversions #2a and #2b both indicate that the inversion is very sensitive to the choice of "t" value and that re-parameterizing the inversion to remove this slab correction factor would likely improve inversion results.

Overall, the inversions' difficulties in converging may be due to several factors. First, the filtered gravity data is very smooth, yielding more possible depth solutions that could fit the data. Second, a two-layer crustal model will have more solutions than a single-layer crustal model, though a two-layer model is necessary based on spectral structure results. Third, the model space is constrained only roughly by gravity spectrally-derived depths and there are no other *a priori* data available with which to constrain these inversions. Finally, a 2D structure approximation may not be an appropriate assumption since the crust in the Byrd Subglacial Basin and Marie Byrd Land is very heterogeneous (Chapter 3). 2D forward modeling is probably adequate for hypothesis testing the crustal structure across West Antarctica, 1. given relatively good correlation between inverse and forward model results, 2. until additional datasets have been collected with which to improve constraints on the area's crustal structure (there are very few locations were seismic results are currently available) and 3. until improvements are made to stabilize this basic inversion scheme.

References

Adam, D. (2002), Amazing Grace, *Nature*, *416*, 10-11.

Alley, R. B. (2002), On Thickening Ice?, *Science*, *295*, 451-452.

Alley, R. B., and R. B. Bindschadler (2001), The West Antarctic Ice Sheet and sea-level change, in *The West Antarctic Ice Sheet: Behavior and Environment.*, edited by R. B. Alley and R. A. Bindschadler, pp. 1-11, American Geophysical Union, Washington, D.C.

Alley, R. B., D. D. Blankenship, C. R. Bentley, and S. T. Rooney (1986), Deformation of Till beneath Ice Stream-B, West Antarctica, *Nature*, *322*, 57-59.

Anandakrishnan, S., D. D. Blankenship, R. B. Alley, and P. L. Stoffa (1998), Influence of Subglacial Geology on the Position of a West Antarctic Ice Stream from Seismic Observations, *Nature*, *394*, 62-65.

Anandakrishnan, S., and J. P. Winberry (2004), Antarctic subglacial sedimentary layer thickness from receiver function analysis, *Global Planet Change*, *42*, 167-176.

Bamber, J., and J. L. Gomez-Dans (2005), The accuracy of digital elevation models of the Antarctic continent, *Earth Planet Sci Lett*, *237*, 516-523, DOI: 10.1016/j.epsl.2005.06.008.

Bannister, S., J. Yu, B. Leitner, and B. L. N. Kennett (2003), Variations in crustal structure across the transition from West to East Antarctica, Southern Victoria Land, *Geophys J Int*, *155*, 870-884.

Behrendt, J. C. (1999), Crustal and Lithospheric Structure of the West Antarctic Rift System from Geophysical Investigations - A Review, *Global Planet Change*, *23*, 25-44.

Behrendt, J. C., D. D. Blankenship, D. Damaske, and A. K. Cooper (1995), Glacial Removal of Late Cenozoic Subglacially Emplaces Volcanic Edifices by the West Antarctic Ice Sheet., *Geology*, *23*, 1111-1114.

Behrendt, J. C., D. D. Blankenship, C. A. Finn, R. E. Bell, R. E. Sweeney, S. M. Hodge, and J. M. Brozena (1994), CASERTZ Aeromagnetic Data Reveal Late Cenozoic Flood Basalts (?) in the West Antarctic Rift System, *Geology*, *22*, 527-530.

Behrendt, J. C., D. D. Blankenship, D. L. Morse, and R. E. Bell (2004), Shallow-source aeromagnetic anomalies observed over the West Antarctic Ice Sheet compared with coincident bed topography from radar ice sounding—new evidence for glacial ‘‘removal’’ of subglacially erupted late Cenozoic rift-related volcanic edifices, *Global Planet Change*, *42*, 177-193.

Behrendt, J. C., and A. K. Cooper (1991), Evidence of Rapid Cenozoic Uplift of the Shoulder Escarpment of the Cenozoic West Antarctic Rift System and Speculation on Possible Climate Forcing, *Geology*, *19*, 315-319.

Behrendt, J. C., C. Finn, D. L. Morse, and D. D. Blankenship (2007), One hundred negative magnetic anomalies over the West Antarctic Ice Sheet (WAIS), in particular Mt. Resnik, a subaerially erupted volcanic peak, indicate eruption through at least one field reversal, in *Antarctica: A Keystone in a Changing World – Online Proceedings of the 10tth ISAES*, edited by A. K. Cooper, et al., p. 4, USGS Open File Report 2007-1047, Extended Abstract 030.

Bell, R. E., D. D. Blankenship, C. A. Finn, D. L. Morse, T. A. Scambos, J. M. Brozena, and S. M. Hodge (1998), Influence of Subglacial Geology on the Onset of a West Antarctic Ice Stream from Aerogeophysical Observations, *Nature*, *394*, 58-62.

Bell, R. E., V. A. Childers, R. A. Arko, D. D. Blankenship, and J. M. Brozena (1999), Airborne gravity and precise positioning for geologic applications, *J Geophys Res*, *104*, 15281-15292.

Bell, R. E., M. Studinger, G. D. Karner, C. A. Finn, and D. D. Blankenship (2006), Identifying Major Sedimentary Basins Beneath the West Antarctic Ice Sheet from Aeromagnetic Data Analysis, in *Antarctica: Contributions to Global Earth Sciences*, edited by D. K. Fütterer, et al., pp. 117-121, Springer, Berlin.

Bentley, C. R. (1964), The structure of Antarctica and its ice cover, in *Research in geophysics*, edited by H. Odishaw, pp. 335-389, Massachusetts Institute of Technology, Cambridge, US.

Bentley, C. R. (1983), Crustal structure of Antarctica from geophysical evidence- a review, paper presented at Antarctic earth science; fourth international symposium, Cambridge University, Adelaide, South Australia.

Bentley, C. R. (1991), Configuration and structure of the subglacial crust, in *Oxford*

Monographs on Geology and Geophysics: The Geology of Antarctica, edited by R. J. Tingey, pp. 335-364, Oxford University Press, Oxford, UK.

Bentley, C. R., and J. D. Robertson (1982), Isostatic gravity anomalies in West Antarctica, in *Antarctic Geoscience*, edited by C. Craddock, p. 1172, University of Wisconsin Press, Madison, WI.

Blankenship, D. D., S. Anandakrishnan, J. L. Kempf, and C. R. Bentley (1987a), Microearthquakes under and alongside Ice Stream B, Antarctica, detected by a new passive seismic array, *Ann Glaciol*, *9*, 30-34.

Blankenship, D. D., R. E. Bell, S. M. Hodge, J. M. Brozena, J. C. Behrendt, and C. A. Finn (1993), Active Volcanism Beneath the West Antarctic Ice Sheet and Implications for Ice-sheet Stability, *Nature*, *361*, 526-529.

Blankenship, D. D., C. R. Bentley, S. T. Rooney, and R. B. Alley (1986), Seismic measurements reveal a saturated porous layer beneath an active Antarctic ice stream, *Nature*, *322*, 54-57.

Blankenship, D. D., C. R. Bentley, S. T. Rooney, and R. B. Alley (1987b), Till beneath Ice Stream B. 1. Properties from seismic travel times, *J Geophys Res*, *9*, 8903-8911.

Blankenship, D. D., D. L. Morse, C. A. Finn, R. E. Bell, M. E. Peters, S. D. Kempf, S. M. Hodge, M. Studinger, J. C. Behrendt, and J. M. Brozena (2001), Geologic controls on the initiation of rapid basal motion for West Antarctic ice streams: A geophysical perspective including new airborne radar sounding and laser altimetry results, in *The West Antarctic Ice Sheet: Behavior and Environment*, edited by R. B. Alley and R. A. Bindschadler, pp. 105-121, American Geophysical Union, Washington, D.C.

Bradshaw, J. D., P. R. J., S. D. Weaver, B. C. Storey, R. J. Muir, and T. R. Ireland (1997), New Zealand Superterranes Recognized in Marie Byrd Land and Thurston Island, in *The Antarctic region; geological evolution and processes; proceedings of the VII international symposium on Antarctic earth sciences*, edited by C. A. Ricci, pp. 429-436, Terra Antarctica Publication, Vienna, Italy.

Brozena, J. M. (1984), A preliminary analysis of the NRL airborne gravimetry system, *Geophysics*, *49*, 1060-1069.

Brozena, J. M., and J. L. Jarvis (1993), CASERTZ 1991-992: Airborne gravity and surface topography measurement, *Antarctica Journal of the United States*, *28*, 1-3.

Brozena, J. M., and M. F. Peters (1988), An airborne gravity study of eastern North Carolina, *Geophysics*, *53*, 245-253.

Busetti, M., G. Spadini, F. M. van der Wateren, S. A. P. L. Cloetingh, and C. Zanolla (1999), Kinematic modeling of the West Antarctic Rift System, Ross Sea, Antarctica, *Global Planet Change*, *23*, 79-103.

Cande, S. C., and D. V. Kent (1995), Revised calibration of the geomagnetic polarity time scale for the late Cretaceous and Cenozoic, *J Geophys Res*, *100*, 6093-6096.

Childers, V. A. (1996), Gravimetry as a geophysical tool: airborne gravimetry and studies of lithospheric flexure and faulting, Ph.D. Dissertation thesis, Columbia University, New York.

Childers, V. A., R. E. Bell, and J. M. Brozena (1999), Airborne gravimetry: An investigation of filtering, *Geophysics*, *64*, 61-69.

Clarke, T. S., P. D. Burkholder, S. B. Smithson, and C. R. Bentley (1997), Optimum seismic shooting and recording parameters and a preliminary crustal model for the Byrd Subglacial Basin, Antarctica, in *The Antarctic Region: Geological Processes and Evolution*, edited by C. A. Ricci, pp. 485-493, Terra Antarctica, Siena, Italy.

Cunningham, A. P., R. D. Larter, P. F. Barker, K. Gohl, and F. O. Nitsche (2002), Tectonic evolution of the Pacific margin of Antarctica 2. Structure of Late Cretaceous-Early Tertiary plate boundaries in the Bellingshausen Sea from seismic reflection and gravity data, *J Geophys Res*, *107*, 2346, DOI: 10.1029/2002JB001897.

Curtis, M. L. (2001), Tectonic History of the Ellsworth Mountains, West Antarctica: Reconciling a Gondwana Enigma, *GSA Bulletin*, *113*, 939-958.

Dalziel, I. W. D (2006), On the extent of the West Antarctic Rift System, *Terra Antarctica Reports*, *12*, 193-202.

Dalziel, I. W. D., and D. H. Elliot (1982), West Antarctica: Problem Child of

Gondwanaland, *Tectonics*, *1*, 3-19.

Dalziel, I. W. D., and L. A. Lawver (2001), The Lithospheric Setting of the West Antarctic Ice Sheet, in *Antarctic Research Series. The West Antarctic Ice Sheet: Behavior and Environment.*, edited by R. B. Alley and R. A. Bindschadler, pp. 29-44, American Geophysical Union, Washington, D.C.

Dalziel, I. W. D., L. A. Lawver, and J. B. Murphy (2000), Plumes, orogenesis, and supercontinental fragmentation, *Earth Planet Sci Lett*, *178*, 1-11.

Davey, F. J., and G. Brancolini (1995), The late Mesozoic and Cenozoic structural setting of the Ross Sea region, in *Geology and stratigraphy of the Antarctic margin*, edited by A. K. Cooper, et al., pp. 167-182, American Geophysical Union, Washington, D.C.

Decesari, R. C., C. C. Sorlien, B. P. Luyendyk, D. S. Wilson, L. R. Bartek, J. Diebold, and S. E. Hopkins (2007a), Regional seismic stratigraphy correlations of the Ross Sea: Implications for the tectonic history of the West Antarctic Rift System, in *Antarctica: A Keystone in a Changing World- Online Proceedings of the 10th ISAES*, edited by A. K. Cooper and C. F. Raymond, SGS Open File Report 2007-1047, Short Research Paper 052, doi: 10.3133/of2007-10447.srp052.

Decesari, R. C., D. S. Wilson, B. P. Luyendyk, and M. Faulkner (2007b), Cretaceous and tertiary extension throughout the Ross Sea, Antarctica, in *Antarctica: A Keystone in a Changing World- Online Proceedings of the 10th ISAES*, edited by A. K. Cooper and C. F. Raymond, p. 6, USGS Open File Report 2007-1047, Short Research Paper 098, doi: 10.3133/of2007-1047.srp098.

Diehl, T. M. (2008) "Field Guide to Antarctic Gravity Stations Visited During the 2004-2005 AGASEA Airborne Campaign." UTIG Technical Report No. 194. 23 pp. Online: http://www.ig.utexas.edu/library/tech_reports/utig_tech_rep_194.pdf

Diehl, T. M., J. W. Holt, D. D. Blankenship, and D. A. Young (2008a), Free-air gravity anomalies over the Thwaites Glacier catchment, West Antarctica, http://ngdc.noaa.gov/mgg/gravity/utig_agasea.html, Natl. Geophys. Data Cent., Boulder, Colo.

Diehl, T. M., J. W. Holt, D. D. Blankenship, D. A. Young, T. A. Jordan, and F. Ferraccioli (2008b), First airborne gravity results over the Thwaites Glacier catchment, West Antarctica, *G-cubed*, *9*, Q04011, DOI: 10.1029/2007GC001878.

Divenere, V., D. V. Kent, and I. W. D. Dalziel (1995), Early Cretaceous paleomagnetic results from Marie Byrd Land, West Antarctica: Implications for the Weddellia collage of crustal blocks, *J Geophys Res*, *100*, 8133-8151, DOI: 95JB00042.

Donnellan, A., and B. P. Luyendyk (2004), GPS evidence for a coherent Antarctic plate and for postglacial rebound in Marie Byrd Land, *Global Planet Change*, *42*, 305-311.

Drewry, D. J. (1983), *Antarctica: Glaciological and Geophysical Folio 2*, Scott Polar Research Institute, Cambridge, U.K.

Eagles, G., K. Gohl, and R. D. Larter (2004), High-resolution animated tectonic reconstruction of the South Pacific and Western Antarctic Margin, *G-cubed*, *5*, Q07002, DOI: 10.1029/2003GC000657.

Engelhardt, H., and B. Kamb (1998), Basal sliding of Ice Stream B, West Antarctica, *J Glaciol*, *44*, 223-230.

Engelhardt, H., N. Munphrey, B. Kamb, and M. Fahnestock (1990), Physical Conditions at the Base of a Fast Moving Antarctic Ice Stream, *Science*, *248*, 57-59.

Fahnestock, M., and J. Bamber (Eds.) (2001), *Morphology and Surface Characteristics of the West Antarctic Ice Sheet*, 13-27 pp., American Geophysical Union, Washington, D.C.

Fairhead, J. D., and C. S. Okereke (1988), Depths to major density contrasts beneath the West African rift system in Nigeria and Cameroon based on the spectral analysis of gravity data, *J Afr Earth Sci*, *7*, 769-777.

Ferraccioli, F., E. Bozzo, and D. Damaske (2002), Aeromagnetic signatures over western Marie Byrd Land provide insight into magmatic arc basement, mafic magmatism and structure of the Eastern Ross Sea Rift flank, *Tectonophys*, *347*, 139-165.

Ferraccioli, F., P. C. Jones, M. L. Curtis, and P. T. Leat (2005), Subglacial imprints of early Gondwana break-up as identified from high resolution aerogeophysical data over western Dronning Maud Land, East Antarctica, *Terra Nova*, *17*, 573-579.

Ferraccioli, F., T. A. Jordan, D. G. Vaughan, J. W. Holt, M. James, H. F. J. Corr, D. D. Blankenship, J. D. Fairhead, and T. M. Diehl (2007), New aerogeophysical survey targets the extent of the West Antarctic Rift System over Ellsworth Land, in *Antarctica: A Keystone in a Changing World- Online Proceedings of the 10th ISAES X*, edited by A. K. Cooper and C. R. Raymond, pp. 1-4, USGS Open-File Report 2007-1047, Extended Abstract 113, Santa Barbara, California.

Ferraccioli, F. F., P. C. Jones, A. P. M. Vaughan, and P. T. Leat (2006), New aerogeophysical view of the Antarctic Peninsula: More pieces, less puzzle, *Geophys Res Lett*, *33*, L05310.

Fitzgerald, P. G. (1989), Uplift and formation of Transantarctic Mountains-- Applications of apatite fission track analysis to tectonic problems, paper presented at International Geological Congress, 28th, Washington, D.C.

Flowerdew, M. J., I. L. Millar, M. L. Curtis, A. P. M. Vaughan, M. S. A. Horstwood, M. J. Whitehouse, and C. M. Fanning (2007), Combined U-Pb geochronology and Hf isotope geochemistry of detrital zircons from early Paleozoic sedimentary rocks, Ellsworth-Whitmore Mountains block, Antarctica, *GSA Bulletin*, *119*, 275-288.

Gohl, K., D. Teterin, G. Eagles, G. Netzeband, J. W. G. Grobys, N. Parsiegla, P. Schlüter, V. Leinweber, R. D. Larter, G. Uenzelmann-Neben, and G. Udintsev (2007), Geophysical survey reveals tectonic structures in the Amundsen Sea embayment, West Antarctica, in *Antarctica: A Keystone in a Changing World - Online Proceedings of the 10th ISAES*, edited by A. K. Cooper and C. F. Raymond, Short Research Paper 047, USGS Open-File Report 2007-1047.

Grant, F. S., and G. F. West (1965), *Interpretation Theory in Applied Geophysics*, 584 pp., McGraw-Hill Book Company, New York.

Grunow, A. M., D. V. Kent, and I. W. D. Dalziel (1987), Mesozoic Evolution of West Antarctica and the Weddell Sea Basin - New Paleomagnetic Constraints, *Earth Planet Sci Lett*, *86*, 16-26.

Hamilton, R. J., B. P. Luyendyk, C. C. Sorlien, and L. R. Bartek (2001), Cenozoic tectonics of the Cape Roberts Rift Basin and Transantarctic Mountains Front, Southwestern Ross Sea, Antarctica, *Tectonics*, *20*, 352-342.

Haran, T., J. Bohlander, T. Scambos, and M. Fahnestock (2005), MODIS mosaic of Antarctica (MOA) image map, http://nsidc.org/data/moa/, National Snow and Ice Data Center, Boulder, CO.

Harlan, R. B. (1968), Eötvös Corrections for Airborne Gravimetry, *J Geophys Res*, *73*, 4675-4679.

Holt, J. W., D. D. Blankenship, D. L. Morse, D. A. Young, M. E. Peters, S. D. Kempf, T. G. Richter, D. G. Vaughan, and H. F. J. Corr (2006a), New boundary conditions for the West Antarctic ice sheet: Subglacial topography of the Thwaites and Smith Glacier catchments, *Geophys Res Lett*, *33*, L09501, DOI: 10.1029/2005GL025561.

Holt, J. W., T. G. Richter, S. D. Kempf, D. L. Morse, and D. D. Blankenship (2006b), Airborne gravity over Lake Vostok and adjacent highlands of East Antarctica, *G-cubed*, *7*, Q11012, DOI: 10.1029/2005GC001177.

Holt, J. W., D. D. Blankenship, F. Ferraccioli, D. G. Vaughan, D. A. Young, S. D. Kempf, and T. M. Diehl (2007), New aeromagnetic results from the Thwaites Glacier catchment, West Antarctica, Extended Abstract 153, 151-154 pp., *USGS Open-File Report*, Santa Barbara, California.

Hughes, T. (1975), The West Antarctic ice sheet; instability, disintegration, and initiation of ice ages, *Reviews of Geophysics and Space Physics*, *13*, 502-526.

Jachens, R. C., and J. Griscom (1985), An Isostatic Residual Gravity Map of California, in *The Utility of Regional Gravity and Magnetic Anomaly Maps*, edited by Hinze, pp. 347-360, SEG Press.

Jacobs, S. S., and J. C. Comiso (1997), Climate variability in the Amundsen and Bellingshausen Seas, *J Clim*, *10*, 697-709.

Jacobs, S. S., C. F. Giulivi, and P. A. Mele (2002), Freshening of the Ross Sea during the late 20th century, *Science*, *297*, 386-389.

Jankowski, E. J., and D. J. Drewry (1981), The structure of West Antarctica from geophysical studies, *Nature*, *291*, 17-21.

Jones, P. C., A. C. Johnson, R. R. B. von Frese, and H. F. J. Corr (2002), Detecting rift basins in the Evans Ice Stream region of West Antarctica using airborne gravity data, *Tectonophys*, *347*, 25-41.

Jordan, T. A., F. Ferraccioli, D. G. Vaughan, J. W. Holt, H. F. J. Corr, D. D. Blankenship, and T. M. Diehl (submitted), West Antarctic Rift System unveiled from aerogravity over the Pine Island Glacier region, *GSA Bulletin*.

Joughin, I., E. Rignot, C. E. Rosanova, B. K. Lucchitta, and J. Bohlander (2003), Timing of recent accelerations of Pine Island Glacier, Antarctica, *Geophys Res Lett*, *30*.

Kadmina, I. N., R. G. Kurinin, V. N. Masolov, and G. E. Grikurov (1983), Antarctic Crustal Structure from Geophysical Evidence: A Review, paper presented at Antarctic earth science; fourth international symposium, Cambridge University Press, Adelaide, South Australia.

Karner, G. D., M. Studinger, and R. E. Bell (2005), Gravity anomalies of sedimentary basins and their mechanical implications: Application to the Ross Sea basins, West Antarctica, *Earth Planet Sci Lett*, *235*, 577-596.

Karner, G. D., and A. B. Watts (1983), Gravity anomalies and flexure of the lithosphere at mountain ranges, *J Geophys Res*, *88*, 10449-10477.

Kaspari, S., P. A. Mayewski, D. A. Dixon, V. B. Spikes, S. B. Sneed, M. J. Handley, and G. S. Hamilton (2004), Climate variability in West Antarctica derived from annual accumulation-rate records from ITASE firn/ice cores, *Ann Glaciol*, *39*, 585-594.

Kern, M., K. P. Schwartz, and N. Sneeuw (2003), A study of the combination of satellite, airborne, and terrestrial gravity data, *J Geodes*, *77*, 217-225.

LaCoste, L. J. B. (1967), Measurement of gravity at sea and in the air, *Rev Geophys*, *5*, 477-526.

LaCoste and Romberg Corp. (2004), *Model "S" air-sea dynamic gravity meter system II: Instruction manual*, Version 1.5 Software ed., 133 pp., LaCoste & Romberg, Austin, Texas.

Lawver, L. A., and L. M. Gahagan (1994), Constraints on Timing of Extension in the Ross Sea Region, *Terra Antarctica*, *1*, 545-552.

Lawver, L. A., J. Y. Royer, D. T. Sandwell, and C. R. Scotese (1991), *Evolution of the Antarctic Continental Margin*, Cambridge University Press, Cambridge.

Le Brocq, A. M., A. J. Payne, and M. J. Siegert (2006), West Antarctic balance calculations: Impact of flux-routing algorithm, smoothing algorithm and topography, *Computers & Geosciences*, *32*, 1780–1795.

LeMasurier, W. E. (2008), Neogene extension and basin deepening in the West Antarctic rift from comparisons with the East African rift and other analogs, *Geology*, *36*, 247-250.

LeMasurier, W. E., and C. A. Landis (1997), The West Antarctic Erosional Surface: Its Role in Determining the Timing of Mantle Plume Activity, Uplift, and Erosion, During Late Cretaceous- Cenozoic Time in Marie Bird Land, paper presented at VII international symposium on Antarctic earth sciences, Terra Antarctica Publication : Siena, Italy, Siena, Italy.

LeMasurier, W. E., and J. W. Thompson (Eds.) (1990), *Volcanoes of the Antarctic Plate and Southern Oceans*, 487 pp., American Geophysical Union, Washington, D.C.

Lichten, S., W. Yoazar-Sever, M. Bertiger, K. Hurst, R. J. Muellersehoen, S.-C. Wu, T. Yunck, and J. Zumberge (1995), GIPSY-OASIS II: A high precision GPS data processing system and general satellite orbit, Tech. Rep. 95-1323, Jet Propulsion Laboratory, CA.

Liu, H., K. C. Jezek, B. Li, and J. L. Zhao (2001), RADARSAT Antarctic Mapping Project digital elevation model version 2, http://nsidc.org/data/nsidc-0082.html, National Snow and Ice Data Center, Boulder, CO.

Luyendyk, B. P. (1997), Slab Capture Versus Ridge Collision as an Explanation for Cretaceous Extension and Rifting of East Gondwana, paper presented at VII international symposium on Antarctic earth sciences, Terra Antarctica Publication : Siena, Italy, Siena, Italy.

Luyendyk, B. P., C. C. Sorlien, D. S. Wilson, L. R. Bartek, and C. S. Siddoway (2001), Structural and tectonic evolution of the Ross Sea rift in the Cape Colbeck region, Eastern Ross Sea, Antarctica, *Tectonics*, *20*, 933-958.

Luyendyk, B. P., D. S. Wilson, and C. S. Siddoway (2003), Eastern margin of the Ross Sea Rift in western Marie Byrd Land, Antarctica: Crustal structure and tectonic development, *G-cubed*, *4*, 1090, DOI: 10.1029/2002GC000462.

Lythe, M. B., D. G. Vaughan, A. Lambrecht, H. Miller, U. Nixdorf, and others (2001), BEDMAP: A new ice thickness and subglacial topographic model of Antarctica, *J Geophys Res B Solid Earth Planets*, *106*, 11335-11351.

Mader, G. L. (1992), Rapid static and kinematic Global Positioning System solutions using the ambiguity function technique, *J Geophys Res*, *97*, 3271-3283.

McAdoo, D., and S. Laxon (1997), Antarctic Tectonics: Constraints from an ERS-1 Satellite Marine Gravity Field, *Science*, *276*, 556-560.

McNutt, M. K. (1983), Influence of plate subduction on isostatic compensation in Northern California, *Tectonics*, *2*, 399-415.

Mercer, J. H. (1978), West Antarctic Ice Sheet and Co2 Greenhouse Effect - Threat of Disaster, *Nature*, *271*, 321-325.

Monaghan, A. J., D. H. Bromwich, R. L. Fogt, S. H. Wang, P. A. Mayewski, D. A. Dixon, A. Ekaykin, M. Frezzotti, I. Goodwin, E. Isaksson, S. D. Kaspari, V I. Morgan, H. Oerter, T. D. Van Ommen, C. J. Van der Veen, and J. H. Wen (2006), Insignificant change in Antarctic snowfall since the International Geophysical Year, *Science*, *313*, 827-831, DOI: 10.1126/science.1128243.

Morelli, A., and S. Danesi (2004), Seismological imaging of the Antarctic continental lithosphere: a review, *Global Planet Change*, *42*, 155-165.

Morse, D. L., D. D. Blankenship, E. D. Waddington, and T. A. Neumann (2002), A site for deep coring in West Antarctica: Results from aerogeophysical surveys and thermo-kinematic modeling, *Ann Glaciol, 35,* 36-44.

Müller, R. D., and W. H. F. Smith (1993), Deformation of the oceanic crust between the North American and South American plates, *J Geophys Res*, *98*, 8275-8291.

National Research Council (1997), *Satellite gravity and the Geosphere : Contributions to the Study of the Solid Earth and its Fluid Envelope*, 112 pp., National Academy Press, Washington, D.C.

Oppenheimer, M. (1998), Global Warming and the Stability of the West Antarctic Ice Sheet, *Nature*, *393*, 325-332.

Pankhurst, R. J., I. L. Millar, A. M. Grunow, and B. C. Storey (1993), The Pre-Cenozoic magmatic history of the Thurston Island crustal block, West Antarctica, *J Geophys Res*, *98*, 11835-11849.

Pankhurst, R. J., S. D. Weaver, J. D. Bradshaw, B. C. Storey, and T. R. Ireland (1998), Geochronology and geochemistry of pre-Jurassic superterranes in Marie Byrd Land, Antarctica, *J Geophys Res*, *103*, 2529-2547, DOI: 97JB02605.

Payne, A. J., A. Vieli, A. Shepherd, D. J. Wingham, and E. Rignot (2004), Recent Dramatic Thinning of Largest West Antarctic Ice Stream Triggered by Oceans, *Geophys Res Lett*, *31*.

Peters, L. E., S. Anandakrishnan, R. B. Alley, J. P. Winberry, D. E. Voigt, A. M. Smith, and D. L. Morse (2006), Subglacial sediments as a control on the onset and location of two Siple Coast ice streams, West Antarctica, *J Geophys Res*, *111*, B01302, DOI: 10.1029/2005JB003766.

Peters, M. F., and J. M. Brozena (1995), Methods to improve existing shipboard gravimeters for airborne gravimetry, paper presented at IAG Symposium on Airborne Gravity Field Determination, IUGG XXI General Assembly, Calgary, Boulder, CO, July 2-14, 1995.

PLATES (1999), The PLATES project, Accessed 2008, Online: http://www.ig.utexas.edu/research/projects/plates/, The University of Texas, Institute for Geophysics, Austin, TX.

Pollard, D., and R. M. deConto (2005), Hysteresis in Cenozoic Antarctic ice-sheet variations, *Global Planet Change*, *45*, 9-21, DOI: 10.1016/j.gloplacha.2004.09.011.

Regan, R. D., and W. J. Hinze (1976), The effect of finite data length in the spectral analysis of ideal gravity anomalies, *Geophysics*, *41*, 44-55.

Rignot, E. (2006), Changes in ice dynamics and mass balance of the Antarctic ice sheet, *Philosophical Transactions of the Royal Society A-Mathematical Physical and Engineering Sciences*, *364*, 1637-1655.

Rignot, E., G. Casassa, P. Gogineni, W. Krabill, A. Rivera, and R. Thomas (2004a), Accelerated ice discharge from the Antarctic Peninsula following the collapse of Larsen B ice shelf, *Geophys Res Lett*, *31*.

Rignot, E., R. H. Thomas, P. Kanagaratnam, G. Casassa, E. Frederick, S. Gogineni, W. Krabill, A. Rivera, R. Russell, J. Sonntag, R. Swift, and J. Yungel (2004b), Improved estimation of the mass balance of glaciers draining into the Amundsen Sea sector of West Antarctica from the CECS/NASA 2002 campaign, *Ann Glaciol*, *39*, 231-237.

Rignot, E., D. G. Vaughan, M. Schmeltz, T. Dupont, and D. MacAyeal (2002), Acceleration of Pine Island and Thwaites Glaciers, West Antarctica, *Ann Glaciol*, *34*, 189-194.

Ritzwoller, M. H., N. M. Shapiro, A. L. Levshin, and G. M. Leahy (2001), Crustal and upper mantle structure beneath Antarctica and surrounding oceans, *J Geophys Res B Solid Earth Planets*, *106*, 30645-30670.

Rose, K. E. (1978), Radio echo sounding of Marie Byrd Land, Antarctica, Ph.D. Thesis, University of Cambridge, Cambridge, UK.

Rose, K. E. (1979), Characteristics of ice flow in Marie Byrd Land, Antarctica, *J Glaciol*, *24*, 63-75.

Rose, K. E. (1982), Radio echo sounding in southern Marie Byrd Land, West Antarctica, in *Antarctic Geoscience*, edited by C. Craddock, pp. 982-992, International Union of Geological Sciences, Oslo.

Roy, L., M. K. Sen, D. D. Blankenship, P. L. Stoffa, and T. G. Richter (2005), Inversion and uncertainty estimation of gravity data using simulated annealing: An application over Lake Vostok, East Antarctica, *Geophysics*, *70*, J1-J12.

Sasagawa, G., T. K. Meunier, J. L. Mullins, D. McAdoo, and F. Klopping (2004), Absolute gravimetry in Antarctica: 1995 observations at McMurdo Station and Terra Nova Bay Station, Open-File Report 2004-1190, 49 pp, US Geological Survey, Department of the Interior.

SCAR- The Scientific Committee on Antarctic Research, (2006), Antarctic Digital Database (ADD), Accessed 2008, Online: http://www.add.scar.org:8080/add/

Scambos, T. A., J. A. Bohlander, C. A. Shuman, and P. Skvarca (2004), Glacier acceleration and thinning after ice shelf collapse in the Larsen B embayment, Antarctica, *Geophys Res Lett*, *31*.

Schoof, C. (2007), Ice sheet grounding line dynamics: Steady states, stability, and hysteresis, *J Geophys Res*, *112*, F03S28, DOI: 10.1029/2006JF000664.

Sen, M. K., and P. L. Stoffa (1995), *Global Optimization Methods in Geophysical Inversion*, 281 pp., Elsevier, Amsterdam.

Shepherd, A., D. J. Wingham, and J. A. D. Mansley (2002), Inland thinning of the Amundsen Sea sector, West Antarctica, *Geophys Res Lett*, *29*, 14183-14186, DOI: 10.1029/2001GL014183.

Shepherd, A., D. J. Wingham, and E. Rignot (2004), Warm ocean is eroding West Antarctic Ice Sheet, *Geophys Res Lett*, *31*, L23402, DOI: 10.1029/2004GL021106.

Siddoway, C. S. (2008), Tectonics of the West Antarctic Rift System: New Light on the History and Dynamics of Distributed Intracontinental Extension, in *Antarctica: A Keystone in a Changing World. Proceedings of the 10th International Symposium on Antarctic Earth Sciences*, edited by A. K. Cooper, et al., The National Academies Press, Washington, D.C. doi:10.3133/of2007-1047.kp09.

Sieminski, A., E. Debayle, and J.-J. Lévêque (2003), Seismic evidence for deep low-velocity anomalies in the transition zone beneath West Antarctica, *Earth Planet Sci Lett*, *216*, 645-661.

Spector, A., and F. S. Grant (1970), Statistical models for interpreting aeromagnetic data, *Geophysics*, *35*, 293-302.

Stern, T. A., A. K. Baxter, and P. J. Barrett (2005), Isostatic rebound due to glacial erosion within the Transantarctic Mountain, *Geology*, *33*, 221-224.

Stern, T. A., and U. S. ten Brink (1989), Flexural Uplift of the Transantarctic Mountains, *J Geophys Res*, *94*, 10315-10330.

Storey, B. C., P. T. Leat, S. D. Weaver, R. J. Pankhurst, J. D. Bradshaw, and S. Kelley (1999), Mantle plumes and Antarctica-New Zealand rifting: evidence from mid-Cretaceous mafic dykes, *Journal of the Geological Society, London*, *156*, 659-671.

Studinger, M., R. E. Bell, D. D. Blankenship, C. A. Finn, R. A. Arko, D. L. Morse, and I. Joughin (2001), Subglacial sediments: A regional geological template for ice flow in West Antarctica, *Geophys Res Lett*, *28*, 3493-3496, DOI: 10.1029/2000GL011788.

Studinger, M., R. E. Bell, W. R. Buck, G. D. Karner, and D. D. Blankenship (2004), Sub-ice geology inland of the Transantarctic Mountains in light of new aerogeophysical data, *Earth Planet Sci Lett*, *220*, 391-408.

Studinger, M., R. E. Bell, C. A. Finn, and D. D. Blankenship (2002), Mesozoic and

Cenozoic extensional tectonics of the West Antarctic Rift System from high-resolution airborne geophysical mapping, *Royal Society of New Zealand Bulletin*, *35*, 563-569.

Talwani, M., J. L. Worzel, and M. Landisman (1959), Rapid Gravity Computations for Two-Dimensional Bodies with Application to the Mendocino Submarine Fracture Zone, *J Geophys Res*, *64*, 49-59.

Tapley, B. D., S. Bettadpur, M. Watkins, and C. Regber (2004), The gravity recovery and climate experiment: Mission overview and early results, *Geophys Res Lett*, *31*, 4pp.

Tapley, B. D., J. C. Ries, S. V. Bettadpur, D. Chambers, M. Cheng, F. Condi, and S. Poole (2007), The GGM03 Mean Earth Gravity Model from GRACE, *EOS Trans., AGU*, *88*, Fall Meet. Suppl., Abstract G42A-03.

ten Brink, U. S., S. Bannister, B. C. Beaudoin, and T. A. Stern (1993), Geophysical Investigations of the Tectonic Boundary Between East and West Antarctica, *Science*, *261*, 45-50.

ten Brink, U. S., R. I. Hackney, S. Bannister, T. A. Stern, and Y. Makovsky (1997), Uplift of the Transantarctic Mountains and the bedrock beneath the East Antarctic ice sheet, *J Geophys Res*, *102*, 27603-27621.

Thomas, R., E. Rignot, G. Casassa, P. Kanagaratnam, C. Acuña, T. Akins, H. Brecher, E. Frederick, P. Gogineni, W. Krabill, S. Manizade, H. Ramamoorthy, A. Rivera, R. Russell, J. Sonntag, R. Swift, J. Yungel, and J. Zwally (2004), Accelerated sea-level rise from West Antarctica, *Science*, *306*, 1-4, DOI: 10.1126/science.1099650.

Trey, H., A. K. Cooper, G. Pellis, B. della Vedova, G. Cochrane, G. Brancolini, and J. Makris (1999), Transect across the West Antarctic rift system in the Ross Sea, Antarctica, *Tectonophys*, *301*, 61-74.

Valliant, H. D. (1992), The LaCoste & Romberg Air/Sea gravity meter: an overview, in *CRC Handbook of Geophysical Exploration at Sea*, edited by R. A. Geyer, pp. 141-176, CRC Press.

van der Wateren, F. M., and S. A. P. L. Cloetingh (1999), Feedbacks of Lithosphere Dynamics and Environmental Change of the Cenozoic West Antarctic Rift

System, *Global Planet Change*, *23*, 1-24.

van der Wateren, F. M., T. J. Dunai, R. T. Van Balen, W. Klas, A. Verbers, S. Passchier, and U. Herpers (1999), Contrasting Neogene denudation histories of different structural regions in the Transantarctic Mountains rift flank constrained by cosmogenic isotope measurements, *Global Planet Change*, *23*, 145-172.

Vaughan, D. G., J. L. Bamber, M. Giovinetto, J. Russell, and A. P. R. Cooper (1999), Reassessment of net surface mass balance in Antarctica, *J Clim*, *12*, 933–947.

Vaughan, D. G., H. F. J. Corr, F. F. Ferraccioli, N. Frearson, A. O'Hare, D. Mach, J. W. Holt, D. D. Blankenship, D. L. Morse, and D. A. Young (2006), New boundary conditions for the West Antarctic ice sheet: Subglacial topography beneath Pine Island Glacier, *Geophys Res Lett*, *33*, DOI: 10.1029/2005GL025588.

Vaughan, D. G., J. W. Holt, and D. D. Blankenship (2007), West Antarctic Links to Sea Level Estimation, *Eos Transactions AGU*, *88*, 485, DOI: 10.1029/2007EO460001.

von Frese, R. R. B., W. J. Hinze, L. W. Braile, and A. J. Luca (1981), Spherical earth gravity and magnetic anomaly modeling by Gauss-Legendre quadrature integration, *J Geophys*, *49*, 234-242.

Wannamaker, P. E., J. A. Stodt, and S. L. Olsen (1996), Dormant State of Rifting Below the Byrd Subglacial Basin, West Antarctica, Implied by Magnetotellurgic (MT) Profiling, *Geophys Res Lett*, *23*, 2983-2986.

Weertman, J. (1974), Stability of the junction of an ice sheet and an ice shelf, *J Glaciol*, *13*, 3-11.

Wessel, P., and W. H. F. Smith (1998), New, improved version of the Generic Mapping Tools released, *EOS Trans., AGU*, *79*, 579.

Winberry, J. P., and S. Anandakrishnan (2004), Crustal Structure of the West Antarctic rift system and Marie Bird Land hotspot, *Geology*, *32*, 977-980.

Wingham, D. J., A. J. Ridout, R. Scharroo, R. J. Arthern, and C. K. Shum (1998), Antarctic elevation change from 1992 to 1996, *Science*, *282*, 456-458.

Wörner, G. (1999), Lithospheric dynamics and mantle sources of alkaline magmatism of the Cenozoic West Antarctic Rift system, *Global Planet Change*, *23*, 61-77.

Young, D. A., D. D. Blankenship, J. W. Holt, D. L. Morse, E. Leuro, S. D. Kempf, and M. E. Peters (2006), Surface state of Thwaites Glacier and implications for its stress state from airborne laser altimetry and radar sounding, *Geophysical Research Abstracts*, *8*, 09866.

Young, D. A., S. D. Kempf, D. D. Blankenship, J. W. Holt, and D. L. Morse (2008), New airborne laser altimetry over the Thwaites Glacier Catchment, West Antarctica, *G-Cubed*, *9*, Q06, DOI: 10.1029/2007GC001935.

Vita

Theresa Marie Diehl was born in Rochester, NY on January 16, 1981 to Donald Richard and Marilyn Ann Diehl. She is the second of five children. Theresa attended Spencerport High School from 1995 to 1999 and The Pennsylvania State University from 1999 to 2003. She was awarded a Bachelors of Science in Geosciences with Honors from Penn State and was Geosciences Marshall in May 2003. She published her undergraduate honors thesis entitled “Determining Crustal Structure beneath the Tibetan Plateau using Receiver Functions” in 2003. The second chapter of this dissertation was published in the journal *Geochemistry, Geophysics, and Geosystems* on April 3, 2008. While at the University of Texas at Austin from fall 2003 to summer 2008, Theresa taught four semesters of classes, three of which were undergraduate laboratory-based classes, in addition to completing the research presented in this dissertation.

Permanent address: 27 Kresswood Drive, Rochester, NY 14624

This dissertation was typed by Theresa Marie Diehl.